University of Massachusetts Amherst
ScholarWorks@UMass Amherst

Doctoral Dissertations 1896 - February 2014

1-1-1975

Rheo-optical studies of poly(N)-vinyl carbazole.

Tien-kuei Su
University of Massachusetts Amherst

Follow this and additional works at: https://scholarworks.umass.edu/dissertations_1

Recommended Citation
Su, Tien-kuei, "Rheo-optical studies of poly(N)-vinyl carbazole." (1975). *Doctoral Dissertations 1896 - February 2014*. 607.
https://doi.org/10.7275/3dms-mb03 https://scholarworks.umass.edu/dissertations_1/607

This Open Access Dissertation is brought to you for free and open access by ScholarWorks@UMass Amherst. It has been accepted for inclusion in Doctoral Dissertations 1896 - February 2014 by an authorized administrator of ScholarWorks@UMass Amherst. For more information, please contact scholarworks@library.umass.edu.

3 1206b 0015 5298 E

RHEO-OPTICAL STUDIES OF

POLY(N)-VINYL CARBAZOLE

A Dissertation Presented

By

Tien-kuei Su

Submitted to the Graduate School of the

University of Massachusetts

in parital fulfillment of the requirements of degree of

DOCTOR OF PHILOSOPHY

July 1975

Major Subject : Polymer Science and Engineering

RHEO-OPTICAL STUDIES OF

POLY(N)-VINYL CARBAZOLE

A Dissertation Presented

By

Tien-kuei Su

Approved as the style and content by:

Richard S. Stein

Dr. Richard S. Stein, Chairman of Committee

Roger S Porter

Dr. Roger S. Porter, Member

William J. MacKnight

Dr. William J. MacKnight, Member

Isaac Chanchez

Dr. Isaac C. Sanchez, Member

William M. Prest

Dr. William M. Prest, Member

R S Porter

Dr. R. S. Porter, Department Head

DEDICATION TO

MY PARENTS, MY WIFE AND MY SON

ABSTRACT

Viscoelastic behavior from the responses of mechanical and optical properties of amorphous poly 9(N)-vinyl carbazole (PVK) is studied with relaxation and vibration techniques over various temperatures, elongations and frequencies. The relaxation study is undertaken using a Table Model Instron with the attachment of a conventional optical system by simultaneous and continuous measurements of birefringence and stress. The behavior of birefringence decay and stress decay are followed in the same fashion during the process of simple relaxation. The vibration study is carried out using a dynamic birefringence apparatus by simultaneous measurements of the dynamic quantities of birefringence, stress and strain. Relaxation and vibration data can be described by the WLF equation through time-temperature superposition and frequency-temperature equivalence principles individually to obtain the master curves of optical and mechanical functions. The shift factors from relaxation data agree quantitatively with those from vibration results. The abnormally high value of C_2 in the WLF expression may be associated with the cubic thermal expansion coefficients.

The stress-optical coefficient (S.O.C.) of PVK measured under the condition of relaxation at constant length is almost constant over the temperatures range from 210°C to 275°C of this study and in a agreement with that under dynamic strain.

Stress induced crystallization occurs with an increase of

birefringence and a decrease of stress by stretching amorphous PVK at high temperature above its glass transition temperature and elongation ratio greater than 2.0. The rate and magnitude of stress decay corresponding to crystallization passes through a maximum at an intermediate extension of elongation ratio 3.0. The isothermal crystallization kinetics is described by the Stein equation. The crystallization rate which is very dependent on the elongation in comparison with temperature increases with increasing extension.

The deformation of amorphous PVK accompanied by crystallization leads to sharp X-ray diffraction patterns, small angle light scattering patterns and an increase of infrared dichroism.

The sharp X-ray diffraction peak from the crystalline component of PVK is located at a Bragg angle 2θ of 8.2^{o} which corresponds to the interplanar spacing of $10.5A^{o}$. The intensity and azimuthal dependence of this diffraction peak increases with extension. At high deformation, the chain direction of the crystalline phase is almost perfectly aligned toward the stretching direction.

The morphology of the PVK superstructure as judged from H_v patterns of small angle light scattering is a function of temperature and extension. It has a rod-like texture below $265^{o}C$. Above $275^{o}C$, it appears to change from spherulitic structure at 100% stretching to a combination of spherulitic and rod-like structures (so called shish-kebab texture) with

further elongation up to 200% extension. Finally it becomes a pure fibrillar texture at higher elongation reflected in the increase of stress level.

ACKNOWLEDGEMENT

The author wishes to express his very sincere appreciation and gratitude to Professor Richard S. Stein, thesis director, for his advice, direction and encouragement throughout the course of this research.

The author wishes to extend his gratitude to the thesis committee, Professor R.S. Porter, Professor W. J. Macknight, Professor I. C. Sanchez and Dr. W. M. Prest for their constructive comments and helpful discussions.

It is also a pleasure to thank Dr. W. M. Prest and Dr. R. C. Penwell for providing a great deal of information about PVK.

The author is also indebted to his wife Su-Jin for her encouragement and invaluable help with the figure copy and the thesis typing.

In addition, he wishes to ackowledge with thanks for the financial assistance from the Xerox Corporation.

TABLE OF CONTENTS

I. Introduction

The objective of this research is to study the optical and mechanical functions of viscoelasticity of amorphous polyvinyl carbazole, and the behavior of isothermal crystallization as well as molecular orientation during and after stretching polyvinyl carbazole under tensile stress by means of rheo-optical techniques.

Poly 9(N)-vinyl carbazole (PVK) used in this study is a commercial sample (trademark "Luvican") by the German (B.A.S.F.) process[1] which is an adiabatic bulk polymerization under a high pressure (40 Atm) of inert gas of nitrogen. This is a radical polymerization initiated by di-tert-butyl peroxide (0.02%) activated by 2:2-azobisisobutylronitile (0.01%) stirred at 80-90°. Its molecular weight distribution has been characterized by gel permeation chromatograph of PVK-THF solution to give M_w / M_n about 7 with $M_w = 1.47 \times 10^6$ and $M_n = 2.18 \times 10^5$.

PVK is a noncrystalline polymer prepared by free radical polymerization[1] or cationic polymerization[14]. PVK can not be polymerized by an anionic mechanism[9]. In 1961, it was reported that PVK had a high degree of stereoregularity and crystalline spherulitic structure with Ziegler-Natta type (butyllithium-titanium tetrachloride) polymerization[15]. Later in 1963, the reproducibility of this result of coordinated polymerization was suspected[16]. Stereoregular polymerization of semi-crystalline of PVK was reported by using catalyst of the type MR_mX_n (M = metal, R = organic radical and X = halogen) such as (C_2H_5) AlCl[14]. PVK produced by solid state polymerization with redox catalyst (ammonium persulfite / sodium

bisulfate) from monomer crystal may be crystallized[18]. It was found that the infrared spectra of PVK from this solid state polymerization system is same as that from radical polymerization.

PVK $(C_{14}H_{11}N)_n$ whose formula is shown on Figure (70b) has a rigid and bulky side group which result in its characteristic property of extreme brittleness at room temperature. Its rigidity is reflected in a high glass transition temperature in the range of 160-250°C[2], which increases with molecular weight and decreases with decreasing solvent content.

PVK is a good dielectric material having a dielectric constant of 3.0, a power factor about 0.001 and permittivity of 3.0 over a wide frequency range[1], has high thermal stability and has very good photoconductive properties[8]. Its refractive index, 1.69 at room temperature, is high for the interest of contact lens[9]. In comparison to polystyrene, PVK has more stable dielectric constant over the change of temperature and frequency, a superior thermal stability and stiffer chains than PS for which the conformational paramer is 2.2[3].

Polymer materials with the presence of hetero atoms, electrons and particularly polyaromatic structure have higher photoresponse than those without containing heterocyclic group or π electrons. The interest of photoelectric properties of vinyl polymers is to have large π electron system as a pendant group[10]. Poly N-vinyl carbazole has larger photoconductivity than any other carbazole derivatives such as poly 2-vinyl carbazole[9]. The photoconductivity of PVK sensitization[11][12]

and PVK-Iodine charge transfer mechanism[13] have been investigated. All of these studies were carried out on the unoriented amorphous PVK and its complexes. The increase of conductivity of π electron system with orientation may be due to increase of the amount of π -orbital overlap between adjacent molecules as the effect of pressure[31]. It was reported that the amorphous oriented films have superior electrical properties[32] than unoriented samples. It was found that crystalline polyacetylene has higher electrical conductivity and oriented polyacrylnitrile pyrolyzate has greater electrical conductivity by stretching before pyrolysis[19].

In the investigation of solution properties of viscosity-molecular weight relation of PVK, Kuwakara et al[3] found that its large value of conformational parameter σ , 2.85 is due to the steric effect of repulsion between carbazole groups which bring about considerable hindrance to free rotation of its chains. This parameter σ, is defined as

$$\sigma^2 = \frac{(\overline{R_o^2})}{(\overline{R_{of}^2})}$$

where $\overline{R_o}^2$ is the mean square end-to-end distance of chains and $\overline{R_o}^2$ is the corresponding value with free internal rotation.

The large magnitude of shielding and nonuniform shielding of aromatic protons from nuclear magnatic resonance spectrum also indicate the mutual interaction of bulky carbazole group[4]. The number of monomer units which is statistically equivalent to one random link is a basis of chain stiffness which may be

measured by evaluating the anisotropy of the random link from the measured value of the stress-optical coefficient and calculating the anisotropy of the monomer unit from bond polarizabilities. The values of the equivalent random link for same polymers have been reported[5].

In the calculation of strain birefringence of polystyrene, Flory et al[6] concluded that its planar phenyl groups are parallel to one another and perpendicular to the chain backbone. In 1970, Crystal[7] proposed that the pendant carbazole groups of PVK lie close to and parallel to one another from the molecular model studies of both isotactic and syndrotactic configuration.

Kimura et al[19] in 1970 found that crystalline PVK precipitated from solution and treated by heat under nitrogen atmosphere is rod like crystal and are packed in pseudohexagonal array with an isotactic 3/1 helix as well as a syndiotactic 2/1 helix. In the study of single crystal morphologies of PVK grown from dilute solution, Crystal[7] postulated that rod-shaped crystals were formed below 115°C and flat thin lamellar crystals were produced due to chain folding above this temperature. Recently, lamellar structure of PVK was observed with substrate induced crystallization[20], and the molecular arrangement of the crystal lattice is a pseudo-hexagonal packing of helical array with the unit cell parameters a =12.00A° and c = 6.47A°.

Crystallinity and orientation affect physical properties of polymer materials e.g. the electrical[21-23] and mechanical

properties[1,24]. For uniaxial orientation, it has been reported[25-30] that the tensile strength along the direction of stretching axis will be improved, because the applied load will be carried largely by the strong covalent bonds of polymer chains. The tensile strength in the transverse direction will be reduced, because the load will be carried primarily by the weak van der Waals bonds. It is recongnized that the crystallites of uncrosslinked elastomer are similar to the crosslink points in a crosslinked rubber giving rise to higher modulus than for the uncrosslinked rubber with no crystallinity.

In view of the effect of crystallinity and orientation on physical properties, overcoming the limitation of physical strength and the interest of unique photoconductivity of PVK, the rheo-optical study of PVK has been carried out.

The rheo-optical technique has been introduced by Stein, and has been reviewed by several authors[33-37]. It is the method of using the electromagnetic radiation to study the deformation and rheology of polymer materials. It includes birefringence, dichroism, polarized fluorescence, polarized raman scattering, X-ray diffraction and small angle light scattering etc. In polymeric systems, the optical properties of birefringence, infrared dichroism etc arise from the long-range orientation and the interference effects of the large size polymer bring about the phenomena of light scattering and X-ray diffraction etc.

The rheo-optical functions of polymer materials can yield

the information about the behavior of particular internal structures while the mechanical responses can only observe the information from a combined contribution of the internal structure units. The range of linearity of the rheo-optical coefficients for polymers usually exceeds that for the mechanical property of modulus. Since the nonlinearity arises primarily from the processes as bond bending, bond stretching and crystal dislocation formation and motion which would not contribute significently to the optical properties[37].

II. Theoretical and Principles of Methods

A. Birefringence

The phenomenon of double refraction which results from the difference in refractive indices in different directions is termed birefringence. The principles of double refraction phenomenon is shown in Figure (1).

Retardation R, the number of wave path difference, is defined as

$$R = \frac{d}{\lambda_1} - \frac{d}{\lambda_2} \qquad (1)$$

where d is the sample thickness, λ_1 and λ_2 are the wavelengths of light along stretching direction and the direction perpendicular in the specimen medium.

From the difinition of refractive index n,

$$n_1 = \frac{\lambda_o}{\lambda_1} \qquad (2)$$

And

$$n_2 = \frac{\lambda_o}{\lambda_2} \qquad (3)$$

where n_1 and n_2 are the refractive index along and perpendicular to the stretching direction, and λ_o is the wavelength of light in vacuum.

Then the birefringence, Δ can be related to retardation by

$$\Delta = n_1 - n_2 = \frac{\lambda_o}{d} R \qquad (4)$$

The order of retardation can be measured with Babinet compensator and evaluated by the following formula

$$R = \frac{\Delta X}{\Delta X_o} \qquad (5)$$

where ΔX is the amount of shift in the fringe pattern along the retardation wedge in the compensator and ΔX_0 corresponds to one wavelength shift.

The birefringence can be described in terms of bond polarizabilities assuming that the relation between the principal refractive indices and polarizabilities per unit volume can follow the Lorenz-Lorentz equation

$$\frac{n^2-1}{n^2+2} = \frac{4}{3}\pi P \qquad (6)$$

where n is the refractive index of the sample and P is the bond polarizabilities per unit volume.

By differentiation

$$\frac{6n\,dn}{(n^2+2)^2} = \frac{4}{3}\pi\, dP \qquad (7)$$

$$dn = \frac{4\pi}{3}\,\frac{(n^2+2)^2}{6n}\,dP \qquad (8)$$

If the difference of refractive indices is small, then the

$$\Delta = n_{\parallel} - n_{\perp} = \frac{2\pi}{9}\,\frac{(n^2+2)^2}{n}\,(P_{\parallel} - P_{\perp}) \qquad (9)$$

where $\bar{n}$ is the mean value of refractive index, $P_{\parallel}$ and $P_{\perp}$ are the bond polarizabilities parallel and perpendicular to the deformation direction.

The birefringence of the multiphase or multicomponent system by assuming the birefringence to be additive has been

described by the expression (38)

$$\Delta = \sum_i (\phi_i \Delta_i) + \Delta_F \qquad (10)$$

where ϕ_i and Δ_i denotes the volume fraction and birefringence in the i-th phase respectively and Δ_F is the form birefringence representing the contribution from the anisotropic boundaries such as boundaries of crystalline and amorphous regions or microvoids due to the distortion of the field of the light wave.

For a semicrystalline polymer, eq (10) can be rewritten as

$$\Delta = \phi_c \Delta_c + (1 - \phi_c)\Delta_a + \Delta_F \qquad (11)$$

where Δ_c and Δ_a are the birefringence contributions from crystalline and amorphous component individually, ϕ_c is the volume fraction crystallinity.

Relating to the orientation function of crystalline phase f_c, and of amorphous phase, f_a, eq (11) can be represented by

$$\Delta = \mathring{\Delta}_c f_c \phi_c + \mathring{\Delta}_a f_a (1 - \phi_c) + \Delta_F \qquad (12)$$

where $\mathring{\Delta}_c$ and $\mathring{\Delta}_a$ are the intrinsic birefringence of perfectly oriented crystalline and amorphous component respectively. The calculation of $\mathring{\Delta}_c$ is illustrated in Section (B.3.)

The linear relationship between birefringence and stress in amorphous materials has been represented by the equation (7)

$$\Delta_a = C \cdot \sigma \qquad (13)$$

where σ is the stress and the proportional constant, C, is called the stress-optical coefficient.

By replacing Δ_a by assuming the stress optical coefficient, C, for the amorphous region of the crystalline polymer to be identical with that for pure amorphous polymer and neglecting the form birefringence, then

$$\Delta = \Delta_c^{\circ} f_c \phi_c + C \cdot \sigma (1 - \phi_c) \qquad (14)$$

By rearranging

$$\phi_c = \frac{\Delta - C \cdot \sigma}{\Delta_c^{\circ} f_c - C \cdot \sigma} \qquad (15)$$

B. Dynamic Birefringence

The mechanical response of viscoelastic behaviors of polymers can be represented by the Maxwell element consisting of a spring of modulus, E, and dashpot of tensile viscosity, η, connected in series. The relaxation time, τ, is defined as

$$\tau = \frac{\eta}{E} \tag{16}$$

The behaviors of viscoelastic polymer subjected to a sinusoidal strain, ε, and a sinusoidal stress, σ, out of phase with the strain by the angle, δ, can be described as

$$\varepsilon(t) = \varepsilon_0 \exp(i\omega t) \tag{17}$$

$$\sigma(t) = \sigma_0 \exp(i(\omega t + \delta)) \tag{18}$$

where ω is the frequency and t is the time.

The complex tensile modulus, E^*, can be given by

$$E^* = E' + iE'' \tag{19}$$

$$= \frac{\sigma(t)}{\varepsilon(t)} \tag{20}$$

$$= \frac{\sigma_0}{\varepsilon_0} \exp(i\delta) \tag{21}$$

$$= |E^*| (\cos\delta + i \sin\delta) \tag{22}$$

Then

$$\tan\delta = \frac{E''}{E'} \tag{23}$$

And

$$E' = |E^*| \cos\delta \tag{24}$$

$$E'' = |E^*| \sin\delta \tag{25}$$

The response of a distribution of Maxwell elements yields

$$E^* = \int_0^\infty \frac{E(\tau)\omega^2\tau^2}{1+\omega^2\tau^2} d\tau + i\int_0^\infty \frac{E(\tau)\omega\tau}{1+\omega^2\tau^2} d\tau \qquad (26)$$

In term of relaxation spectra function H ($\ln \tau$), E^* can be expressed as

$$E^* = \int_{-\infty}^{+\infty} \frac{\omega^2\tau^2}{1+\omega^2\tau^2} H(\ln\tau) d\ln\tau + i\int_{-\infty}^{+\infty} \frac{\omega\tau}{1+\omega^2\tau^2} H(\ln\tau) d\ln\tau \qquad (27)$$

The relaxation spectra function, H ($\ln \tau$), is always positive and stress always leads strain.

Similarly, the optical property of birefringence, Δ , in a polymer specimen subjected to a periodic tensile strain, ε , will generally be out of phase by the angle, α , and can be written as

$$\Delta(t) = \Delta_0 \exp(i(\omega t + \alpha)) \qquad (28)$$

The complex strain optical coefficient, K^*, obtained by dividing strain, ε ,

$$K^* = \frac{\Delta(t)}{\varepsilon(t)} \qquad (29)$$

$$= \frac{\Delta_0}{\varepsilon_0} \exp(i\alpha) \qquad (30)$$

$$= |K^*|(\cos\alpha + i\sin\alpha) \qquad (31)$$

$$= K' + iK'' \qquad (32)$$

$$K' = |K^*| \cos\alpha \qquad (33)$$

Then

$$K'' = |K^*| \sin\alpha \qquad (34)$$

$$\tan\alpha = \frac{K''}{K'} \qquad (35)$$

Related to elastic birefringence spectra function A ($\ln\tau$) and viscous birefringence spectra function B ($\ln\tau$), K^* can be formulated as(39)

$$K^* = \int_{-\infty}^{+\infty} \frac{A(\ln\tau)\omega^2\tau^2 + B(\ln\tau)}{1+\omega^2\tau^2} d\ln\tau + i\int_{-\infty}^{+\infty} \frac{(A(\ln\tau)-B(\ln\tau))\omega\tau}{1+\omega^2\tau^2} d\ln\tau \quad (36)$$

The birefringence spectra functions, A ($\ln\tau$) and B ($\ln\tau$) may be positive or negative to make the strain optical coefficient increase or decrease and phase difference, α , be positive or negative as a function of frequency.

The complex stress optical coefficient, C^* and the phase difference, β , between birefringence and stress can be derived to give the following formula.

$$C^* = \frac{\Delta(t)}{\sigma(t)} \quad (37)$$

$$= \frac{K^*}{E^*} \quad (38)$$

$$= C' + iC'' \quad (39)$$

Then

$$C' = |C^*|\cos\beta \quad (40)$$

$$C'' = |C^*|\sin\beta \quad (41)$$

And

$$\tan\beta = \frac{C''}{C'} \quad (42)$$

$$= \tan(\delta-\alpha) \quad (43)$$

$$= \frac{\tan\delta - \tan\alpha}{1+\tan\delta\tan\alpha} \quad (44)$$

The transmission of light, T , shown on Figure (2a) with a sample between two cross polaroids with polarization direction at 45^{o} to the stretching direction of the sample as Figure (8) is

$$T = A\sin^2\left(\frac{R}{2}\right) + T_s \tag{45}$$

where T_s is the internal scattering resulted from locally oriented structures (such as spherulite) with the sample is placed between two crossed polaroids. A, which is an attenuation factor due to the reduction of transmission intensity from other factors than retardation can be written as

$$A = (1-r)^{-(K+\tau)d} \tag{46}$$

where r is the reflectivity, K is the absorption coefficient, τ , is the turbidity, and d is the thickness of the specimen.

R is the retardation consisting of the retardation of retarding plates placed in the optical path, R_r , and the retardation from sample, R_s. R_r is a constant retardation from reatrding plates and R_s gives the same formula as eq (4)

$$R_s = \frac{2\pi d}{\lambda}\Delta_s \tag{47}$$

which upon differentiation to a small value of strain, ε , yields

$$\left(\frac{\partial R}{\partial \varepsilon}\right) = \frac{2\pi}{\lambda}\left[\Delta_s\left(\frac{\partial d}{\partial \varepsilon}\right) + d\left(\frac{\partial \Delta_s}{\partial \varepsilon}\right)\right] \tag{48}$$

The Poisson's ratio, μ , by the application of small

tensile strain is defined as

$$\mu = \frac{1}{2}\left[1 - \frac{1}{V}\left(\frac{dV}{d\varepsilon}\right)\right] \tag{49}$$

Another alternative definition of, μ, in shear deformation is

$$\mu = \frac{\left|\frac{\partial d}{\partial \varepsilon}\right|}{d} \tag{50}$$

For the incompressible material i.e. assuming constant volume deformation as, ε, is small, then

$$\frac{dV}{d\varepsilon} = 0 \tag{51}$$

And
$$\mu = \frac{1}{2} \tag{52}$$

Thus
$$\frac{\partial d}{\partial \varepsilon} = \frac{d}{2} \tag{53}$$

By differentiation of eq (45)

$$\left(\frac{\partial T}{\partial \varepsilon}\right) = A\sin\left(\frac{R}{2}\right)\cos\left(\frac{R}{2}\right)\left(\frac{\partial R}{\partial \varepsilon}\right) + \sin\left(\frac{R}{2}\right)\left(\frac{\partial A}{\partial \varepsilon}\right) + \left(\frac{\partial T_s}{\partial \varepsilon}\right) \tag{54}$$

The quantities A and $\left(\frac{\partial A}{\partial \varepsilon}\right)$ can be obtained by removing the analyzer during vibrating sample. In which case, $T_A = T$ and $\left(\frac{\partial A}{\partial \varepsilon}\right) = \left(\frac{\partial T_A}{\partial \varepsilon}\right)$.

To make a linear response and maximum sensitivity of transmission one should adjust R_r so that $R = \pi/2$ or $3\pi/2$ etc, Then one will obtain

$$\sin\frac{R}{2}\cos\frac{R}{2} = \sin^2\frac{R}{2} = \frac{1}{2} \tag{55}$$

From eq (47), (54), (55) and neglecting $\left(\frac{\partial T_s}{\partial \varepsilon}\right)$ term, the

strain optical coefficient, K, will become

$$K = \frac{\partial \Delta_s}{\partial \varepsilon} \tag{56}$$

$$= \frac{\lambda}{2\pi d A}\left[2\left(\frac{\partial T}{\partial \varepsilon}\right) - \left(\frac{\partial A}{\partial \varepsilon}\right) + \frac{1}{2}\Delta_s \right. \tag{57}$$

When the retardation, R has values of odd integer multiple of $\pi/2$, shown on Figure (2a) the slope of $\partial T/\partial R$ is maximum and the linear relationship between T and R is

$$T = K \cdot R \tag{58}$$

where k is a proportional constant.

The Lissajous figure corresponding to the relation between transmission of light and strain is shown in Figure (3). In order to make sure the validity of eq (58), a standard retarding plate with a known small retardation R_c is inserted in the optical path, parallel $R_c^{\parallel}$, and perpendicular $R_c^{\perp}$, to the vibration direction successively to increase or decrease the total retardation and bring about upper or lower Lissajous figures from the displacement of the original one shown in Figure (3).

The displacement, h, of the Lissajous figures due to the higher and lower retardation by R_c shown on Figure (3) is

$$h = \frac{1}{2}(h_1 + h_2) \tag{59}$$

$$R = R_c^{\parallel} + R_c^{\perp} \tag{60}$$

The deviation H_2 of base line P_1P_3 from the correct base line P_1P_2 by removing the analyzer during vibration is caused

by the reflectivity and turbidity of the sample.

Then the dynamic birefringence of the sample, Δ , can be expressed as

$$\Delta = \frac{R_c}{h}(H+H_2)\frac{\lambda}{2\pi d} \tag{61}$$

The sine function of the phase angle difference is

$$\sin\alpha = \frac{H_\Delta^*}{H} \tag{62}$$

The strain optical coefficient K can be given by

$$|K^*| = \frac{R_c}{\varepsilon h}(H+H_2)\frac{\lambda}{2\pi d} + \frac{1}{2}\Delta_s \tag{63}$$

Then

$$K' = |K^*|\cos\alpha \tag{64}$$

$$K'' = |K^*|\sin\alpha \tag{65}$$

$$\tan\alpha = \frac{K''}{K'} \tag{66}$$

The Lissajous figure represents the relationship between force and strain is shown on Figure (2b). The stress, σ , is

$$\sigma = \frac{L\cdot m}{S} \tag{67}$$

where m is the slope of linear calibration for load voltage relationship, and S is the cross section area of the sample. By dividing strain, ε , the dynamic modulus E^* becomes

$$|E^*| = \frac{\sigma}{\varepsilon} \tag{68}$$

The phase angle, δ , which stress leads strain is

$$\delta = \sin^{-1} \frac{H_\sigma^*}{H_\sigma} \tag{69}$$

Then

$$E' = |E^*| \cos\delta \tag{70}$$

$$E'' = |E^*| \sin\delta \tag{71}$$

$$\tan\delta = \frac{E''}{E'} \tag{72}$$

The birefringence-stress relationship can be decuced either by Lissajous figure method or using birefringence-strain and stress-strain data to follow eq (37) - (44) to get stress optical coefficient C^* and phase difference β .

C. Infrared Dichroism

Infrared spectroscopy depends on the absorption caused by changes in the dipole moment accompanying vibration of the various chromophoric groups in the molecules. The technique of dichroism concerns the use of the relative absorption characteristris of the chromorphoric groups to study the orientation of polymer molecules.

The absorpance A , of a certain chromophoric group can be described by

$$A = C(\varepsilon \cdot \mu)^2 \tag{73}$$

$$= |\varepsilon|^2 |\mu|^2 \cos^2\theta \tag{74}$$

where C is a constant depending on the extinction coefficient and instrumental correction, ε is the electic vector of the polarized incident beam, μ is the oscillating dipole coupled with the vibration, and θ is the angle between μ and ε . The absorption is a maximum when μ and ε are parallel and is zero when they are perpendicular. The ratio of absorbance for polarization parallel to that perpendicular to the stretching direction is called dichroism.

For a certain absorption band, the absorbance for a polarized electric vector parallel to the stretching direction $A_{\parallel}$, has the relation

$$A_{\parallel} = N a \cos^2\theta \tag{75}$$

where N is the number of chromophoric groups per unit volume and,a, is another constant.

For the assumption of cylindrical symmetry systems, the overall average absorption $\bar{A}$, is

$$\bar{A} = \frac{A_{\parallel}+2A_{\perp}}{3} \tag{76}$$

$$= \frac{Na}{3} \tag{77}$$

Then the absorption for polarized light perpendicular to the stretching direction, $A_{\perp}$, is

$$A_{\perp} = \frac{Na-A_{\parallel}}{2} \tag{78}$$

$$= \tfrac{1}{2}[Na-Na\cos^2\theta] \tag{79}$$

$$= \tfrac{1}{2}Na\sin^2\theta \tag{80}$$

The ratio of the intensities of the optical absorption spectrum for polarized infrared with the electric vector parallel, $A_{\parallel}$, and perpendicular, $A_{\perp}$, to the direction of deformation is called dichroic ratio, D.

$$D = \frac{A_{\parallel}}{A_{\perp}} \tag{81}$$

$$= 2\cot^2\theta \tag{82}$$

Then

$$D-1 = 2\cot^2\theta - 1 \tag{83}$$

$$= \frac{3\cos^2\theta-1}{\sin^2\theta} \tag{84}$$

$$D+2 = \frac{2}{\sin^2\theta} \tag{85}$$

The Herman's orientation function of second moment is defined as

$$f' = \frac{3\langle\cos^2\theta\rangle - 1}{2} \tag{86}$$

Thus the orientation function f', of the absorption band can be expressed in terms of dichroic ratio D, as

$$f' = \frac{D-1}{D+2} \tag{87}$$

Then the orientation function f, of the polymer chain can be ralated by

$$f = \frac{D-1}{D+2}\,\frac{D_o+2}{D_o-1} \tag{88}$$

And

$$= 2\cot^2\beta \tag{89}$$

where β is the angle between the transition moment of the chromophoric group and the polymer chain, and D_o is the intrinsic dichroism as the chain have perfectly aligned.

In the conventional determination of the dichroic ratio, the orientation sample and the infrared polarizer are placed in the sample beam path of a double beam spectrometer. $A_{\parallel}$ and $A_{\perp}$ are the absorption determined successively with the polarizer inclined to the transmit radiation polarized parallel first and then perpendicular to the direction of elongation shown on Figure (4).

Then

$$A_{\parallel} = \text{Log}\,\frac{I^{o}_{\parallel}}{I_{\parallel}} \tag{90}$$

$$A_{\perp} = \text{Log}\,\frac{I^{o}_{\perp}}{I_{\perp}} \tag{91}$$

The infrared dichroism can be employed to determine the orientation of different fraction of chain segments corresponding to different absorption bands within the same polymer chain, provided that the directions of transition moment are known.

The low degree of orientation of the polymer chain or an unfavorable angle to the chain axis will result in the dichroic ratio D, close to unity[40]. The method for measuring these cases has been shown by Stein[41] and differential method has been described[42] and more recently used by Stein[43] and Read et al[44,45].

D. Small Angle Light Scattering (SALS)

The photographic method to record directly the complete scattering pattern caused by the presence of optical isotropic or anisotropic heterogeneities to characterize the crystalline superstructure of polymer film has been developed by Stein et al[46]. The notation of a V_V scattering pattern indicates the vertical alignment of the electric vertors of both polarizer and analyzer, while the H_V pattern represents the vertical alignment of polarizer and horizontal arrangement of analyzer with the polarizer in the same vertical position as that of deformation. The optical arrangements for the H_H and V_H patterns are the same as V_V and H_V scattering respectively, but the electric vector of polarizer is perpendicular to the stretching direction.

Both the anisotropic sphere[46,47] and disk[48,49] models predict the so-called four leaf clover pattern with a distinct maximum in the H_V scattering as a function of scattering angle, θ, at odd multiples of $\pi/4$ of the azimuthal angle, μ defined in Figure (5). It is a characteristic of a spherulitic texture. The formula to calculate the average size of the spherulite, R, has been derived as[46]

$$\frac{4R}{\lambda_m} \sin\left(\frac{\theta_{max}}{2}\right) = 4.09 \qquad (92)$$

where λ_m is the wave length of light in the scattering medium.

The basic scattering theory of the anisotropic rods has been documented to explain the scattering pattern for polytetrafluoroethyiene[46,50]. The scattering amplititude E_{H_v} for H_v polarization from the rods of infinitesimal thickness and length L in 2-dimensional space (i.e. $\beta = 0$) shown on Figure (5) was given by[50]

$$E_{H_v} = \rho L \delta \sin(\alpha+\omega)\cos(\alpha+\omega)\left[\sin(\tilde{k}aL/2)/\tilde{k}aL/2\right] \quad (93)$$

and

$$a = -\sin(\alpha+\mu)\sin\theta \quad (94)$$

where ρ is the scattering power per unit length of the rod, δ is the optical anisotropy of the rod, ω is the angle between long axis of rod and stretching direction, α is the angle between maximum polarizability direction and long axis of rod, and the wave number k is defined as

$$\tilde{k} = \frac{2\pi}{\lambda_m} \quad (95)$$

The intensity of scattering, I, proportional to the square of the amplititude as

$$I = C \cdot \int N(\alpha) E_{H_v}^2 \, d\alpha \quad (96)$$

where $N(\alpha)$ is the distribution function of rods. This equation assumes incoherence of the scattering from different rods.

The scattering patterns from anisotropic rods depend upon the distribution of orientation of the rods, the angle between optic axis and rod axis, and the relationship between the refractive index of the rod and that of the surroundings. It has been extended to describe the 1-dimensionsl[51] and 2-dimensional[52] rods in 3 dimensional space. The H_v pattern can change their shapes from X-type (having maximum and minimum intensities at odd and even multiples of $\pi/4$ of μ angle) , to circular-type (intensities at even multiples of $\mu=\pi/4$) by variation with polarizability angle[51,52]. The monotonic decrease in intensity with increasing scattering angle in the H_v pattern is a characteristic of rod-like models.

E. X-ray Diffraction

Wide angle X-ray diffraction (WAXD) which reveals the degree of ordering in the solid materials has been applied to investigated the degree of crystallinity, the size and the perfection of crystals, and the orientation behaviors of crystals in the semicrystalline polymers.

The geometry of the diffraction pattern from the uniaxial orientation sample by photographic method is illustrated in Figure (6). The polymer sample is placed normal to the incident X-ray beam, the direction on the photographic film parallel to the stretching axis is the meridian and the perpendicular direction is the equator. The position of the diffraction pattern on the film can be designated by a radial distance, R, from the undeviated beam and an azimuthal angle, μ , with respect to the meridian.

The "d" spacing corresponding to the set of diffraction planes (h,k,l) can be ccrrelated with diffraction angle, θ , by Bragg equation

$$n\lambda = 2d\sin\theta \tag{97}$$

And

$$\tan 2\theta = \frac{R}{L} \tag{98}$$

where λ is the wavelength of X-ray, R is the distance from the center of the photographic film to the diffraction peak and L is the distance between sample and photographic film.

From the intensity and the distribution along the azimuthal angle, μ , of the diffraction pattern, the crystallinity and orientation of the crystal planes can be described qualitatively. The uniaxial prefered orientation of the crystallographic plane can be determined from the azimuthal angle dependence taken as the value of the breadth of the diffraction arcs or spots. The smaller this orientation angle corresponds to the greater degree of orientation.

III. Experimental and Apparatus

A. Sample Preparation

The technique of preparing films by solution casting has been applied during this study, because the polymer is unstable with the melt-pressing at high flow temperature. This method involves forming a viscous solution in a volatile solvent then drying by vaporizing the solvent. The procedures to make the film are as follows.

1. Prepare about 10% polyvinyl carbazole-tetrahydrofuran solution.
2. Pour about 20 ml to 60 ml of this viscous solution into the pyrex glass dish of 6" diameter to make 3 mil to 10 mil thick of dry sample. The glass dish is positioned on the even surface checked with level.
3. Cover the dish with aluminum foil then beaker to allow an atmosphere rich in THF solvent and to prevent the solvent drying too fast from the surface with consequent wrinkling.
4. After tetrahydrofuran evaporates completely, remove the dry transparent film from the dish with methanol.
5. Place the film in the vacuum oven at room temperature overnight the heat to about 160^{o}C then to 250^{o}C.
6. Cut the film into rectangular shape on a hot stage at the temperature about 200^{o}C.

B. Birefringence

The Instron equipped with optical system is used to obtain birefringence from the measurement of retardation by using Babinet compensator and the mechanical response of stress or modulus from the trace of the recorder after amplification from the load cell. The schematic diagram of the Table Model Instron (Model TM) with the attachment of conventional optical arrangement is shown in Figure (7).

1. Optical System

A mercury vapor lamp (GE A100H4) has been used as the light source and rendered parallel by condensing lens then monochromatized by a monochromatic filter of wavelength 5460 A^{o}. The polarizer and analyzer are placed perpendiculat to each other and 45^{o} to the stretching direction of the sample. The light ray is collimated with pinhole after passing through the polarizer. The method of measuring birefringence by using Babinet compensator has been described[5,53,54].

2. Mechanical System

The full scale of the force can be controlled with different range of load cell or by adjusting sensitivity button in the recorder and has been calibrated by hanging known weight before experiment. The "Dial Assembly" is used to set

the specified strain, and the proper gear ratio is chosen to regulate the deformation rate.

3. Temperature Control System

The constant temperature cylindrical chamber is made of two solid aluminum hemicylinders with two circular holes on the opposite sides to permit the light to pass through the sample. It is sufficiently insulated with glass fiber and heated with Chromalox tubular heating element surrounded with Wood's metal ($T_m = 68^o$) to increase heat conduction between heating element and walls of wells in chamber. The heating elements are regulated a by Fenwal regulator (Series 141). The thermo-couple placed close to the specimen indicates the temperature of the system on the panel of Fenwel Proportional temperature controller (Series 542) which can preset the desired temper-ature and connected with the power supply. The nitrogen gas is purged into the chamber during the experiment to avoid thermal decomposition of the sample. The fixed rod between the upper clamp and load cell is made of glass fiber to reduce heat conduction through it.

4. Procedures

The sample is put between the two clamps at the temperature near the preset temperature and is so adjust that there is no initial strain on the strip. After the temperature reaches equilibrium, the sample of original thickness d_o is stretched

to the desired extension ratio, λ . Simultaneously, the output of force, f , is recorded continuously on the recorder and the retardation, R, is read from Babinet compensator. With the assumption of affine deformation, the stress is evaluated by

$$\sigma = \frac{f}{(A/\lambda)} \tag{99}$$

where A is the cross section area of original sample.

The birefringence, Δ , can be calculated using eq(4) with correction of sample thickness as

$$\Delta = \frac{\lambda_o}{(d/\lambda)} R \tag{100}$$

C. Dynamic Birefringence

The dynamic birefringence equipment is schematically illustrated in Figure (8).

1. Optical System

The optical arrangement for dynamic birefringence apparatus is similar to the optical attachments of the Instron. The mercury vapor lamp served as the light source is operated on the D.C. power from a 125 volt motor-generator, filtered through a condenser choke circuit consisted of inductor and capacitor components. The intensity of light can be regulated by a variable resistor in series with the lamp. The photo-resistive cell is made of CdS with a fixed polaroid and a rotatable polaroid facing the light source. The battery-powered photoresistor is a D.C. level compensator located near the lamp and it is a solid state device whose resistance increases with intensity of radiation. It is employed to balance the D.C. level from the output of photomultiplier such that the signal of Lissajous figure of light transmission-strain relation can be located at the optimum position on the screen of cscilloscope by rotating the rotatable polaroid. It has another function of compensating the fluctuation in intensity of light source to a certain extent.

The retardation plates which are made of mica and inserted between the sample and the analyzer are supplemented to adjust

the transmission of light into the linear region with maximum sensitivity. Then the beam passes through a neutral density filter to avoid saturation of light intensity then into the photomultiplier tube powered by a battery.

2. Mechanical System

The frequency of vibration is regulated by changing the pully belts to different ratios and dynamic strain is controlled by the eccenticity of the cams which produce a sinusoidal vertical diplacement of the upper end of the polymer strip. A force compensator powered by battery which is a circuit device composed of resistor and capacitor components is used to balance the output of force and position the signal of force-strain Lissajous figure at desired position on the screen of the oscilloscope by adjusting the resistor. A Schaevitz TDC-4M miniature Dynamometer using a linear variable differential transducers (LVDT) have been used to transform the dynamic strain and force responses into electrical signals. The LVDT's are powered by the audio frequency osielators and their output signals are traced on the oscilloscope through the amplifiers.

3. Procedures

The retardation plates and the response of the photo-multiplier have been calibrated with a Babinet compensator and the function of force transducer (LVDT) has been calibrated

to have linear force-voltage relation. An output of linear Lissajous signals (no phass difference) of modulus-strain and birefringence-strain relations during vibration are attained by adjusting the capacitor of the attached circuits by using the elastic spring and quartz wedge instead of the sample. In order to have the sample taut between the clamps during vibration, an intial 5% static strain has been applied after temperature equilibrium is attained. The static birefringence is evaluated from the measurement of retardation by using Babinet compensator and the static force is balanced with another stress tranducer in a differential manner. After a certain period (about 30 minutes) of vibration to assure stability, the Lissajous figures representing transmission of light-strain and force-strain relations are traced on the different channels of Tektronix dual-beam oscilloscope subsequently. The dynamic optical and mechanical coefficients can be evaluated according to the equations in the part B of Chapter II.

D. Small Angle Light Scattering

The experimental arrangement for photographic low-angle light scattering is shown on Figure (9). The plane polarized Helium-Neon, Spectra 130 laser light is the light source with wavelength of 6328A^{o} in air. A red filter is used for eliminating the blue fluorescent light from the laser and a neutral filter may be used when the scattered light is too intense. A shutter controls the exposure time and the pinhole adjusts the diameter of the beam.

After completeing the measurements in part B, the sample is quenched to room temperature rapidly. It has been found that the birefringence keeps constant while the stress increases greatly. Light scattering study is carried out at room temperature with these specimen positioned between glass plates and immersed with silicon oil to minimize surface scattering.

IV. Results and Discussions

AA. Glass transition temperature of PVK

The glass transition temperature, T_g , for amorphous polymers is the temperature at which they change from the glassy state to the rubbery state. It is associated with the onset of main-chain segmental motion. There are various factors[111, 112] which will influence the glass transition in amorphous polymers, but only three kinds of effect will be pointed out in this section. Regarding the chemical strusture, the bulky nature of the side group of carbazole molecule makes internal rotation of the chains restricted so that polyvinyl carbazole is a rigid plastic with one of the highest glass transition temperatures of vinyl polymers[2]. With the assumption of equal free volume for all molecular weight fractions, the effect of molecular weight on the glass transition temperature has been proposed as[113, 114].

$$T_g = T_g^{\infty} - \frac{K}{\bar{M}_n} \qquad (A1)$$

The quantities of T_g^{∞} and K have been obtained as 500° and 2.27×10^5 respectively for PVK[115]. The number average molecular weight, $\bar{M}_n$, for this study is 2.18×10^5 which gives the value of T_g about 225°C according to eq (A1). Low molecular weight material soluble in the polymer such as solvent will soften the polymer materials so as to reduce the glass transition temperature[116].

The static thermodynamic property of heat capacity which characterizes the glass transition temperature has been measured by using differential scanning calorimetry (DSC) in this study. Figure (2) represents the temperature dependence of the heat capacity for the commercial PVK. This gives a T_g of 220.8°C. Figure (3) which indicates the heat capacity-temperature relation for the PVK solution cast film without heat treatment yields T_g at 158.8°C. Figure (4) and Figure (5) illustrate the same function for the PVK film heated to 180°C and 220°C in vacuum oven and T_g are 195.3°C and 217.5°C respectively. The latter sample has solvent content about 0.01 percent analyzed by gas chromatograph[117]. The difference of T_g in this study seems to be due to the different amount of solvent trace remained in the sample.

A. Optical and Mechanical Viscoelastic Behaviors of Amorphous Polyvinyl Carbazole

1. Relaxation Method

a. Birefringence and Stress Relaxation

After a step function strain performed by stretching the polymer sample to a specified extension rapidly then keeping at constant length and constant temperature, the isothermal relaxation of optical property of birefringence and mechanical property of stress of amorphous PVK were measured simultaneously and continuously against time over a certain range of temperature and elongations.

The optical response of birefringence versus time at elongation ratio 1.1 (10% stretching) over the temperature range from 210°C to 275°C is plotted logarithmically in Figure (14). The corresponding mechanical response of stress relaxation is shown on Figure (15). Under 30% deformation (extension ratio 1.3) with the same temperature range as 10% elongation, the logarithmic birefringence decay and the corresponding stress decay are shown on Figure (16) and Figure (17) respectively. Figure (18) describes the stress-time relation of 50% elongation at the temperature of 220°C over a relatively longer time scale. Under the same deformation, a family curves of the birefringence and the stress as a function of time over the temperature range of 210°C to 275°C

are plotted separately on Figure (19) and Figure (20).

The isothermal optical function of birefringence and isothermal mechanical function of stress increases with extension but decrease with rising the temperature for the corresponding deformation in the temperature range of this study. The amount of decay and the rate of relaxation for both birefringence and stress decrease with lowering the temperature.

The isothermal birefringence relaxation and the isothermal stress relaxation behave in the same fashion under the above conditions. The stress optical coefficient (S.O.C.) during relaxation at constant length under 30% elongation as a function of temperature is shown on Figure (21). The value of , C, (S.O.C.) is almost constant with time and is around 1.2×10^{-8} cm^2/dynes for all the temperatures of this study. The reciprocal relation between S.O.C. and the temperature has been documented[5]. The C value with which is not temperature dependent over this temperature range may be due to the temperature interval being small. It has been reported[55] that both stress and birefringence relax in a similar way during the course of decay for the rubbery polyisobutylene to elucidate the same molecular mechanism between optical and mechanical relaxation processes. It was also presented[56] that the ratio of birefringence to stress for the rubbery polystyrene during relaxation and creep is independent of time, molecular weight, stress and strain up to 95% elongation, and depends only very slightly on temperature.

b. Time-Temperature Superposition

The time and temperature dependence of the optical and mechanical viscoelastic behaviors can be separated by the phenomenological theory of linear viscoelasticity to have the interconversion between time and temperature function of any experimental measurements of viscoelastic responses.

Time-temperature correspondence is the procedure of superimposing a family of creep curves or relaxation curves at different times and temperatures. The increase in temperature with respect to the reference temperature is converted into longer time by an appropriate value of shift factor, a_T, and vice versa. A typical superimposed master curve of relaxation is for the well investigated polymer of polyisobutylene[57,58].

The master curve of the logarithmic plot of the reduced optical function of birefringence relaxation at 10% deformation is illustrated on Figure (22) obtained using time-temperature superposition with a reference temperature at 220°C. Figure (23) depicts the master curve of stress relaxation (stress versus reduced time, t/a_T) corresponding to Figure (15) with horizontal shift and same reference temperature as Figure (22). Similarly, by horizontal translation along log t from a family curves of birefringence relaxation at 30% elongation in Figure (16) and stress relaxation in Figure (17) with the same standard temperature of 220°C, the composite curves of

birefringence and stress responses with reduced variable of time were obtained and are illustrated in Figure (24) and Figure (25). The resulting superimposed curves of birefringence decay and stress decay at 50% elongation reduced to a standard temperature of 220°C shown on Figure (26) and Figure (27) respectively.

There is good agreement between Figure (18) and Figure (27). The former curve comes from the direct experimental measurement of stress decay over a longer time scale at 220°C and the latter is the composite curve from a family of curves of stress relaxation over the temperature range from 210°C to 275°C obtained by shifting horizontally along the time axis using 220°C as the reference temperature. This evidence indicates that the linear viscoelastic behavior of time-temperature superposition is applicable to optical and mechanical relaxation phenomena of amorphous PVK. The vertical shift factor of relaxation curves $T\rho/T_o\rho_o$, due to temperature variation which accounts for the inherent temperature dependence and density change is slight and has been neglected over the temperature range of this study.

The temperature dependence at all the relaxation times is the same according to molecular theory[59,60,61] of dilute solution and bulk polymers. The shift factor, a_T, which is represented by the ratio of relaxation time at the temperature T to that at the reference temperature T_o characterizes the composite curves. The logarithmic plot of the shift factor,

a_T as a function of temperature using 220°C as the standard temperature is illustrated on Figure (23a).

An empirical formula to describe the general curve of log a_T as a function of temperature has been introduced[62] and called the WLF equation

$$\text{Log } a_T = \frac{-C_1^\circ (T-T_o)}{C_2^\circ + T - T_o} \tag{101}$$

which by rearrangement, gives

$$\frac{T-T_o}{\text{Log } a_T} = -\frac{C_2^\circ}{C_1^\circ} - \frac{1}{C_1^\circ}(T-T_o) \tag{102}$$

Then, the WLF plot of $T - T_o$ / log a_T against $T - T_o$ will give a straight line with the slope m and intercept i related to constant C_1° and C_2° as

$$C_1^\circ = \frac{1}{m} \tag{103}$$

$$C_2^\circ = \frac{i}{m} \tag{104}$$

The parameters of C_1 and C_2 characterize the temperature dependent of shift factor, a_T , for several polymers have been reported[63,64]. The plot of WLF expression with reference temperature of 220°C is shown on Figure (23b). The constant C_1° and C_2° are 11.4 and 226.0 respectively. Choosing another standard temperature T_1, the form of WLF relation is same as eq (101) and the coefficients C_1' and C_2' can be transformed in terms of the values at T_o by

$$C_1' = \frac{C_1^\circ C_2^\circ}{C_2^\circ + T_1 - T_\circ} \tag{105}$$

$$C_2' = C_2^\circ + T_1 - T_\circ \tag{106}$$

With the reference temperature at 250°C, Figure (29a) shows the logarithm of the shift factor against temperature and Figure (29b) is the WLF plot. This provides the coefficients C_1 and C_2 as 9.3 and 245.0 individually from the slope and intercept of this plot.

2. Vibrational Method

a. Dynamic responses of optical and mechanical functions

The dynamic optical properties and dynamic mechanical properties were measured simultaneously as a function of temperature and frequency with the dynamic birefringence apparatus. The dynamic birefringence technique for the study of the relationship between structural changes (molecular orientational variation) and mechanical properties in the high polymer field has been introduced and developed by Stein et al[39,65-67] for low density and high density polyethylene, nylon 6, polypropylene and polybutene; Yamada et al[68] for rubber, low density polyethylene and polypropylene; Read[69-70] for polyacetaldehyde; Rudd[71] for polystyrene and Legrand[72]

for polytetrafluoroethylene, silicon rubber, PMMA etc. Recently, the π -sector technique[73,74] which can achieve a high precision by averaging out the fluctuation over many cycles has been applied for dynamic birefringence measurements for polyethylene[75].

The dynamic optical response of the variation of the real part of dynamic strain optical coefficient, K', with frequency over the temperature range of this study is plotted logarithmically on Figure (30). Figure (31) illustrates the behaviors of the imaginary component of dynamic strain optical coefficient, K'', as a function of frequency. The logarithm of dynamic mechanical responses of the change of the storage component of dynamic modulus, E', and the loss part of dynamic modulus, E'', with logarithmic frequency over the same temperature region are shown in Figure (32) and Figure (33) respectively.

The real component of stress optical coefficient at a vibration frequency of 0.545 cycles/sec over the temperature range of this study is depicted in Figure (34). The constant value of stress optical coefficient (S.O.C.) is about 1.4×10^{-8} cm^2 / dynes which is comparable with that from relaxation data (1.2×10^{-8} cm^2 /dynes).

The temperature dependence of optical functions K', K'' and mechanical function E'' at constant frequency pass through the maximum at a temperature in the vicinity of the glass transition temperature. The temperatures of these maxima

increase with frequency over the frequency range of this study. The temperature corresponding to the dispersion of the optical responses are higher than that in correspondence with the dispersion of the mechanical responses.

b. Frequency-Temperature Superpositions

The frequency and temperature dependence of the optical and mechanical viscoelastic functions can be correlated and superimposed[63,76]. The effect of an increase in temperature with respect to the standard temperature corresponds to a decrease in frequency by parallel translation along the log frequency axis.

The master curve of reduced function from a family of curves of real part of strain optical corfficient, K', by frequency-temperature correspondence with respect to the reference temperature at 220°C is shown on Figure (36). The composites curve of the imaginary component of strain optical coefficient, K'', against reduced frequency by horizontal shift along frequency scale is plotted in Figure (37). For reduction to the same standard temperature of 220°C, the master curves of the vs, frequency are shown on Figure (38) and Figure (39) respectively. This linear viscoelastic theory is applicable to both mechanical and optical viscoelastic properties for amorphous PVK.

The logarithmic plot of the reduction factor, a_T, against temperature from the master curves of mechanical function E', E'' and optical function K', K'' using 220°C as a standard temperature is shown on Figure (40a). The magnitudes of a_T, employed for frequency-temperature superposition of the dynamic optical and mechanical data agree quantitatively with those from time-temperature correspondence of the birefringence and stress relaxation results.

The corresponding WLF plot from the vibration data is illustrated on Figure (40b). The constants of C_1 and C_2 values in WLF formula with the reference temperature at 220°C are obtained from the slope and intercept of WLF plot as 10.0 and 202.5 respectively.

The concept of the diffusion and viscosity of transport phenomena depending on the molecular mobility-free volume relation leads the constant C_2^o in WLF equation to[63]

$$C_2^o = \frac{f_o}{\alpha_f} \tag{107}$$

where f_o is the fractional free volume at the reference temperature T_o and thermal expansion coefficient, α_f, of free volume V_f can be expressed by

$$\alpha_f = \frac{1}{V_f}\frac{dV_f}{dT} \tag{108}$$

By the assumption of a parallel relation between glass volume and occupied volume[63], the thermal expansion coefficient difference above and below glass transition temperature, α_f,

equals to, α_f.

The abnormal high value of C_2^o from relaxation and vibration studies may be associated with the small difference of the thermal expansivities between rubbery and glassy states. The unusual small value of thermal expansivities of the relative free volume, α_f, was found for the dynamic mechanical properties of methacrylate polymers[77,78,79,80,81]. According to the concept of iso-free volume state posulated by Fox and Flory[82], Simha and Boyer[83] proposed a general relation between thermal expansion coefficient and glass transition temperature for amorphous as

$$(\alpha_\ell - \alpha_g) \cdot T_g = K \qquad (109)$$

$$\Delta\alpha = \alpha_\ell - \alpha_g \qquad (110)$$

where α_ℓ and α_g are the coefficients of thermal cubical expansion for amorphous material above and below T_g and K is a constant. This indicates that the higher the glass transition temperature, the closer the thermal expansion coefficients in rubbery and glassy states. Recently, the relation in eq (109) has also been described by hole theory[84].

B. Stress Induced Crystallization

1. Birefringence and Stress Behaviors During Oriented Crystallization

Oriented crystallization in polymer materials due to deformation has been investigated by means of simple extension of solid state of polymers[85-92], shearing of melt[93-96], and stirring in solution[97,98]. It is generally recognized that crystallization and orientation under stress can enhance the physical properties of polymer substances through a special arrangement of molecular configuration. In general, the polymer materials will be deformed resulting in crystallization and orientation during the processing operations with the application of heat and stress, e.g. extrusion[99,100], injection molding[101], fiber spinning[102], blow molding[103] of molten state and elongation flow of solution[104]. The rate of crystallization affects the rate of production in processing and the morphology and the nature of crystallites influence the properties of the products.

The crystallization of linear and crosslinked rubber in the solid state can be produced by stretching so as to have one axis of the crystallites oriented parallel to the direction of the extension[5]. Such stress induced crystallization has been conveniently studied by following its birefringence[90,91] or stress[85,86,88]. In this study, the amorphous PVA is

stretched to the specified extension ratio at the preset constant temperature, then the simultaneous and continuous measurements on the stress and birefringence are performed to follow crystallization in the deformed state at constant length and at constant temperature.

a. Step by Step Elongation (M1)

The deformation treatment by stretching amorphous PVK by 50% intervals to the final specified extension at constant temperature presented in this section will be called process M1 thereafter.

The isothermal variation of birefringence with time at the temperature of 220°C over the various elongation ratios from 1.5 to 6.0 is plotted on Figure (41). The same negative sign of birefringence is observed as in the relaxation study (A.1.) and it is attributed to the greater contribution of bond polarizabilities from the side group of the carbazole monomer units than that from the vinyl backbones. The decay of birefringence is reduced with further stretching up to 200% elongation. At a further extension to a draw ratio 4.0, the birefringence at first remains constant after deformation and then after about 5 min. starts to rise . The corresponding variation of stress with time at 220°C over the same range of extension is shown on Figure (42). In all the cases, the stress decreases with time and stress decay is reduced with increasing elongation. The normal relaxation phenomena

presented in Section A.1. show that the birefringence and stress relaxation behave in the same manner so as to keep the stress optical coefficient constant during the progress of relaxation. In other words, this suggests that the stress decay due to the rearrangement of molecular configuration under the deformed state at constant length is always accompanied by a decrease of birefringence for a simple relaxation process. Consequently, the increase in birefringence with time at higher extension is believed to arise from the growth of crystallites which have prefered molecular orientation with respect to stretching direction. It has been found that the birefringence falls initially during stretching from the deformed sample at extension ratio 4.0, then rises to a higher value again. This phenomenon can result from some degree of breakdown of the original crystal pattern at leongation ratio 4.0 to rearrange the molecular chains into new positions. It was reported[105] that the orientation function determined by X-ray diffraction becomes broader during the process of further stretching the vulcanized polychloroprene in the presence of crystallites and was interpreted due to the interaction between the crystallites.

At a temperature of 240°C, the isothermal birefringence changes as a function of time over a range of draw ratios from 1.5 to 6.0 is illustrated on Figure (43). The birefringence begins to increase at the later stage of relaxation at elongation ratio 4.0, with a lower rate as well as magnitude than at a 220°C. The isothermal curve of stress decay under the

same condition as Figure (43) is depicted in Figure (44). The variation of birefringence and stress with time at 250°C over the range of extension ratios from 1.5 to 4.0 are plotted on Figure (45) and Figure (46) respectively. There is no indication of birefringence rising with time in this range of elongation. At the higher temperature of 260°C, Figure (47) shows a family curves of isothermal birefringence relaxation for various extension ratios from 1.5 to 6.0. The corresponding stress-time curves at 260°C are shown on Figure (48). In all of these elongations at 260°C, both the birefringence and stress always decreases with time, The rate as well as magnitude of stress decay is reduced with increasing deformation.

The behavior of birefringence and stress with time for various temperatures and degrees of elongation are essentially similar to the standard relaxation phenomena discussed in Section A.1. i.e. birefringence and stress increases with elongation but decrease with temperature, expect that the sign of slope of birefringence-time curve changes due to crystallization at high elongation with lower temperature. At high extension, the tendency for the isothermal birefringence with time to undergo a transition from the falling to the rising type of curve decreases with increasing the temperature due to the more significant motion of molecular chains at higher temperatures.

b. Initial Elongation of 50% followed by elongation to the desired extension (M2)

In this section, a different history of deformation (Model M2) was studied there the amorphous PVK was first extended to 50% strain, then stretched to the preset elongation. Figure (49) shows a family curves of isothermal birefringence changes with time at the temperature of 240°C over the elongation ratio range from 2.0 to 6.0. The variation of stress as a function of time corresponding to the same conditions at 240°C is illustrated on Figure (50). Birefringence begins to rise just after deformation at extension ratio 3.0 instead of at elongation ratio 4.0 for M1 type treatment as shown on Figure (43). Above the draw ratio 3.0, the birefringence response is seen to reach a high value immediately after stretching and its rate as well as magnitude of rising decreases at higher elongation. It is also found that the rate and amount of stress decay with time is higher for M2 type stretching shown on Figure (50) than M1 type stretching shown on Figure (43).

These facts that the faster rise of birefringence ammompanied with faster rate of stress fall can be accounted for in terms of the higher crystallization rate, i.e. M2 type of deformation treatment is more favorable for developing crystallites than M1 type stretching.

c. Direct stretching to specified elongation from undeformed state (M3)

The following results have been carried out by stretching

the original unextended sample directly to the final stage at constant temperature (mechanism M3). There are no data for temperatures below 260°C, because the sample necked or broke at high elongation under these conditions.

The isothermal birefringence variation with time for a series of various extension ratio ranging from 1.5 to 3.0 at constant temperature of 260°C is shown on Figure (51). At low elongation such as λ = 1.5, birefringence always decreases with time due to simple relaxation as presented in section B.1.a. As the elongation ratio reaches 2.0, the response of birefringence falls first after stretching, then it rises with time after 10 minutes of birefringence relaxation, It has been interpreted in Section B.1. a that the rising of birefringence in the deformed state is due to strain induced crystallization with the produced crystallites lining parallel to the stretching axis. As the elongation ratio greater than 2.1, the sample becomes very high by birefringent after deformation and the birefringence always increases with time monotonously. The isothermal stress-time behavior corresponding to the same condition as the birefringence-time relation at this temperature of 260°C is illustrated in Figure (52). It is seen that the stress always decreases with time towared zero. The rate and magnitude of birefringence increase is shown in Figure (51) where it is seen to decrease with increasing elongation, but the rate and amount of decrease in stress increases with increasing elongation over the extension

range of this study from elongation ratio 2.0 to 3.0 at 260°C. And it is found that the time for the stress decay at zero gets shorter at higher elongation.

In comparing M2 type and M3 type of deformation at the temperature of 260°C ranging the extension ratio from 2.0 to 3.0, it is deduced that. (1) the response of birefringence always falls with time for M2 type stretching shown on Figure (52) but it rises against time for M3 type stretching shown on Figure (47). (2) It is seen in Figure (52) that the rate and magnitude of stress decay decrease with increasing elongation for M2 type deformation, but they bahave in opposite way for M3 type deformation. (3) The sample is more birefringent by M3 type extension for a given elongation ratio and it is a rising function of deformation. Thus it can be concluded that M3 type deformation is a better mechanism for producing crystallites from amorphous polyvinyl carbazole and the rate of crystallization increases with increasing elongation.

The isothermal response of birefringence as a function of time at the temperature of 265°C ranging the elongation ratio from 2.0 to 5.0 is plotted in Figure (53). When the extension ratio is 2.0, it is found that the birefringence decreases with time initially after stretching then starts to increase after 5 minutes of birefringence decay. From extension ratio 3.0 and above, the isothermal birefringence always rises with time due to crystallization with the resulting crystallites orienting

toward the direction of the reference axis. The absolute value of birefringence increases with increasing elongation, but the rate and amount of birefringence increase are reduced with increasing elongation. In other words, the PVK sample becomes more birefringent at higher extension. The isothermal decay of stress against time at the same temperature of 265°C over the same range of elongation is shown on Figure (54). It is demonstrated that the stress always falls with time for all range of extension and the most drastic reduction of stress occurs at elongation ratio 3.0. In other words, the rate as well as the magnitude of stress decay pass through the maximum at the point of extension ratio 3.0 over the draw ratio from 2.0 to 5.0 at 265°C.

A family of curves of isothermal variation of birefringence with time at the temperature of 275°C over a wide range of elongation ratio from 1.5 to 5.0 is illustrated in Figure (55). The standard relaxation phenomenon which is seen for the sample at extension ratio 1.5 describes the monotonous falling of birefringence with time. As the sample is stretched to 75% at this temperature of 275°C, the birefringence of the sample drops first for 10 minutes after stretching and then rises with time after that. With further stretching to draw ratio 2.0, the birefringence falls after stretching then rises upward against time after about 2 minutes of birefringence relaxation. From the extension ratio of 2.1 up, the high birefringent sample of

PVK shows an increase of birefringence with time immediately after stretching and the rate as well as the magnitude of the increase of birefringence decreases with increasing elongation. A family of curves of monotonous stress decay versus time corresponding to the same temperature of 275°C and same range of extension from elongation ratio 1.5 to 5.0 is plotted in Figure (56). It is seen that the initial stress after stretching is a simple function of deformation, i.e. it becomes higher with further elongation. However, the rate and magnitude of stress decay with time increase to a maximum at the intermediate extension of elongation ratio 3.0 then fall again as the extension is further increased.

It is known that when a polymer material is subjected to deformation such as hot stretching, there occur three types of deformation. The first one is the instaneous elastic deformation with bond stretching or valence angle deformation which is independent of time and temperature of stretching. The second sort is the high elastic or time dependent deformation by rotation of molecular segment. And the third kind is a viscous deformation or plastic flow with molecular sliding past each other. The behavior of simple relaxation is mostly attributed to plastic flow, which results from the breakdown of the cohesive links due to van der Waal's force or due to physical entanglements. It has been found in this part and in relaxation study that the tension in the rubbery

state of PVK for a given elongation decreases with raising the temperature. These results are not consistent with what is concluded according to the application of the statistical theory of ideal rubber elasticity, which predicts that the stress of rubber is linearly prop rtional to absolute temperature at a constant strain. The discrepan may be due to the contribution of energy term and plastic flow.

From Flory's crystallization theory[106], if crystallites develop in an elastomer under strain, the stress is consequently reduced due to the crystalline state being no energy. And the plastic flow will increase with increasing elongation and temperature. Thereby the rate of stress decay willbe accelerated and its magnitude of reduction will be increased with increasing elongation at constant temperature due to the complementary actions of plastic flow and crystallization. However, at higher elongation, the crystallites formed during stretching can act as the effective multifunctional crosslinkages which will prevent any further breakdown of the cohesive links due to plastic flow with the slippage of chain molecule past each other. Therefore, the rate and magnitude of stress decay will increase with elongation and pass through a maximum after which it will decrease again with further stretching. It has been shown before that the maximum rate and magnitude of stress reduction of PVK occurs at an extension ratio 3.0 for all the temperature from 260°C to 300°C in this study.

Among other studies, it was reported[107] that the process

of volume decrease of vulcanized natural rubber during crystallization under stress is reflected in hastening the onset of stress relaxation at higher elongation over the extension range from 50% to 200% stretching. In that work, highest elongation ratio is 3.0 and the rate of stress decrease does not slow down with increasing elongation. In 1955, Tobolsky et al[92] found that the rate of stress decay of natural rubber after simple stretching increases with increasing extension up to elongation ratio 3.0 then it becomes slower for further stretching to elongation ratio 3.5.

As the temperature increases to 285°C, Figure (57) shows a family of curves of isothermal birefringence plotted against time over various elongation ratio ranges from 2.0 to 5.0. Similarly, at elongation 2.0, birefringence decreases initially after stretching then increases with time after 2 minutes of birefringence relaxation. At elongation ratio 3.0 and above, the PVK sample becomes more birefringent with time at once after being deformed. Up to an elongation ratio of 4.0, the birefringence rises with time monotonously in the period of performing the experiment, the rate and amount of birefringence rising decrease with increasing extension. However, at elongation ratio 5.0, the abnormal behavior of birefringence-time relation is observed in that birefringence rises with time immediately after stretching then falls against time after 15 minutes of rising. The isothermal stress change as a function of time at 285°C over the same range of extension is shown on Figure (58). It is

also seen that the stress decay becomes faster with increasing extension in the region from elongation ratio 2.0 to 3.0 then becomes slower at higher elongation.

When the temperature reaches 300°C, the variation of birefringence with time at elongation ratio from 2.0 to 5.0 is illustrated on Figure (59). At draw ratio 2.0, the birefringence starts to increase against time after 2 minutes of birefringence decay. At higher extension up to draw ratio 3.0, the birefringence increases with time monotonously right away after stretching. With further extension up to elongation ratio 4.0 and above, it is observed that birefringence rises with time initially after stretching then falls against time after a certain period of birefringence rising. The birefringence begins to fall in about 30 minutes after stretching for elongation ratio 4.0, and in 10 minutes for elongation ratio 5.0. It has also been found that PVK sample during stretching becomes more birefringent with increasing elongation up to extension ratio around 4.5 then the birefringence drops with further elongation at this temperature of 300°C. This is the same phenomenon which has been described in Section (B.1.) and it results in a lower magnitude of birefringence at extension ratio 5.0 than that of extension ratio 4.0. A family of stress-time curves at 300°C over the same range of extension is plotted on Figure (60). At elongation ratios lower than 3.0, the stress decreases with time monotonously and the rate as well as the magnitude of stress decay are increased with increasing extension.

The unusual stress-time behaviors at this temperature of 300°C are observed for higher elongation ratio at 4.0 and 5.0. It is shown that the stress falls with time after stretching then rises after a certain period of time of stress falling. It has been found that the time for changing the sign of the slope of birefringence-time curve at elongation ratic 5.0 is shorter for 300°C than 285°C, and it is shorter at elongation ratio 5.0 than elongation ratio 4.0 at 300°C. This suggests that the tendency of the abnormal transition of the slope of birefringence-time curve from positive to negative becomes greater at higher temperature and elongation.

At the highest temperature of 320°C in this study, the isothermal birefringence change as a function of time for different elongation ratio from 2.0 and 3.0 is plotted on Figure (61). At elongation ratio 2.0, the time for birefringence rising begins at 5 minutes after stretching. The corresponding isothermal stress change using time as a variable at 320°C is shown on Figure (62). The stress decreases with time monotonously to zero and the sample at elongation ratio 3.0 reaches zero stress faster than the sample at elongation ratio 2.0.

Summarizing the birefringence-time relation at elongation ratio 2.0 for all the temperature in this study, it is found that the time for birefringence to start to rise after stretching gets shorter from the temperature of 260°C to 275°C then becomes longer with further raising the temperature. This may

suggest that 275°C is the temperature for the maximum rate of crystallization at elongation ratio 2.0. However, the crystallization rate is not very temperature dependent and will be discussed in Section (B.2.).

The significant upturn phenomenon of stress-strain curve for PVK during stretching has been found arcund elongation ratio 4.0 for all the temperatures from 265°C to 300°C in this study. It nas been interpreted as being characteristic of the crystallization process in previous paragraphs. This noteworthy behavior of the stress-strain curve of PVK at high elongation is shown on Figure (63) which is a typical trace of stress-strain behavior from recorder at the temperature of 275°C. It is evident that the slcpe of stress-strain curve starts to rise slowly above extension ratio 3.1 and increasing extension results in the pronounced upward curvature at extension ratio 4.0 with a steep linear upward slop on further elongation. The extension ratio 3.1 showing the increasing slope of the stress-strain curve agrees with the stress-time curve shown on Figure (56) which indicates that the rate as well as magnitude of stress decay starts to decrease above this extension ratio.

A similar explanation of crystallization process developed for butyl rubber was reported[108] by observing an apparent increasing slope of stress-strain curve at 400% extension and a linear ateep slope after 700% elongation. By measuring the rise of temperature due to crystallization on fast stretching

of butyl rubber[109] and natural rubber[110], it was shown that the slope of temperature rise-strain curve is a slowly rising function of the extension with a steep upward turn and almost linear continuation at high extension.

2. Crystallization Kinetics

For a uniaxially oriented crystallization of rubbery polymers, the change of volume fraction crystallinity with time can be described in terms of the two phase model using the Stein equation through the simultaneous and continuous measurements of birefringence and stress. In order to depict the variation of crystallinity reflected by the increase of birefringence accompanied with the decrease of stress, the effect of the orientation of the crystalline component, f_c , and the behavior of the strained amorphous region have to be considered. If the resulting crystallites are perfectly oriented with their chain axes parallel to the stretching direction (as discussed in Section (B.4)), then the orientation function of the crystalline phase is equal to 1. Provided that the amorphous phase during crystallization behaviors like pure amorphous material in simple relaxation study and the total tension is loaded on the amorphous region, then the expression for the crystallinity becomes[38].

$$X_c = \frac{\Delta - \sigma \cdot C}{\Delta_c^{\circ} - \sigma \cdot C} \qquad (111)$$

where Δ and σ are measured quantities, Δ_c° has been calculated shown in Section (B.3), and C is attained from relaxation data.

The isothermal crystallinity change calculated in this way as a function of time at temperature of 260°C over the elongation range from 2.0 to 3.0 is shown on Figure (64). It

is seen that the volume fraction crystallinity increases with higher extension. Figure (65) illustrates the crystallinity-time curve at 275°C over a wide range of elongation ratio from 1.75 to 5.0. The crystallization rate may be represented by the half time, $t_{1/2}$, which is the characteristic parameter for crystallization indicates the time required for 50% of total phase transformation from amorphous to crystalline phase. The values of $t_{1/2}$ for various elongation ratios from 2.0 to 3.0 at 275°C are tabulated on Table (I). This tabulation doesn't include higher extension, beacuse under these conditions, the PVK sample possesses high crystallinity representing more than half of the final quantity immediately after stertching. The fact that $t_{1/2}$ decreases with increasing elongation shows that the crystallization rate increases with elongation in this range of extension. This observation is consistent with the birefringence and stress responses which are presented in section (B.1.c). The accelerating effect on crystallization process by increasing extension has been studied and interpreted[85,86] as resulting from the corresponding increase in the equilibrium melting temperature associated with decrease in the entropy of melt upon stretching. This leads to an increase in the degree of supercooling. The equations which describe the relationship between the equilibrium melting point and elongation ratio have been derived[106]. The isothermal crystallization characteristic curves of crystallinity-time

relation for the temperature at 265°C, 285°C and 300°C over a range of extension ratios from 2.0 to 5.0 are shown on Figure (66), Figure (67), and Figure (68). The decrease of crystallinity for 285°C at elongation ratio 5.0 in 30 minutes after stretching corresponds to the drop of birefringence shown in Figure (57). The same phenomena are observed for 300°C at elongation ratios 4.0 and 5.0. At 320°C, the variation of crystallinity with time for extension ratios 2.0 and 3.0 is plotted in Figure (69).

In all cases, the PVK sample is more crystalline after stretching at higher elongations. This suggests that the crystallization process under stress occurs during the course of stretching. The half times, $t_{1/2}$, for the elongation ratio 3.0 over the temperature range of this study from 260°C to 320°C are presented on Table (II). This suggest the surprising observation that there is no significant effect of temperature on crystallization rate. Thus it may be concluded that the elongation effect on the crystallization kinetics is much more important than the temperature effect from the following facts:

(1). At elongation ratio 2.0, birefringence first falls after stretching then rises after a certain period time. However, this is abcut the same time from temperatures from 265°C to 285°C.

(2). The maximum rate and magnitude of stress decay occurs at elongation ratio 3.0 for all the temperatures in this study.

(3). The upward turn of stress strain curve shows up at around

an Elongation ratio 4.0 for all the cases. (4). The magnitude of crystallinity and crystallization rate are more elongation dependent than temperature dependent. The above statements may indicate that the crystallization rate-temperature relation of PVK sample under stress is a relative broad curve. In the nature rubber system, it was reported[139, 140] that the temperature has little effect on the value of the elongationratio at which the force shows the apparent upturn behavior. However, its crystallization kinetics is dependent upon both temperature and extension apparently.

The decrease of crystallinity of PVK at the later atage of isothermal oriented crystallization accompanied by the falling type of birefringence-time curve and the rising type of stress-time curve is observed at higher temperatures and higher elongations. It was found[86] that a substantial rise in the retractive force at the later stage of isothermal stretched crystallization occurs at low elongation rather than at high elongation of crosslinked trans-polyisoprene. It was interpreted as the volume contraction which will occur in a highly oriented state and is more apparent at higher temperatures. A similar behavior of stress rise has been observed[141] in polyethylene and attributed to the formation of folded-molecule crystallites. This interpretation seems incompatible with PVK system which shows rod-like structure judged from H_v light scattering patterns. The thermal

degradation of PVK at high temperature is not ruled out even through it can only account for the drop of birefringence but not for the rise of stress.

3. Calculation of Intrinsic Birefringence of Polyvinyl Carbazole

The intrinsic birefringence of PVK molecules will be calculated from bond polarizabilities in this section.

The coordinate system of the film (YZ plane) and the angles associated with the orientation functions are shown on Figure (70a). The X-axis is perpendicular to the plane of the film. The set of a,b and c axes and the set of d,e and f axes which characterize the orientation of backbone and planar carbazole molecule respectively are illustrated on Figure (70b). The c axis is the chain direction; the a axis perpendicular to the c axis and coplanar with it and C-C backbone. The b axis is perpendicular to both a and c axes. The d axis is perpendicular to the planar pendant group, the f axis is along the C-N bond and in this plane of carbazole molecule; the e axis is perpendicular to d and f axes and also in this plane of carbazole froup. The angle, ω , represents the angle between the d axis and the plane difined by a and c axes.

The relationship between the refractive index differences and the polarizability differences in Z and Y direction formulated in eq (9) is[5]

$$\Delta = (n_z - n_y) = \frac{2\pi}{9}\left[\frac{(n^2+2)^2}{n}\right](P_z - P_y) \qquad (112)$$

assuming the applicability of the Lorenz-Lorentz equation.

For uniaxial stretching along Z direction, the quantity of $(P_Z - P_Y)$ has been derived as[118]

$$(P_x - P_Y) = n_m f_r \left\{ P_c - \left(\frac{P_a + P_b}{2}\right) + \frac{1}{2}\left[\frac{P_d(1+3f_\omega)}{2} + \frac{P_e(1-3f_\omega)}{2} - P_f \right] \right\} \quad (113)$$

where n_m is the number of monomer unit per unit volume and is expressed as

$$n_m = \frac{\rho N_o}{M_m} = 3.74 \times 10^{21} \quad (114)$$

where ρ is the density of PVK, N_o is Avogardro's number and M_m is the molecular weight of the monomer unit of PVK. P_K is the polarizability along K direction. The orientation function f_r and f_ω which are associated with orientation of vinyl chain and rotation of carbazole molecule resprectively are defined as[118]

$$f_r = \frac{3\langle \cos^2 \gamma \rangle - 1}{2} \quad (114a)$$

$$f_\omega = 2\langle \cos^2 \omega \rangle - 1 \quad (114b)$$

The perfect orientation of monomer unit will give the intrinsic birefringence corresponding to the maximum polarizability differences. Under this condition, f_r is equal to 1. Then eq(113) can be rewritten as

$$(P_x - P_Y)^\circ = 3.74 \times 10^{21} \left\{ P_c - \left(\frac{P_a + P_b}{2}\right) + \frac{1}{2}\left[\frac{P_d(1+3f_\omega)}{2} + \frac{P_e(1-3f_\omega)}{2} - P_f \right] \right\} \quad (115)$$

Using the assumption of additivity of bond polarizabilities[119] the polarizability in a certain K direction can be represented as

$$P_k = \sum_i \left[(b_l - b_t)_i \cos^2 \theta_{ik} + (b_t)_i \right] \qquad (116)$$

where b_l and b_t are the longitudinal and transverse polarizabilities of the ith bond, θ_{ik} is the angle between axis and the axis of the i-th bond.

The vinyl chain which is the repeating unit of PVK, consists of two C-C bonds and three C-H bonds. Taking the tetrahedral angle 109.8° as the angle between C-C bonds of the main chain, then the polarizabilities along a, b and c axes are given as

$$P_a = 2(b_l - b_t)_{C-C} \cos^2 \frac{109.8^\circ}{2} + 2(b_t)_{C-C} + 3(b_l - b_t)_{C-H} \cos^2 \frac{109.8^\circ}{2} + 3(b_t)_{C-H} \qquad (117)$$

$$P_b = 2(b_t)_{C-C} + 3(b_l - b_t)_{C-H} \sin^2 \frac{109.8^\circ}{2} + 3(b_t)_{C-H} \qquad (118)$$

$$P_c = 2(b_l)_{C-C} \sin^2 \frac{109.8^\circ}{2} + 3(b_t)_{C-H} + 2(b_t)_{C-C} \qquad (119)$$

The principal polarizabilities of planar benzene ring are considered as the coplanar polarizability $(b_{\parallel})_B$ as well as perpendicular polarizability $(b_{\perp})_B$ and are calculated as follows:

$$(b_{\parallel})_B = 2\left[(b_l)_{C-C_{ar}} + (b_l)_{C-H}\right] + 4\cos^2 60^\circ \left[(b_l - b_t)_{C-C_{ar}} + (b_l - b_t)_{C-H}\right] + 4\left[(b_t)_{C-C_{ar}} + (b_t)_{C-H}\right] \qquad (120)$$

$$(b_{\perp})_B = 6\left[(b_t)_{C-C_{ar}} + (b_t)_{C-H}\right] \qquad (121)$$

Using Denbeigh's bond polarizabilities[119], $(b_{\parallel})_B$ and $(b_{\perp})_B$ are 123.0 x 10^{-25} cm^3 and 63.8 x 10^{-25} cm^3 respectively, and they are 124.5 x 10^{-25} cm^3 by using Bunn's bond polarizabilities[120,121] shown on Table (IIIA). These values have been reported as[122] 123.1 x $10^{-25}cm^3$ and 63.5 x $10^{-25}cm^3$ individually.

The planar carbazole group is composed of one C-C bond, three C-N bonds and two benzene rings subutracting four C-H bonds from them. The polarizabilities along d, e and f directions are given as

$$P_d = 2(b_{\perp})_B + (b_t)_{C-C} + 3(b_t)_{C-N} - 4(b_t)_{C-H} \qquad (122)$$

$$P_e = 2(b_{\parallel})_B + (b_\ell)_{C-C} + 2(b_\ell - b_t)_{C-N}\cos^2 30^\circ + 3(b_t)_{C-N} - 4[(b_\ell - b_t)_{C-H}\cos^2 30^\circ + (b_t)_{C-H}] \qquad (123)$$

$$P_f = 2(b_{\parallel})_B + (b_t)_{C-C} + (b_\ell)_{C-N} + 2(b_\ell - b_t)\cos^2 120^\circ + 2(b_t)_{C-N} - 4[(b_\ell - b_t)_{C-H}\cos^2 60^\circ + (b_t)_{C-H} \qquad (124)$$

The evaluated values for P_d, P_e and P_f by using different source of bond polarizabilities are also shown on Table (IIIB).

Using Denbigh's bond polarizabilities, eq(115) can be rewritten as

$$(P_x - P_y)^\circ = -(0.0c527 - 0.0414 f_\omega) \qquad (125)$$

If the planar bulky side groups of PVK are restricted to being perpendicular to the chain direction, then $\omega = 0^\circ$, $\langle\cos^2\omega\rangle = 1$ and $f_\omega = 1$. In this case, the intrisic birefringence of PVK, Δ°, is obtained as -0.457 according to eq (112).

Using Bunn's bond polarizabilities, eq(115) becomes

$$(P_Z - P_Y) = - (0.00875 - 0.0388\ f_\omega) \qquad (125a)$$

Under the same restriction for the rotation of the side of group, the intrinsic birefringence becomes -0.476.

The intrinsic birefringence of -0.457 has been used through this study to evaluate the crystallinity according to eq (111) through this study. The magnitude of crystallinity will become lower if the intrinsic birefringence calculated from Bunn's bond polarizabilities is employed. For instance, the crystallinity at 260°C with elongation ratio 3.0 is (20.1 ± 1.0)% by using Denbigh's bond polarizabilities, but it is (18.0 ± 0.9)% by using Bunn's .

4. X-ray Diffraction Pattern and Orientation of Crystalline Phase

Generally, a polycrystalline polymer material is not made of a single crystal but rather of many crystallites. The resulting wide angle X-ray diffraction is the superposition of the diffraction from individual crystallites with no coherent interference among different crystals. In this study, a North American Philips water cooled X-ray diffraction unit (type No. 12045) has been used. The X-ray beam is CuKα radiation with wavelingth 1.5418A° obtained by filtering the CuKβ spectrum with nickel. The X-ray beam after passing through the β-filter is collimated with a pinhole system then penetrates the polymer

specimen. A beam stop has been used to reduce the darkness around the central region of the film due to air scattering from the intense transmitted beam. The flat-film technique has been employed by using a plate camera consisting of a stationary specimen stand assembly and reflection standard assembly with motor-driven cassette designed to take standard 4'' x 3 - 1/4'' film or smaller.

The X-ray diffraction studies have been performed at room temperature using the sample subjected to isothermal crystallization in the deformed state for various temperatures and elongations as described in Section (B.1). The deformed PVK sample retained its extension after quickly cooling down to room temperature. This is consistent with the evidence that the stretched PVK specimen retains the same birefringence after it is quenched fast to lower than 200°C. Such a process of treating deformed PVK sample freezes the PVK molecules in their strained positions. It is known that the retaractive forces existing in the material become apparent only when the internal viscosity of the material is reduced at high temperature. Similar behavior was reported[123] with stretched polystyrene which remains in the deformed state after cooling below its glass transition temperature.

A series of X-ray diffraction patterns of PVK at 275°C over the range of elongation ratio from 1.5 to 3.0 are shown on Figure (71). At elongation ratio 1.5, it is seen that two amorphous interference haloes occur resulting from the quasi-

short-range order with diffraction angle 2θ at 7.2^{o} and 20.5^{o} respectively. This is similar to the diffraction picture of undeformed PVK as shown in Figure (77). At elongation ratios of 2.0 and above, the sharp diffraction due to the crystalline phase with Bragg angle 2θ at 8.2^{o} becomes apparent. This diffraction peak corresponds to the interplanar spacing, d , as $10.5A^{o}$ according to

$$d = \frac{\lambda}{2 \sin\theta} \qquad (126)$$

The structure of PVK crystal was reported[20] in which the rod-like PVK molecules are packed parallel in a pseudonexagonal array where the nearest chain-to-chain distance, a , is approximately $12.3A^{o}$. Then the diffraction peak at $2\theta = 8.2^{o}$ can be interpreted as $(10\bar{1}0)$ reflection from the hexagonal lactice. The intensity of this crystalline diffraction peak increases with further elongation accompanied by a decrease of intensity of the amorphous diffraction peaks. However, it becomes difficult to resolve these changes by photographic technique for elongation ratio above 2.0, since the resulting diffraction patterns look alike. It has also been observed that the azimuthal dependence of this crystalline diffraction peak increases with increasing extension i.e. the width of this diffraction arc is reduced with further stretching.

In the hexagonal system like PVK crystal with sixfold symmetry about c-axis, it has been shown[124,125] that only one

plane is necessary to determine the independent orientation of crystal axis. The limiting case for the orientation of c-axis of chain molecules, f_c , was proposed[125] as

$$f_c = -2 f_{10\bar{1}0,Z} \qquad (127)$$

where $f_{10\bar{1}0,Z}$ is the orientation function of the normal of $(10\bar{1}0)$ plane with respect to the stretching axis Z. This reflection has the maximum intensity on the equator with a narrow arc having a shape which indicates that these crystal planes tend to align toward the stretching direction. Consequently, it suggest that theassumption of perfect orientation of crystalline PVK molecules with c-axis parallel to the extension axis above an elongation ratio 2.0 is reasonable.

The qualitative determination of degree of crystal orientation from X-ray diffraction pattern has been determined[126] for isotactic polypropylene. A uniform Debye-Scherrer ring is observed for randomly oriented crystallites, which changes to an arc under uniaxial orientation with incident X-ray beam perpendicular to the stretching direction. The Debye-Scherrer power pattern is obtained as for an undeformed sample again with the incident X-ray beam parallel to the reference axis of a uniaxially oriented sample. Finally the pattern becomes a single rotation pattern composed of sharp spots in the limit of perfect orientation. The determination of molecular structure for stretch crystallized rubber from its X-ray diffraction

pattern has been presented[127] where it is suggested that the c-axis of each crystal becomes nearly parallel to the drawing direction. The arclike shape for the diffraction patterns of PVK crystallites for deformed sample instead of sharp spot may arise from the presence of lattice imperfections or from the PVK crystallites not being perfectly oriented.

By means of a counter diffractometer, the direct recording of the diffraction angle scan for the undeformed PVK and for an elongation ratio 3.0 at 275°C are shown on Figure (72). The azimuthal angle scan with respect to crystalline diffraction peak at $2\theta = 8.2^{\circ}$ for the latter sample is plotted on Figure (73). It is seen that the X-ray diffraction photographic patterns are in agreement with the corresponding counter scans. The prefered molecular orientation in the form of an intersification of amorphous halo at $2\theta = 20.5^{\circ}$ in the meridianal region is also observed. However, it was reported[128] that the application of X-ray diffraction to investigate the presence of orientation of amorphous phase has little quantitative value.

Figure (74a) shows the X-ray diffraction patterns for an elongation ratio of 6.0 over the various temperatures from 220°C to 260°C. All of them show the sharp arc corresponding to $2\theta = 8.2^{\circ}$ along the equatorial region indicating prefered orientation of the c-axis of crystals toward the stretching axis. Similar X-ray diffraction photographs at the temperature of 240°C ranging the elongation ratio from 4.0 to 6.0 is shown on Figure

(74b). The diffraction patterns over the various elongation ratios from 2.0 to 5.0 for the 265°C, 285°C and 300°C are shown on Figure (75), Figure (76) and Figure (77) individually. Figure (78a) and Figure (78b) represent the diffraction pictures for 260°C and 320°C over the various extension ratio 2.0 and 3.0. Similar to the case for 275°C, it is seen in all cases that the crystal diffraction peak has the sharp of arc at elongation ratio 2.0, then it becomes very sharp narrow arc and increases in intensity accompanied with a decrease in the intensity of amorphous peaks with further extension. At 300°C, the diffraction patterns for the PVK sample stretched to an elongation ratio 5.0 for different times corresponding to the isothermal crystallization period after stretching are shown on Figure (77). It is seen that the shape of the two diffraction patterns for times of 30 minutes and 120 minutes are similar, but the intensity at the crystalline peak reflection for the latter is reduced. This is associated with the phenomena of birefringence decrease and stress increase presented in Section (B.1.c). The corresponding diffraction patterns to a Bragg angle scan along the stretching direction are shown on Figure (99). The evidence which shows that the decrease of diffraction intensity at the crystalline peak for the PVK sample at 120 minutes is reflected in the increase of intensity for the amorphous peaks which is more apparent than in the photographic patterns.

5. Determination of Orientation with Infrared Dichroism

For infrared absorption measurements, a Perkin-Elmer Model 180 Infrared Spectrometer has been used in which the radiation source comes from an air-cooled globar. This is a double-beam, ratio-recording instrument with a range of wave number from 4200 to 180 cm^{-1} covered by a set of five gratings. The deformed PVK sample is placed in the beam with the drawing axis being aligned at 45^{o} to the extrance slit to minimize machine polarization effects. The polarizer is located between the monochrometer and the specimen. This experiment is undertaken at room temperature for a series of PVK sample in the stretched state under the same treatment as in Section (B.4).

The assignments of infrared absorption bands for carbazole crystal have been reported[115]. The absorption band which represents the out-of-plane vibration of the carbazole ring has been chosen to study infrared dichroism. The transition moment angle of a certain absorption band is the molecular structure parameter for the quantitative determination of molecular orientation. The 924 cm^{-1} band is of B_1 symmetry representative of its direction of transition moment perpendicular to the plane of the carbazole group. With the assumption that the planar carbazole molecule is perpendicular to the vinyl backbone, then the transition moment of this band is in the same direction as the chain molecules. In other words, the angle between chain and transition moment direction of this absorption

band, , is zero. Therefore, the intrinsic dichroism, D_o, becomes[42]

$$D_o = 2\cot^2\beta \qquad (128)$$
$$= \infty$$

$$\frac{D_o+2}{D_o-1} = 1 \qquad (129)$$

Consequently, the expression for the orientation function of molecular chain can be simplified to be the same as eq(87).

Since the density in the amorphous and the crystalline phases for PVK sample is about same[20], it is assumed that the intrinsic birefringence of both regions are equal. Therefore, eq (12) can be rearranged to yield

$$\Delta = \Delta^\circ [f_c x_c + f_a(1-x_c)] \qquad (130)$$
$$= \Delta^\circ f \qquad (131)$$

Below an elongation ratio of 2.0, no apparent crystalline contribution is observed. Then the measured birefringence can be related to amorphous orientation by

$$\Delta = \Delta^\circ f_a \qquad (132)$$

The orientation function data for PVK deformed at various temperature and elongation from IR dichroism measurements and birefringence measurements are shown on Table (IV) to Table(VII). A typical trace infrared absorption spectra for PVK stretched to elongation ratio 3.0 at the temperature of 275°C with polarization parallel and perpendicular to the stretching direction

are shown on Figure (80).

All of the data indicate that the orientation function determined from infrared dichroism has the same trend as the birefringence which increases with increasing extent of elongation. At low elongations, it is seen that the orientation function measured from both sources is in reasonable agreement. This fact also suggests that the rotation of carbazole molecule is restricted. The rotation of benzene ring in polystyrene molecules has been studied[130] by the correlation between infrared dichroism and birefringence measurements.

6. Morphology

The superstructure of PVK crystal resulting from the stress induced crystallization is studied by using small angle light scattering. This technique has been applied[87,91,131] in this laboratory to investigate the morphology of rubber crystallities under strain. This study is performed at room temperature by sandwiching the deformed PVK sample between microscope cover glasses using silicone oil as the immersion fluid. The light scattering patterns of H_v polarization are obtained by setting the stretching direction parallel to the polarization direction of the incidnet beam.

The H_v scattering patterns at the temperature of 240°C over the elongation ratio range from 2.0 to 6.0 are shown on Figure (81). Figure (82) represents the H_v patterns for the undeformed PVK and for various elongation at 250°C. Figure (83a) illustrates the H_v patterns for elongation ratio 2.0 and 3.0 at 260°C. No scattering patterns are observed for the unstretched and low extension PVK sample. The H_v scattering patterns at high elongation in this temperature range up to 260°C, show the X-type patterns with monotonous decrease in intensity along the scattering angle.

Figure (84a) and Figure (84b) illustrate a sequence of H_v light scattering patterns at the 275°C over a wide range of extension. They demonstrate the effect of elongation on the

superstructure of PVK crystallites at 275°C, since these optical heterogenieties are not present in the undeformed and low elongation PVK sample, but they are developed with stretching in the same range of extension where the crystallization process has been described in previous sections. It is seen that the scattering pattern starts to show the oriented four leaf clover appearence characteristic of spherulitic structure at an elongation ratio 2.0. Subsequently it is accompanied by an X-type pattern with no maximum intensity along the scattering angle which is characteristic of fibrillar scattering by increasing extension up to an elongation ratio of 3.0. Above an elongation ratio 3.0, only the X-type patterns corresponding to a rod-like structure are observed. The change of PVK superstructure from the coexistence of spherulitic and rod-like texture which is so called shish-kebab superstructure[132] to pure fibrillar texture is consistent with the observation of increasing stress level above elongation ratio 3.0 presented in Section (B.1.c).

Similar effects of stress or strain on the superstructure growing in the deformed crystallization systems have been studied by other authors[94,133,134]. By means of electron microscopy, the morphology of natural rubber crystallized under strain was reported[133] where the α-filments consisting of lamellae are formed perpendicular to the strain axis at low elongation. Then it coexists with γ-fibril having chains of

nuclear running in the direction of strain up to the intermediate strain at 200% and becomes pure γ-filament at higher strain. By observing the X-ray diffraction patterns and electron microscopic pictures from the crystallization of polyethylene melt under stress, it was proposed[94] that the polyethylene crystal texture is in the form of twisted lamellae as in normal polyethylene spherulites at low stress. Then it becomes incompletely twisted lamellae at intermediate stress level and finally reaches the fibrillar texture under higher stress. Using small angle light scattering technique during annealing of draw polyethylene, it was found[135] that there coexist fibriller symmetrical texture and spherulitic texture at intermediate strain. The solution crystallization of polyethylene oxide-ethyl alcohol system was reported[97] where the lamellar superstructure is formed without stirring and the fibrillar texture is obtained at high rate of stirring.

The common morphologic feature for crystallization under strain appears to be that the lamellar crystals, the shish-kebab supersturcture then the fibrillar texture will be formed with increasing the extent of strain or stress. The similar results were reported[136,137,138] for the pressure effect on the morphology of polyethylene that the fold-chain crystals are formed at low pressure and the extended-chain crystals are developed under high pressure.

The similar trend of the superstructure of PVK changing with elongation has been found for other temperatures. Figure (85) and Figure (86) represents the series of H_v scattering patterns 265°C and 285°C respectively over the extension ratio range from 2.0 to 5.0. A sequence of H_v scattering patterns at 300°C ranging the elongation ratio from 2.0 to 3.0 are shown on Figure (83b).

V. Summary and Conclusion

In this research, the rheo-optical techniques have been applied to investigate the mechanical and optical properties of PVK during and after deformation.

The behaviors of the simple isothermal birefringence relaxation and isothermal stress relaxation of amorphous PVK have been observed in the same manner over temperatures from 210°C to 275°C and elongations from 10% to 50%. The magnitudes of birefringence and stress become higher at higher extension but become lower at higher temperature. In other words, PVK has higher extent of molecular orientation when it is stretched at lower temperature. The stress-optical coefficient remains constant during the process of simple relaxation and almost independent of temperature over the temperature range of this study. It is in a agreement with that from dynamic measurement.

In the case where the planar carbazole molecule is restricted to be prependicular to the backbone, the orientation determined from birefringence measurement is in a reasonable agreement with that from infrared dichroism result. The intrinsic birefringence of PVK repeating unit is -0.457 by using Denbigh's bond polarizabilities. The contribution of bond polarizabilities from the perdent group of the carbazole monomer unit is much greater than that from vinyl chain. This can account for the negative quantity of birefringence response.

The phenomenological theory of linear viscoelasticity is applicable to optical functions and mechanical functions of

amorphous PVK for the time-temperature superposition of relaxation data and for the frequency-temperature correspondence of vibration results. The shift factors which characterize the master curve of optical and mechanical properties are in a agreement for relaxation and vibration studies. The parameter C_2 in WLF formula which has an unusual high value from both relaxation and vibration measurements may be due to an exceptionally small difference in thermal expansion coefficient between rubbery and glassy states.

The crystallization behaviors of deformed PVK under tensile stress have been observed from the simultaneous responses of birefringence and stress, X-ray diffraction patterns, small angle light scattering patterns, and infrared dichroism.

The birefringence begins to increase with time after stretching above elongation ratio 2.0. During the process of crystallization, the accelerating decrease of stress accompanying the increase of birefringence up to the intermediate elongation ratio 3.0. However, the rate of decrease of stress slows down with further extension. An apparent upturn of the stress-strain curve of PVK occurs at elongation ratio 4.0. The decrease of birefringence at later atages of isothermal crystallization occurs at elongation ratio 5.0 for 285°C and at elongation ratio 4.0 and 5.0 for 300°C. This phenomenon is accompanied by a decrease of infrared dichroism and the decrease of X-ray diffraction intensity from PVK crystal along with an

increase of intensity from amorphous halo. This is the opposite behavior from what is observed during crystallization.

The deformation treatment by direct stretching PVK to the desired extension gives the most favorable dondition for stress induced crystallization. Regarding to this point, M2 type deformation is next and better than mechanism M1.

The crystallization rate is accelerated with increasing elongation. The stretching has much more significant effect on the crystallization kinetics than the temperature does.

The X-ray diffraction peak at diffraction angle $2\theta = 8.2^{o}$ corresponding to $(10\ \bar{1}0)$ reflection of PVK crystal starts to show up at elongation ratio 2.0. The intensity of this sharp diffraction peak increases with increasing extension reflected in the decrease of intensity in amorphous peaks at diffraction angle $2\theta = 7.2^{o}$ and $2\theta = 20.5^{o}$. The breadth of this diffraction arc is reduced at higher elongation so as to indicate the chain axis of the PVK crystallites oriented toward the direction of stretching axis.

The H_v scattering of PVK crystal shows the X-type pattern with monotonous decrease in intensity along the scattering angle blow the temperature of $265^{o}C$. They represent the fibrillar-like structures. Above the temperature of $275^{o}C$, The H_v scattering pattern shows four leaf clovers representing the spherulitic structure of PVK crystal at elongation ratio 2.0. It becomes the coexistence of spherulitic texture and rod-like

texture with further extension up to elongation ratio 3.0. It yields the pure rod-like structure at higher extension reflected in the increase of stress level.

VI. Future Work

The brittle PVK sample in the form of film is very difficult to handle at room temperature. It can be improved by reducing T_g by mixing the polymer with platicizer or by performing the experiment in solvent atmosphere. It will be interesting to run similar experiment for these kinds of samples as the current study. No real equilibrium stage has been reached and abnormal rubber elasticity has been found in this current study. By studying a crosslinked PVK sample one can test rubber elasticity and obtain equilibrium data. The crystallization of crosslinked material is generally reduced. This may result in the apparent temperature dependence on the crystallization kinetics.

The thermal expansion coefficient can be determined by thermal-mechanical analysis. However, there is the difficulty in making suitable dimensions of PVK specimens for testing at the present time.

In preliminary experiment, it is found that the birefringence and stress increase with stretching rate. It will be interesting to study the effect of extension rate on the orientation, crystallization behaviors and morphology. However, the PVK sample is constantly broken at high deformation rates.

Since the temperature effect on the crystallization kinetics is not apparent in this current study, it may become more obvious to observe this effect by studying the crystallization behavior by annealing after melting the deformed PVK crystal.

It will be interesting to observe the effect of elongation and temperature of stretching on the melting point of deformed PVK samples, since the melting temperature can be correlated with the degree of supercooling for the isothermal crystallization kinetics. It has been tried to locate the melting point of PVK crystal by differential scanning calorimeter, but there is no any trace of an endothermic peak. Perhaps the PVK sample decomposes before T_m or the heat of fusion is too small. It was reported[142] that the melting behavior of PVK-PBBA (poly P-biphenyl acrylate) copolymer is not observable with DSC technique because of the decomposition of PVK. It is possibly by microscope to observe optical anisotropy at the temperature at which the birefringence disappears or else to observe the disappearance of the light scattering pattern.

It would be worthwhile to measure crystallinity by X-ray diffractometer and by density column in order to compare with the result from birefringence and stress responses. The intensity from the diffraction peak at $2\theta = 8.2$ corresponding to PVK crystals contains a contribution from the amorphous halo centered at $2\theta = 7.2^{\circ}$. This should be subtracted out. Since the density in amorphous phase and crystalline phase is very close, a tall density column is required to determine density with sufficient accuracy.

The quantitative determination of the orientation function of PVK crystal by X-ray diffractometer can check the assumption of perfect alignment of chain molecules and give more

accurate quantity of crystallinity.

There is no observation of the occurrance of a new infrared absorption band for crystalline PVK. However, it may be interesting to characterize the orientation function by infrared dichroism by choosing another abosrption band besides the band at wave number 924 Cm^{-1}. Some preliminary data are shown on Table (VII).

To see the effect of temperature, the X-ray diffraction, light scattering, and infrared measurements of deformed PVK can be performed with and without constraint at elevated temperatures. It would also be worthwhile to perform these measurements during the process of stretching, relaxation and crystallization. The maximum intensity of spherulitic structure of PVK crystal can be located accurately by using photometric light scattering.

To analyze the status of PVK sample after thermal and stretching treatments, it is interesting to study the temperature and stretching effects on the thermal and mechanical degradation. In the preliminary outlook, the free radical frozen in glassy PVK specimen after stretching at the temperature of 275°C for two hours has been detected by electron paramagnetic resonance, but not the case after thermal treatment at 275°C for 3 hours. The increase of weight average molecular weight accompaning the decrease of number average molecular weight

for the former sample, have been found by gel permeation chromatograph. This results in broadening and flatening the molecular weight distribution profile. However, it almost does not change for the latter sample.

Finally, it is valuable to test the physical properties, e.g. the electrical conductivity ductility, tensile strength for these PVK sample treated in this study. However, it has been found that the oriented PVK becomes easier to be broken along the stretching direction than unoriented PVK. Perhaps, the biaxial orientation can be tried to improve the drutility and tensile strength in both directions.

CAPTIONS FOR FIGURES

1. Schematic diagram for the double refraction phenomenon.
2a. Schematic illustration of variation of light transmission versus retardation.
2b. Lissajous' figure of the force-strain relationship.
3. Lissajous' figures of the light intensity-strain relationship.
4. The transmittance-wave number curves for polarizer parallel and perpendicular to the direction of stretching axis.
5. Coordinate system for light scattering of one-dimensional rod in three-dimensional space.
6. Geometric system for the X-ray diffraction of uniaxial oriented polymer film.
7. Schematic diagram of Table Instron with conventional optical attachments.
8. Sketch of dynamic birefringence apparatus.
9. Schematic diagram of small angle light scattering system.
10. Schematic plot of temperature dependence of heat capacity for the original commercial PVK.
11. Schematic plot of temperature dependence of heat capacity for the solution casting PVK film without heat treatment.
12. Schematic plot of temperature dependence of heat capacity for the solution casting PVK film heated to 180^{o}C in vacuum oven.

13. Schematic plot of temperature dependence of heat capacity for the solution casting PVK film heated to 220°C in vacuum oven.
14. The birefringence relaxation with time at 10% extension over the temperature range from 210°C to 275°C.
15. The stress relaxation with time at 10% extension over the temperature range from 210°C to 275°C.
16. The birefringence relaxation with time at 30% extension over the temperature range from 210°C to 275°C.
17. The stress relaxation with time at 30% extension over the temperature range from 210°C to 275°C.
18. The stress relaxation with time at the temperature of 220°C by 50% stretching.
19. The birefringence relaxation with time at 50% extension over the temperature range from 210°C to 275°C.
20. The stress relaxation with time at 50% extension over the temperature range from 210°C to 275°C.
21. The ratio of birefringence to stress during relaxation at 30% extension ranging the temperature from 210°C to 275°C.
22. The master curve of birefringence relaxation at 10% deformation using the temperature at 220°C as the reference temperature.
23. The master curve of stress relaxation at 10% deformation using the temperature at 220°C as the reference temperature.

24. The master curve of birefringence relaxation at 30% deformation using the temperature at 220°C as the reference temperature.

25. The master curve of stress relaxation at 30% deformation using the temperature at 220°C as the reference temperature.

26. The master curve of birefringence relaxation at 50% deformation using the temperature at 220°C as the reference temperature.

27. The master curve of stress relaxation at 50% deformation using the temperature at 220°C as the reference temperature.

28a. Plot of logarithmic shift factor, a_T, from relaxation data against temperature using the temperature at 220°C as the standard temperature.

28b. Plot of $-\frac{T-T_r}{\text{Log } a_T}$ versus $T-T_r$ using the temperature at 220°C as the standard temperature T_r.

29a. Plot of logarithmic shift factor, a_T, against temperature using the temperature at 250°C as the standard temperature.

29b. Plot of $-\frac{T-T_r}{\text{Log } a_T}$ versus $T-T_r$ using the temperature at 250°C as the standard temperature T_r.

30. Logarithmic plot of real component of strain optical coefficient, K', versus frequency.

31. Logarithmic plot of imaginary component of strain optical coefficient, K'', versus frequency.

32. Logarithmic plot of real component of modulus, E', versus frequency.

33. Logarithmic plot of imaginary component of modulus, E'', versus frequency.
34. The variation of stress optical coefficient (S.O.C.) with respect to temperature at different frequency.
35. The master curve of real part of strain optical coefficient using the reference temperature of 220°C.
36. The master curve of imaginary part of strain optical coefficient using the reference temperature of 220°C.
37. The master curve of real part of modulus using the reference temperature of 220°C.
38. The master curve of imaginary part of modulus using the reference temperature of 220°C.
39. Plot of logarithmic shift factor, a_T , from vibration data versus temperature using the standard temperature of 220°C.
40. Plot of $-\frac{T-T_r}{\text{Log } a_T}$ versus $T-T_r$ using the standard temperature, T_r, of 220°C.
41. The variation of birefringence with time at 220°C over the elongation ratio range from 1.5 to 6.0 by M1 type of deformation.
42. The variation of stress with time at 220°C over the elongation ratio range from 1.5 to 6.0 by M1 type of deformation.
43. The variation of birefringence with time at 240°C over the elongation ratio range from 1.5 to 6.0 by M1 type of deformation.

44. The variation of stress with time at 240°C over the elongation ratio range from 1.5 to 6.0 by M1 type of deformation.

45. The variation of birefringence with time at 250°C over the elongation ratio range from 1.5 to 4.0 by M1 type of deformation.

46. The variation of stress with time at 250°C over the elongation ratio range from 1.5 to 4.0 by M1 type of deformation.

47. The variation of birefringence with time at 260°C over the elongation ratio range from 1.5 to 6.0 by M1 type of deformation.

48. The variation of stress with time at 260°C over the elongation ratio range from 1.5 to 6.0 by M1 type of deformation.

49. The variation of birefringence with time at 240°C ranging the extension ratio from 2.0 to 6.0 stretched by M2 mechanism.

50. The variation of stress with time at 240°C ranging theextension ratio from 2.0 to 6.0 stretched by M2 mechansim.

51. The variation of birefringence with time at 260°C over the various elongation ratio from 2.0 to 3.0.

52. The variation of stress with time at 260°C over the various elongation ratio from 2.0 to 3.0.
53. The variation of birefringence with time at 265°C over the various elongation ratio from 2.0 to 5.0.
54. The variation of stress with time at 265°C over the various elongation ratio from 2.0 to 5.0
55. The variation of birefringence with time at 275°C over the various elongation ratio from 1.5 to 5.0.
56. The variation of stress with time at 275°C over the various elongation ratio from 1.75 to 5.0.
57. The variation of birefringence with time at 285°C over the various elongation ratio from 2.0 to 5.0.
58. The variatoon of stress with time at 285°C over the various elongation ratio from 2.0 to 5.0.
59. The variation of birefringence with time at 300°C over the various elongation ratio from 2.0 to 5.0.
60. The variation of stress with time at 300°C over the various elongation ratio from 2.0 to 5.0.
61. The variation of birefringence with time at 320°C over the various elongation from 2.0 to 3.0.
62. The variation of stress with time at 320°C over the various elongation ratio from 2.0 to 3.0.
63. The trace of force-strain curve at 275°C with elongation ratio up to 5.0.

64. The variation of crystallinity with time at 260°C ranging the elongation ratios from 2.0 to 3.0.

65. The variation of crystallinity with time at 275°C ranging the elongation ratios from 1.75 to 5.0.

66. The variation of crystallinity with time at 265°C ranging the elongation ratios from 2.0 to 5.0.

67. The variation of crystallinity with time at 285°C ranging the elongation ratios from 2.0 to 5.0.

68. The variation of crystallinity with time at 300°C ranging the elongation ratios from 2.0 to 5.0.

69. The variation of crystallinity with time at 320°C ranging the elongation ratios from 2.0 to 3.0.

70a. The coordinate system of the film and the angles associated with the orientation functions.

70b. The formula of the repeating unit of PVK and the axes characterizing the orientation of backbone and planar carbazole molecule.

71. The X-ray diffraction patterns at 275°C over the range of elongation ratios from 1.5 to 3.0.

72. The X-ray diffraction scans for the undeformed PVK and for elongation ratio 3.0 at 275°C.

73. The X-ray azimuthal angle scans with respect to crystalline diffraction peak for PVK stretched to 200% at 275°C.

74a. The X-ray diffraction patterns for an elongation ratio of 6.0 over the various temperature from 220°C to 260°C.

74b. The X-ray diffraction patterns at 240°C ranging the elongation ratios from 4.0 to 6.0.

75. The X-ray diffraction patterns at 265°C over the various elongation ratios from 2.0 to 5.0.

76. The X-ray diffraction patterns at 285°C over the various elongatiin ratios from 2.0 to 5.0.

77. The X-ray diffraction patterns of undeformed PVK and stretched to the various elongation ratios from 2.0 to 5.0 at 300°C.

78a. The X-ray diffraction patterns at 260°C over the various elongation ratios from 2.0 to 3.0.

78b. The X-ray diffraction patterns at 320°C over the various elongation ratios from 2.0 to 3.0.

79. The X-ray diffraction scans for PVK stretched to the elongation ratio 5.0 at 300°C.

80. The infrared absorption spectra for PVK stretched to the elongation ratio 3.0 at 275°C with polarization parallel and perpendicular to the stretching direction.

81. The H_v light scattering patterns at 240°C ranging the elongation ratio from 2.0 to 6.0.

82. The H_v light scattering patterns for the underformed PVK and for various elongation at 250°C.

83a. The H_v light scattering patterns at 260°C for elongation ratio 2.0 and 3.0.

83b. The H_v light scattering patterns at 300°C ranging the elongation ratio from 2.0 to 3.0.

84a. The H_v light scattering patterns at 275°C over the elongation ratio range from 1.75 to 3.0.

84b. The H_v light scattering patterns at 275°C over the elongation ratio range from 3.1 to 5.0.

85. The H_v light scattering patterns at 265°C over the elongation ratio range from 2.0 to 5.0.

86. The H_v light scattering patterns at 285°C over the elongation ratio range from 2.0 to 5.0.

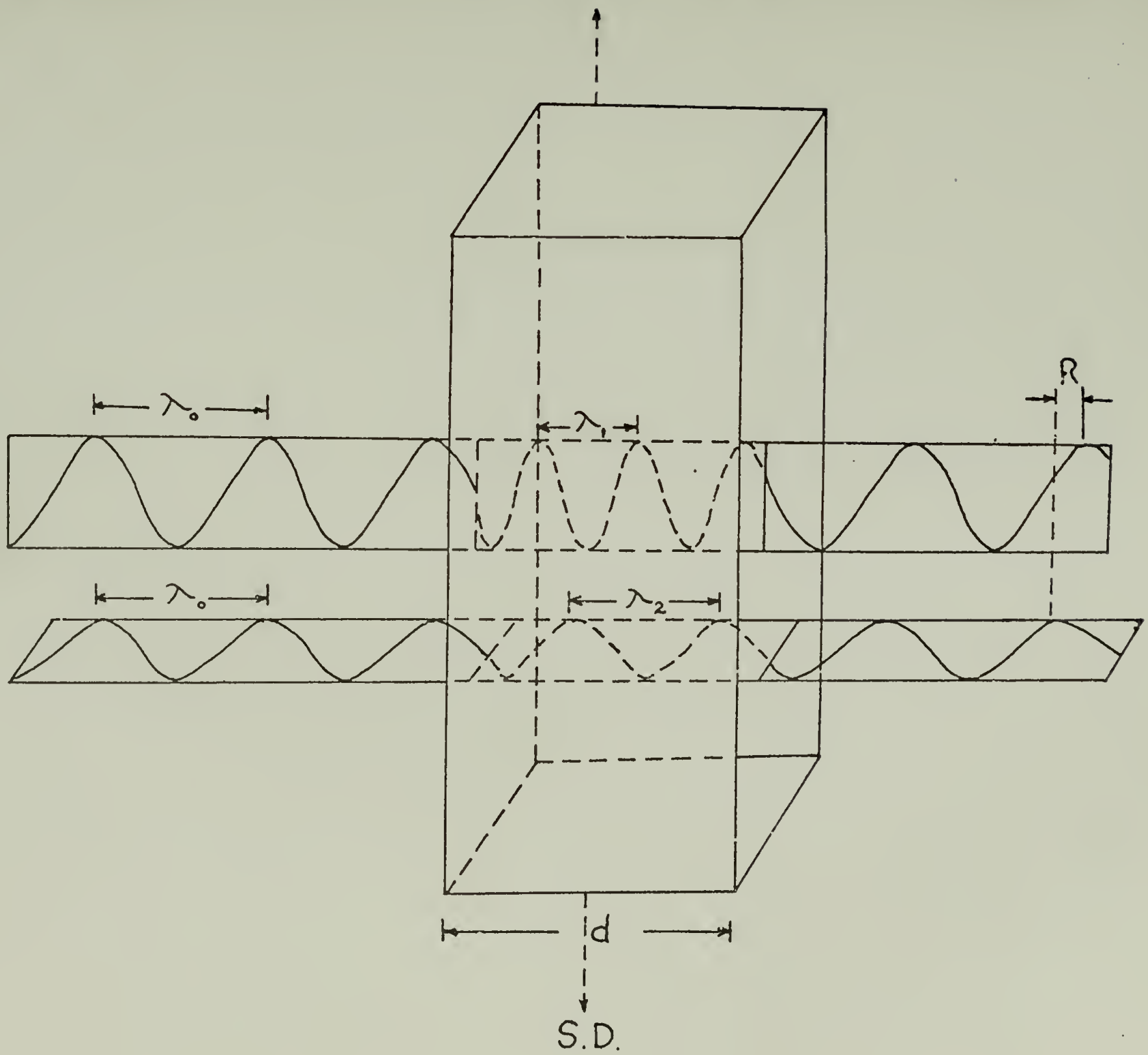

Figure 1. Schematic Diagram for the Double Refraction Phenomenon

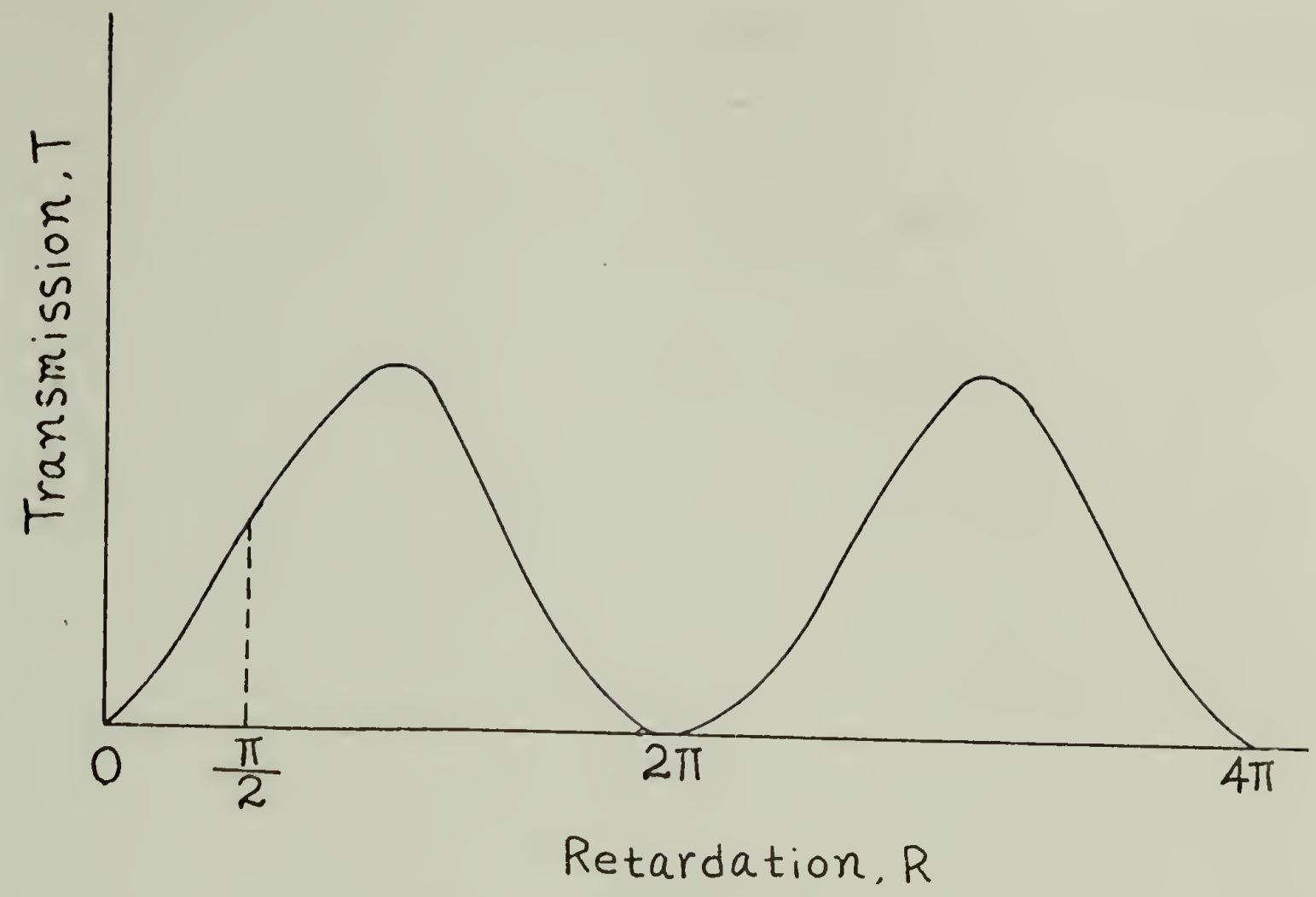

Figure 2a

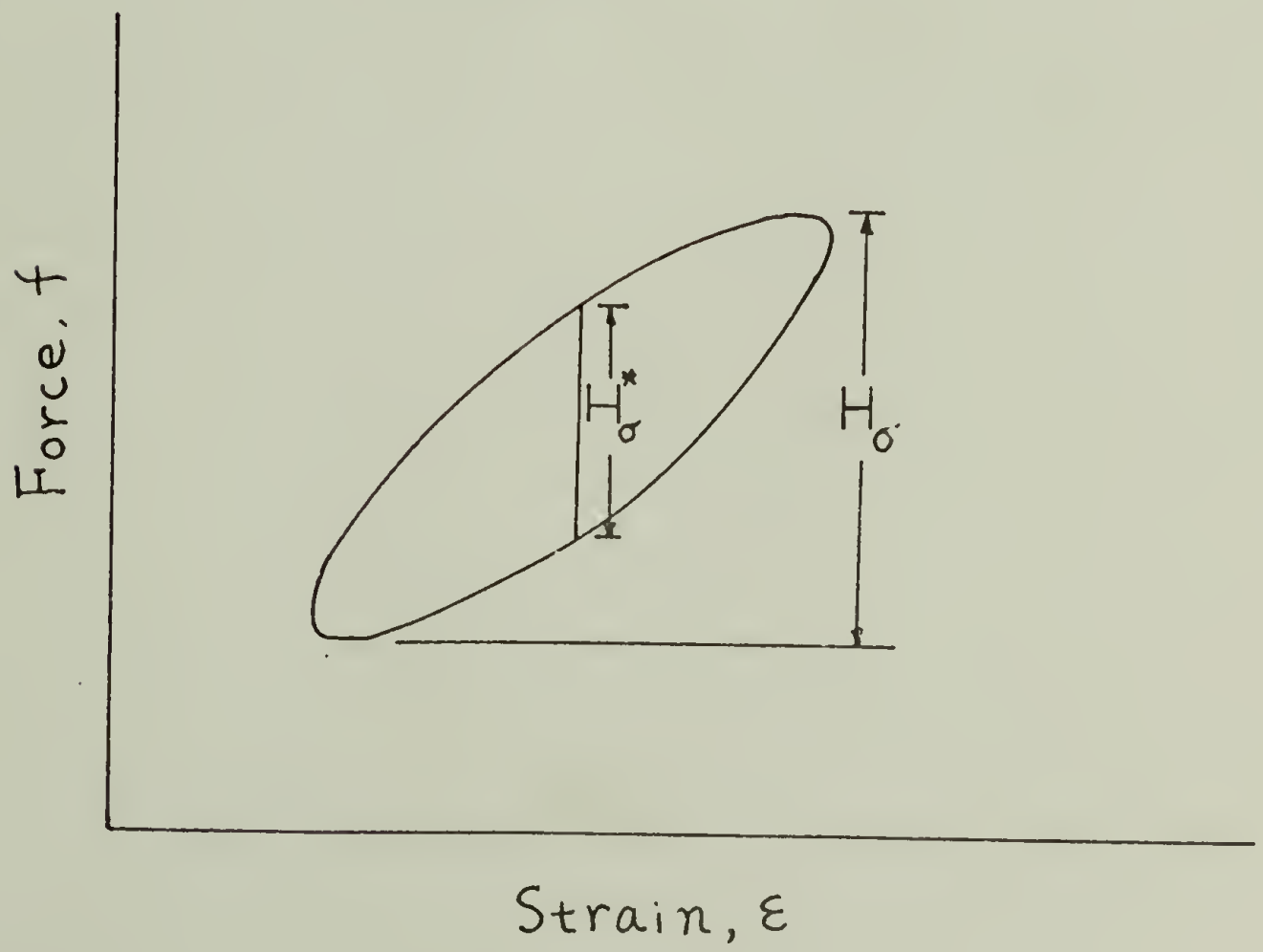

Figure 2b

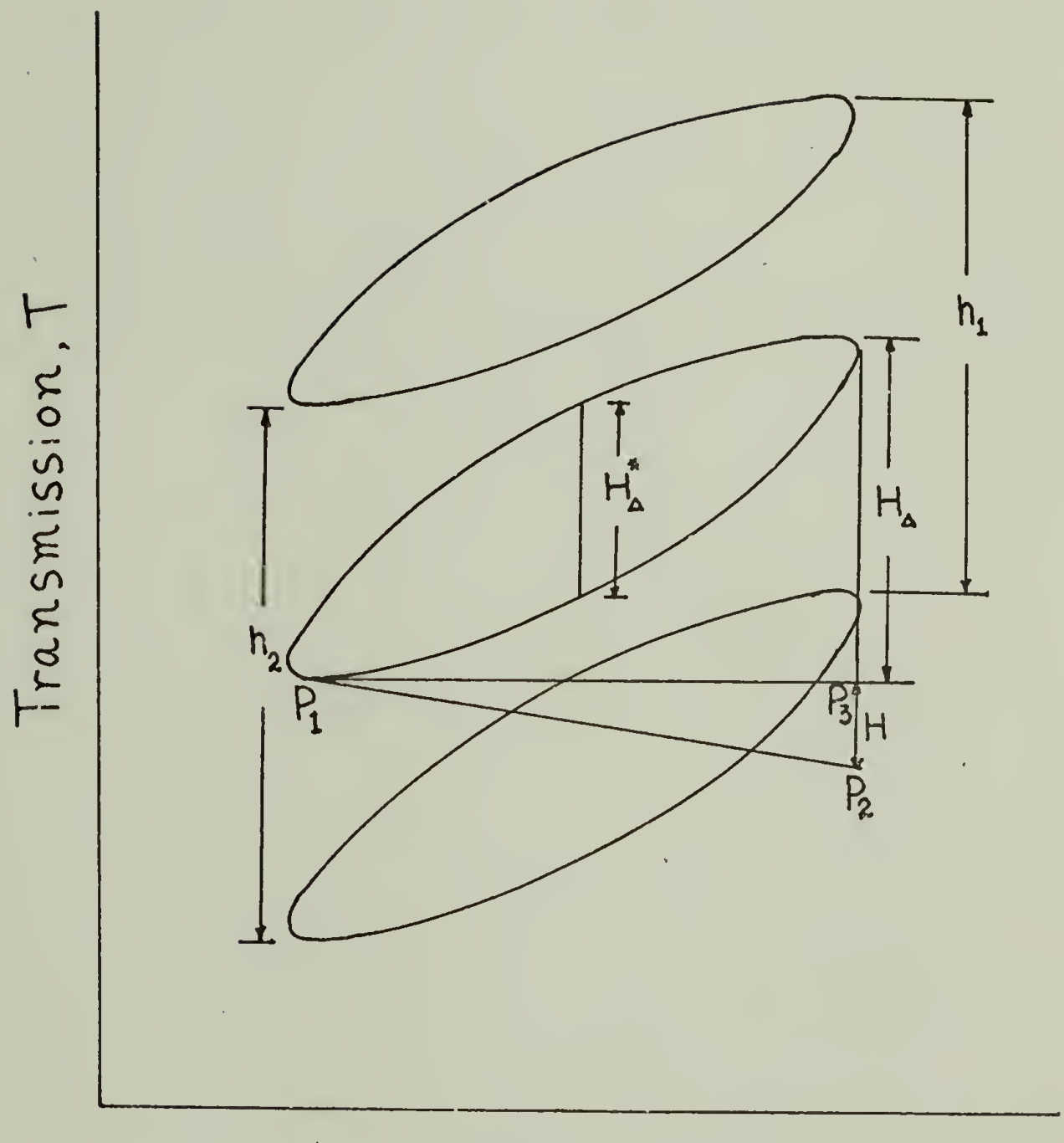

Figure 3

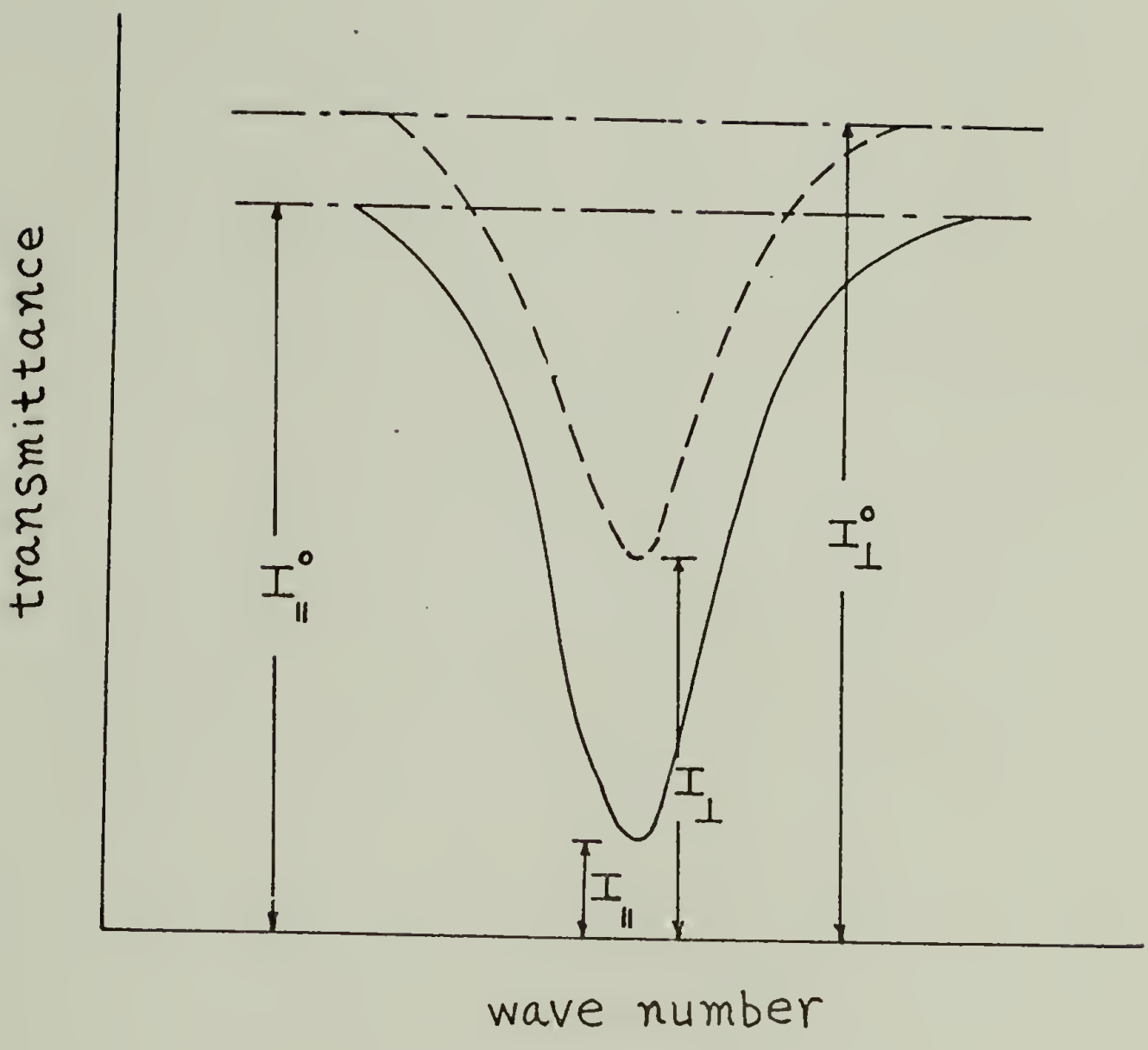
transmittance
$H^\circ_{\parallel}$
$H^\circ_{\perp}$
$I_{\perp}$
$I_{\parallel}$
wave number

Figure 4

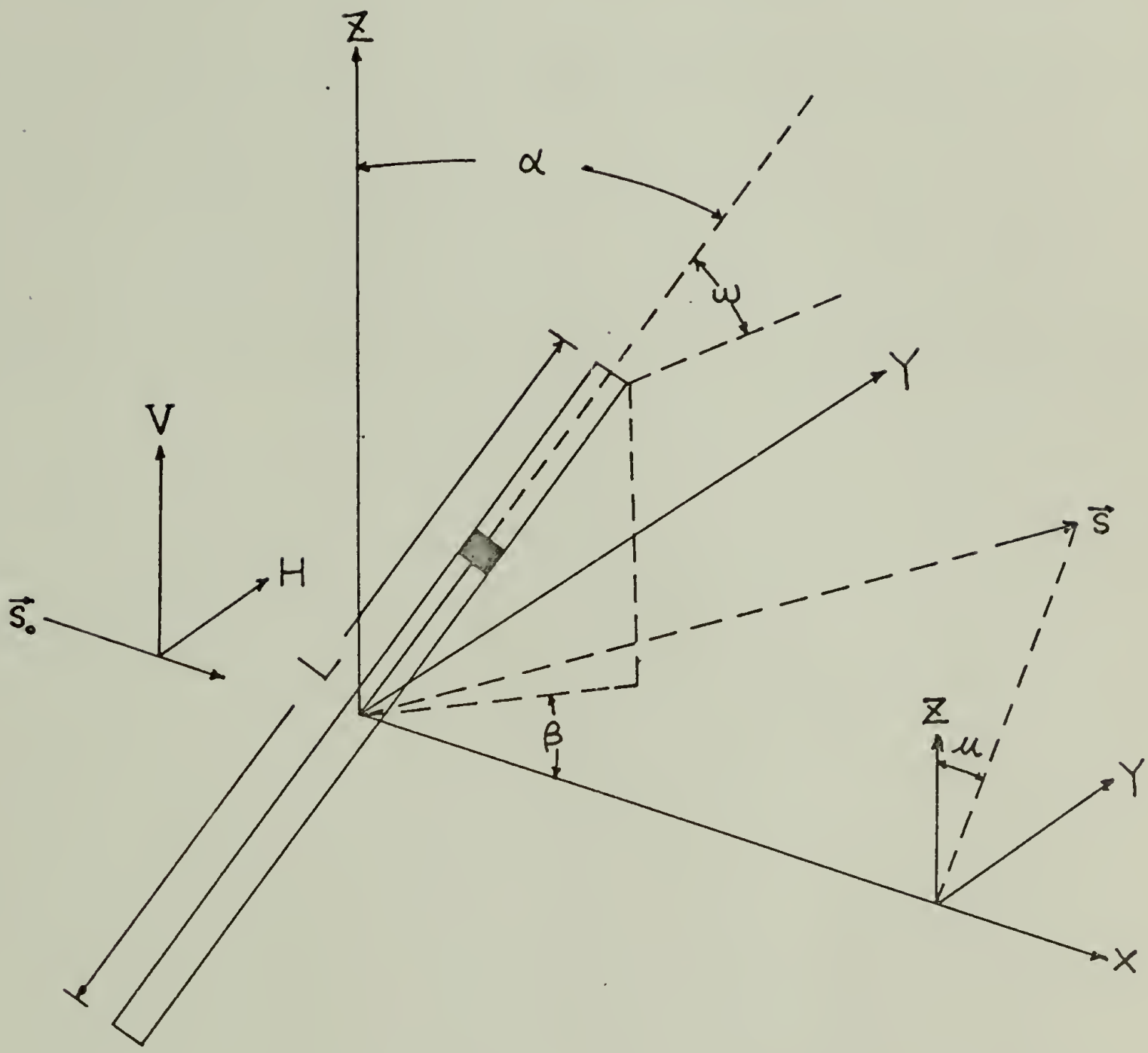

Figure 5. Coordinate System for Light Scattering of One-Dimensional Rod in the Three-Dimensional Space

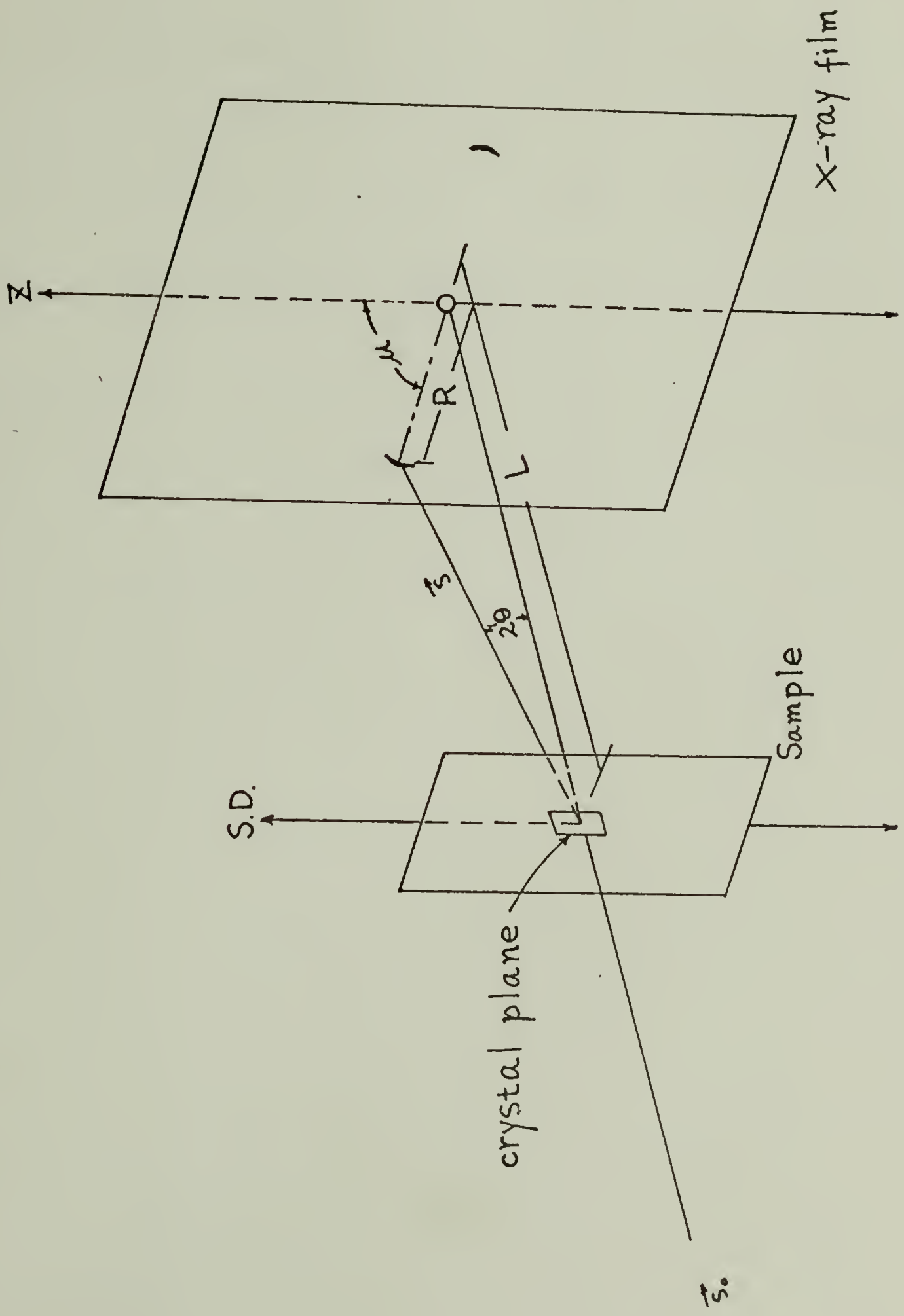

Figure 6. Geometric System for the X-Ray Diffraction of Uniaxial Oriented Polymer Film

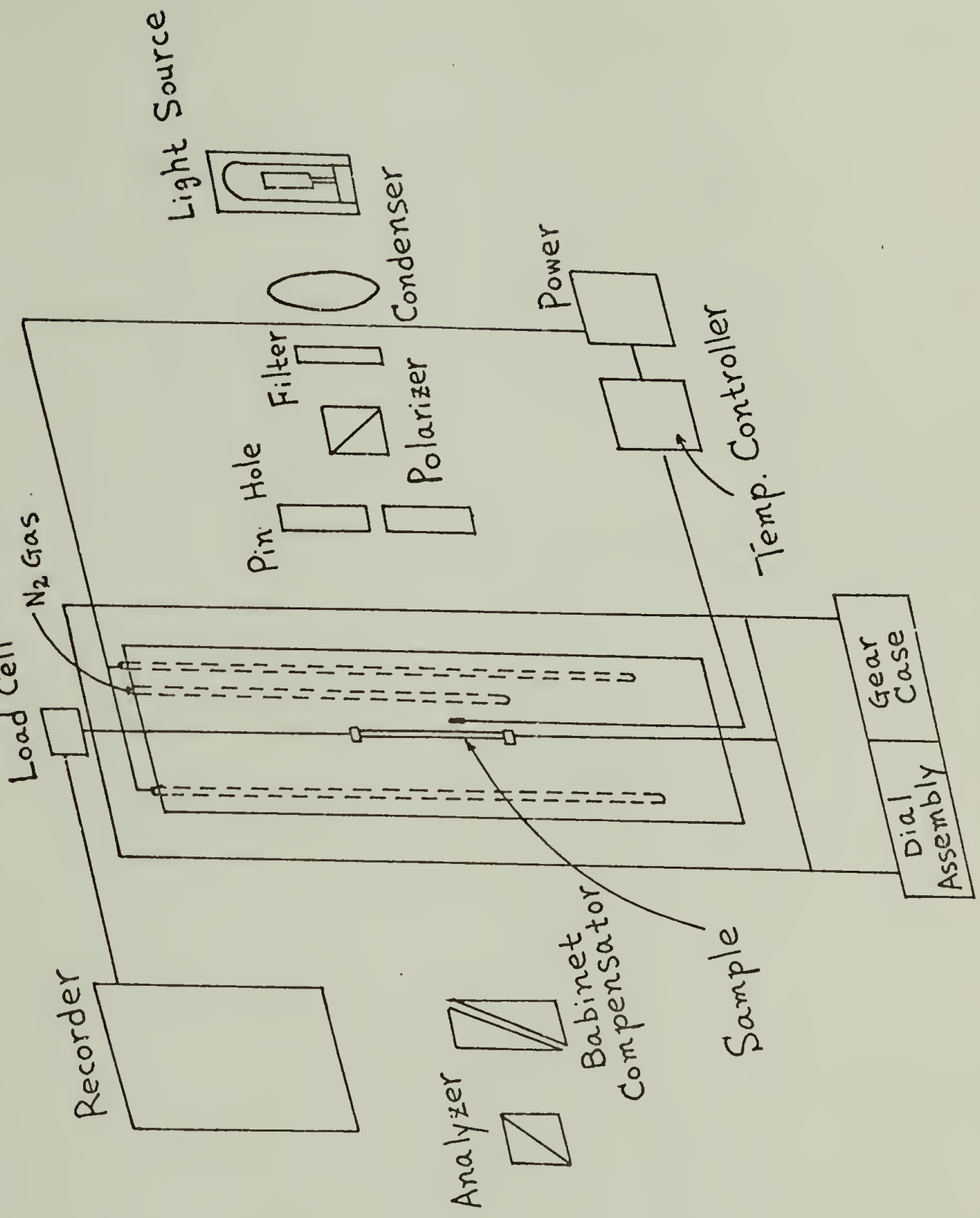

Figure 7. Schematic Diagram of Table Model Instron with Optical Attachment

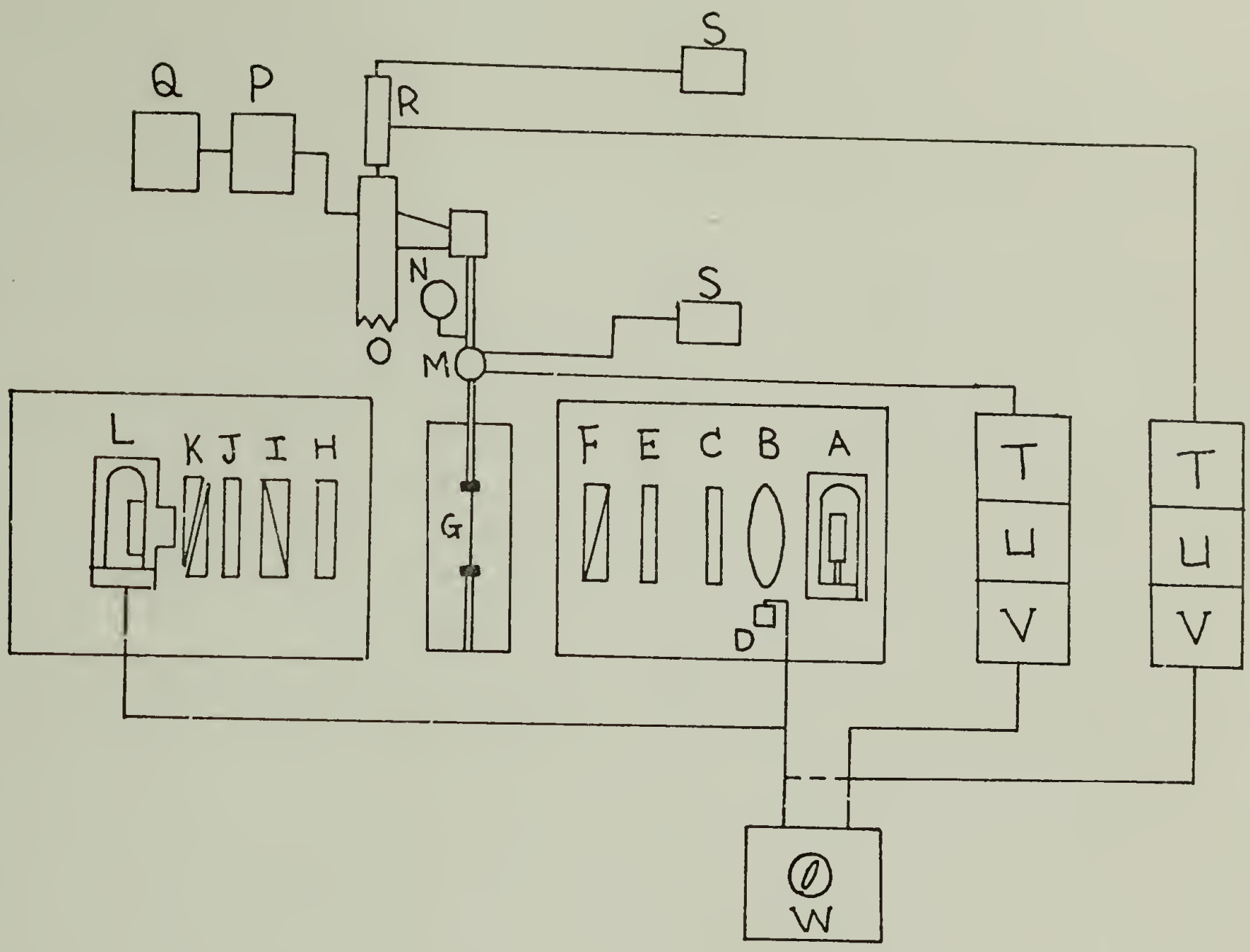

Figure 8. Sketch of Dynamic Birefringence Appratus

(A) Light Source (B) Condensing Lens (C) Monochromic Filter

(D) Phtoresistive Cell (E) Pinhole (F) Polarizer

(G) Sample (H) Retardation Plate (I) Analyzer

(J) Neutran Density Filter (K) Babinet Compensator

(L) Photomultiplier Tube (M) Force Tranducer (N) Dial Guage

(O) Arm of Mechanical Vibrator (P) Worm Gear Reducer

(Q) Transmission System (R) Linear Variable Differential Transformer (S) Oscillator (T) Rectifier (U) Preamplifier

(V) DC amplifier (W) Dual-Beam Oscilloscope

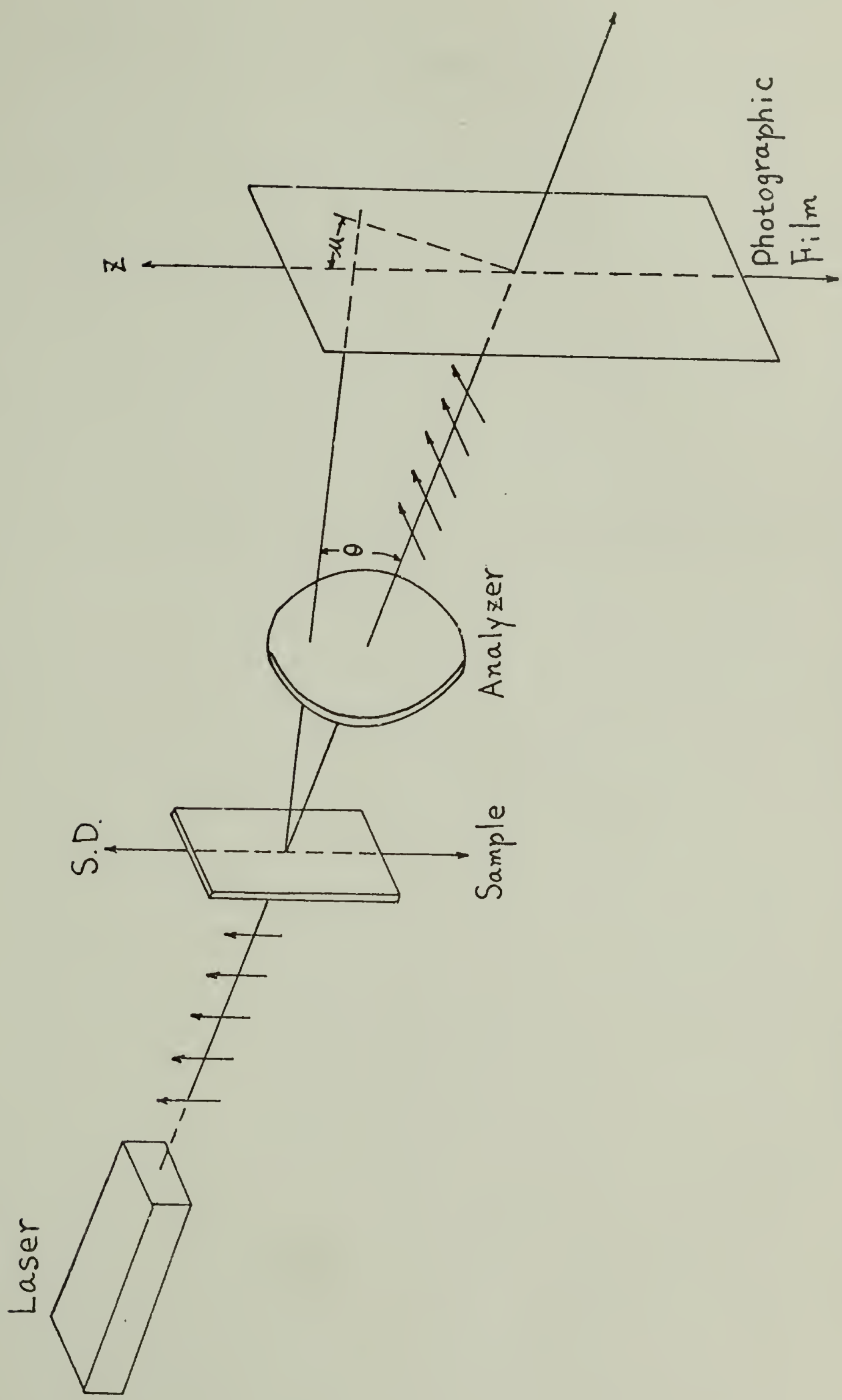

Figure 9. Schematic Diagram of Small Angle Light Scattering System

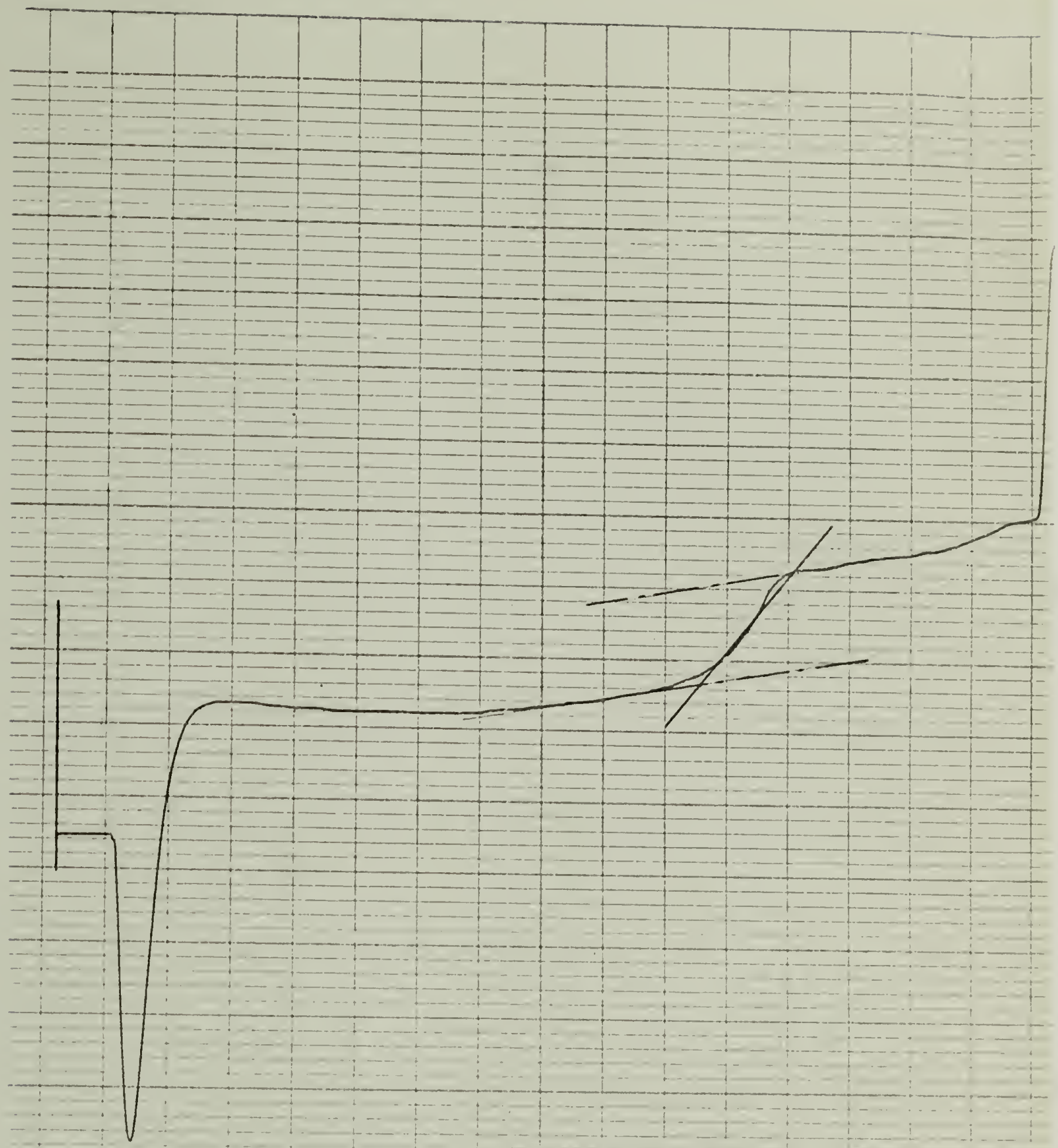

Figure 10

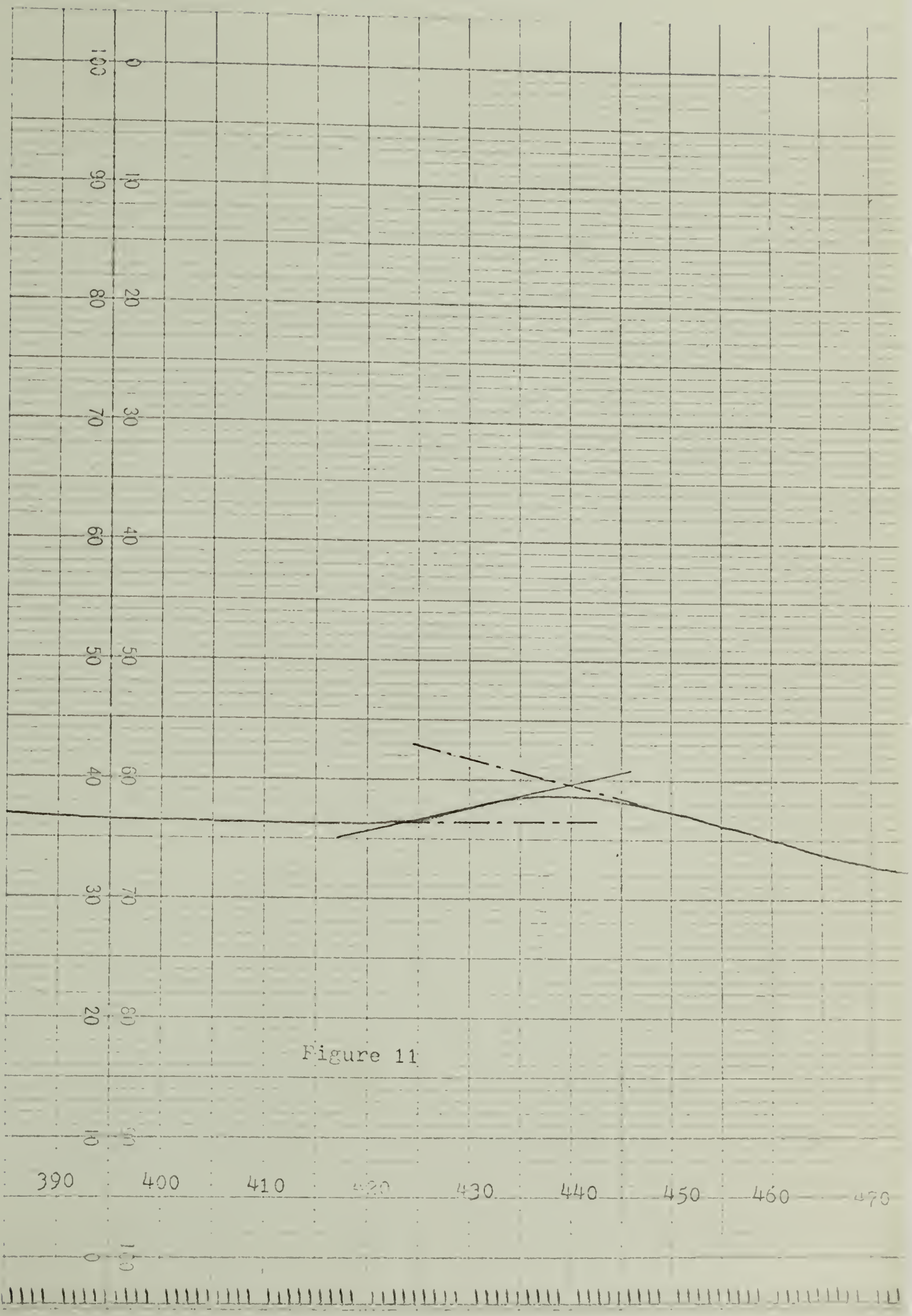
100
90
80
70
60
50
40
30
20
10
0
0
10
20
30
40
50
60
70
80
90
100
390
400
410
420
430
440
450
460
470

Figure 11

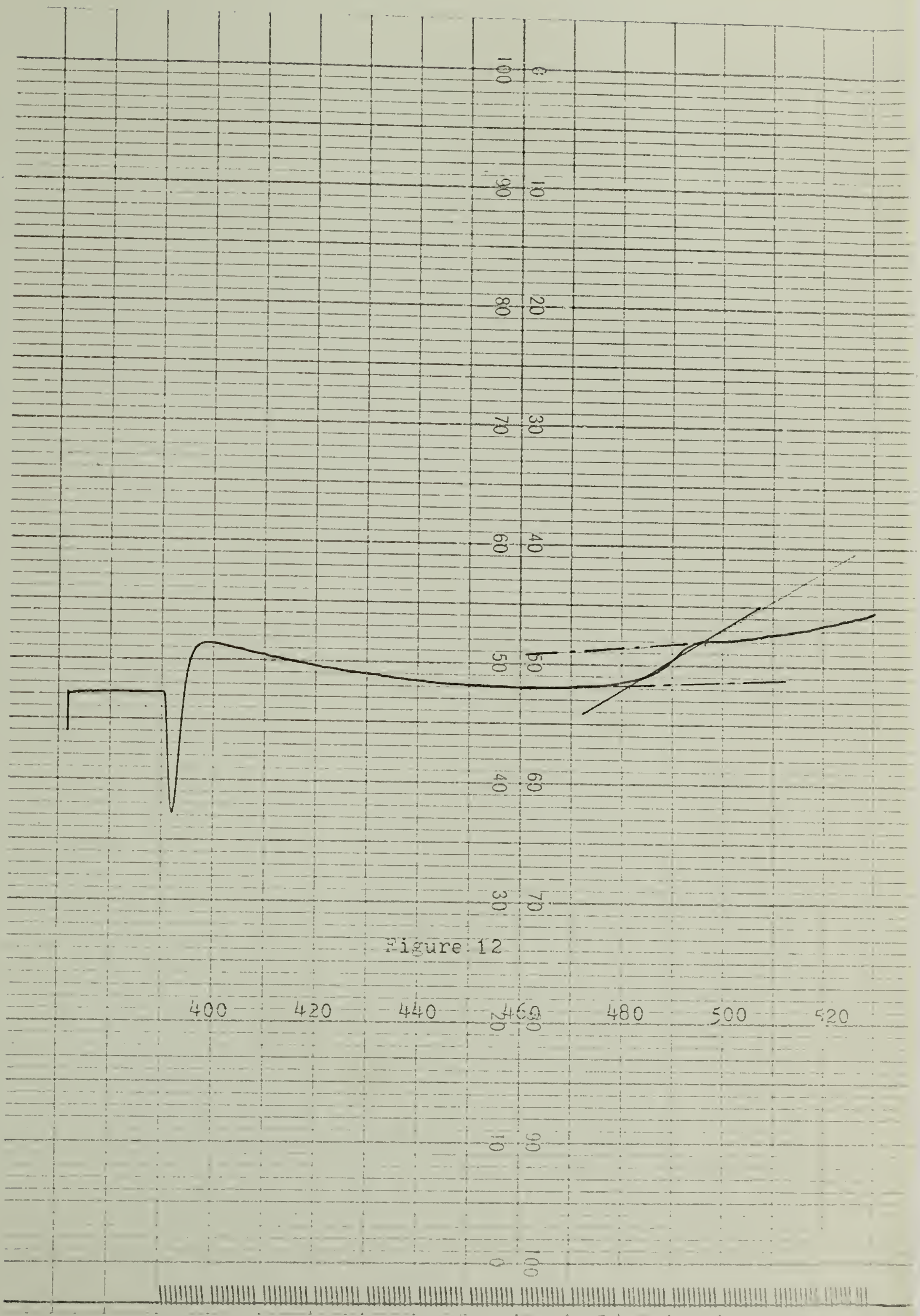
100
90
80
70
60
50
40
30
20
10
0
10
20
30
40
50
60
70
80
90
100
400
420
440
460
480
500
520

Figure 12

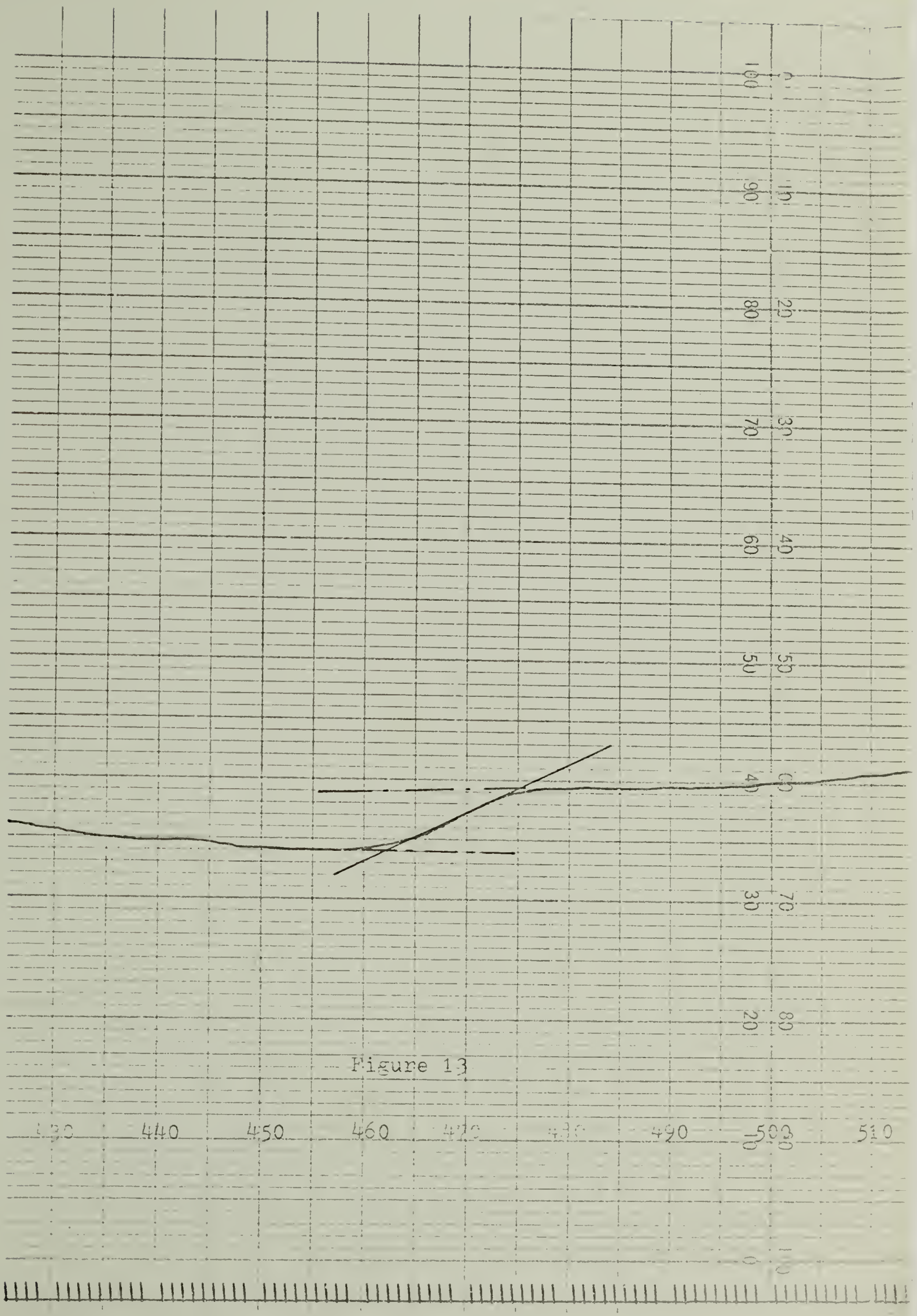

Figure 13

10 %

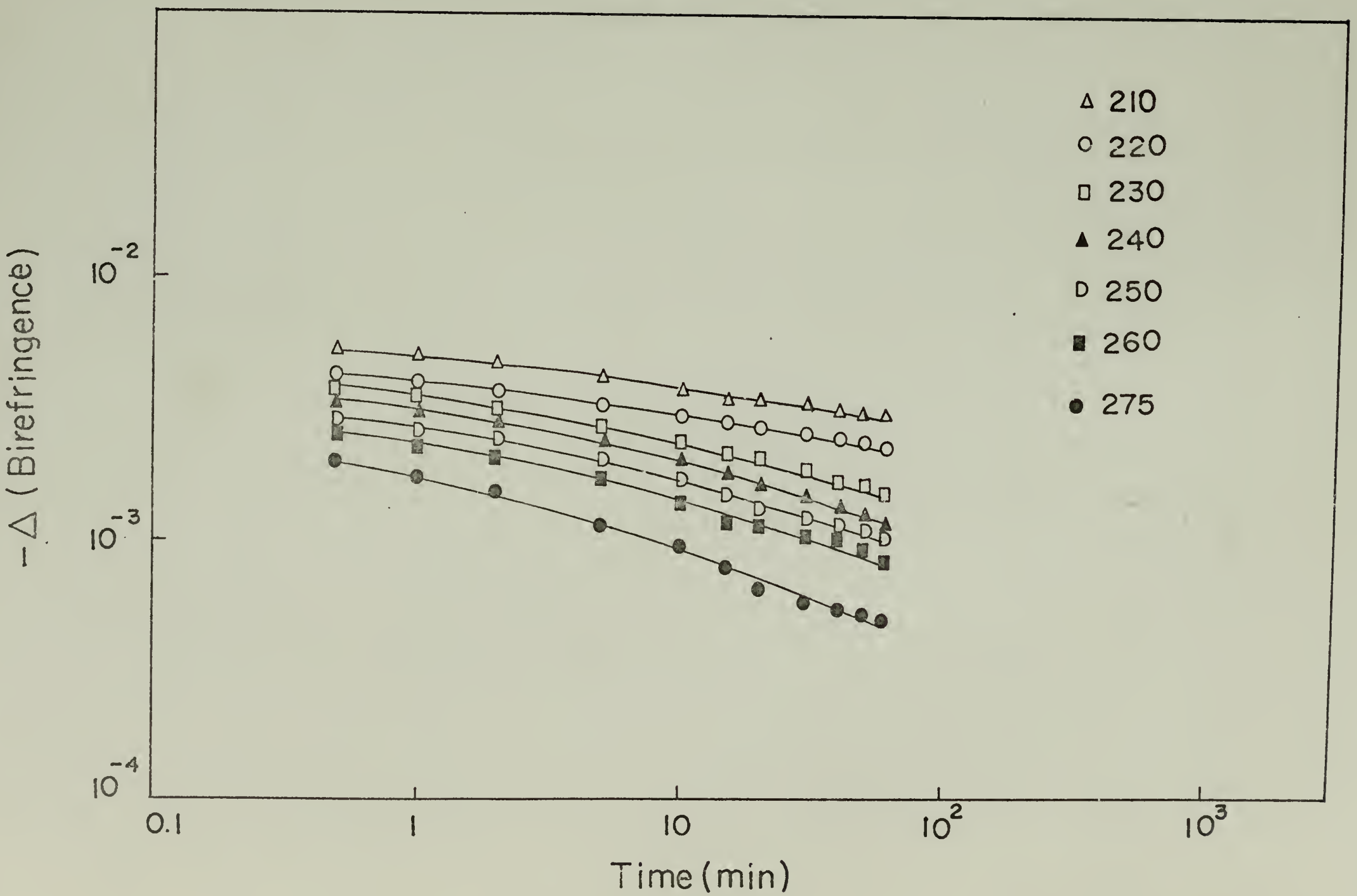
Δ (Birefringence)
10^{-2}
10^{-3}
10^{-4}
0.1
1
10
10^2
10^3
Time (min)
210
220
230
240
250
260
275

Figure 14

10%

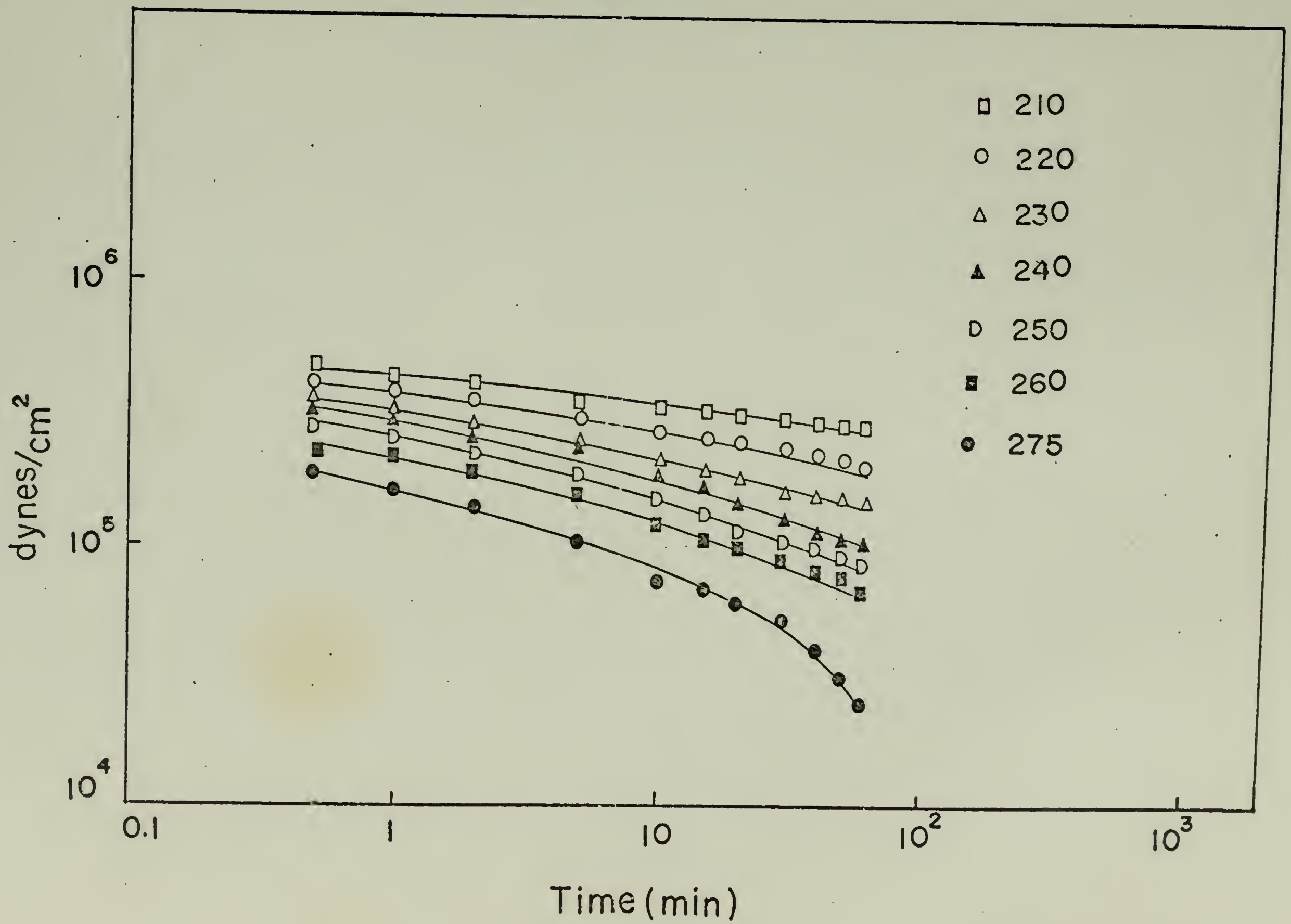
σ
dynes/cm²
10⁶
10⁵
10⁴
0.1
1
10
10²
10³
Time (min)
210
220
230
240
250
260
275

Figure 15

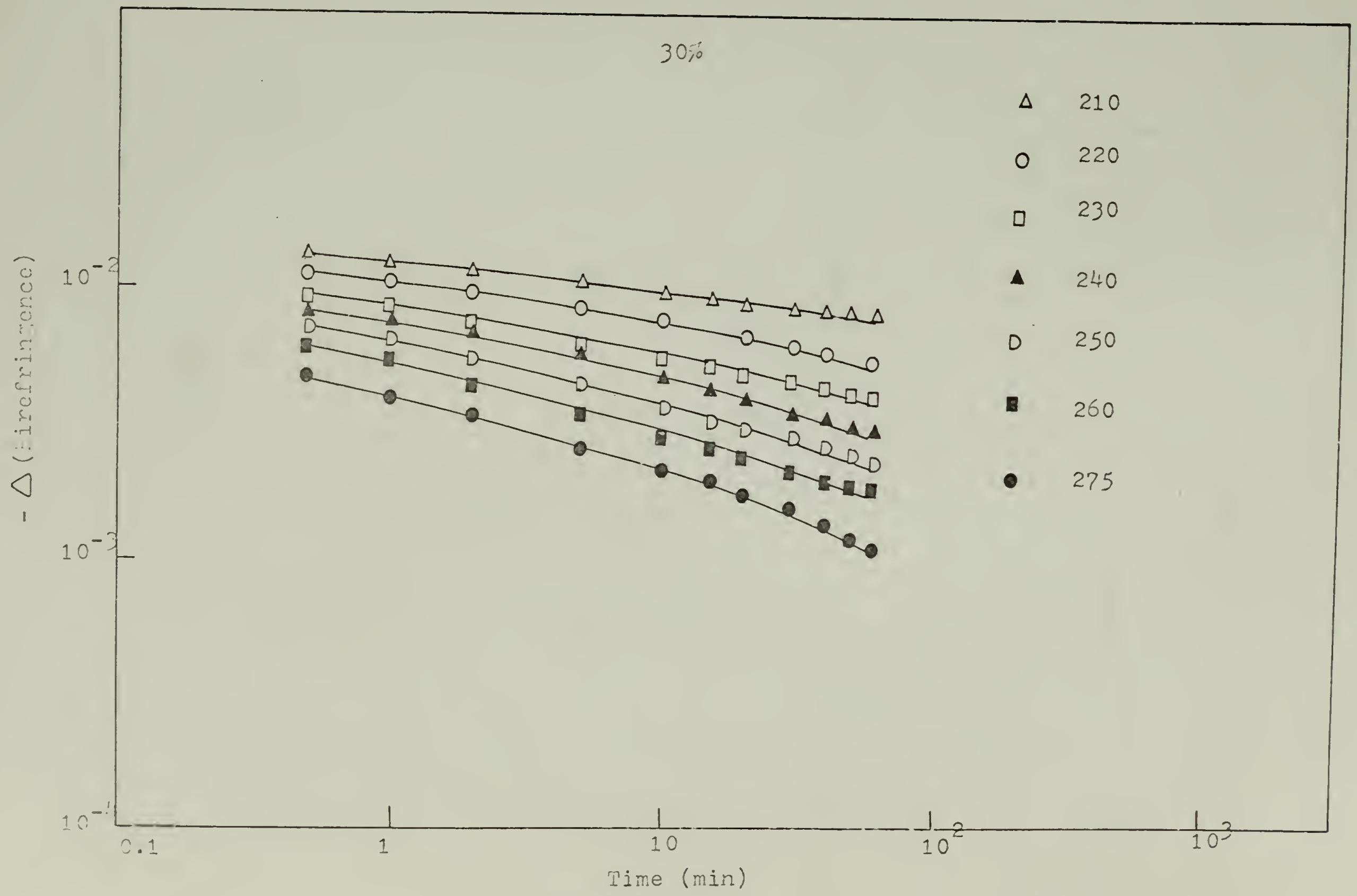
30%
210
220
230
240
250
260
275
10^{-2}
10^{-3}
10^{-4}
0.1
1
10
10^{2}
10^{3}
Time (min)

Figure 16

30%

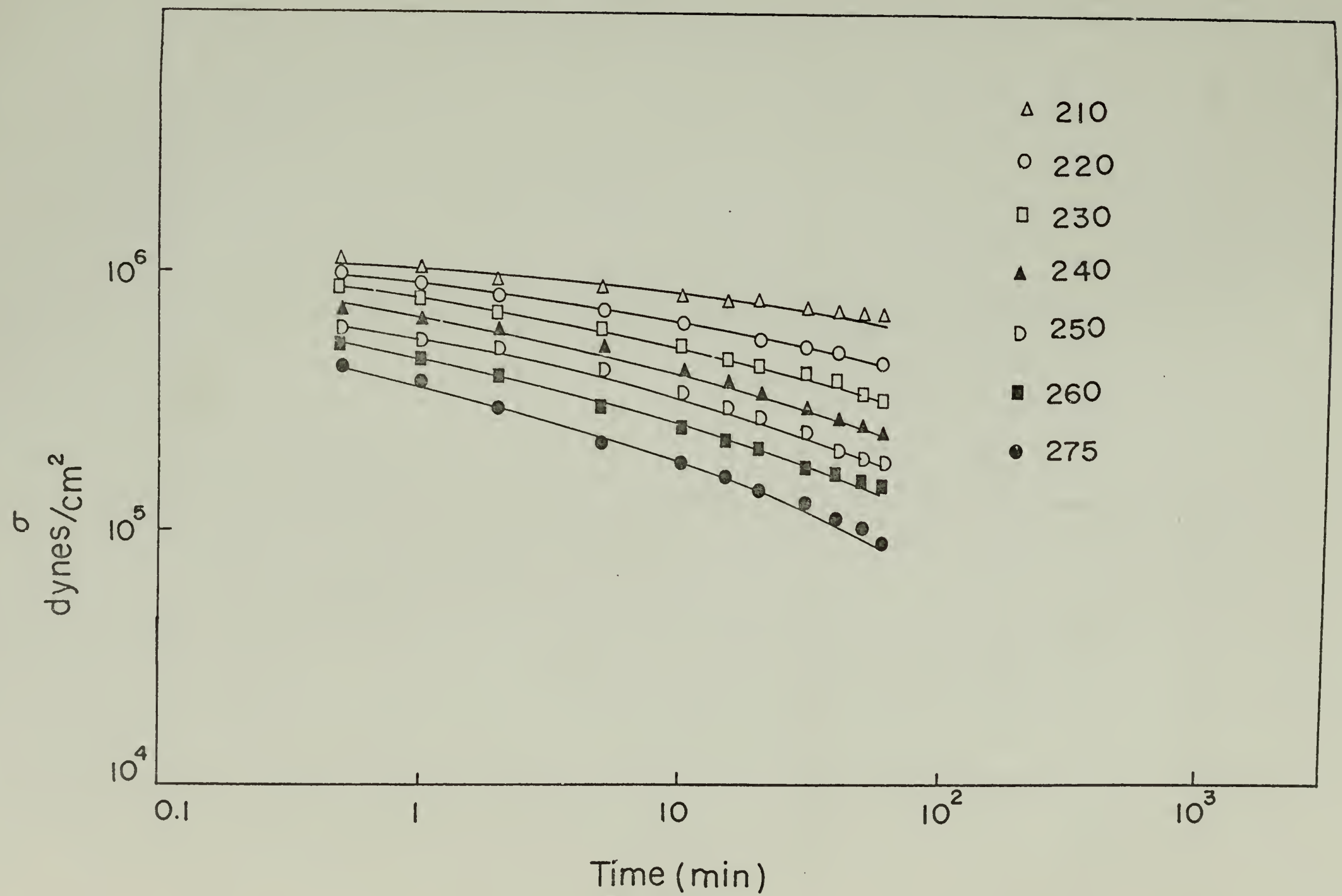
210
220
230
240
250
260
275
10^6
10^5
10^4
σ dynes/cm²
0.1
1
10
10^2
10^3
Time (min)

Figure 17

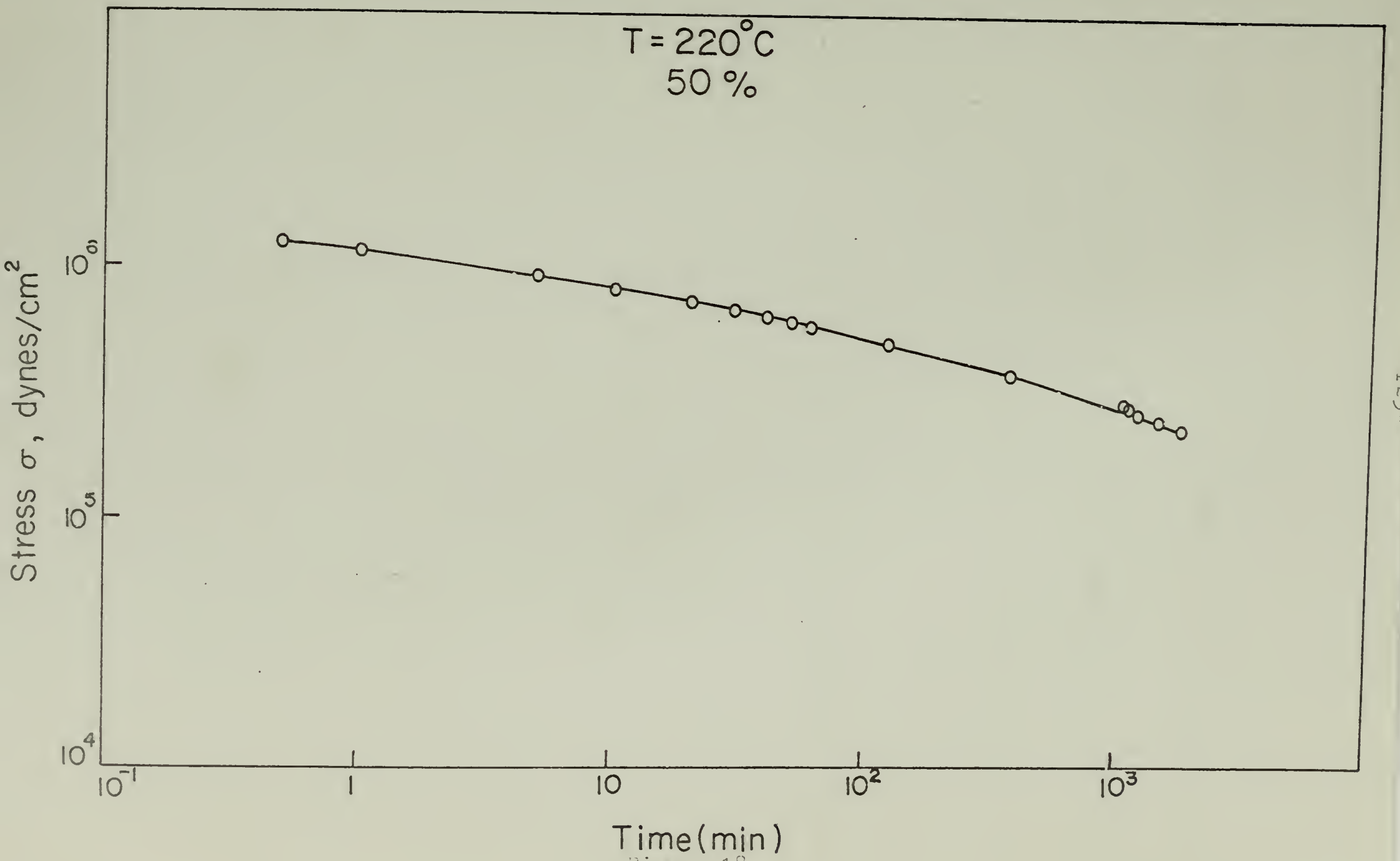
T = 220°C
50 %
$\bar{\sigma}_\infty$
$\bar{\sigma}_5$
Stress σ, dynes/cm²
10^4
10^{-1}
1
10
10^2
10^3
Time(min)

Figure 18

50 %

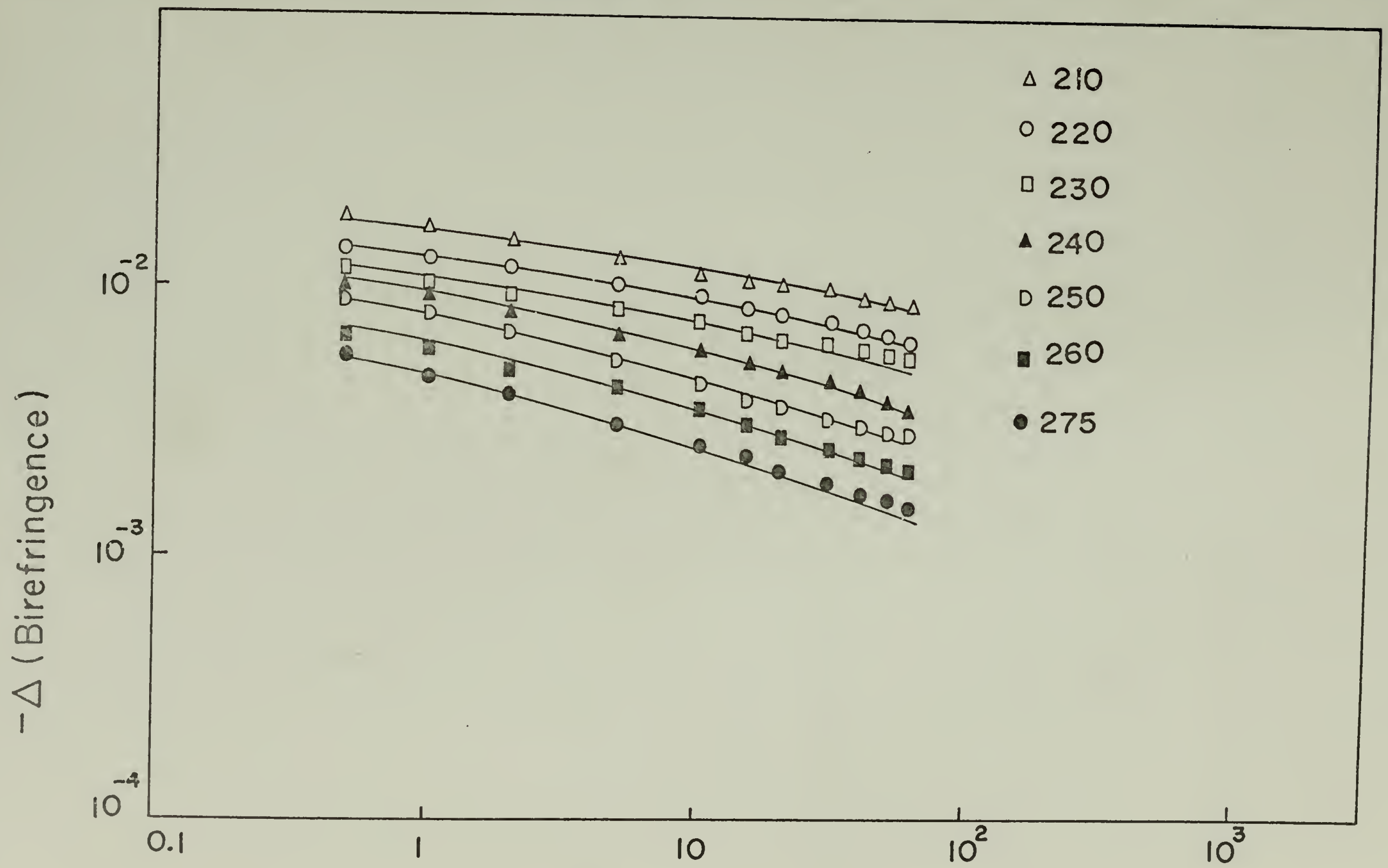
△ 210
○ 220
□ 230
▲ 240
D 250
■ 260
● 275
10^{-2}
10^{-3}
10^{-4}
$-\Delta$ (Birefringence)
0.1
1
10
10^2
10^3
Time (min)

Figure 19

50 %

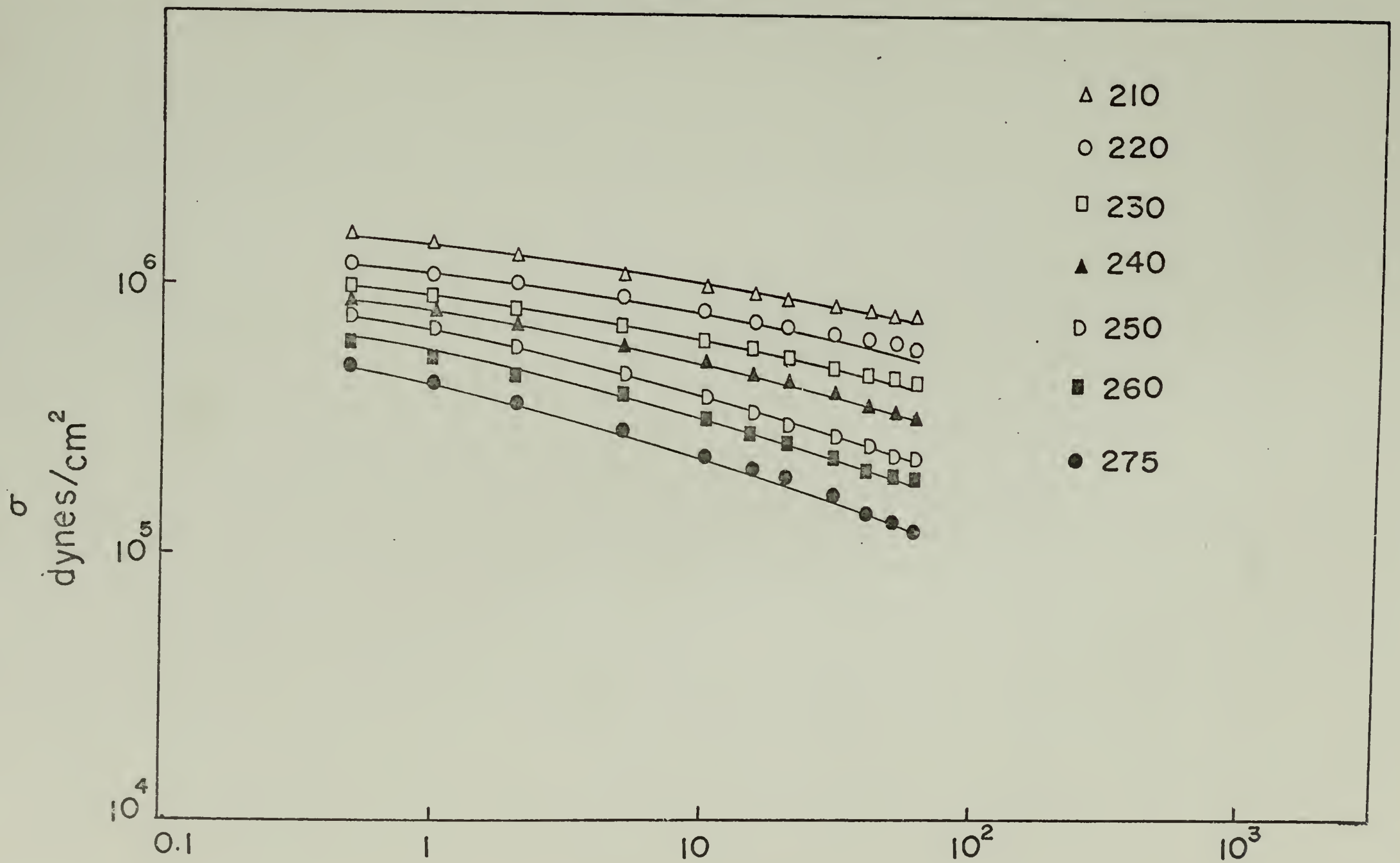
210
220
230
240
250
260
275
10^6
10^5
10^4
0.1
1
10
10^2
10^3
σ dynes/cm²
Time (min)

Figure 20

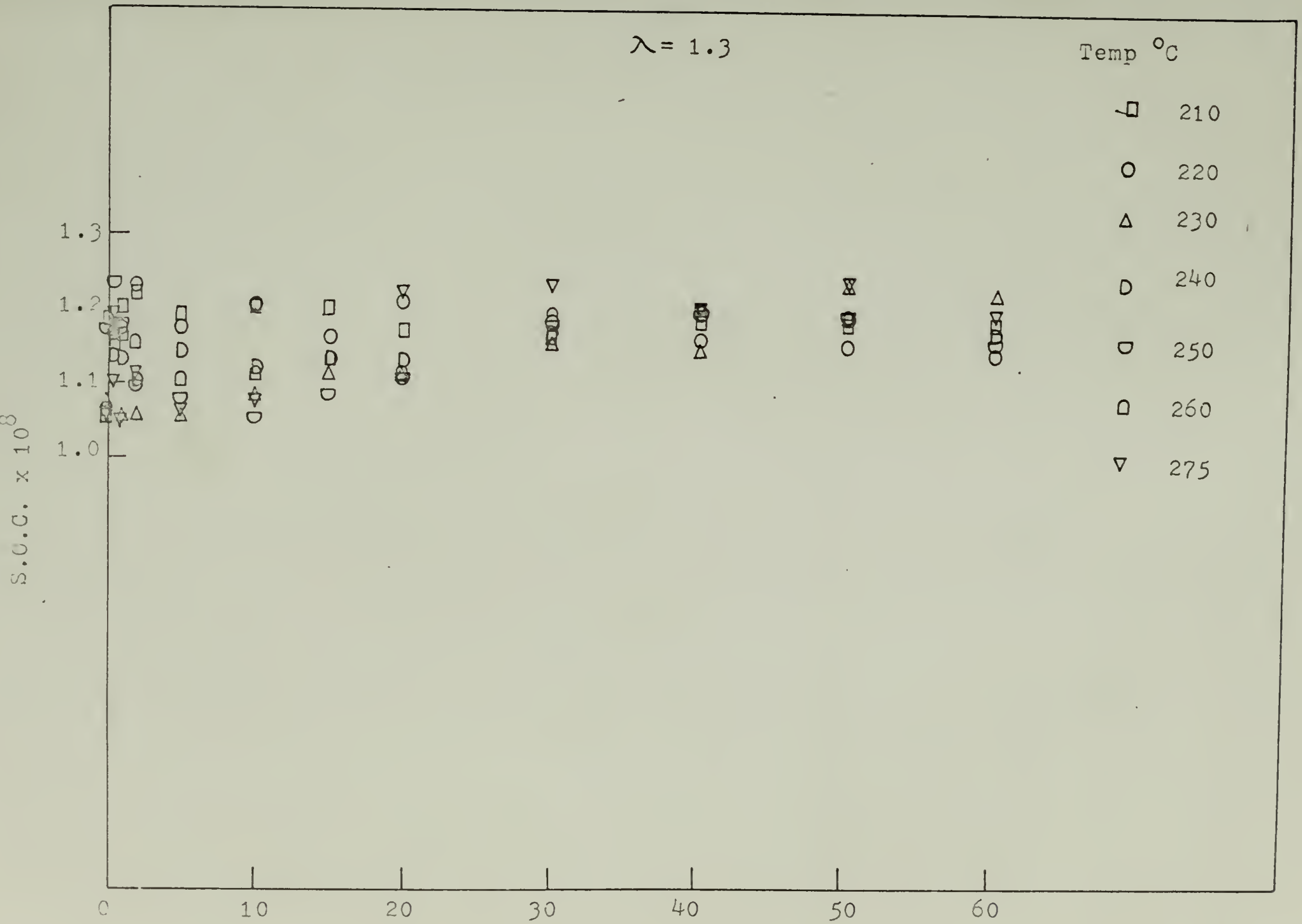
λ = 1.3
Temp °C
210
220
230
240
250
260
275
S.C.C. x 10^8
1.3
1.2
1.1
1.0
0
10
20
30
40
50
60
Time (min)

Figure 21

10 %

$T_{ref} = 220°C$

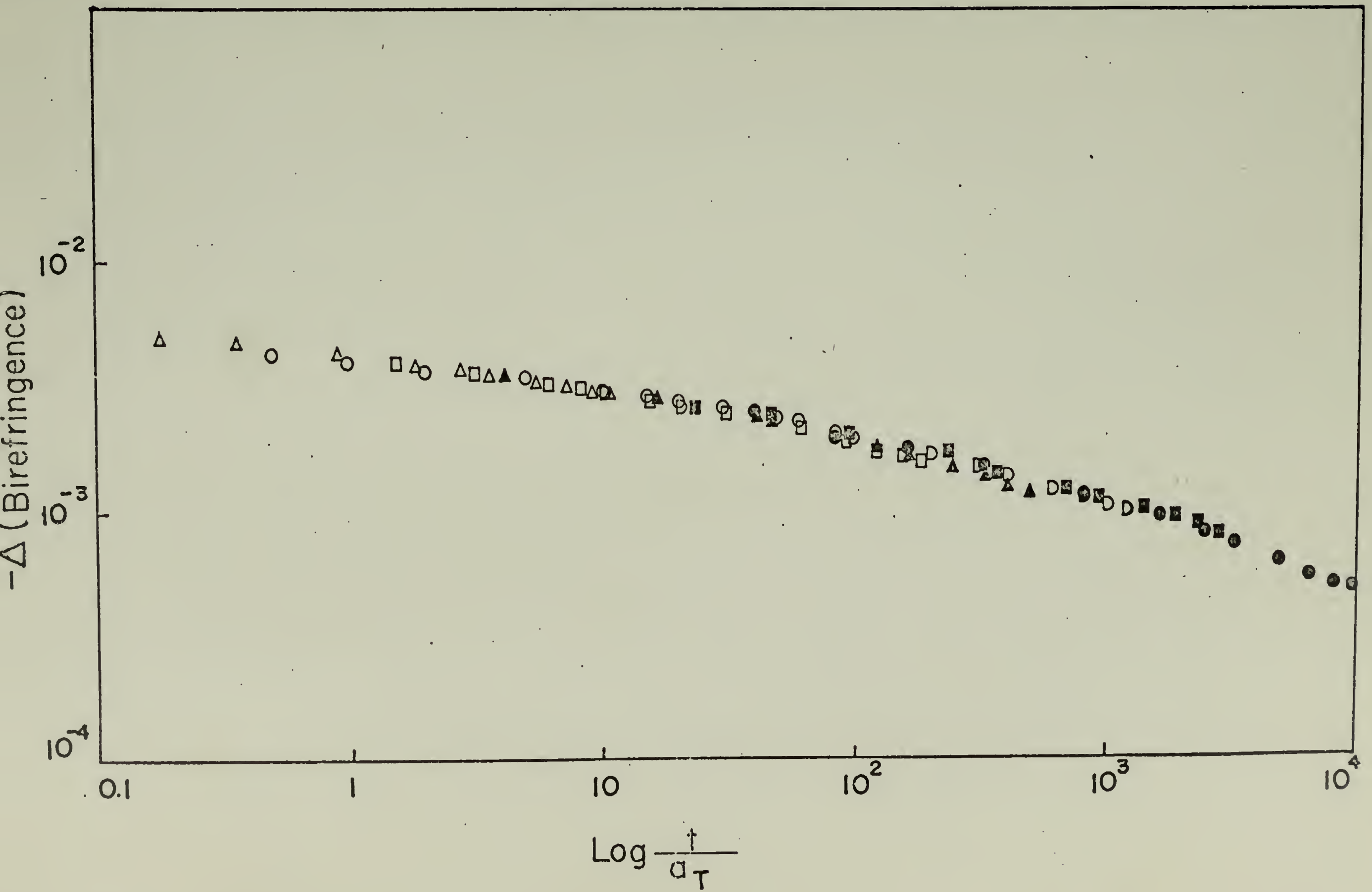

Figure 22

10 %
Tref = 220°C

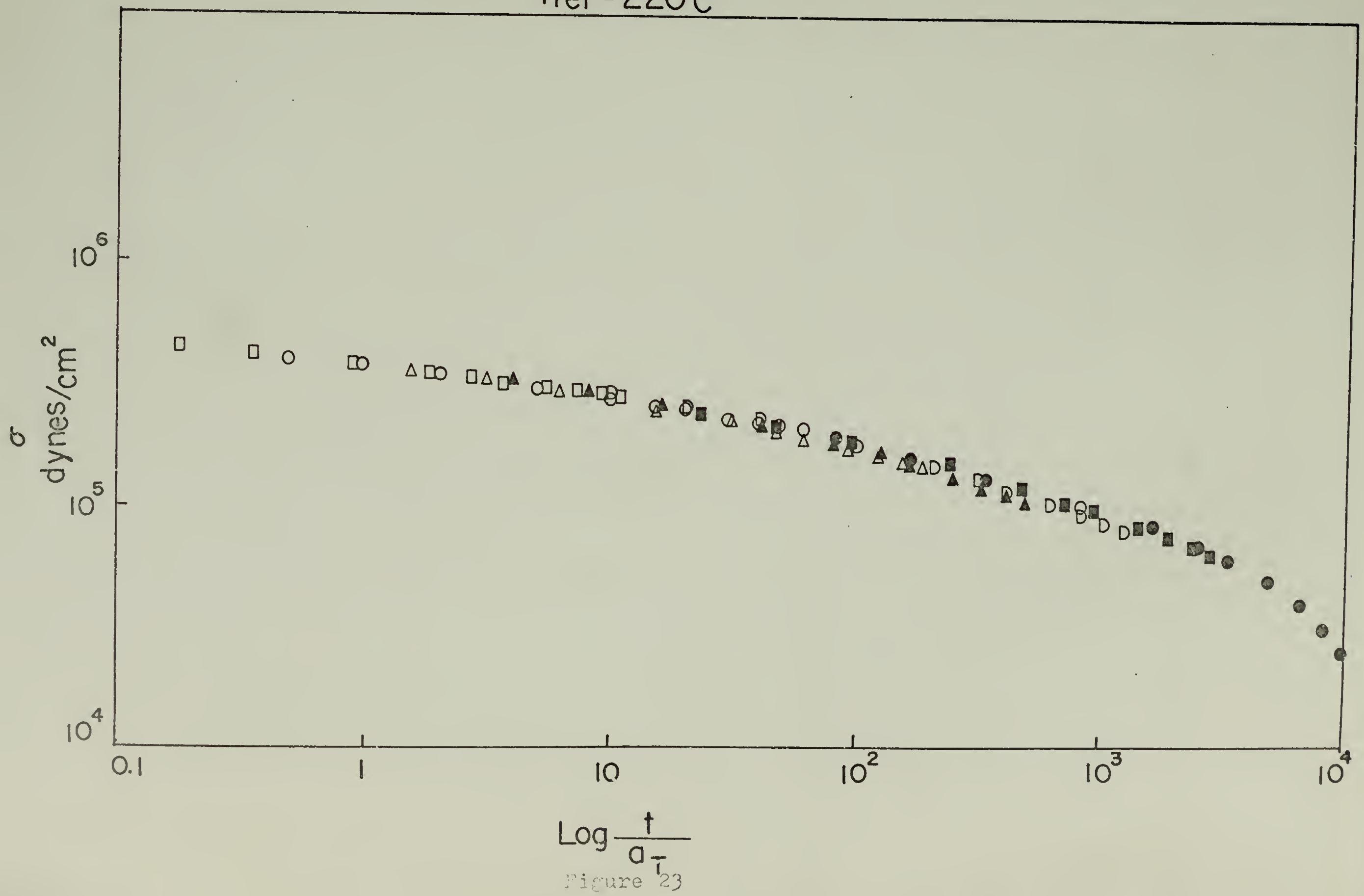

Figure 23

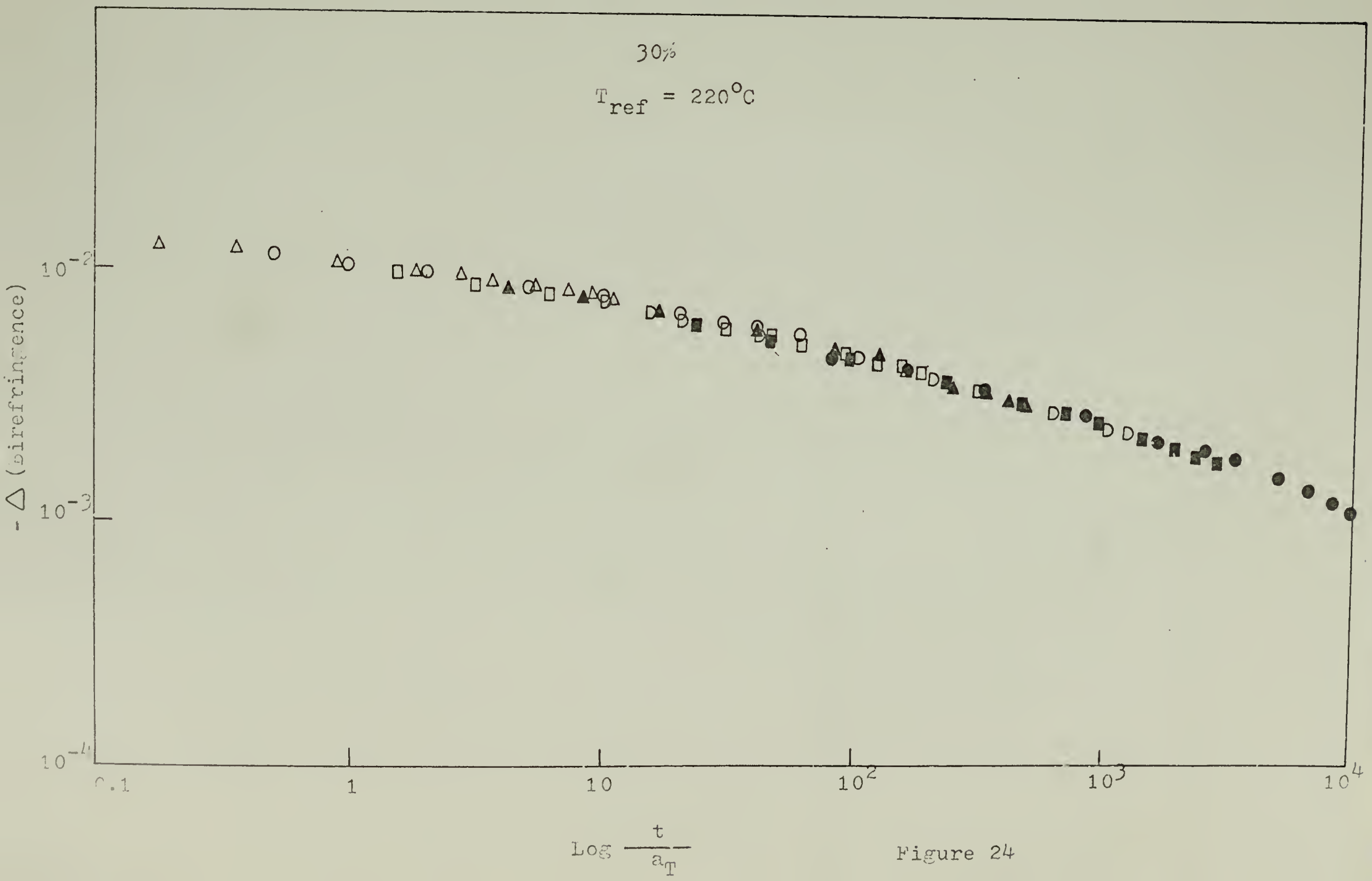
30%
T_{ref} = 220°C
10^{-2}
10^{-3}
10^{-4}
- Δ (birefringence)
0.1
1
10
10^2
10^3
10^4
Log $\frac{t}{a_T}$

Figure 24

30%

$T_{ref} = 220^{\circ}C$

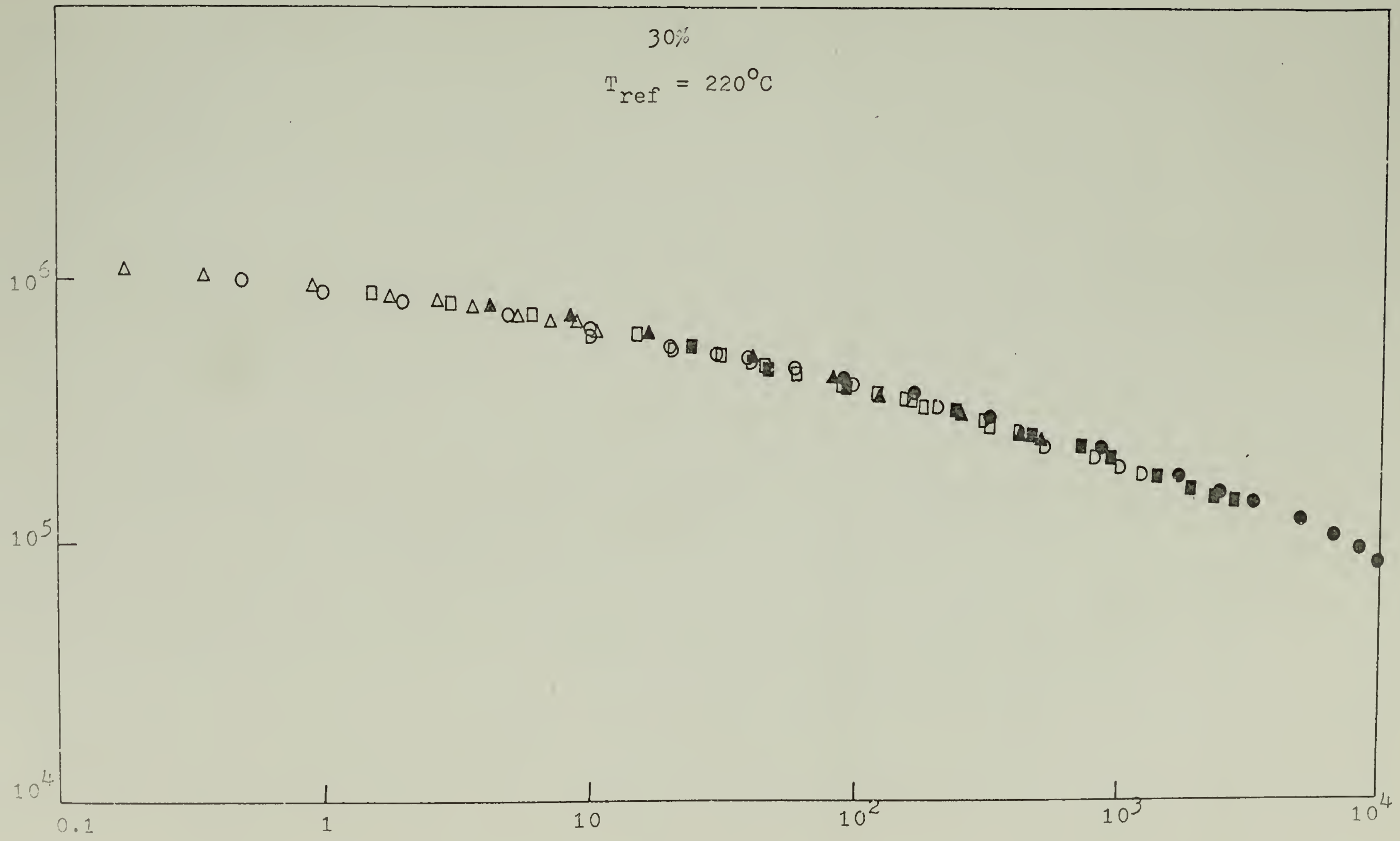

$\text{Log } \frac{t}{a_T}$

Figure 25

50 %
Tref = 220°C

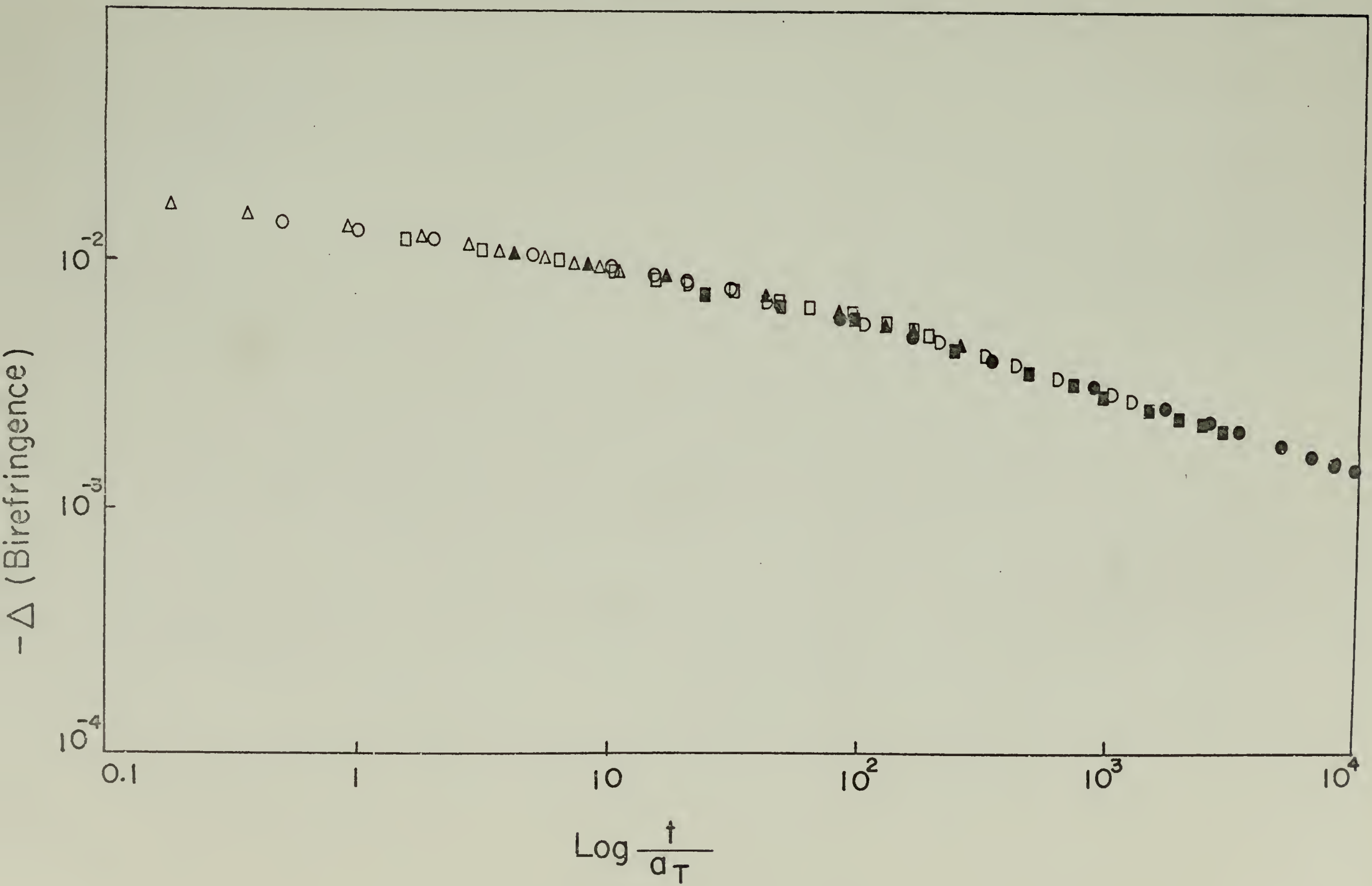

Figure 26

50 %

$T_{ref} = 220^{\circ}C$

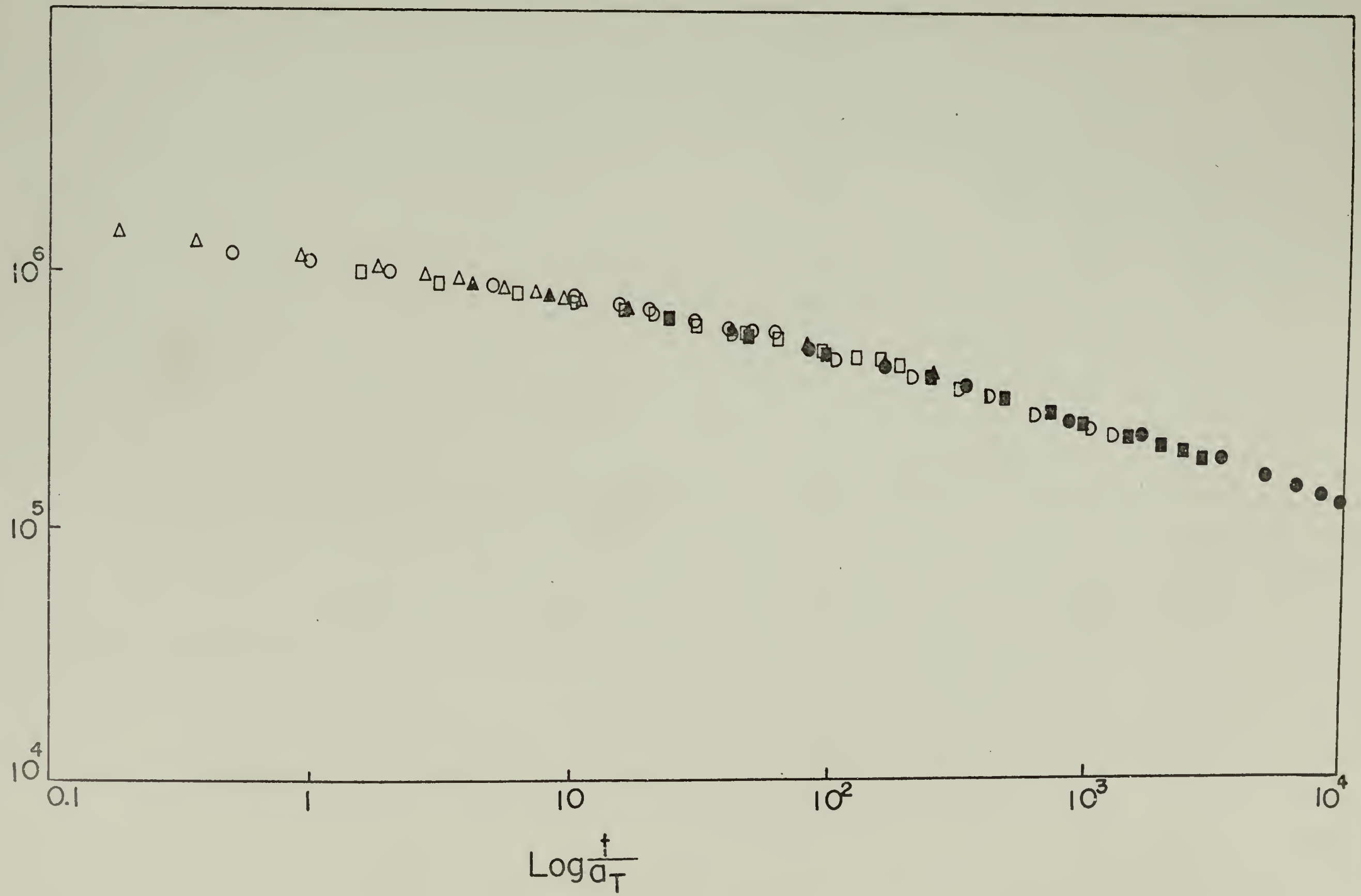

Figure 27

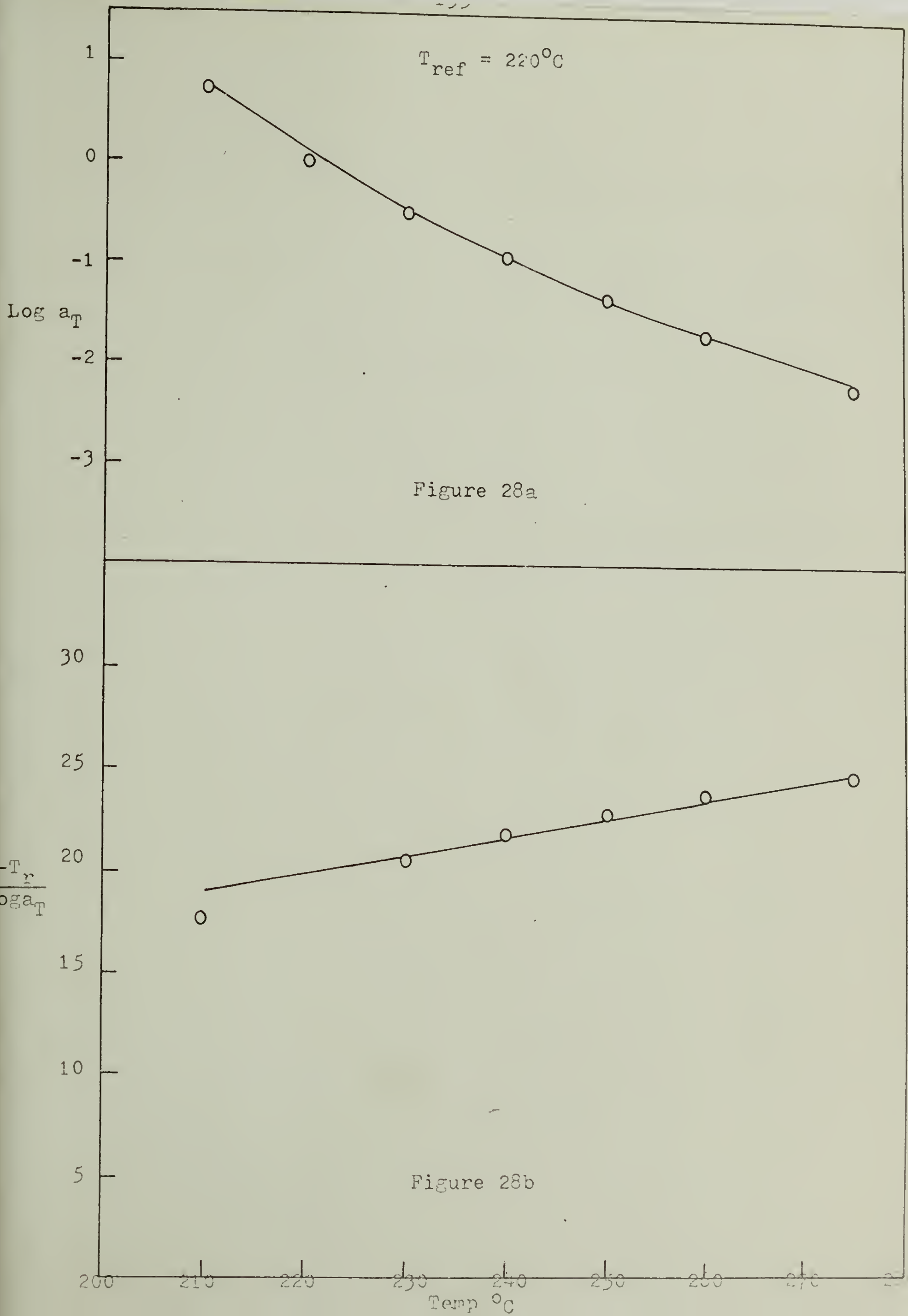

Figure 28a

Figure 28b

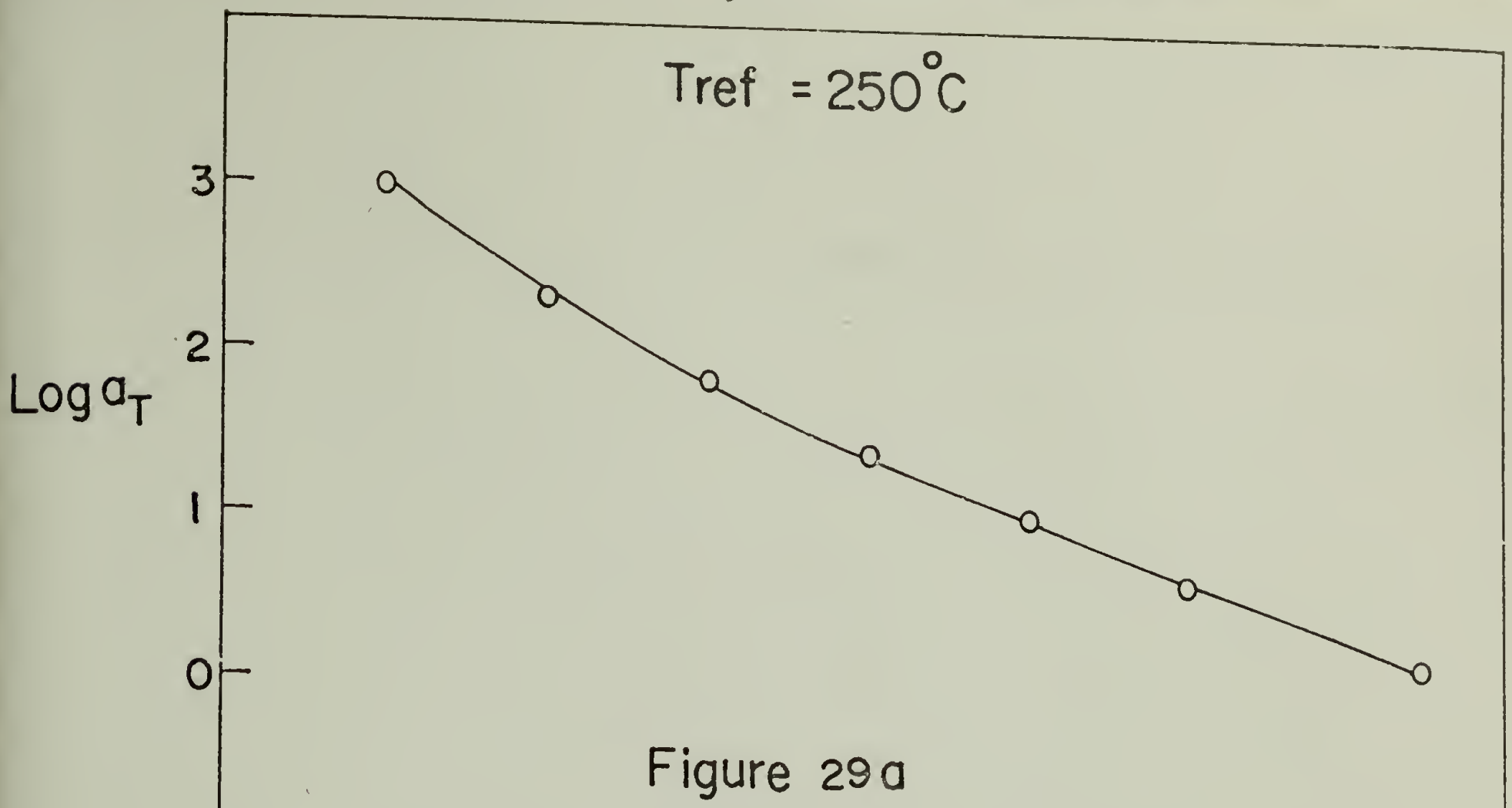

Figure 29a

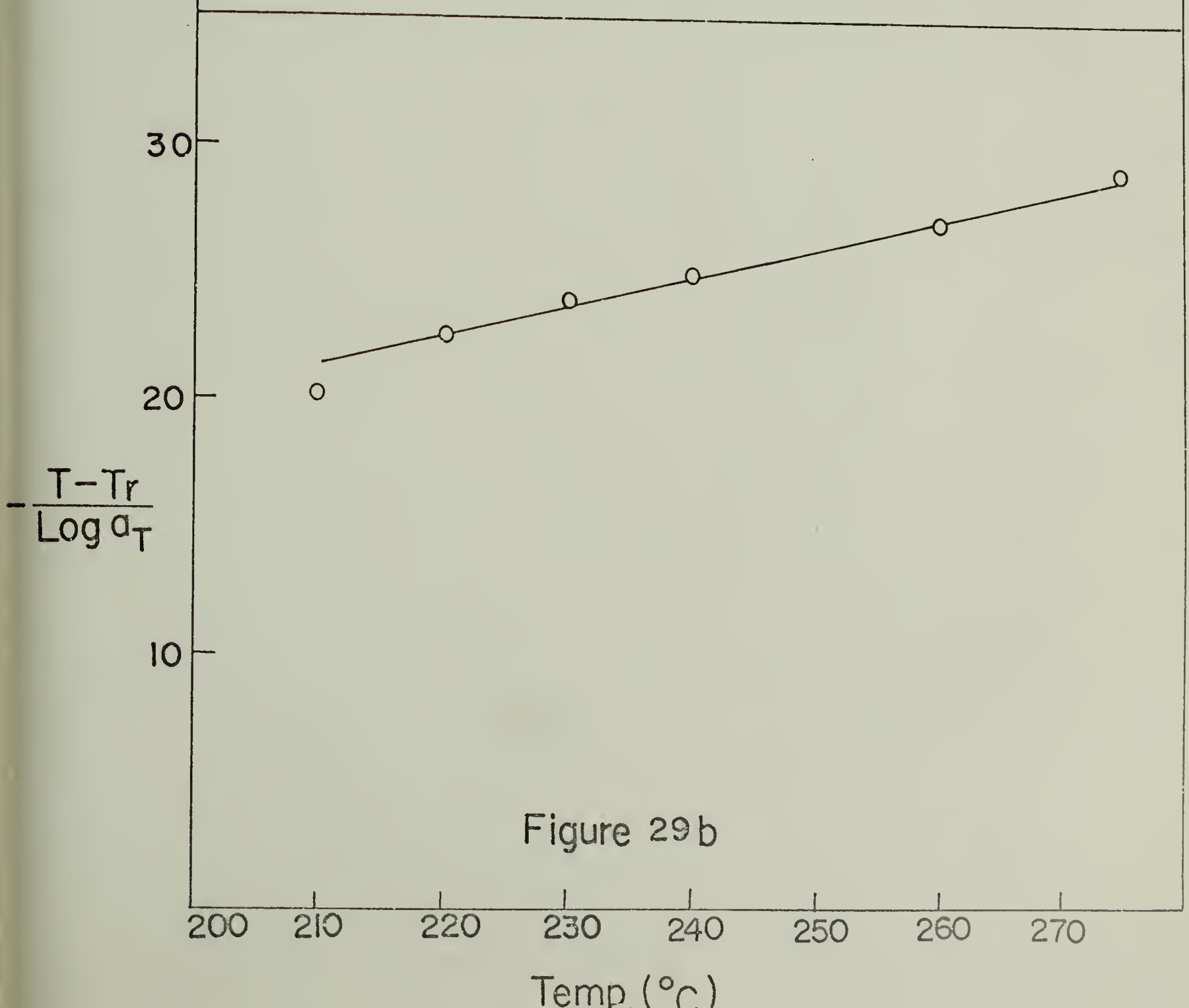

Figure 29b

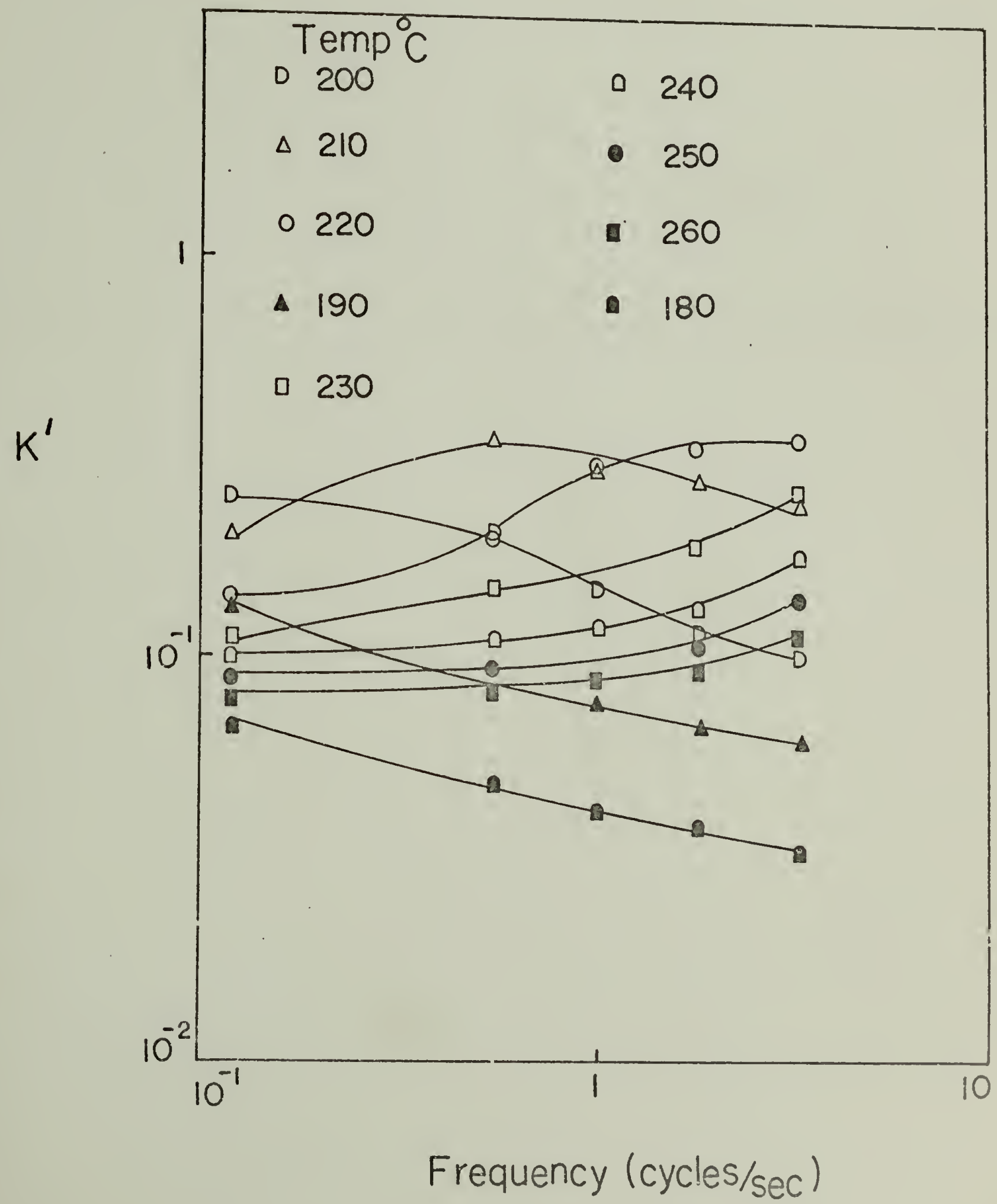
Temp °C
200
210
220
190
230
240
250
260
180
K'
1
10^{-1}
10^{-2}
10^{-1}
1
10
Frequency (cycles/sec)

Figure 30

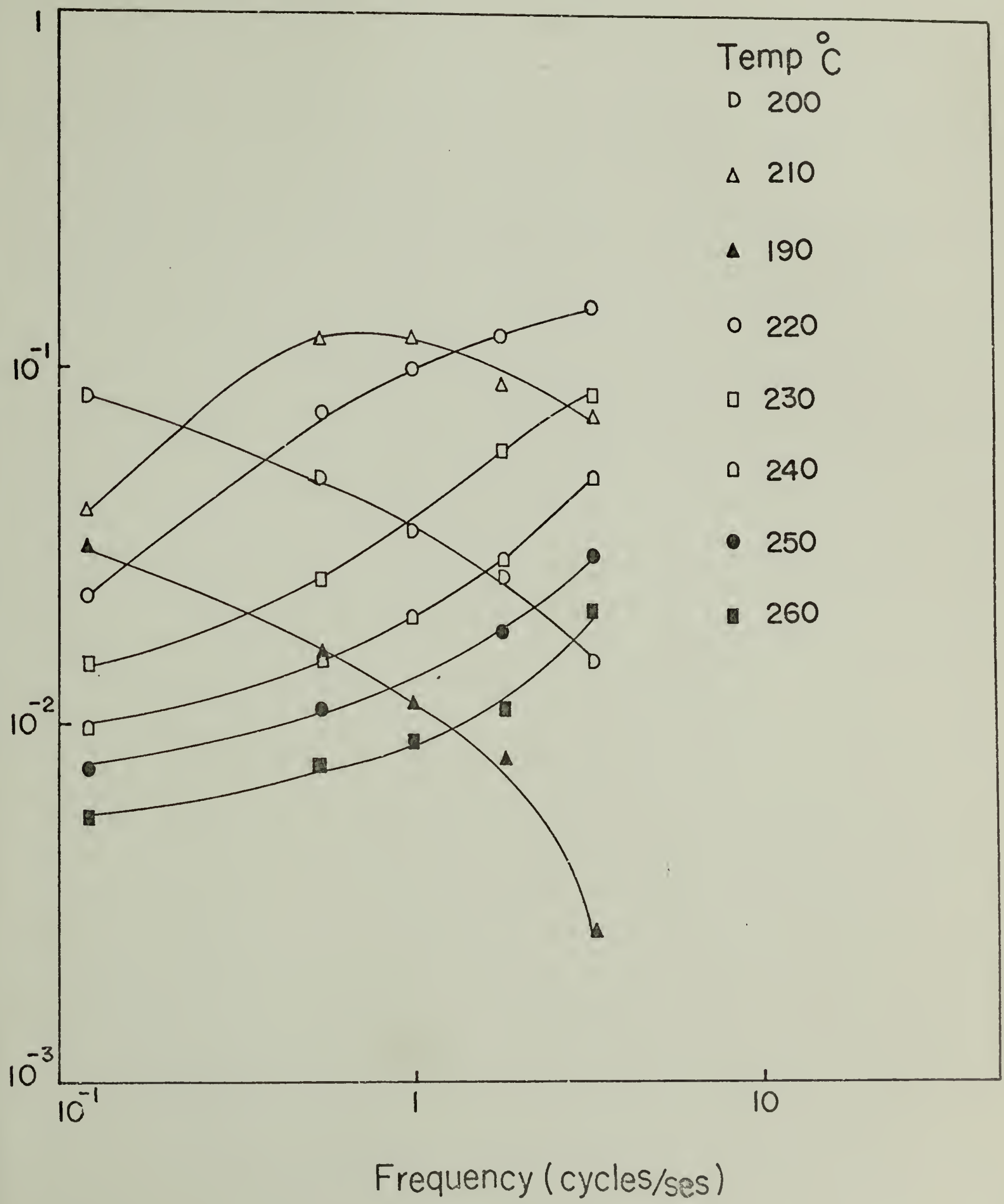
1
10^{-1}
10^{-2}
10^{-3}
K''
Temp °C
D 200
Δ 210
▲ 190
o 220
□ 230
▯ 240
● 250
■ 260
10^{-1}
1
10
Frequency (cycles/ses)

Figure 31

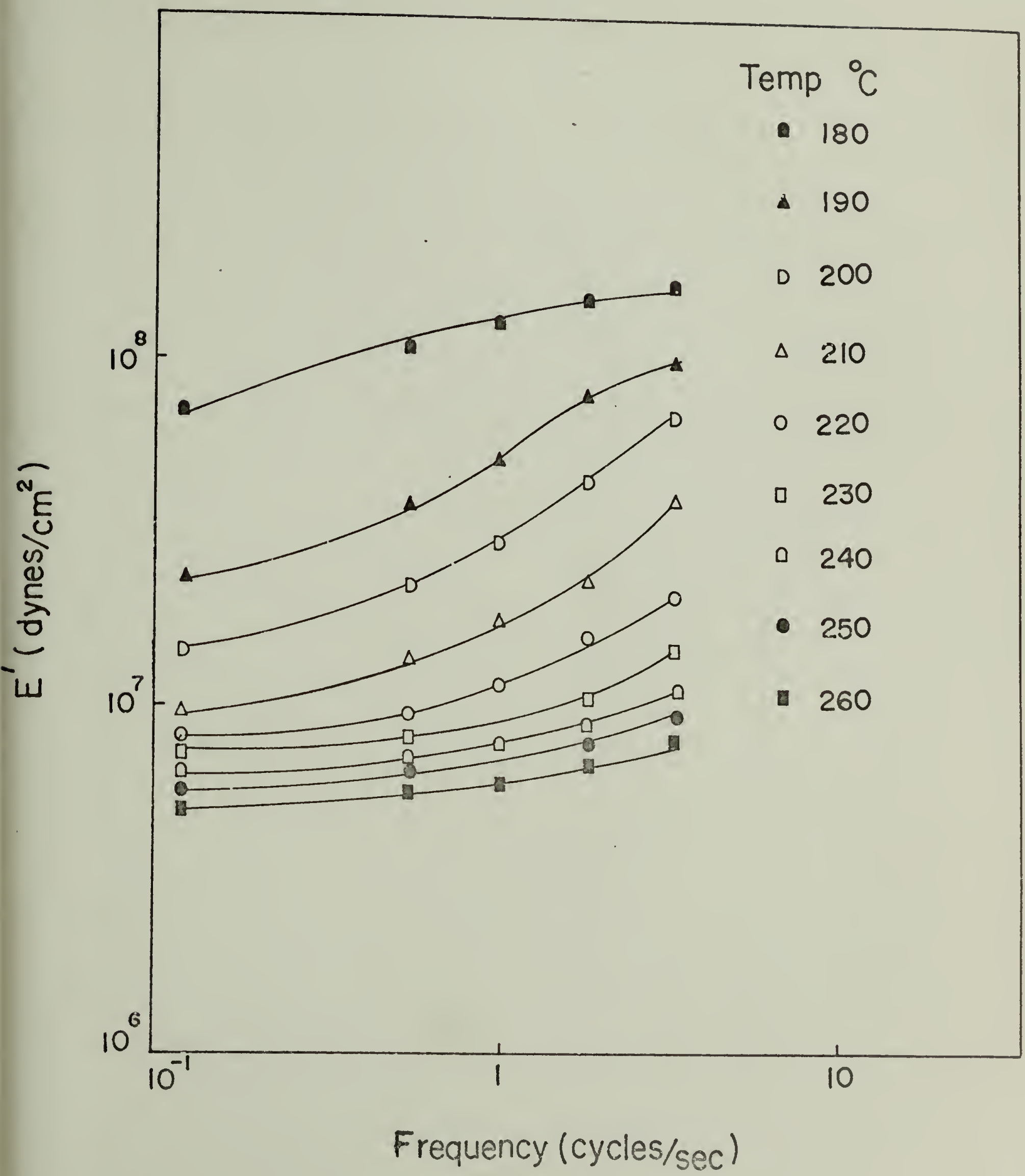
Temp °C
180
190
200
210
220
230
240
250
260
10^8
10^7
10^6
E' (dynes/cm^2)
10^{-1}
1
10
Frequency (cycles/sec)

Figure 32

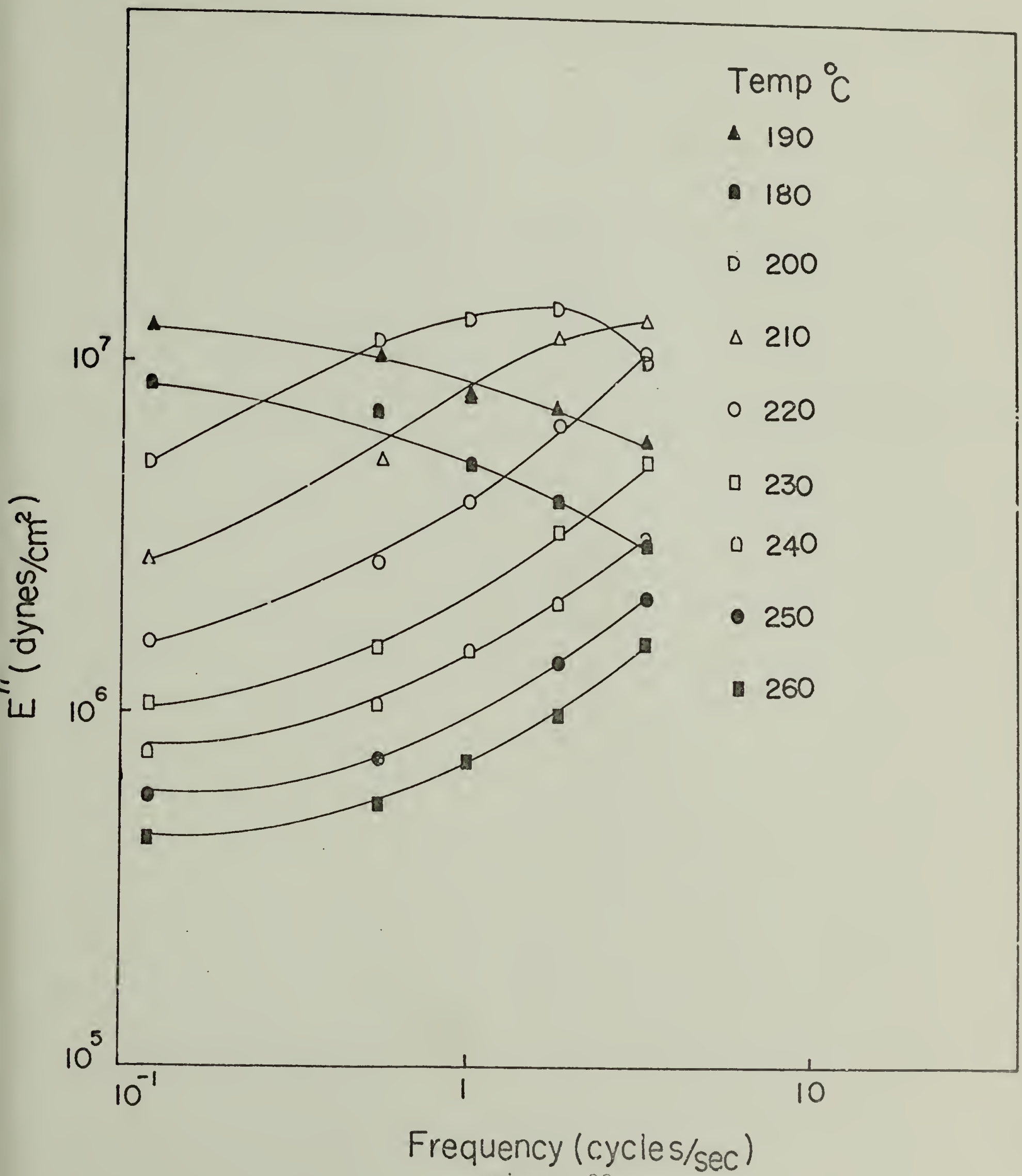
Temp °C
190
180
200
210
220
230
240
250
260
10^7
10^6
10^5
E'' (dynes/cm²)
10^{-1}
1
10
Frequency (cycles/sec)

Figure 33

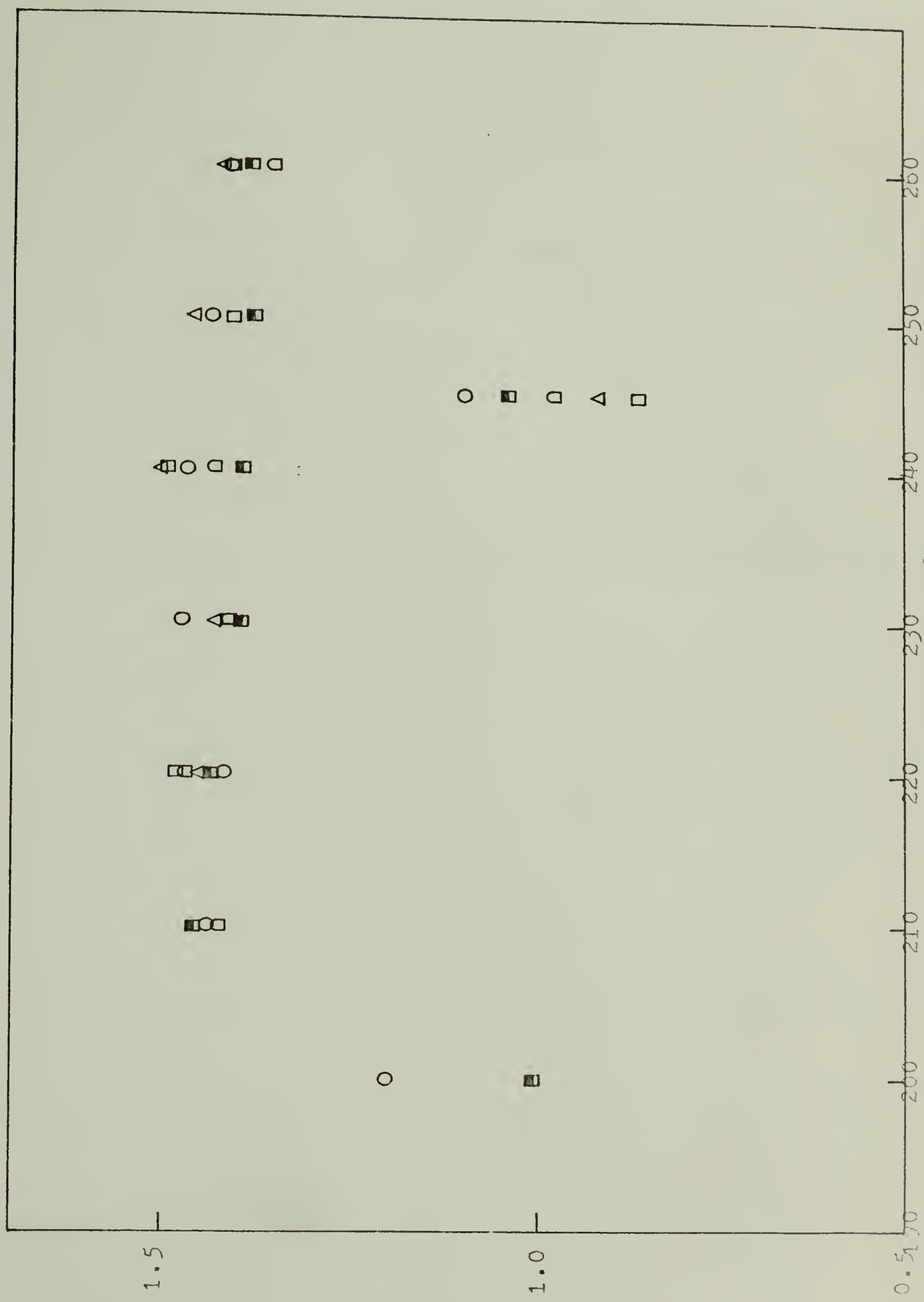
S.O.C. x10³ cm²/dynes
1.5
1.0
0.5
Temperature°C
190
200
210
220
230
240
250
260

Figure 34

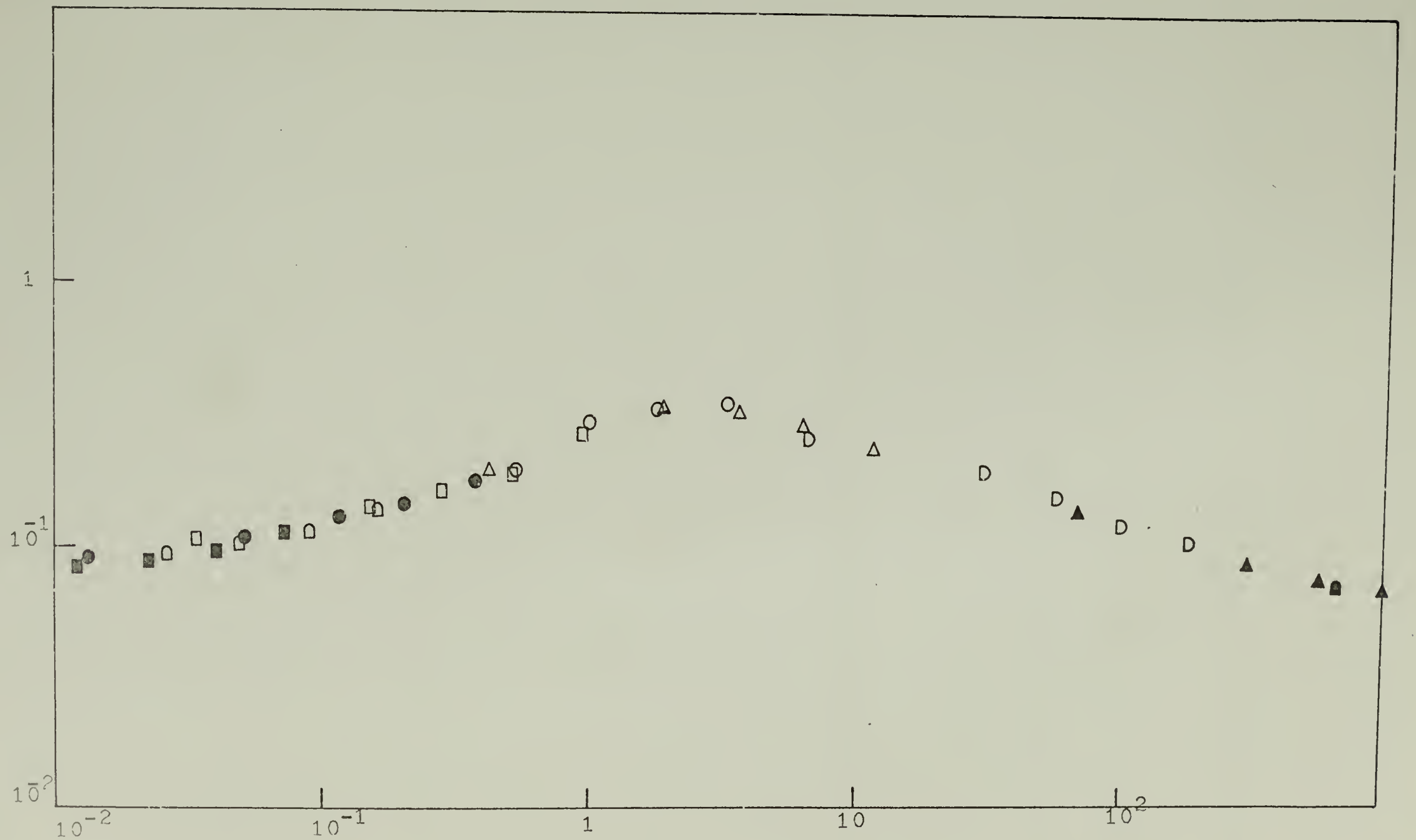

Frequency (cycles/sec)

Figure 35

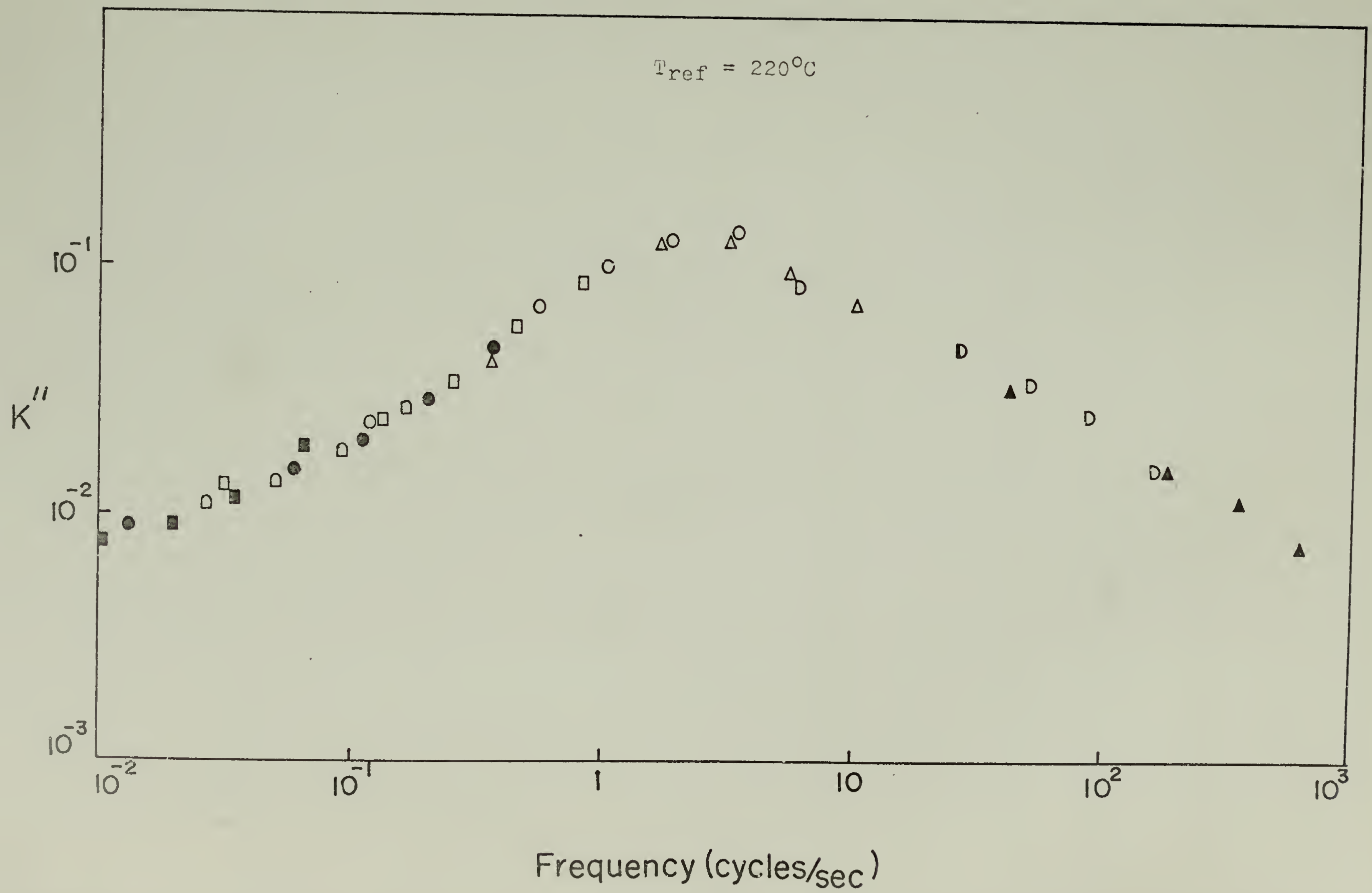
T_{ref} = 220°C
K''
10^{-1}
10^{-2}
10^{-3}
10^{-2}
10^{-1}
1
10
10^{2}
10^{3}
Frequency (cycles/sec)

Figure 36

$T_{ref.} = 220^{\circ}C$

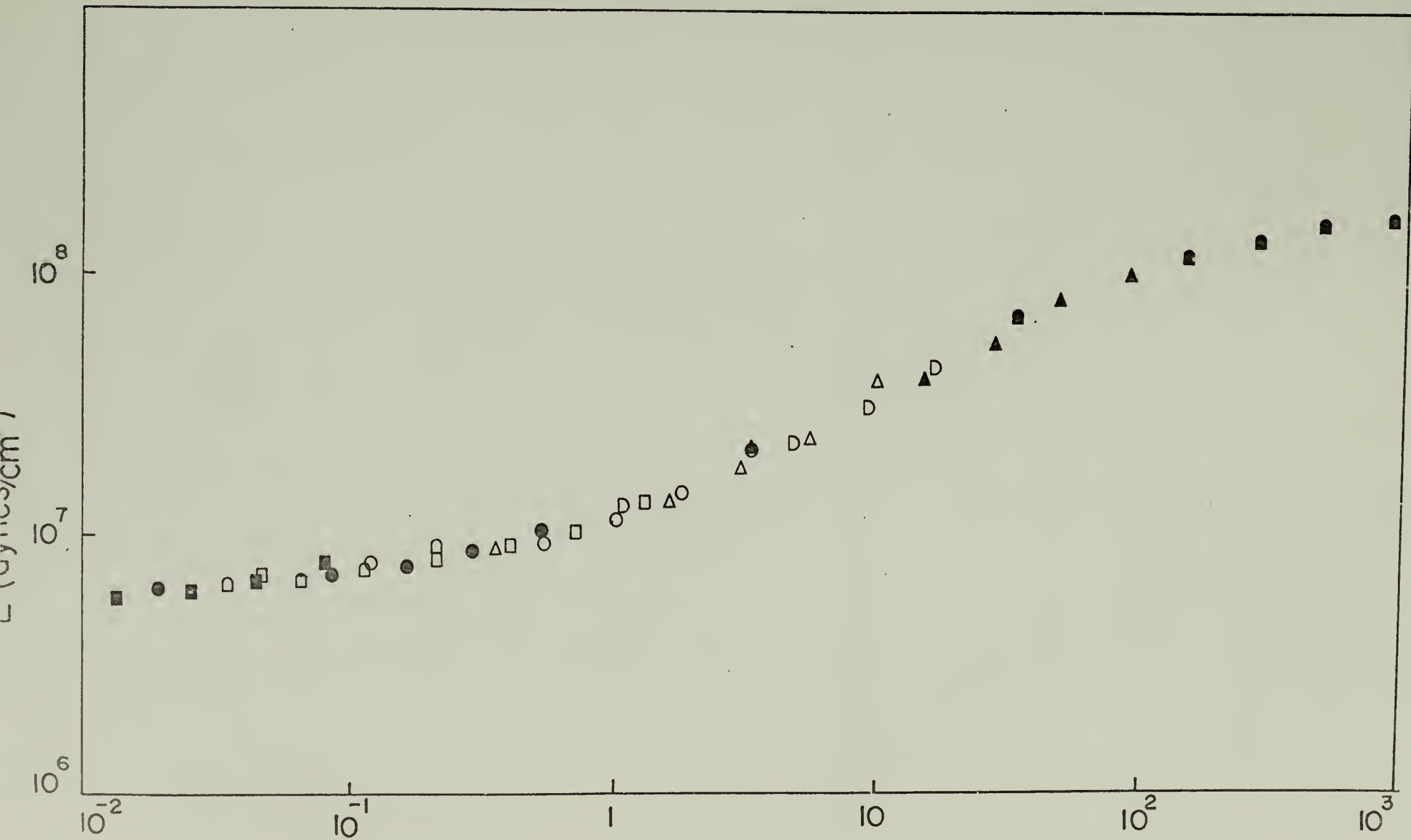

Figure 37

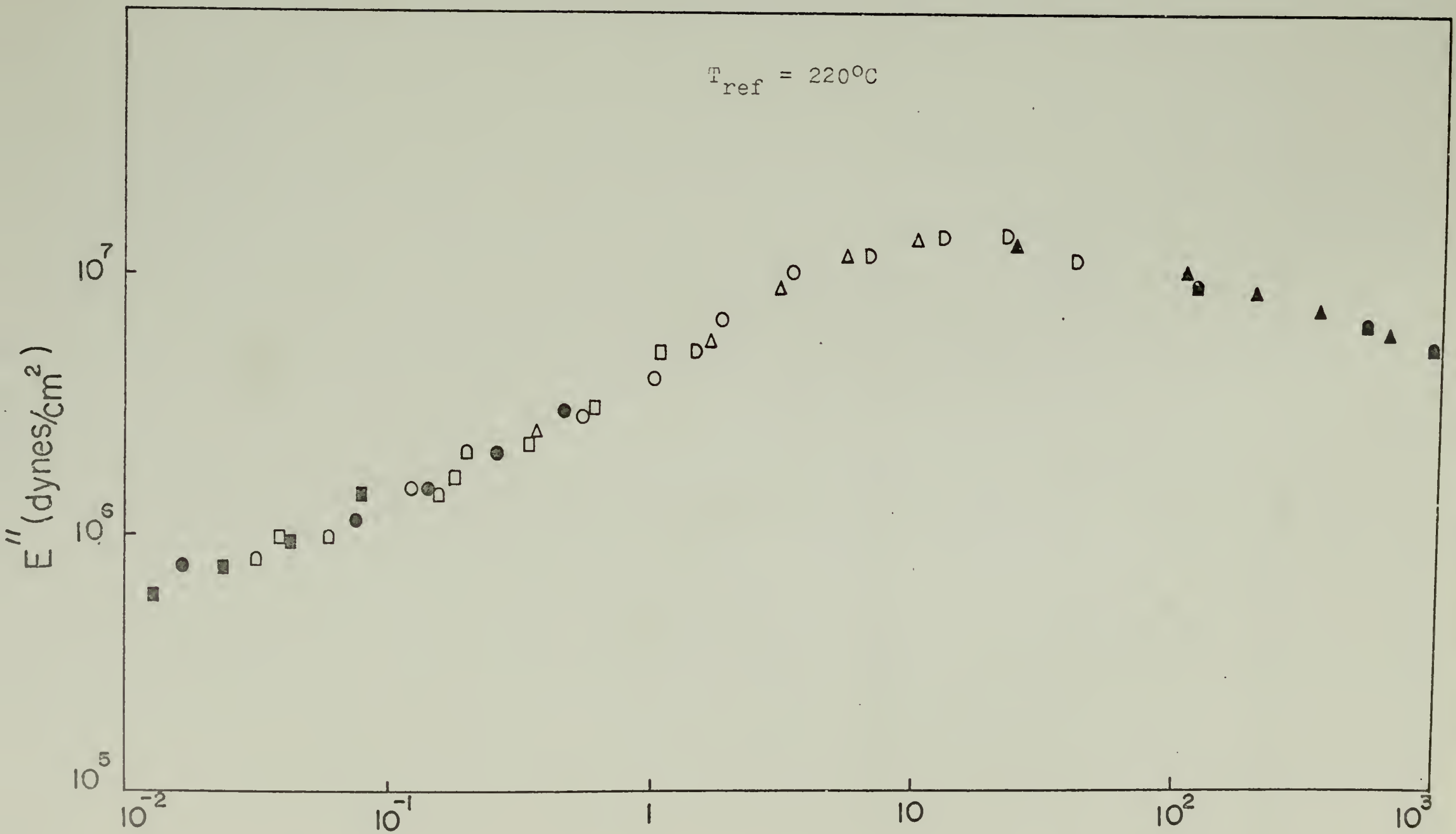
T_{ref} = 220°C
10^7
10^6
10^5
E'' (dynes/cm²)
10^{-2}
10^{-1}
1
10
10^2
10^3
Frequency (cycles/sec)

Figure 38

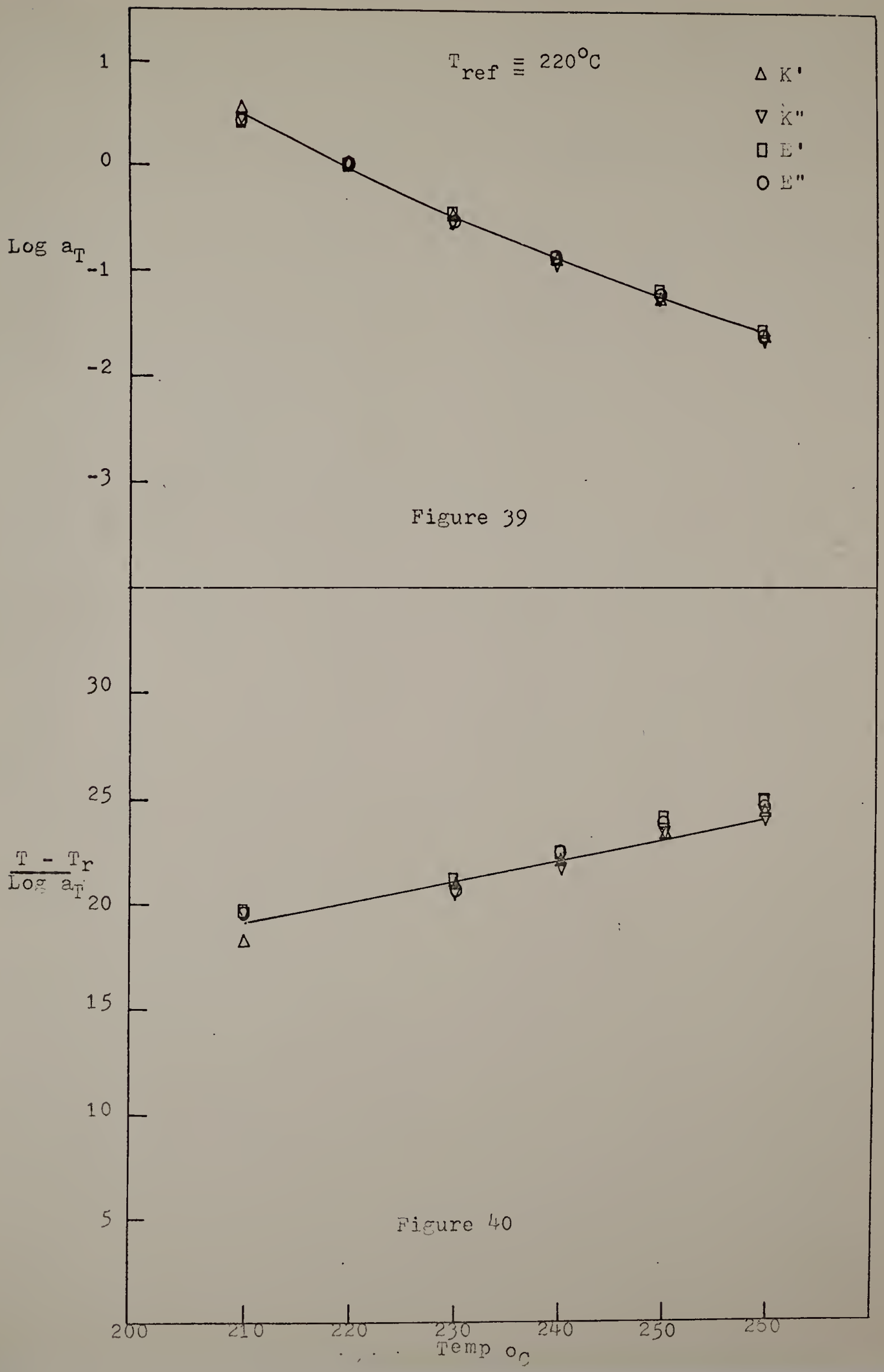

Figure 39

Figure 40

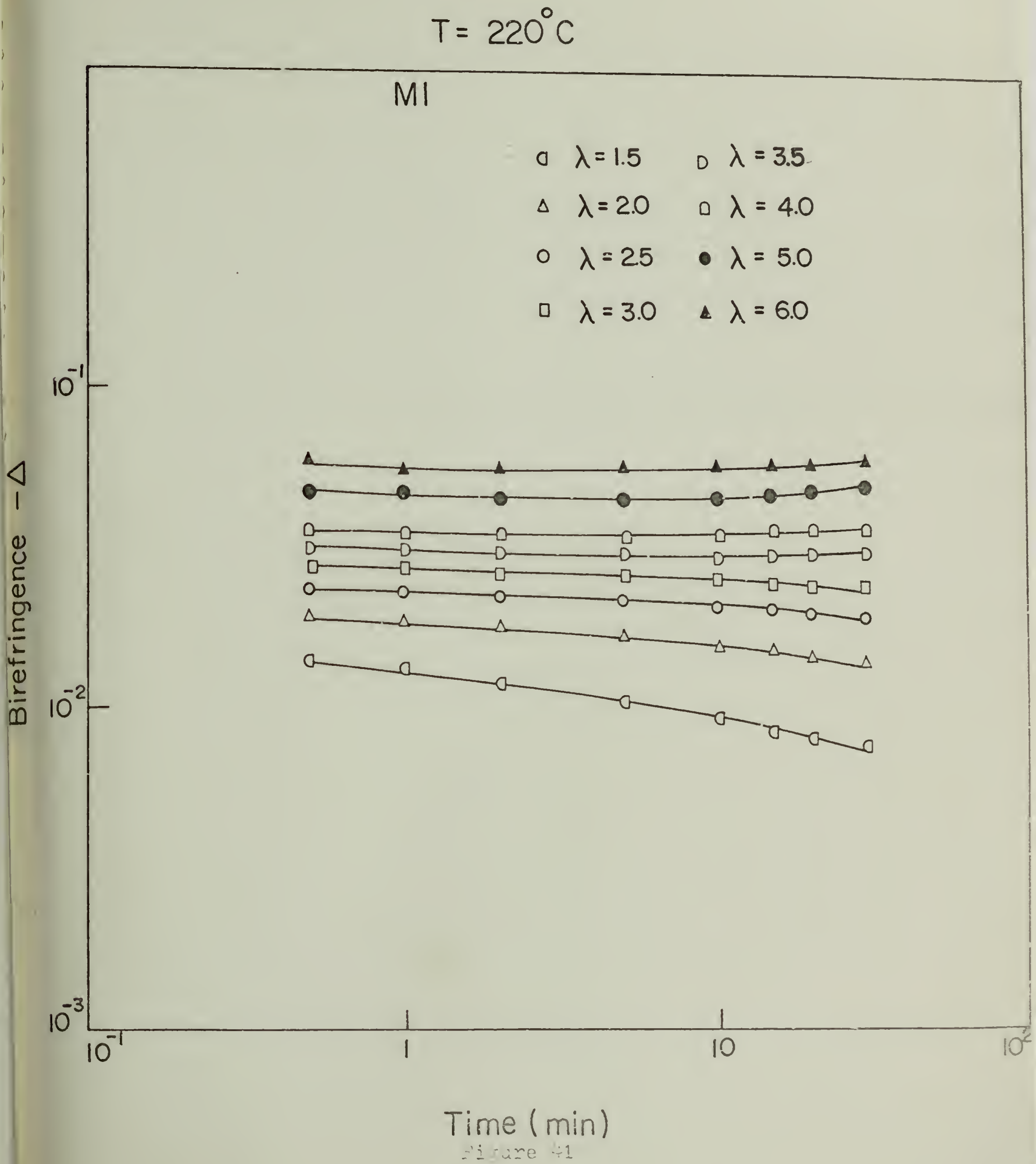
T = 220°C
M1
λ = 1.5
λ = 2.0
λ = 2.5
λ = 3.0
λ = 3.5
λ = 4.0
λ = 5.0
λ = 6.0
Birefringence - Δ
10⁻¹
10⁻²
10⁻³
10⁻¹
1
10
10²
Time (min)

Figure 41

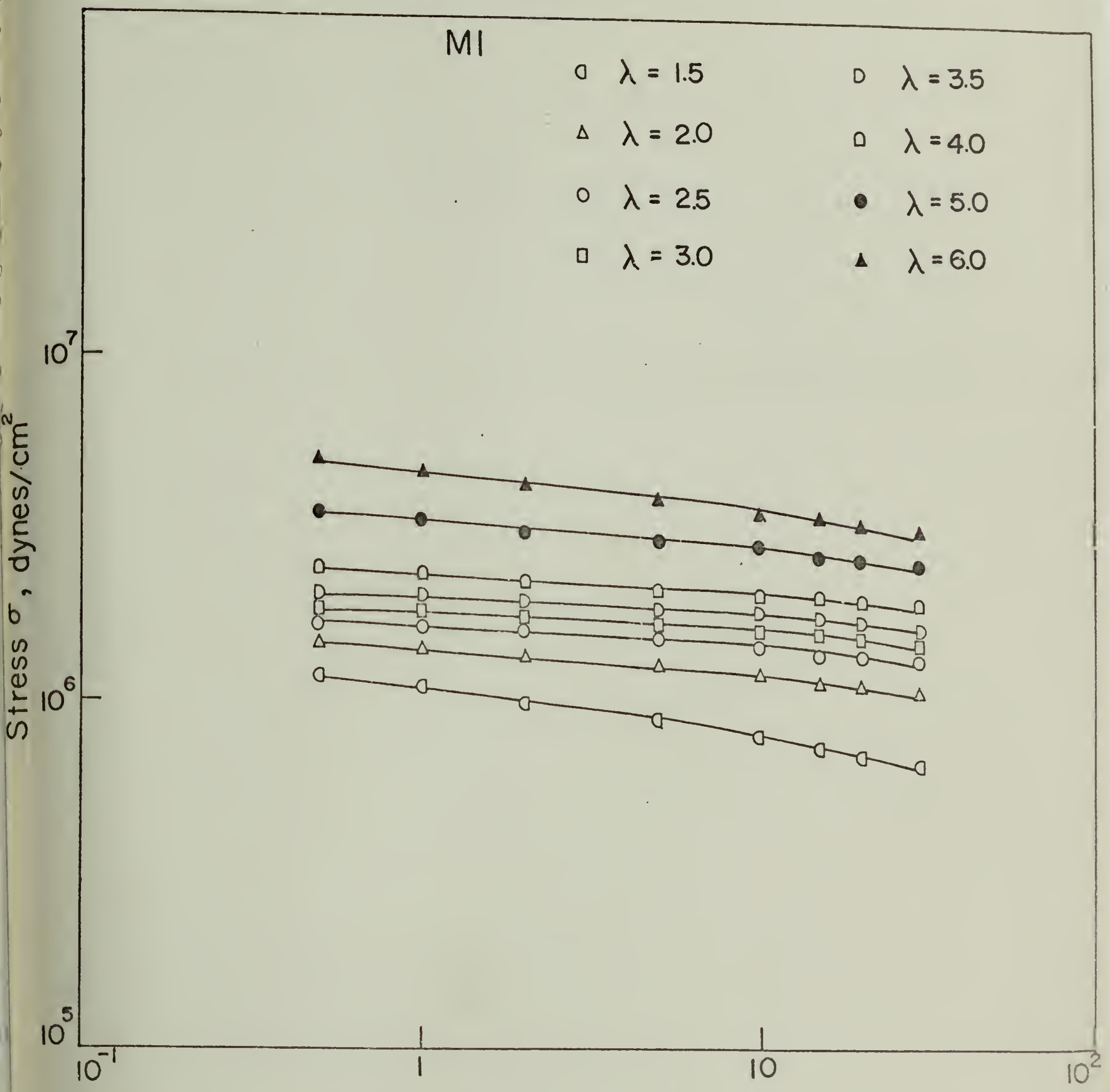
T = 220°C
MI
□ λ = 1.5
△ λ = 2.0
○ λ = 2.5
□ λ = 3.0
▷ λ = 3.5
▭ λ = 4.0
● λ = 5.0
▲ λ = 6.0
Stress σ, dynes/cm²
10⁷
10⁶
10⁵
10⁻¹
1
10
10²
Time (min)

Figure 42

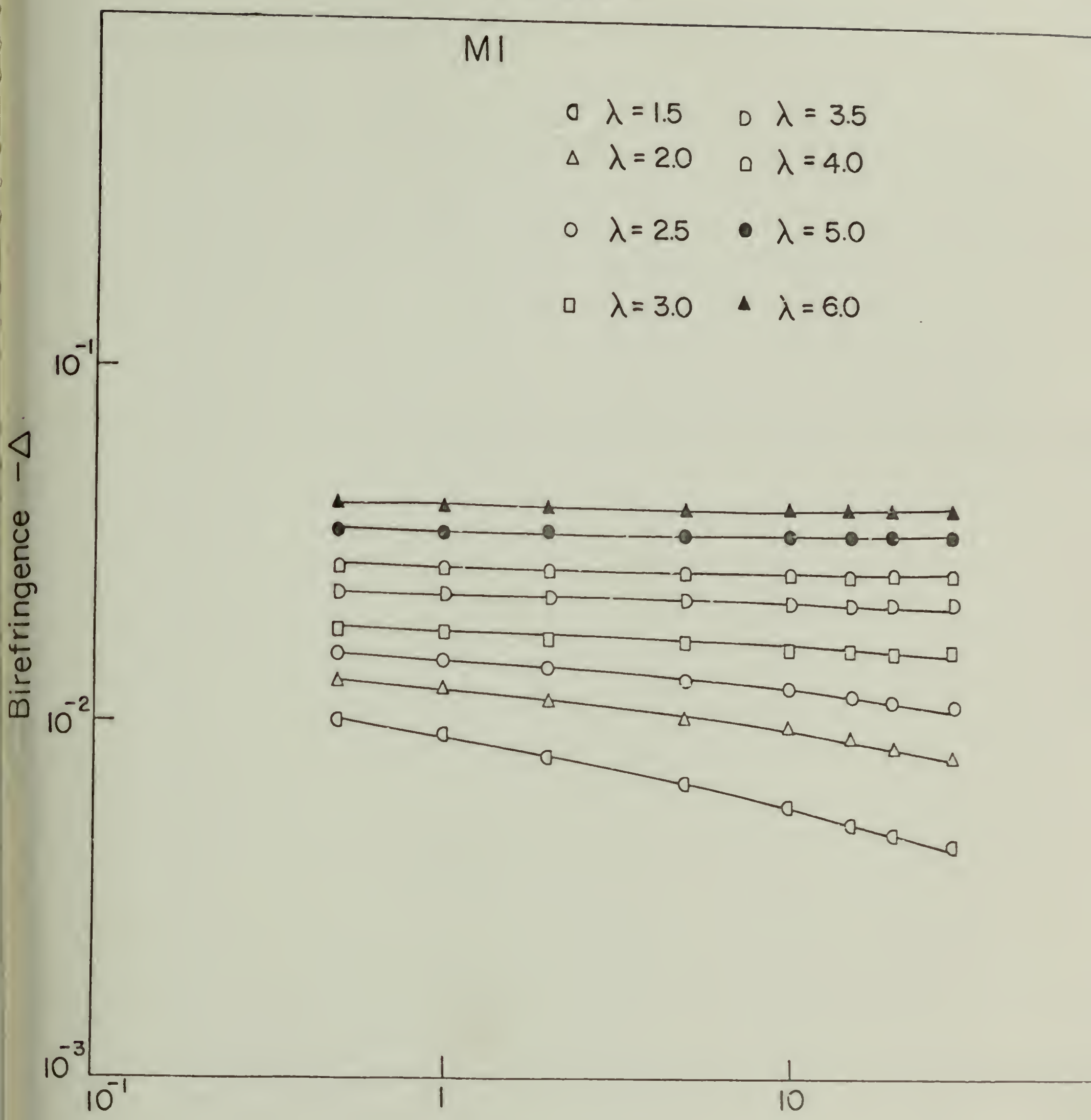
T = 240°C
M1
λ = 1.5
λ = 2.0
λ = 2.5
λ = 3.0
λ = 3.5
λ = 4.0
λ = 5.0
λ = 6.0
Birefringence -Δ
10⁻¹
10⁻²
10⁻³
10⁻¹
1
10
Time (min)

Figure M3

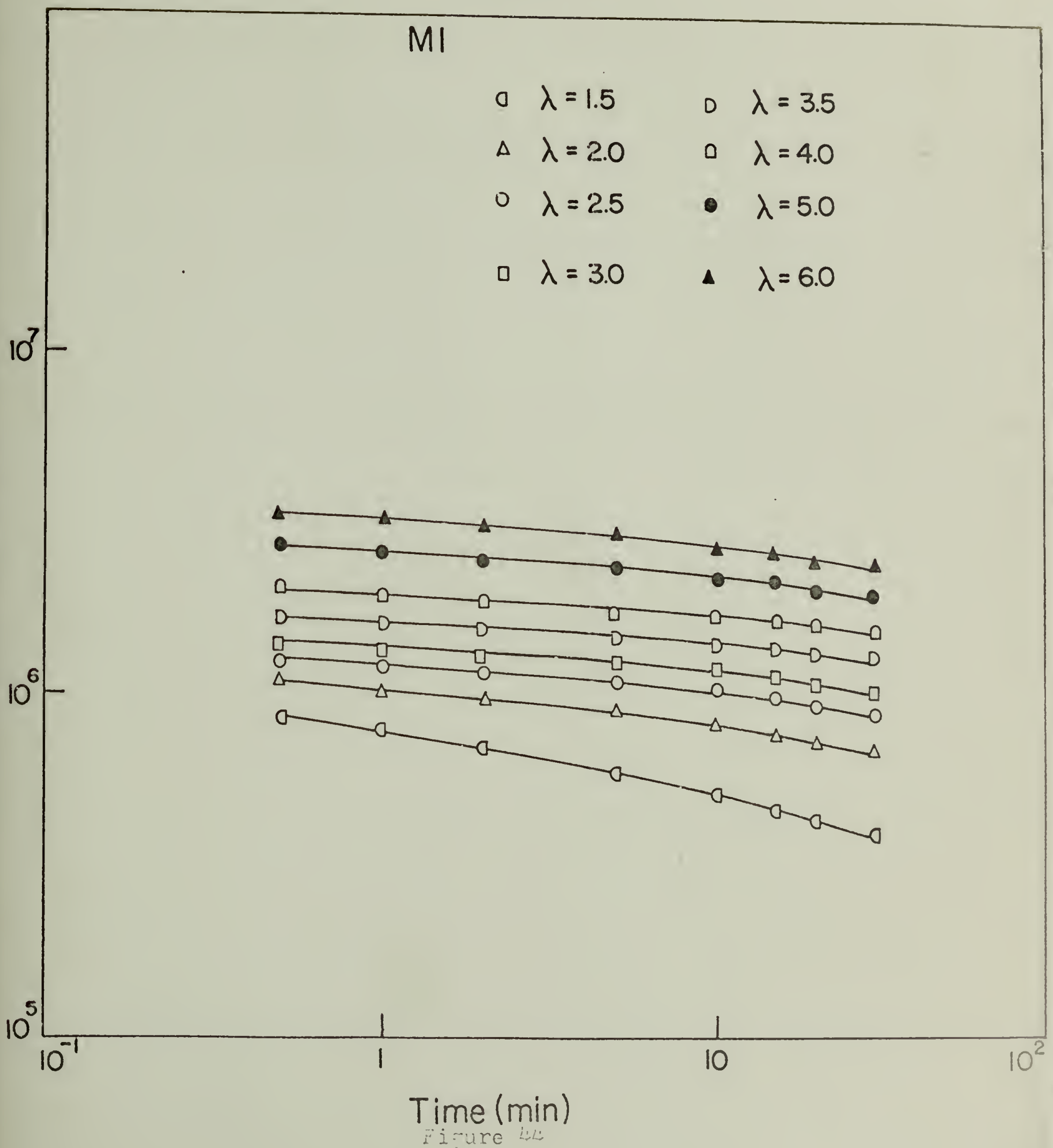
T = 240°C
MI
□ λ = 1.5
△ λ = 2.0
○ λ = 2.5
□ λ = 3.0
▷ λ = 3.5
▭ λ = 4.0
● λ = 5.0
▲ λ = 6.0
Stress σ , dynes/cm²
10⁷
10⁶
10⁵
10⁻¹
1
10
10²
Time (min)

Figure 44

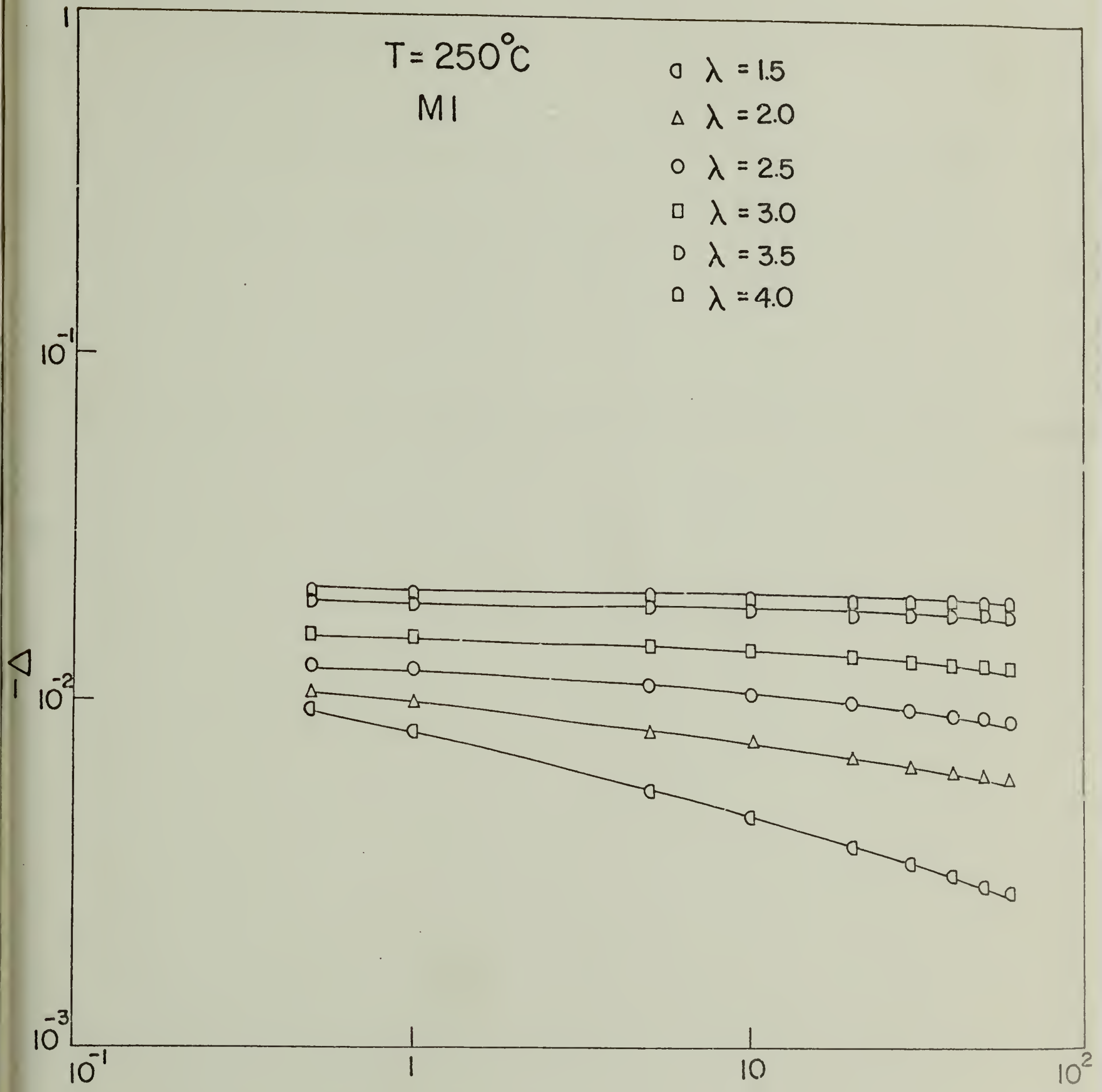
T = 250°C
M I
□ λ = 1.5
△ λ = 2.0
○ λ = 2.5
□ λ = 3.0
D λ = 3.5
□ λ = 4.0
1
10^-1
10^-2
10^-3
-Δ
10^-1
1
10
10^2
Time (min)

Figure 45

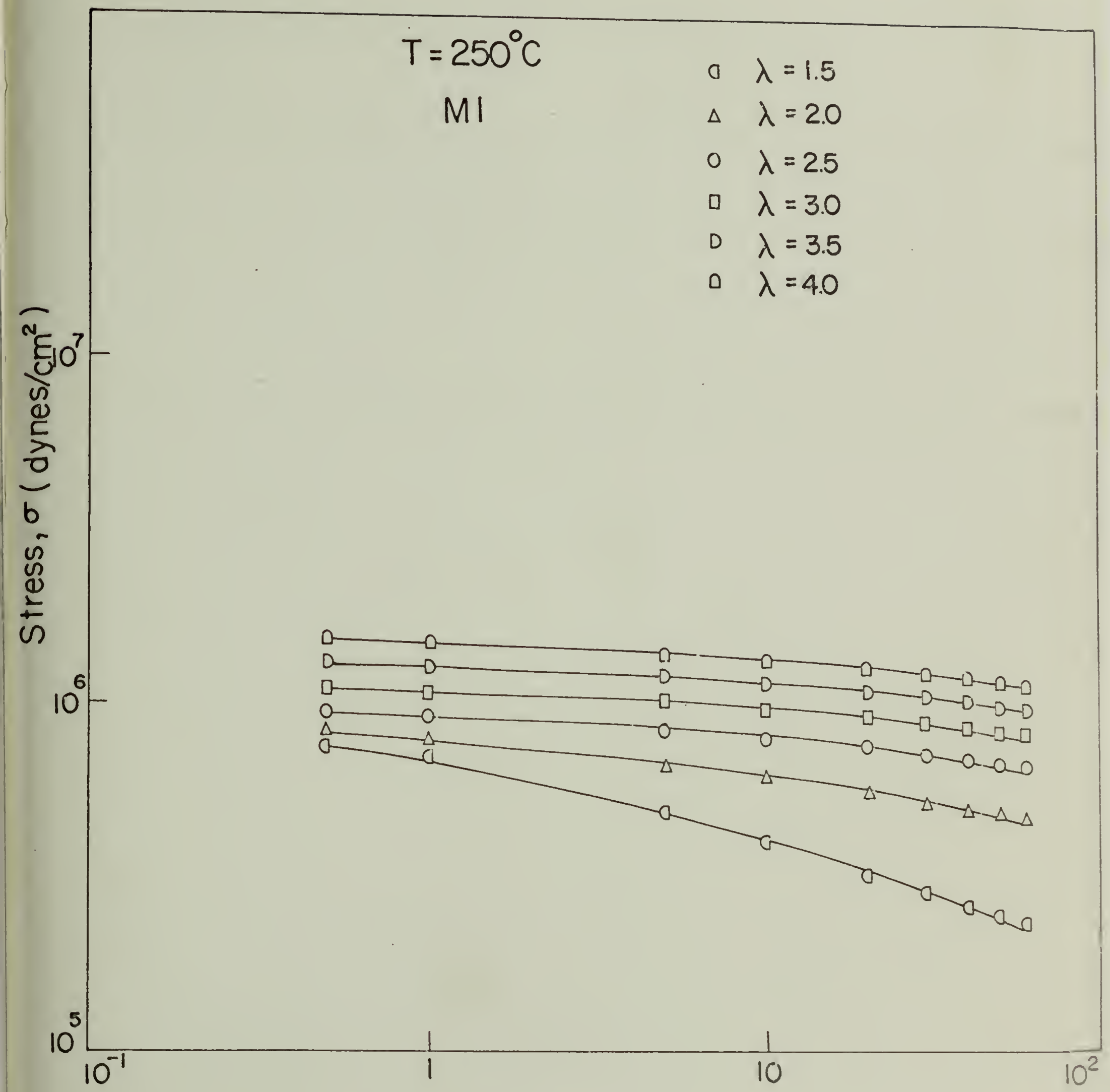
T = 250°C
MI
□ λ = 1.5
△ λ = 2.0
○ λ = 2.5
□ λ = 3.0
D λ = 3.5
□ λ = 4.0
Stress, σ (dynes/cm²)
10⁷
10⁶
10⁵
10⁻¹
1
10
10²
Time (min)

Figure 46

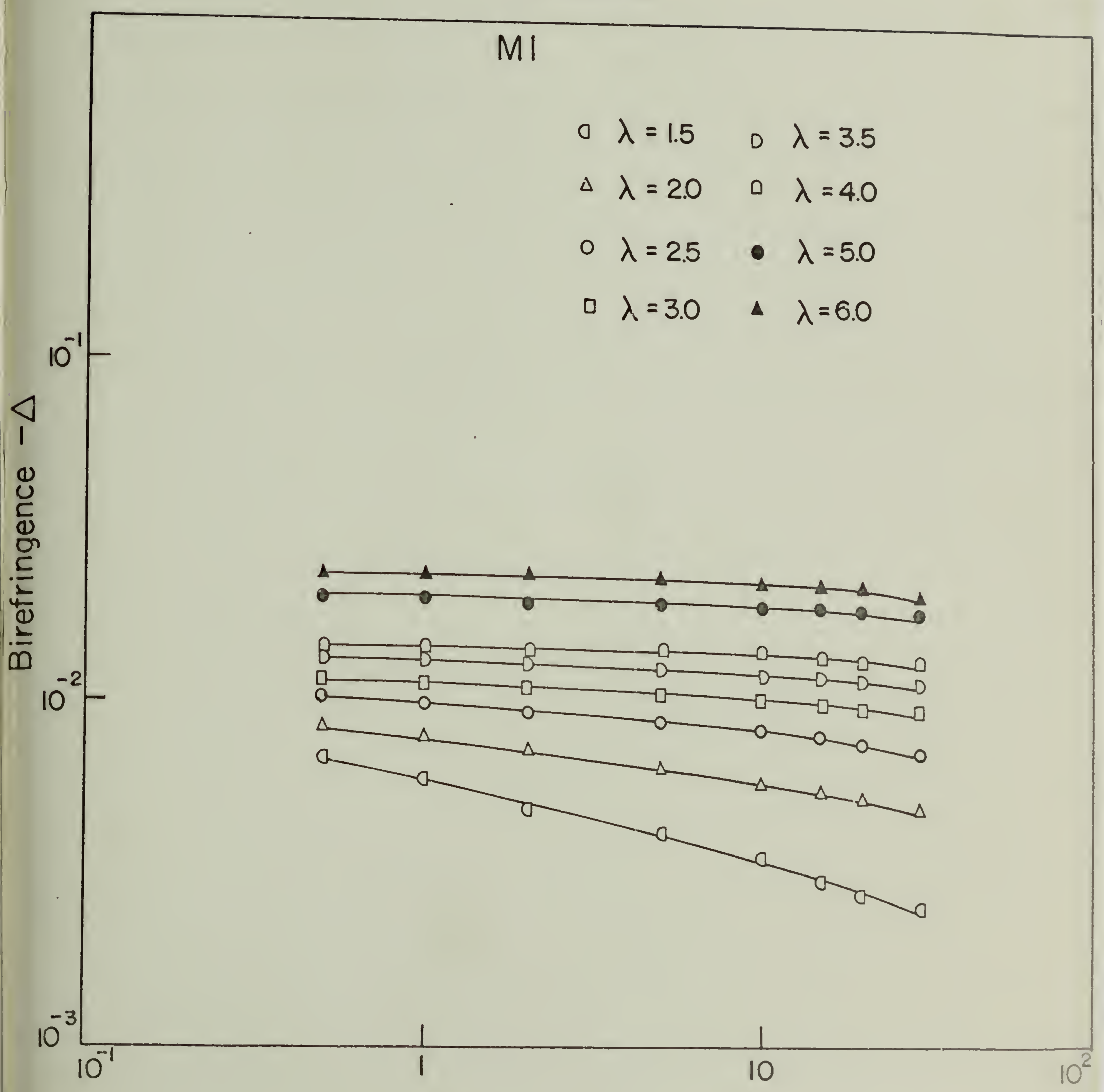
T = 260°C
MI
λ = 1.5
λ = 2.0
λ = 2.5
λ = 3.0
λ = 3.5
λ = 4.0
λ = 5.0
λ = 6.0
Birefringence - Δ
10⁻¹
10⁻²
10⁻³
10⁻¹
1
10
10²
Time (min)

Figure 47

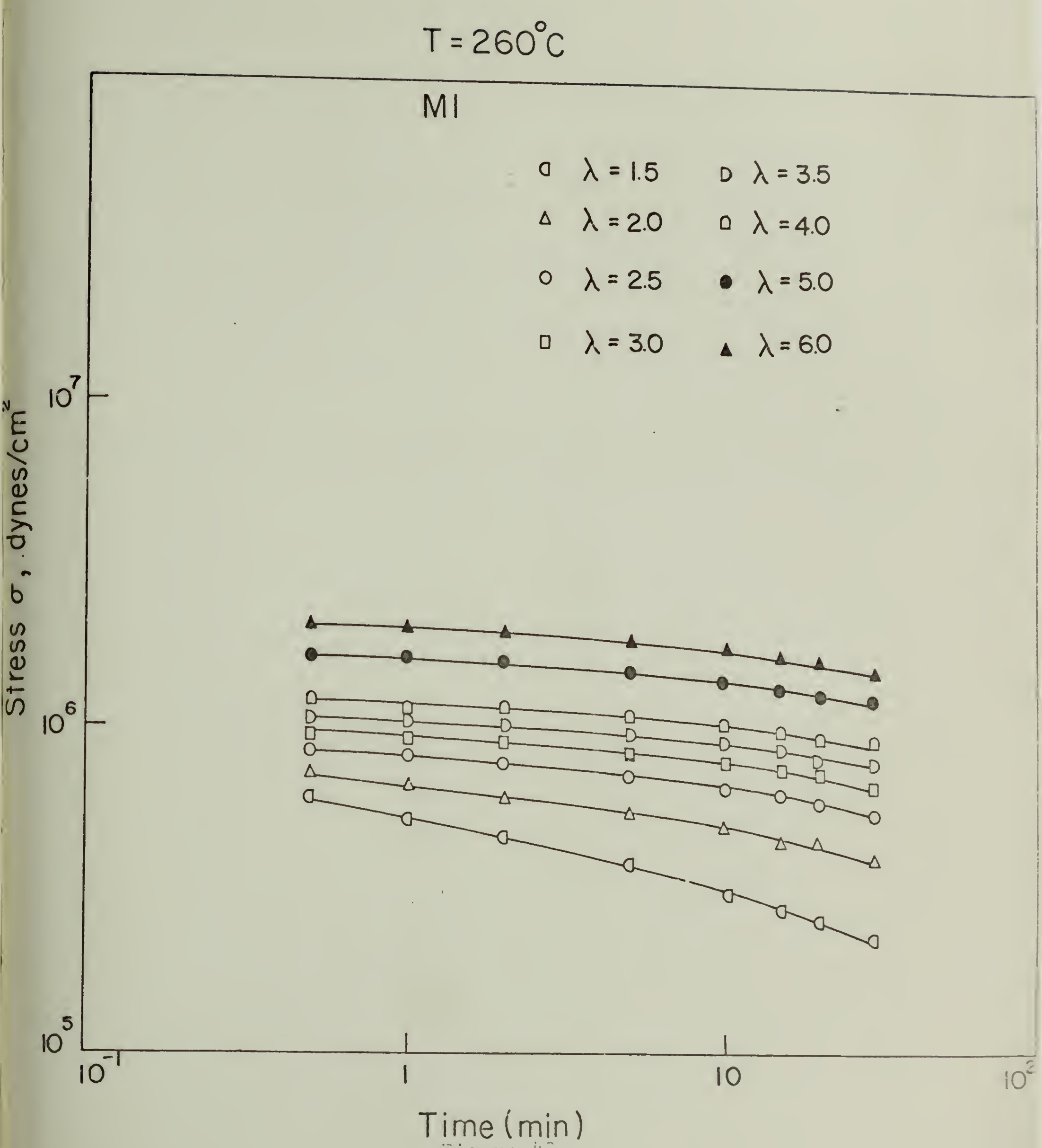
T = 260°C
MI
λ = 1.5
λ = 2.0
λ = 2.5
λ = 3.0
λ = 3.5
λ = 4.0
λ = 5.0
λ = 6.0
Stress σ, dynes/cm²
10⁷
10⁶
10⁵
10⁻¹
1
10
10²
Time (min)

Figure 43

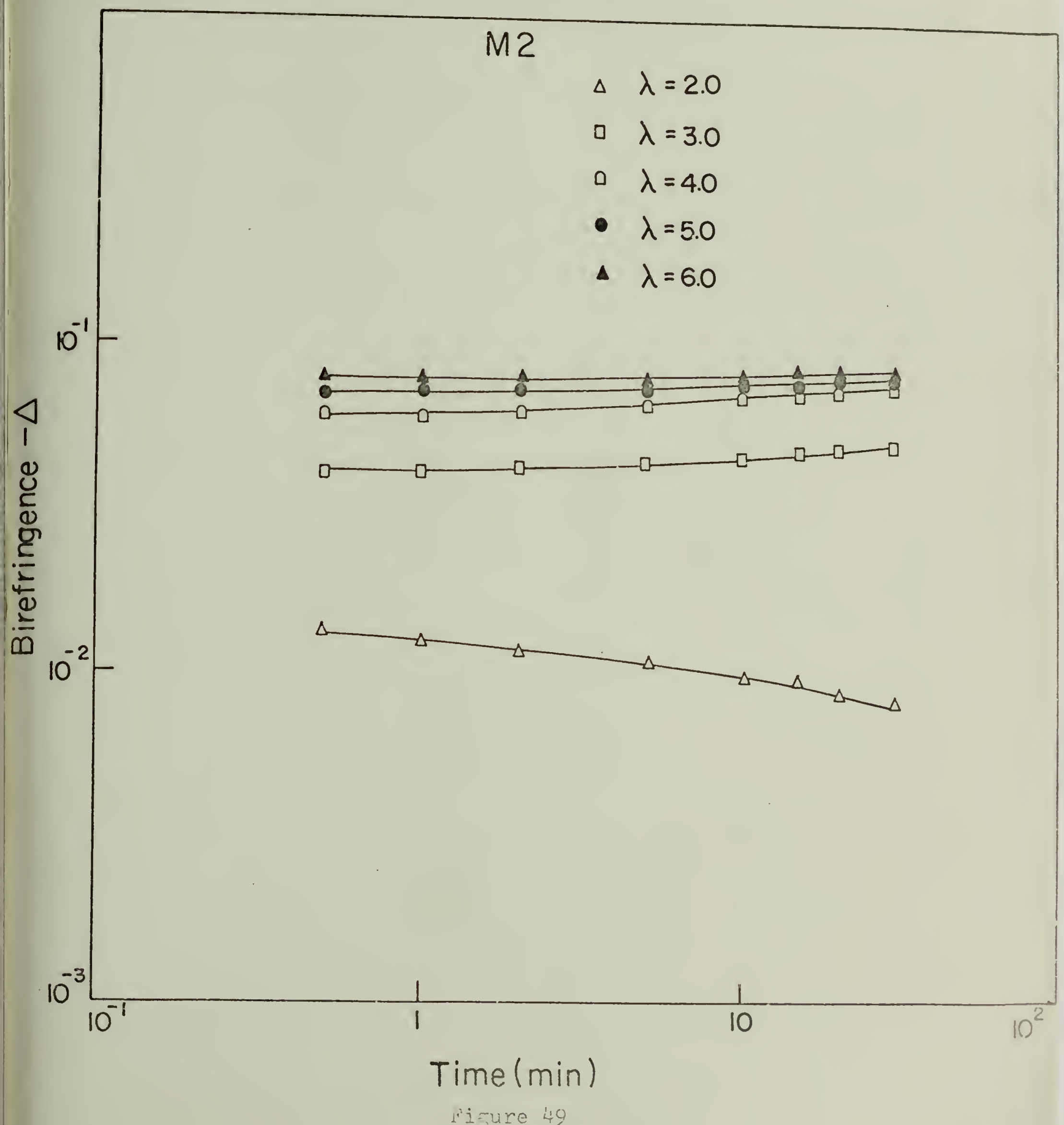
T = 240°C
M2
△ λ = 2.0
□ λ = 3.0
○ λ = 4.0
● λ = 5.0
▲ λ = 6.0
Birefringence -Δ
10⁻¹
10⁻²
10⁻³
10⁻¹
1
10
10²
Time (min)

Figure 49

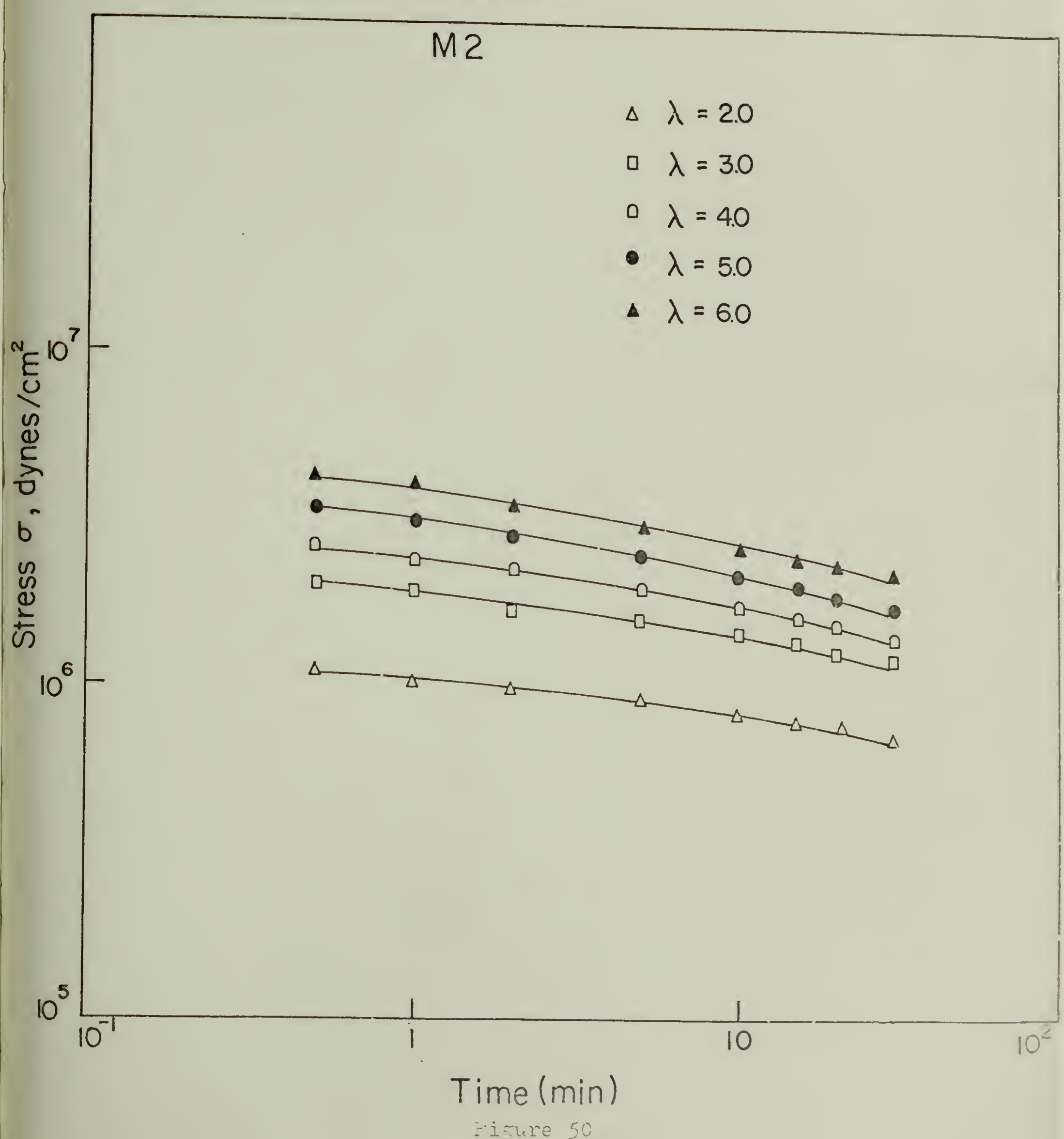
T = 240°C
M2
△ λ = 2.0
□ λ = 3.0
□ λ = 4.0
● λ = 5.0
▲ λ = 6.0
Stress σ, dynes/cm²
10⁷
10⁶
10⁵
10⁻¹
1
10
10²
Time (min)

Figure 50

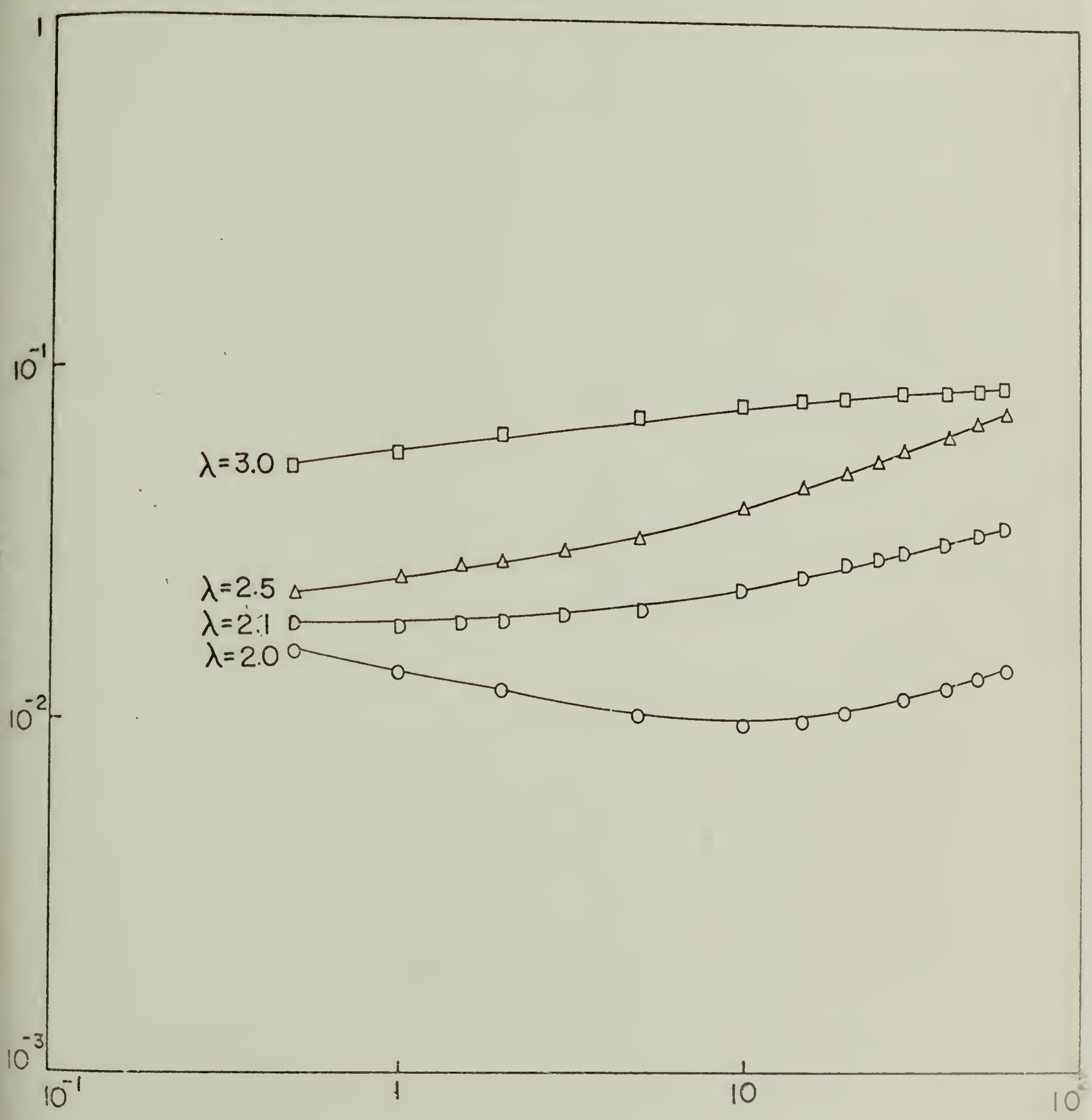
T = 260°C
1
10⁻¹
10⁻²
10⁻³
-Δ (Birefringence)
λ=3.0
λ=2.5
λ=2.1
λ=2.0
10⁻¹
1
10
10²
Time (min)

Figure 51

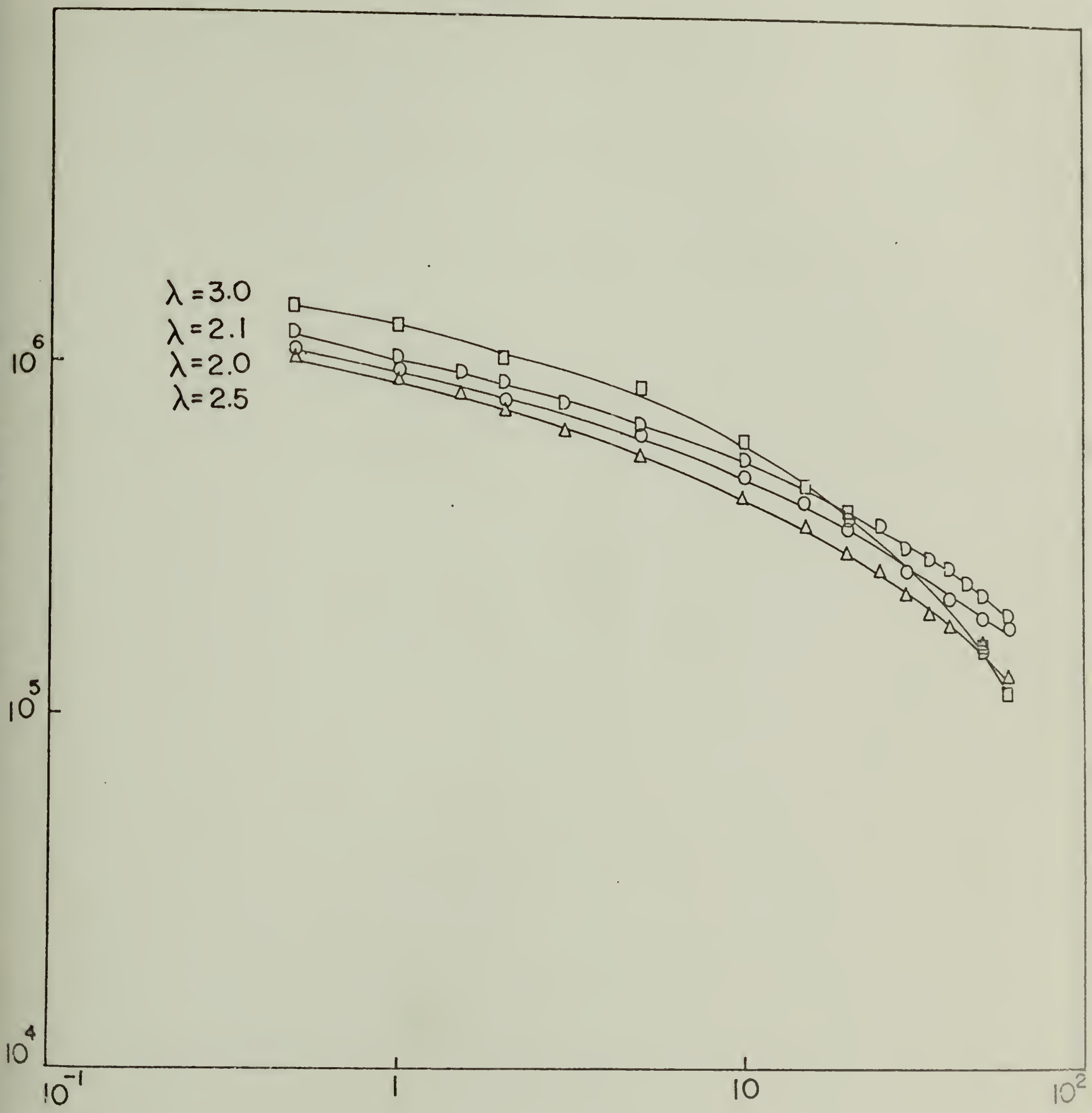
T = 260°C
λ = 3.0
λ = 2.1
λ = 2.0
λ = 2.5
σ, Stress (dynes/cm²)
10⁶
10⁵
10⁴
10⁻¹
1
10
10²
Time (min)

Figure 52

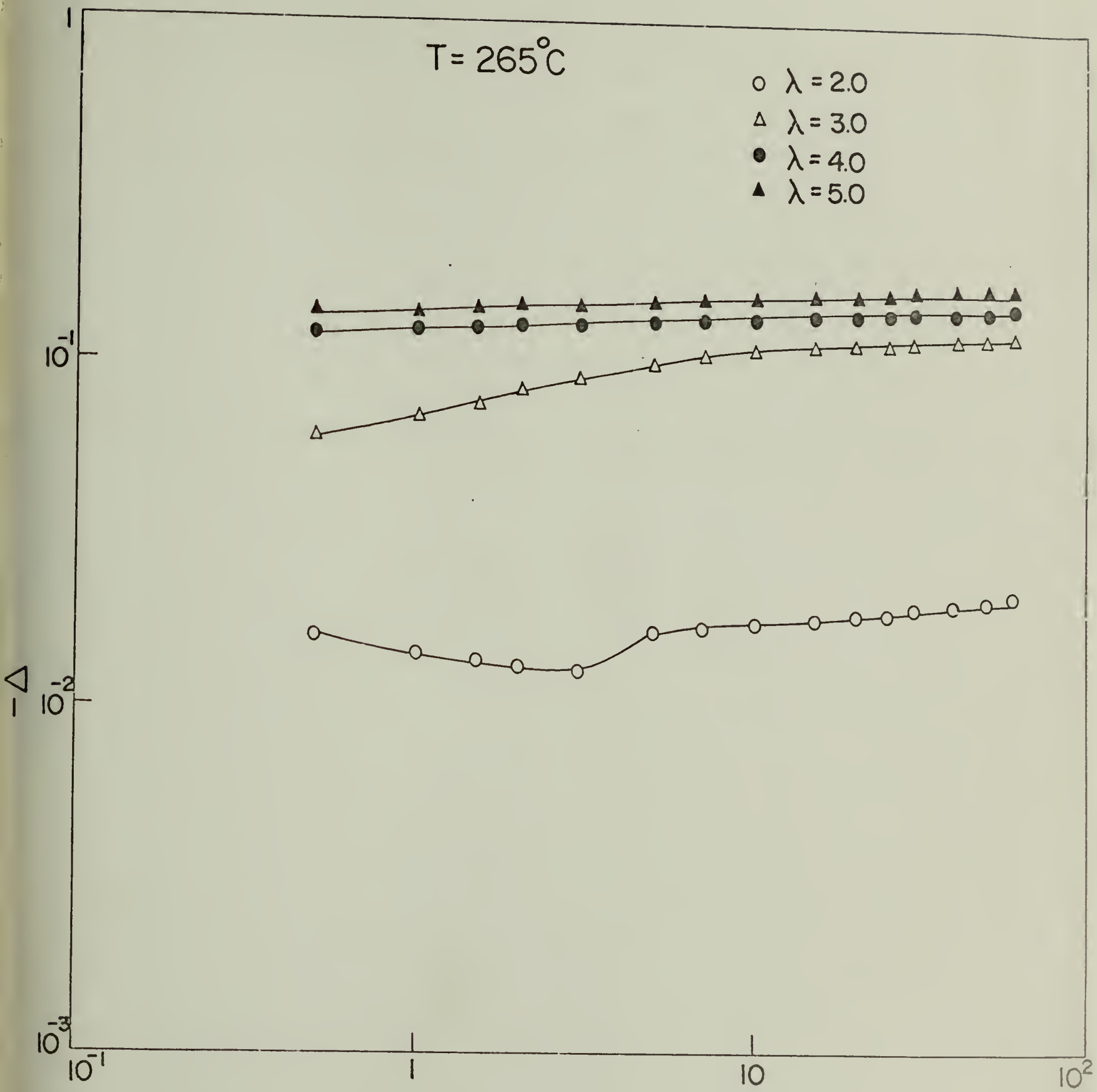

Figure 53

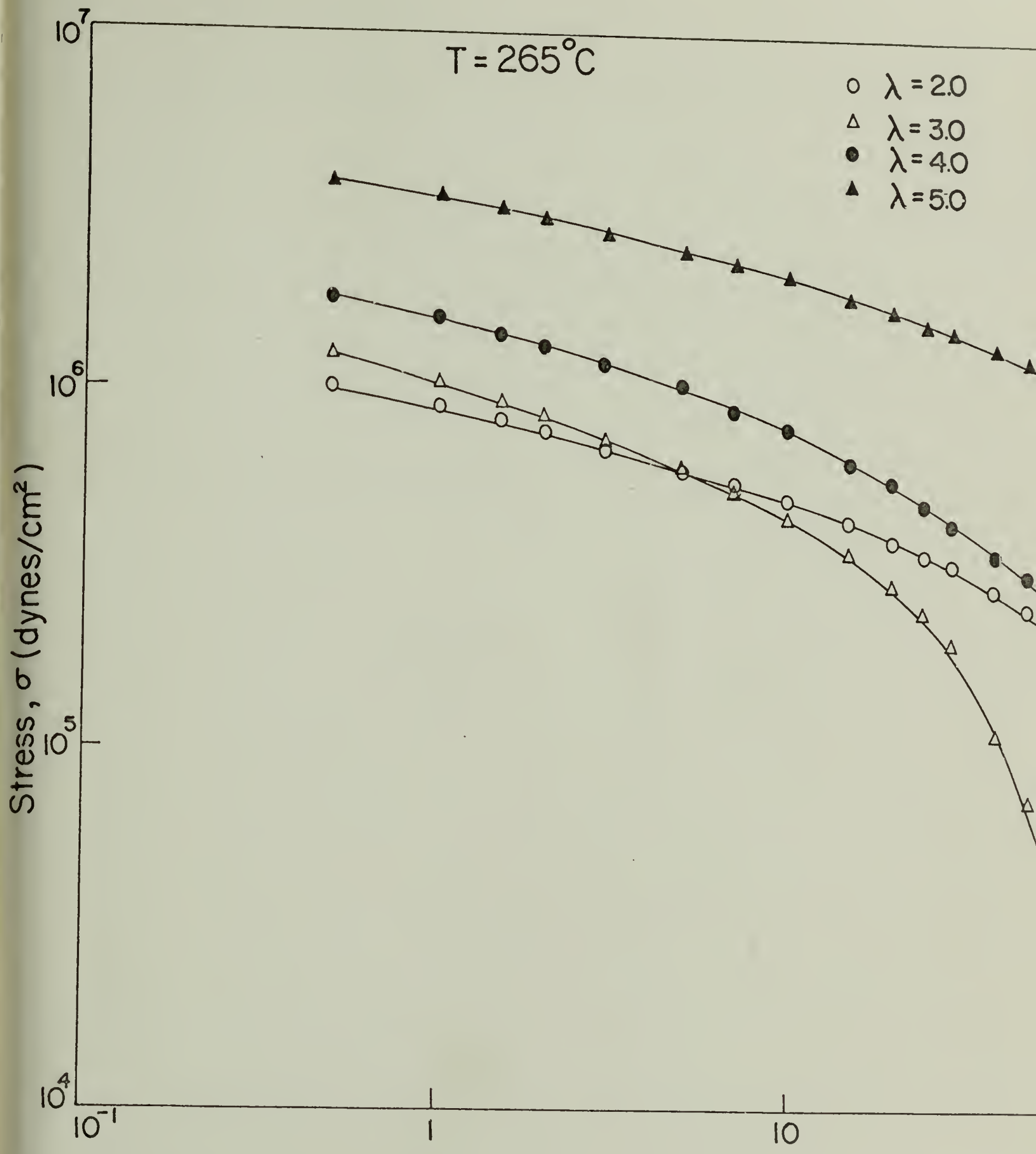
T = 265°C
λ = 2.0
λ = 3.0
λ = 4.0
λ = 5.0
Stress, σ (dynes/cm²)
10⁷
10⁶
10⁵
10⁴
10⁻¹
1
10
Time (min)

Figure 54

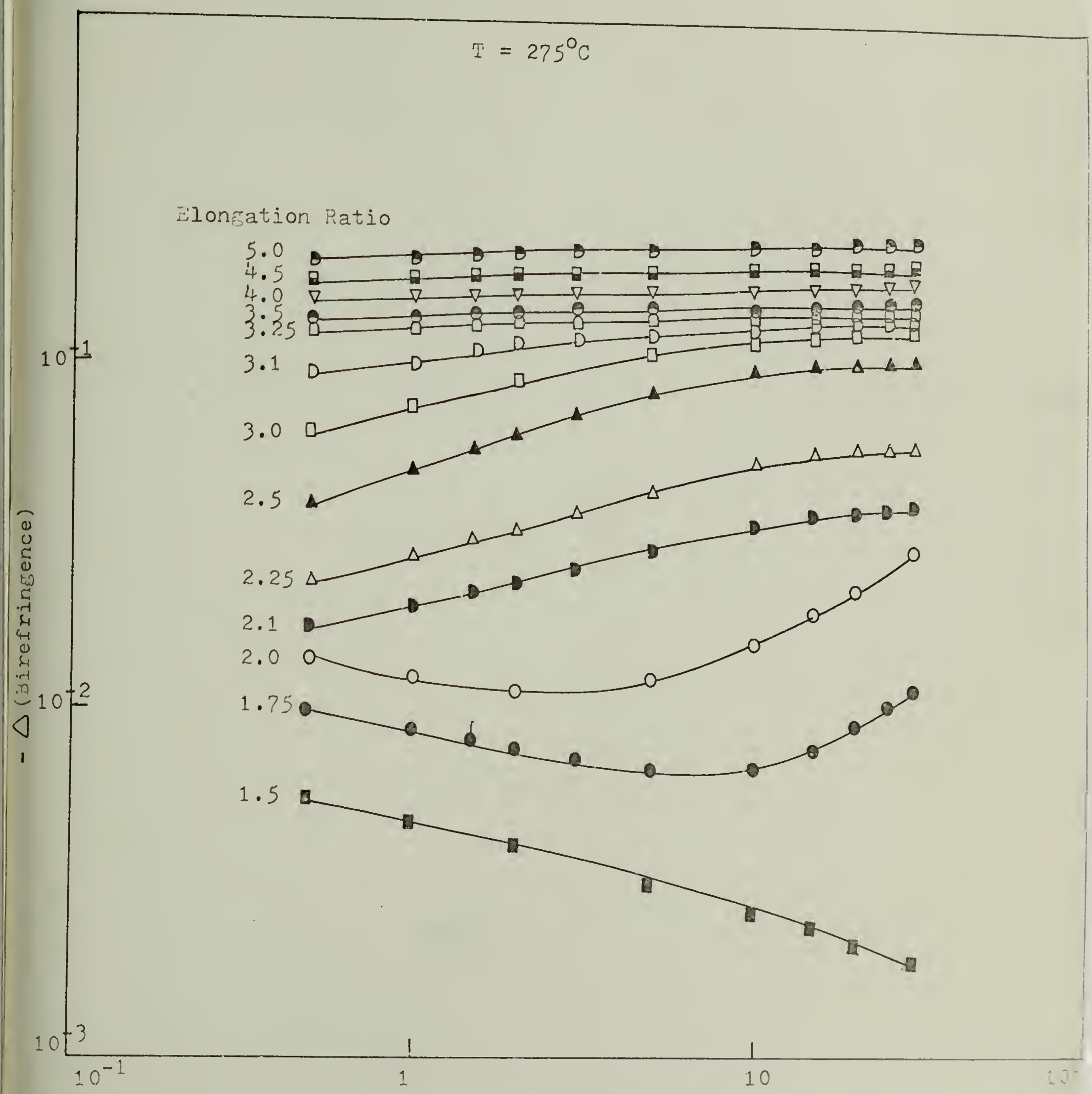
T = 275°C
Elongation Ratio
5.0
4.5
4.0
3.5
3.25
3.1
3.0
2.5
2.25
2.1
2.0
1.75
1.5
- Δ (Birefringence)
10^-1
10^-2
10^-3
10^-1
1
10
Time (min)

Figure 55

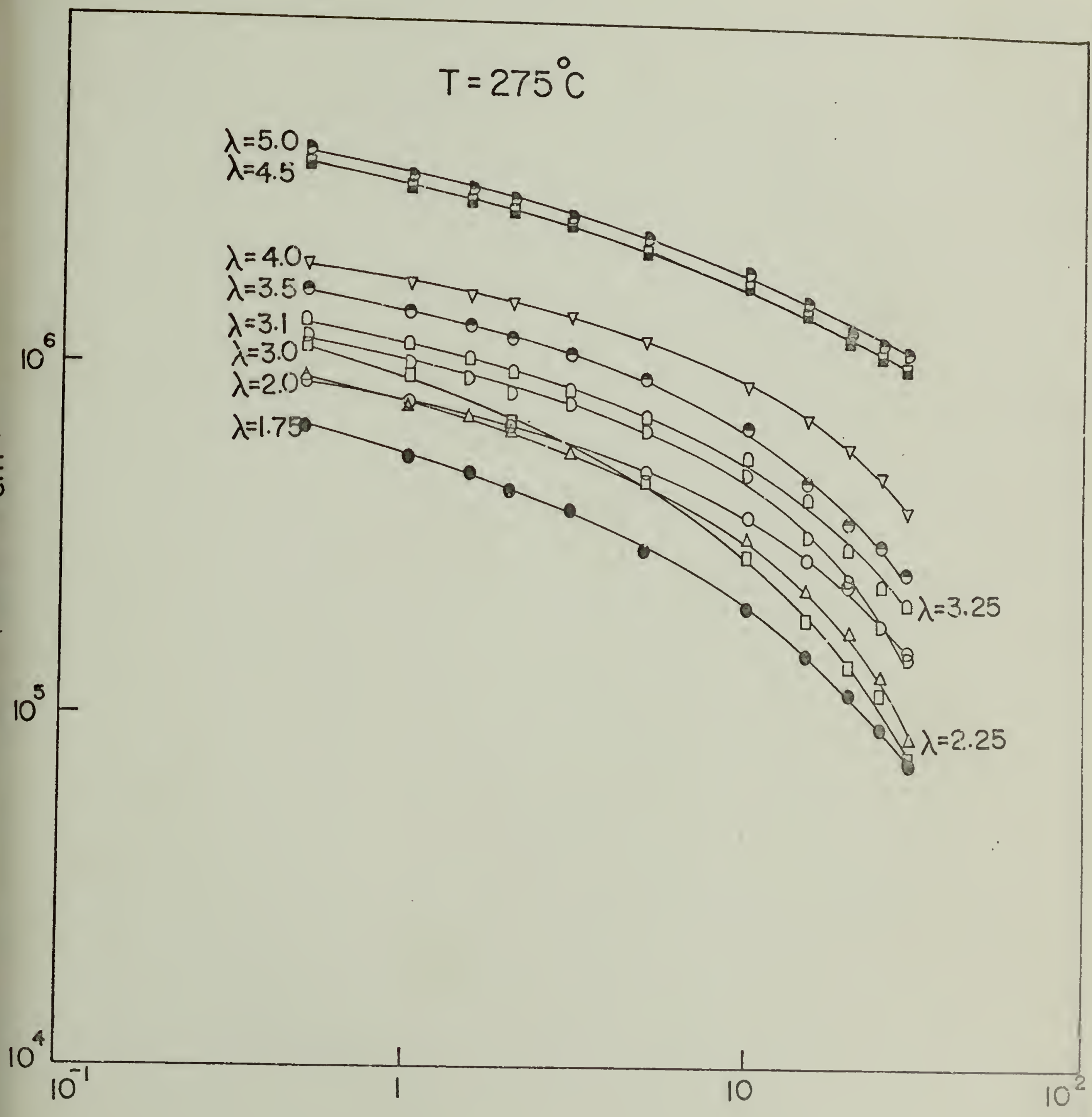
T = 275°C
λ=5.0
λ=4.5
λ=4.0
λ=3.5
λ=3.1
λ=3.0
λ=2.0
λ=1.75
λ=3.25
λ=2.25
10⁶
10⁵
10⁴
σ, Stress (dynes/cm²)
10⁻¹
1
10
10²
Time (min)

Figure 56

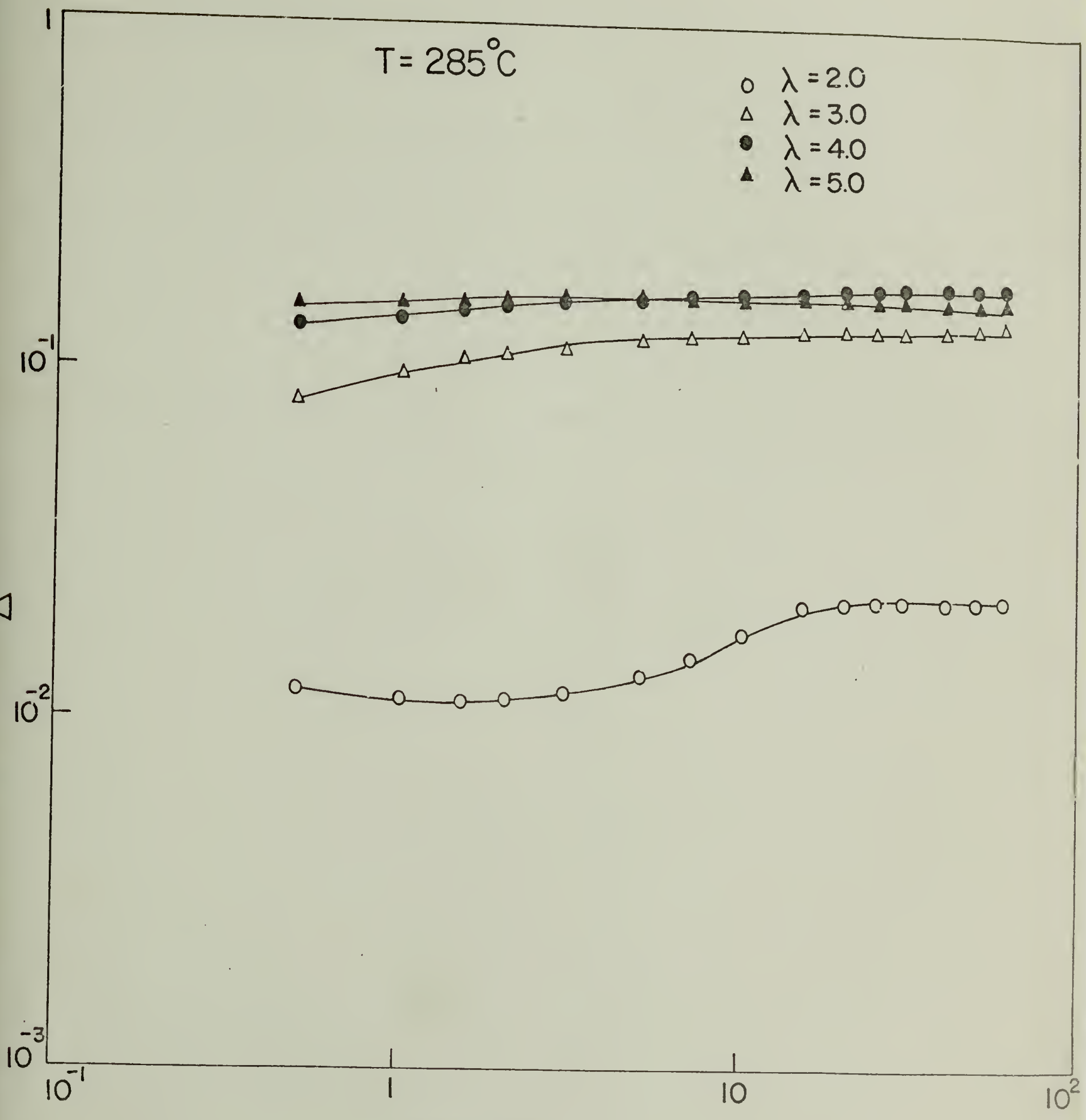

Figure 57

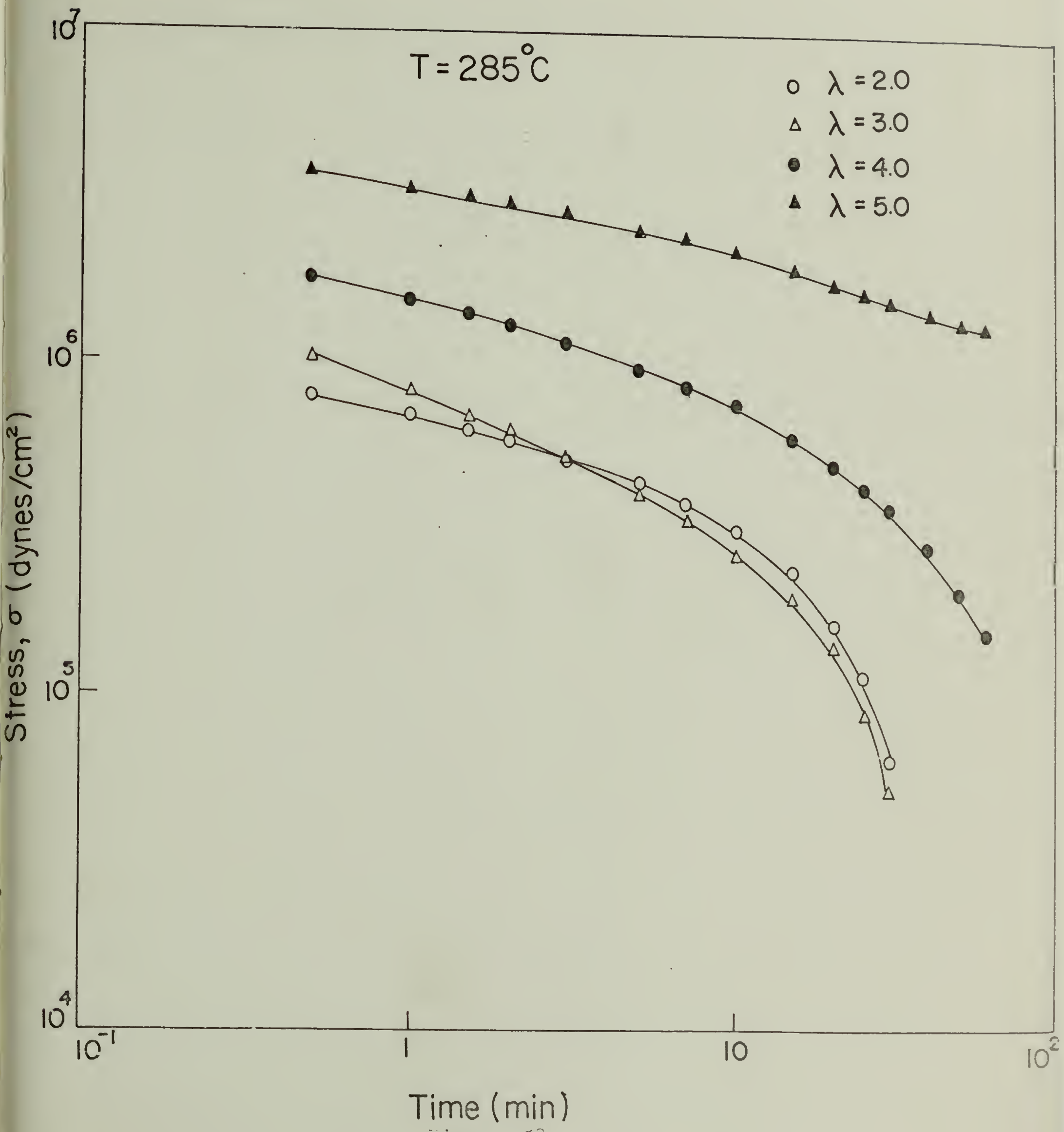
T = 285°C
λ = 2.0
λ = 3.0
λ = 4.0
λ = 5.0
Stress, σ (dynes/cm²)
10⁷
10⁶
10⁵
10⁴
10⁻¹
1
10
10²
Time (min)

Figure 53

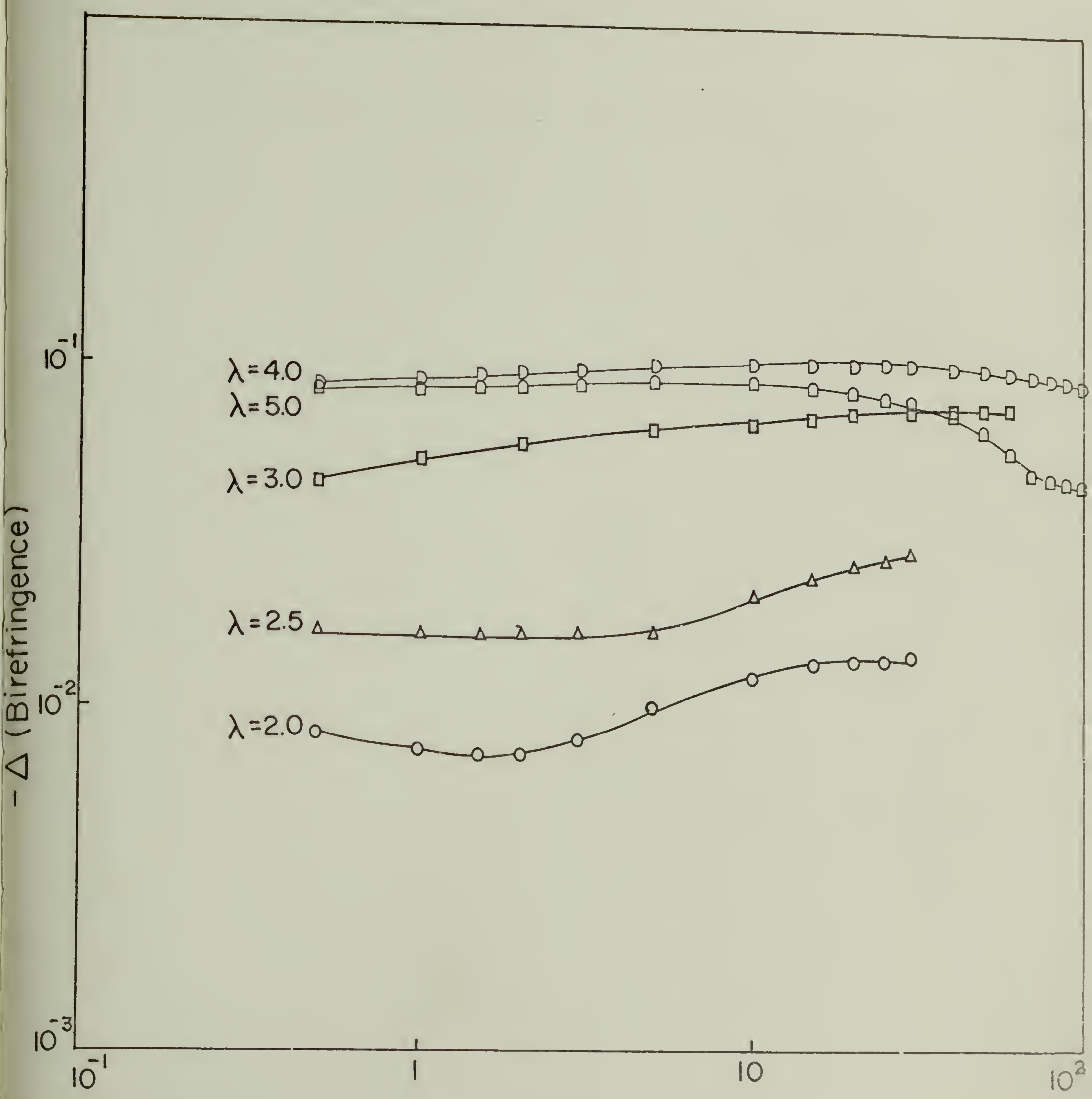
T = 300°C
λ = 4.0
λ = 5.0
λ = 3.0
λ = 2.5
λ = 2.0
- Δ (Birefringence)
10⁻¹
10⁻²
10⁻³
10⁻¹
1
10
10²
Time (min)

Figure 59

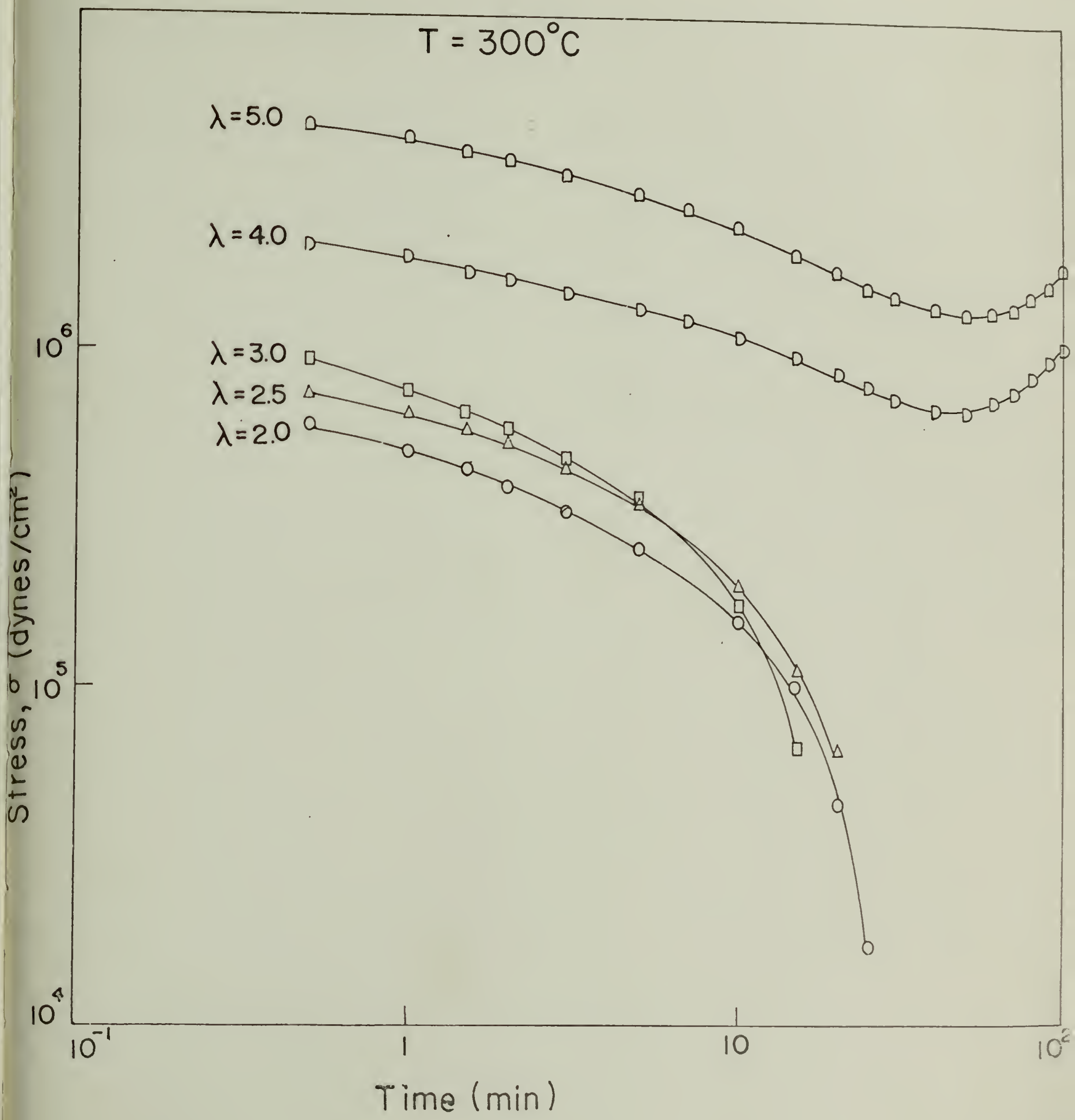
T = 300°C
λ=5.0
λ=4.0
λ=3.0
λ=2.5
λ=2.0
10^6
10^5
10^4
Stress, σ (dynes/cm²)
10^-1
1
10
Time (min)

Figure 60

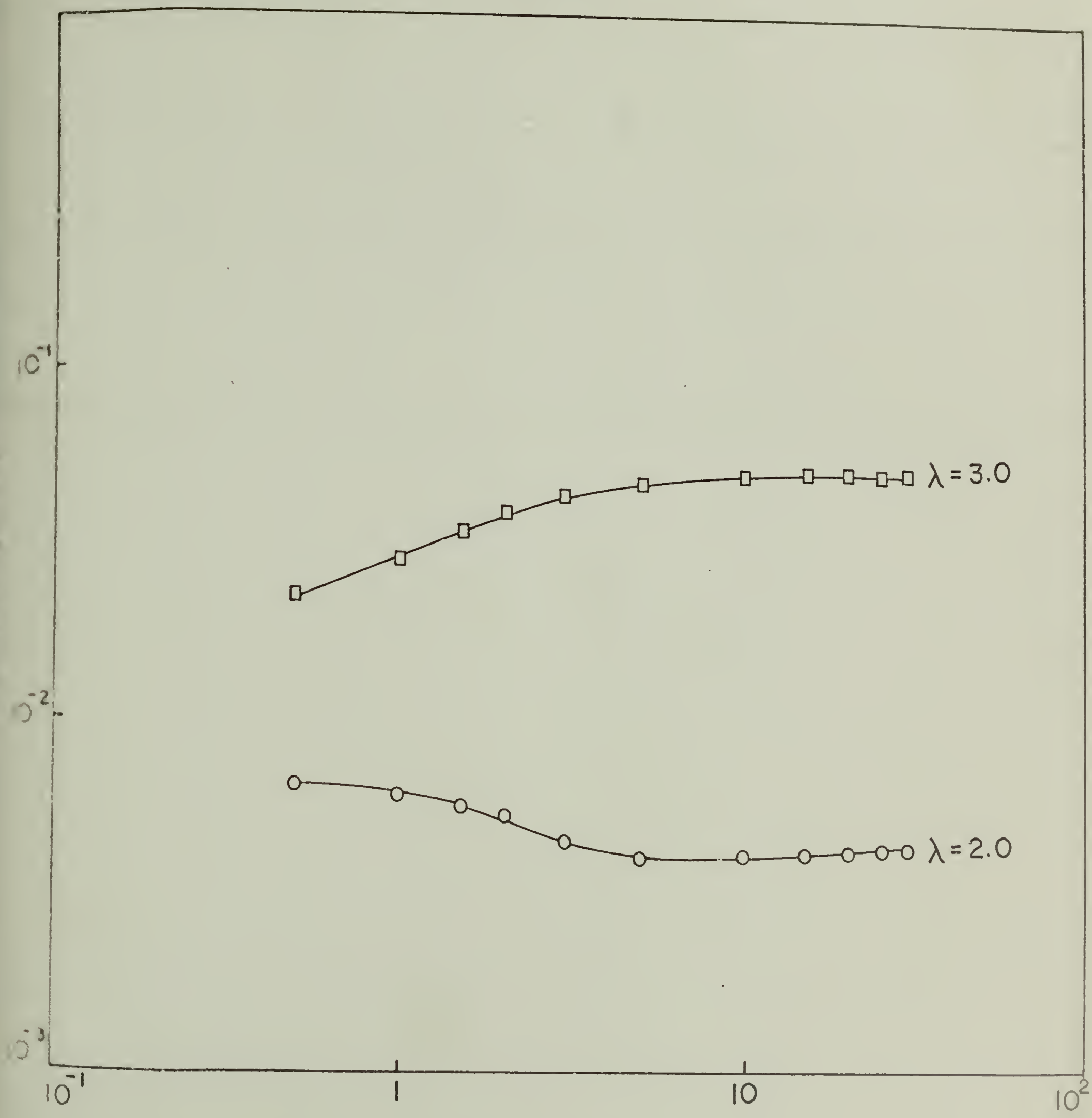

Figure 61

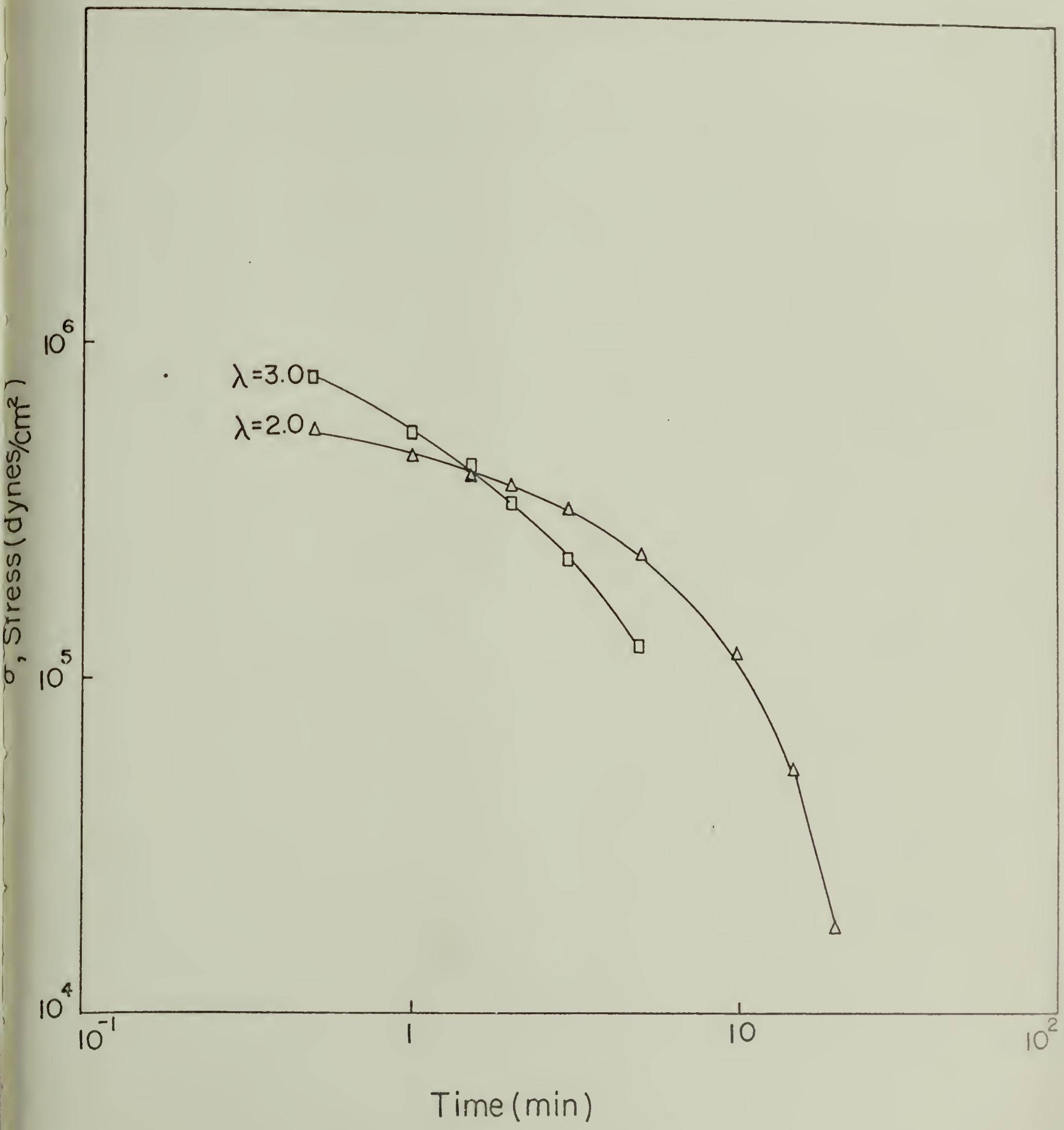
T = 320 °C
σ, Stress (dynes/cm²)
10⁶
10⁵
10⁴
λ = 3.0
λ = 2.0
10⁻¹
1
10
10²
Time (min)

Figure 62

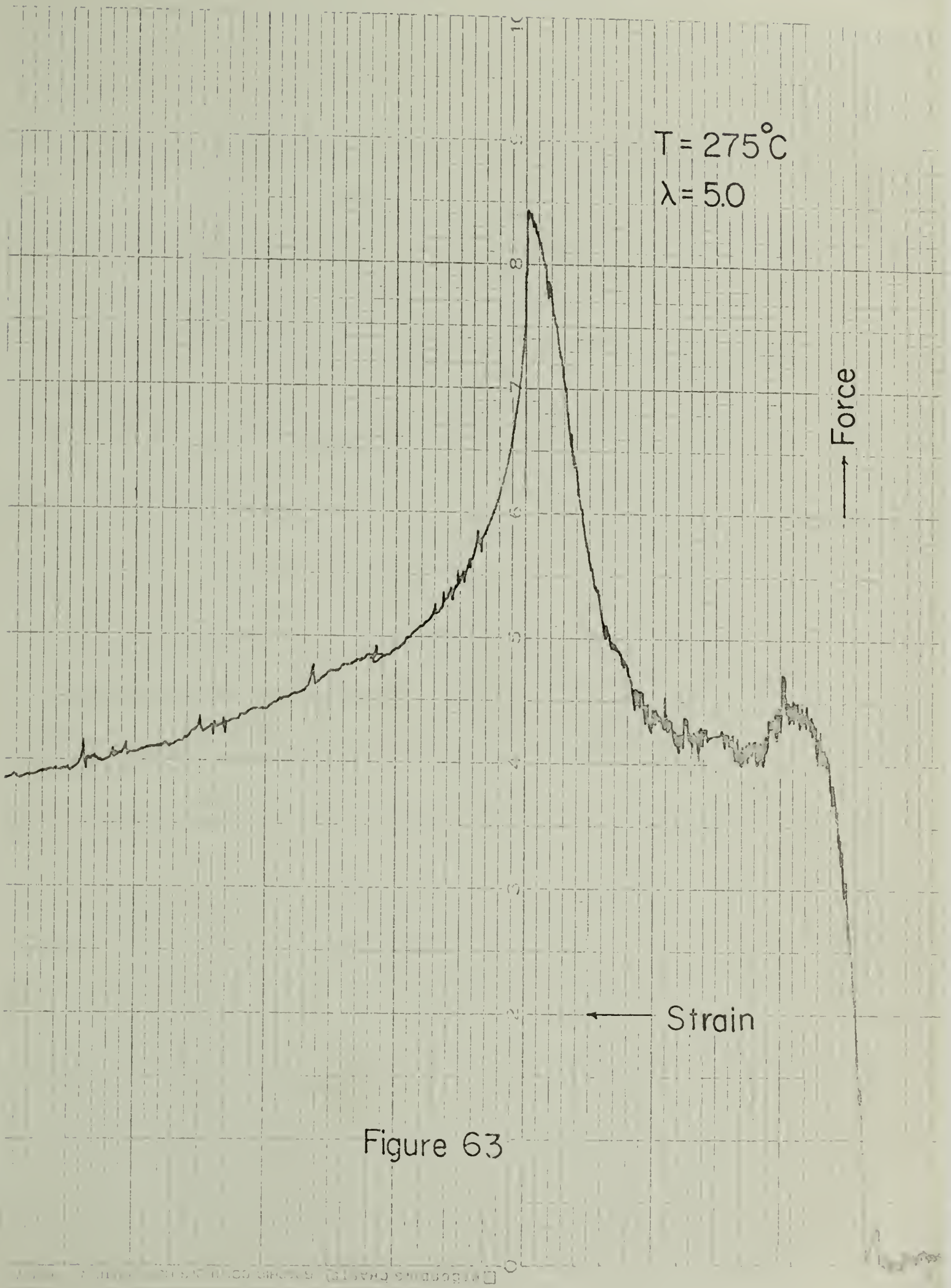

Figure 63

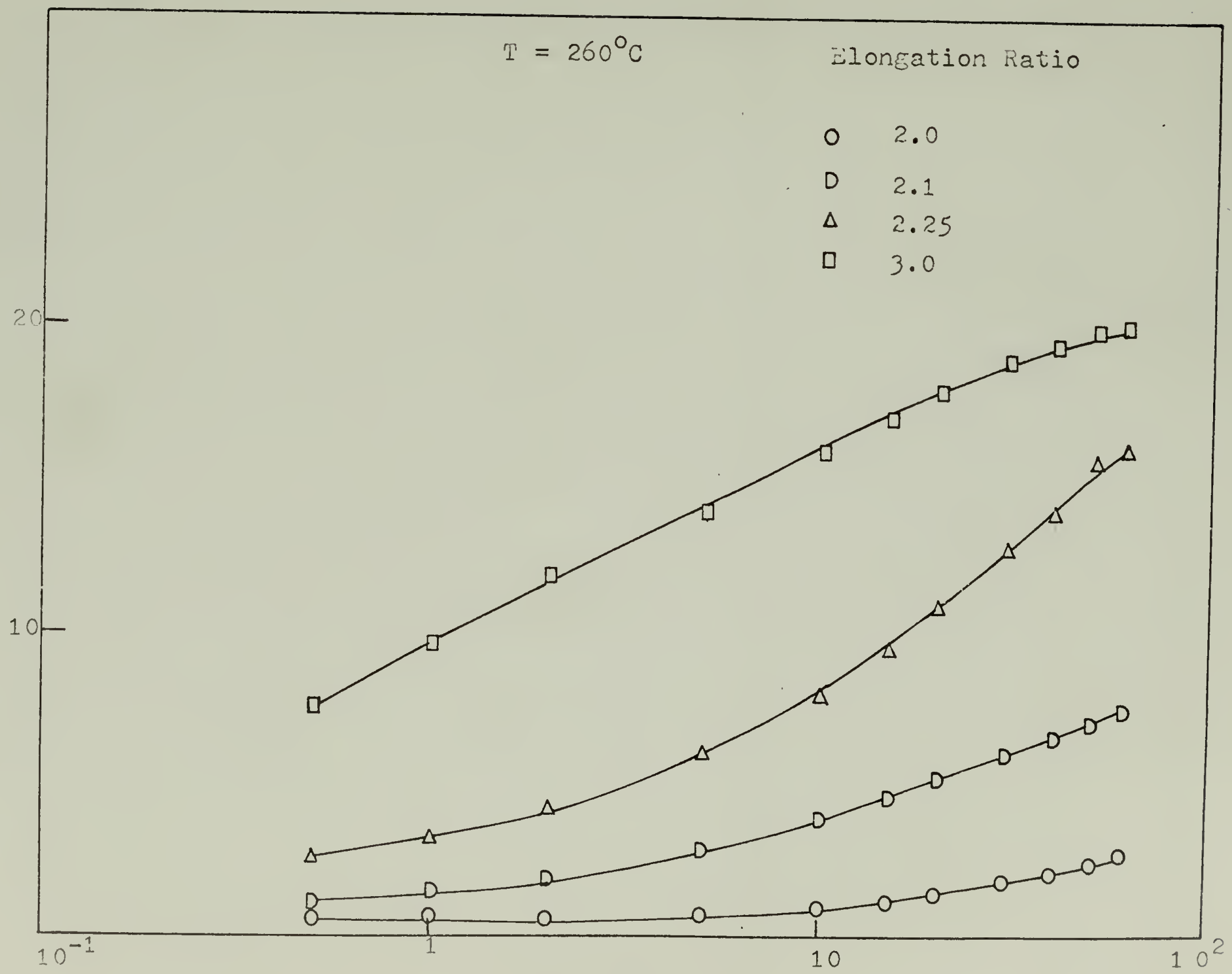
T = 260°C
Elongation Ratio
2.0
2.1
2.25
3.0
20
10
χ_c %
10^{-1}
1
10
10^2
Time (min)

Figure 64

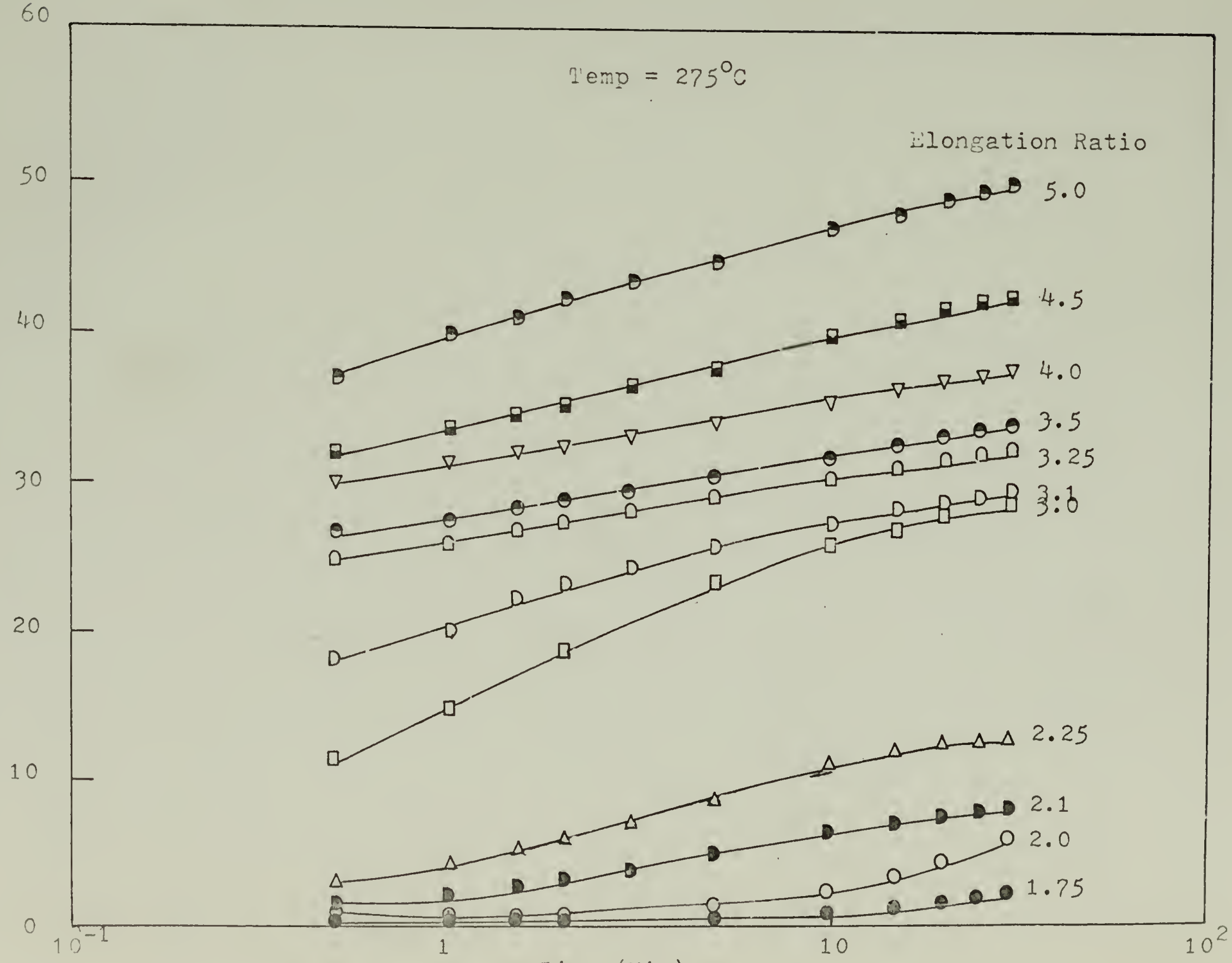
Temp = 275°C
Elongation Ratio
5.0
4.5
4.0
3.5
3.25
3.1
3.0
2.25
2.1
2.0
1.75
60
50
40
30
20
10
0
X_c%
10^{-1}
1
10
10^2
Time (Min)

Figure 65

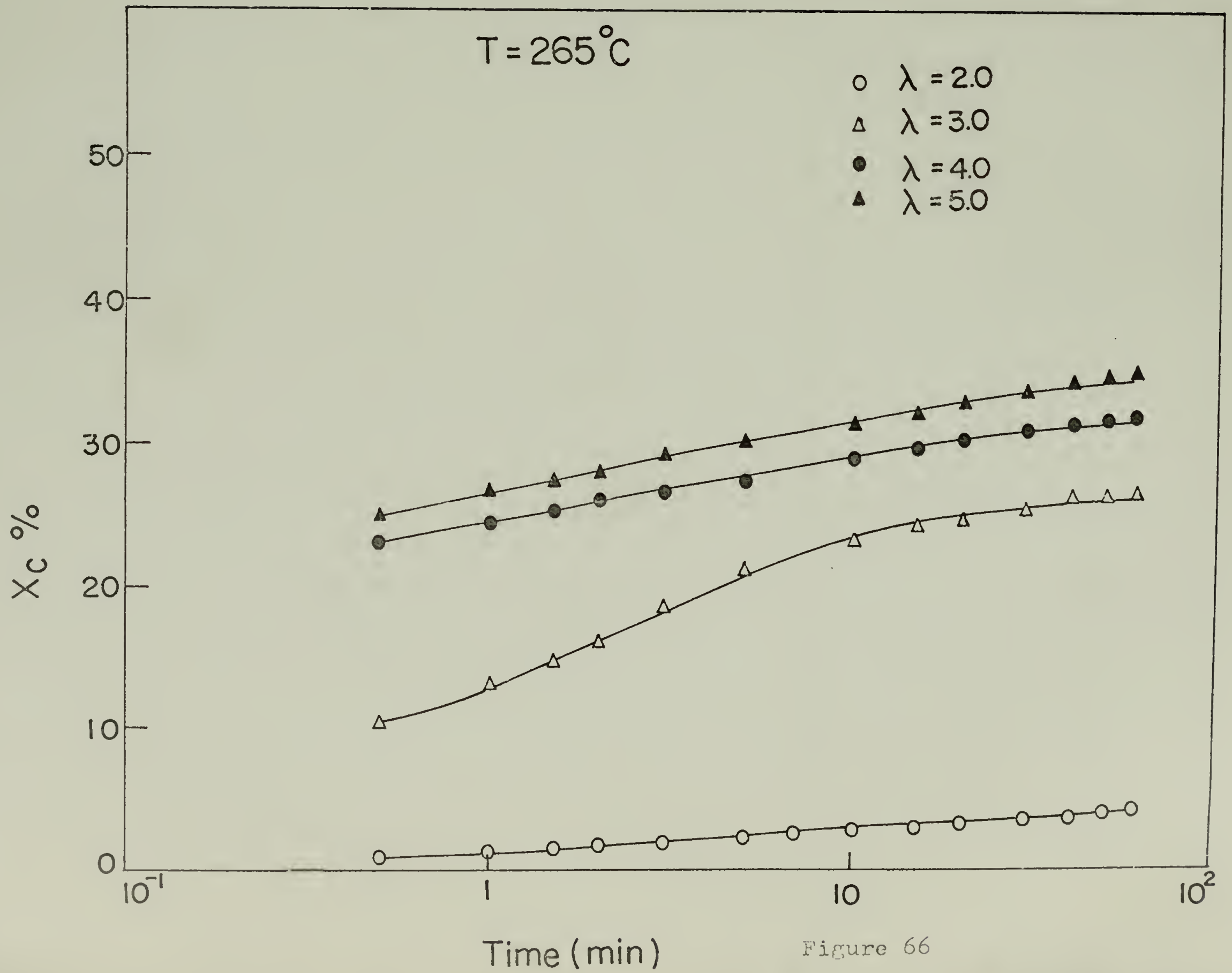

Figure 66

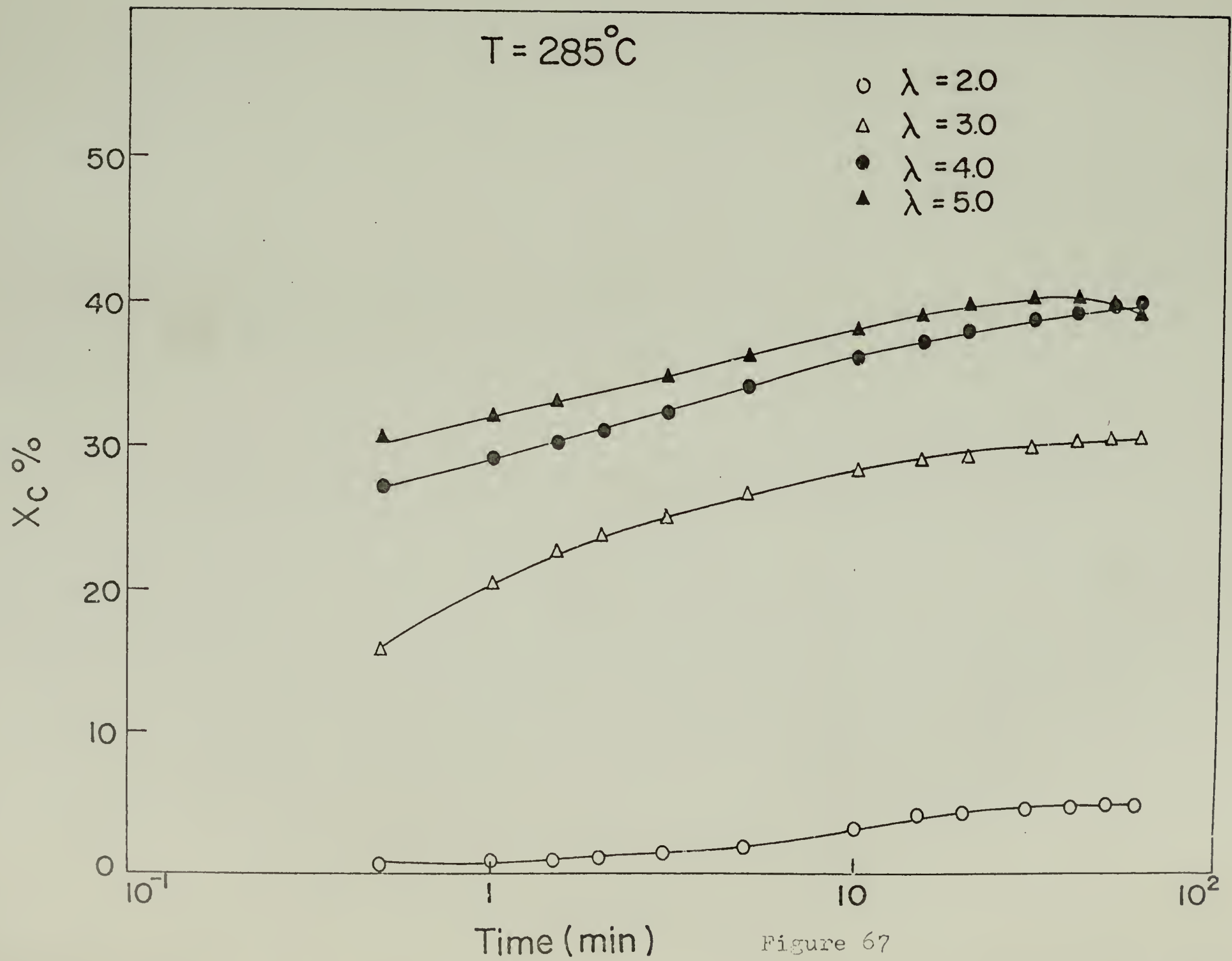

Figure 67

T = 300°C

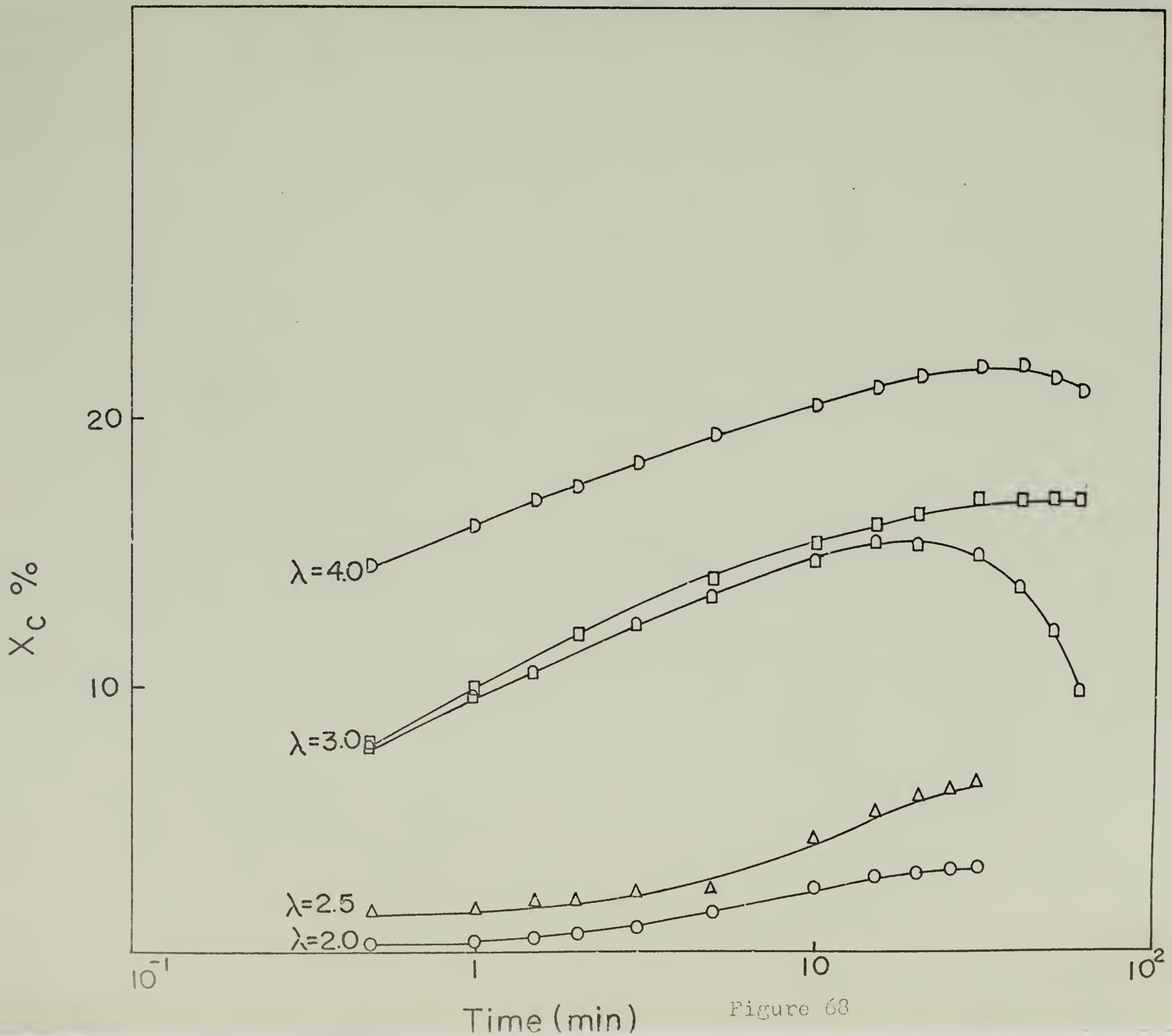

Figure 68

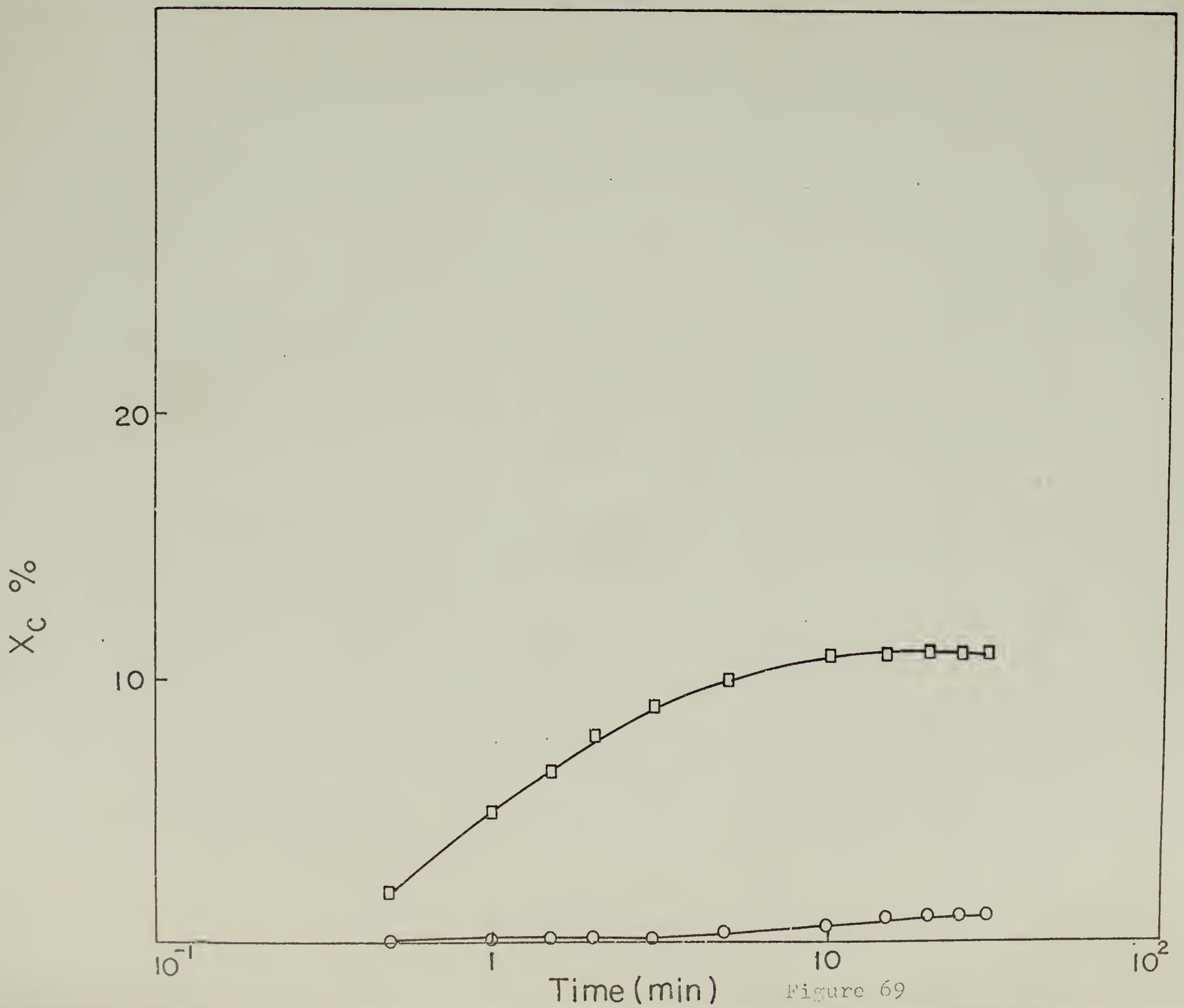

Figure 69

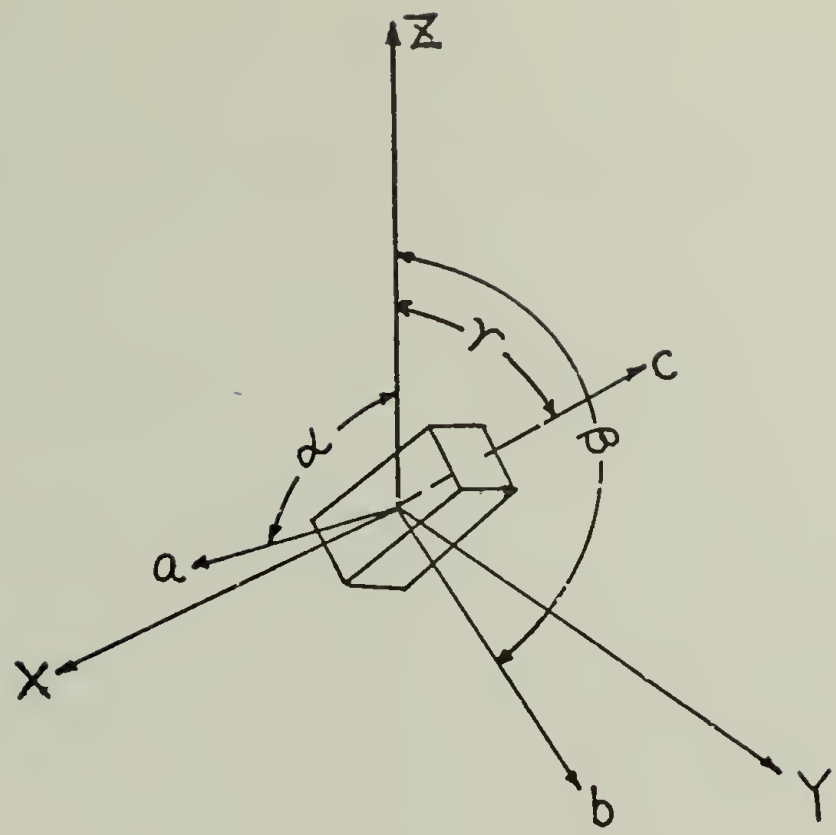

Figure 70a

Figure 70b

T = 275°C

λ = 1.5

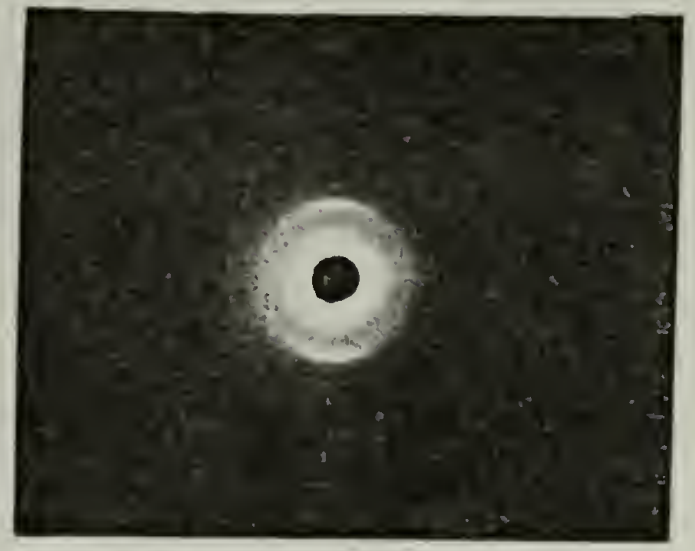

λ = 2.0

S.D.

λ = 2.25

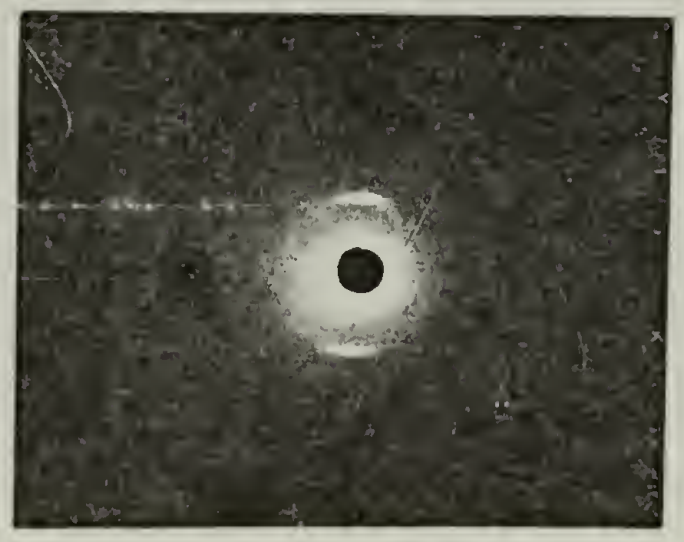

λ = 2.5

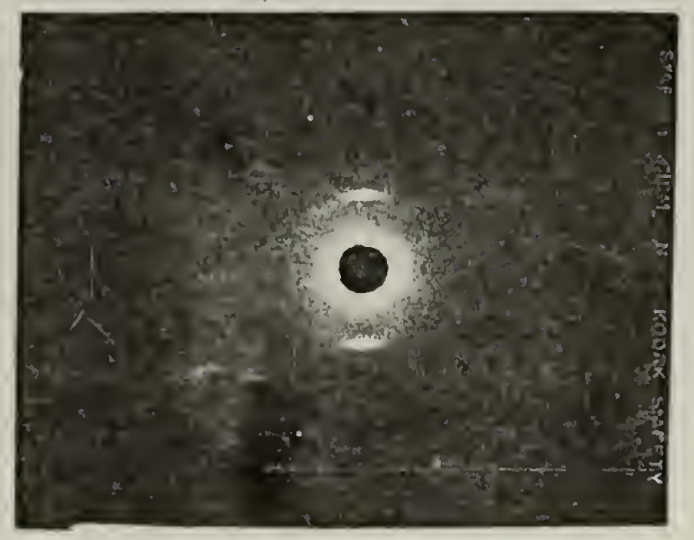

λ = 3.0

Figure 71

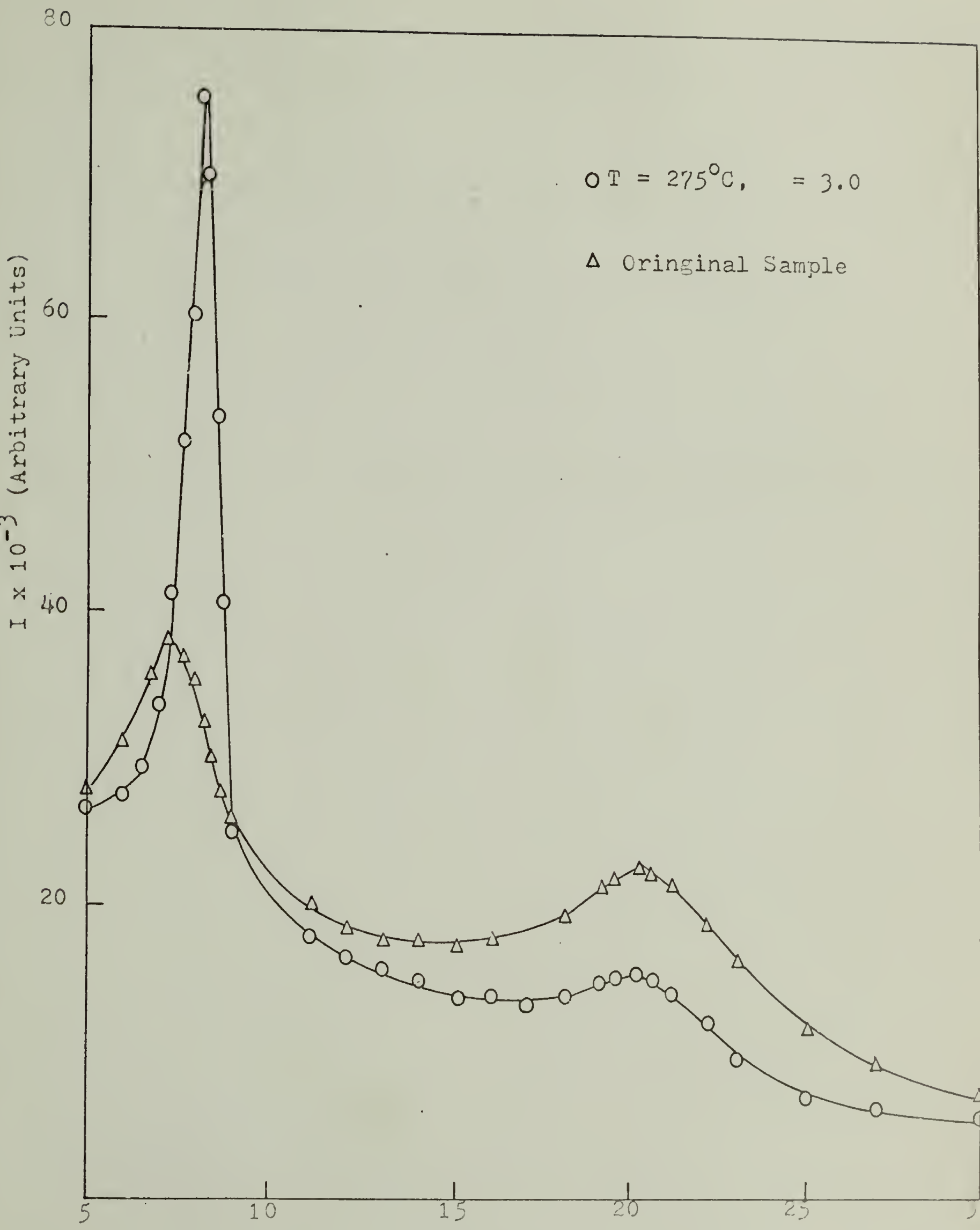
80
60
40
20
I x 10^{-3} (Arbitrary Units)
O T = 275°C, = 3.0
Δ Oringinal Sample
5
10
15
20
25
2θ Degree

Figure 72

Figure 73

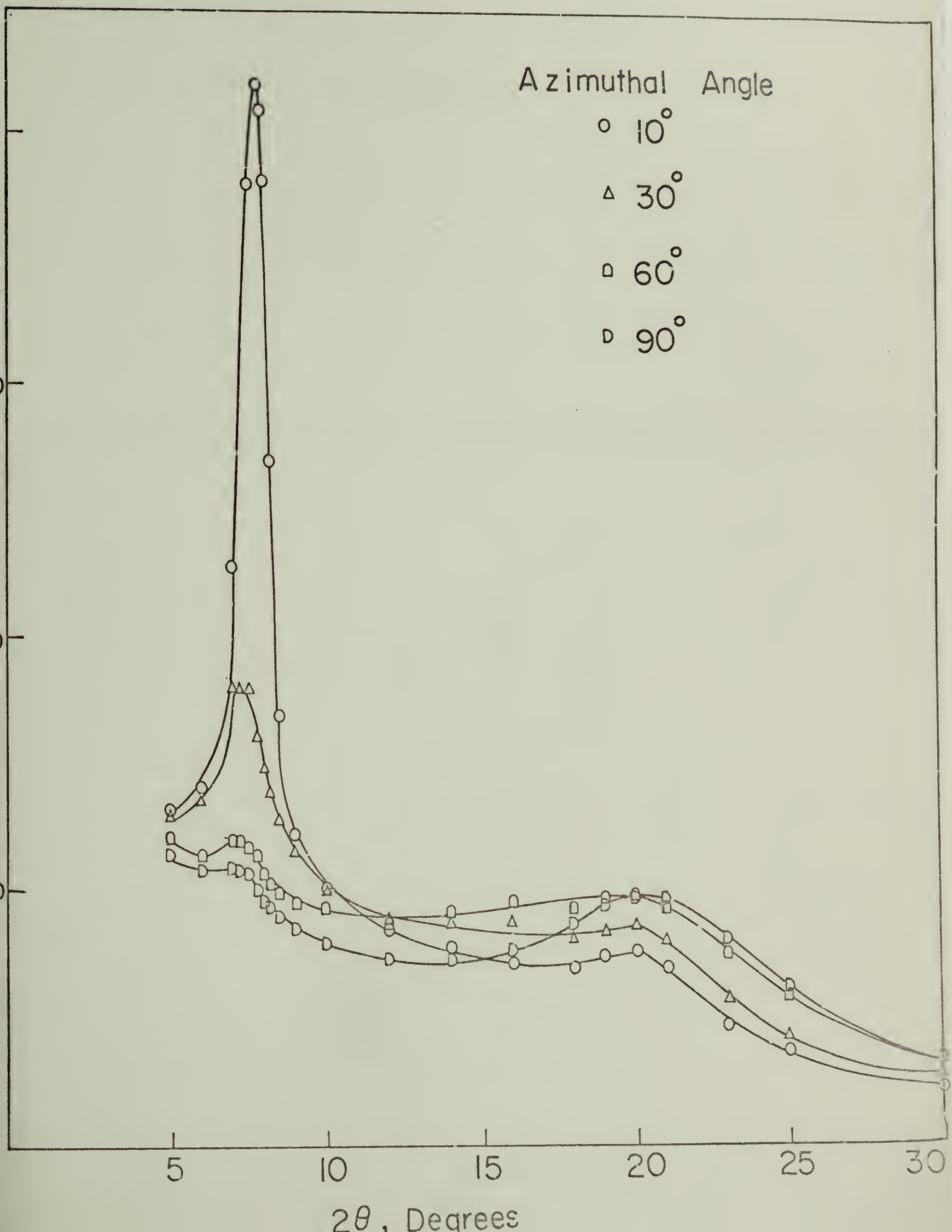
Azimuthal Angle
10°
30°
60°
90°
80
60
40
20
I x 10 (Arbitrary Units)
5
10
15
20
25
30
2θ, Degrees

λ=6.0

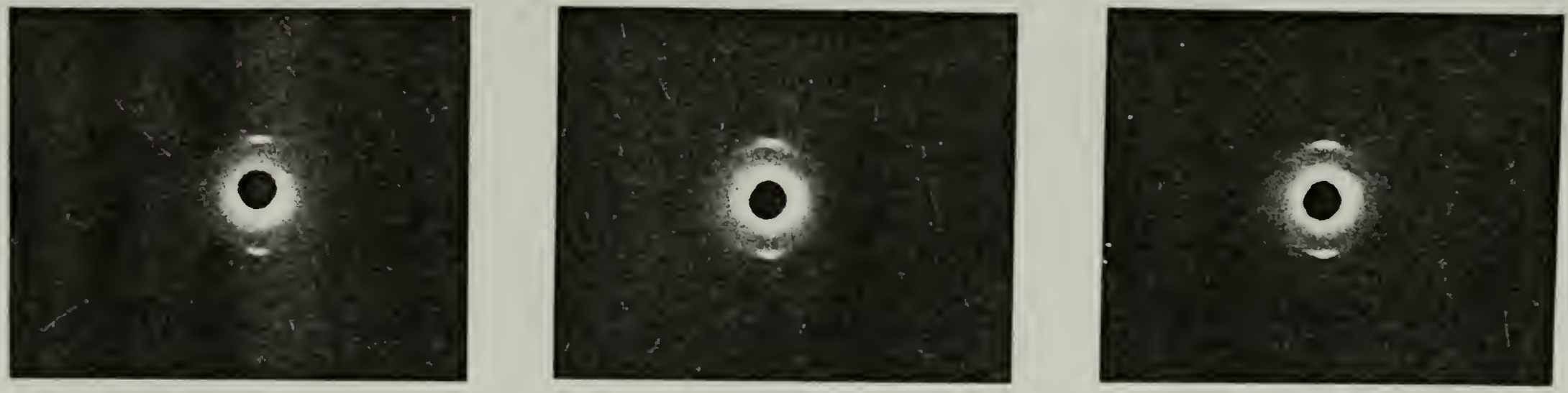

T = 220°C

T = 240°C

T = 260°C

Figure 74a

←→ S.D.

T = 240°C

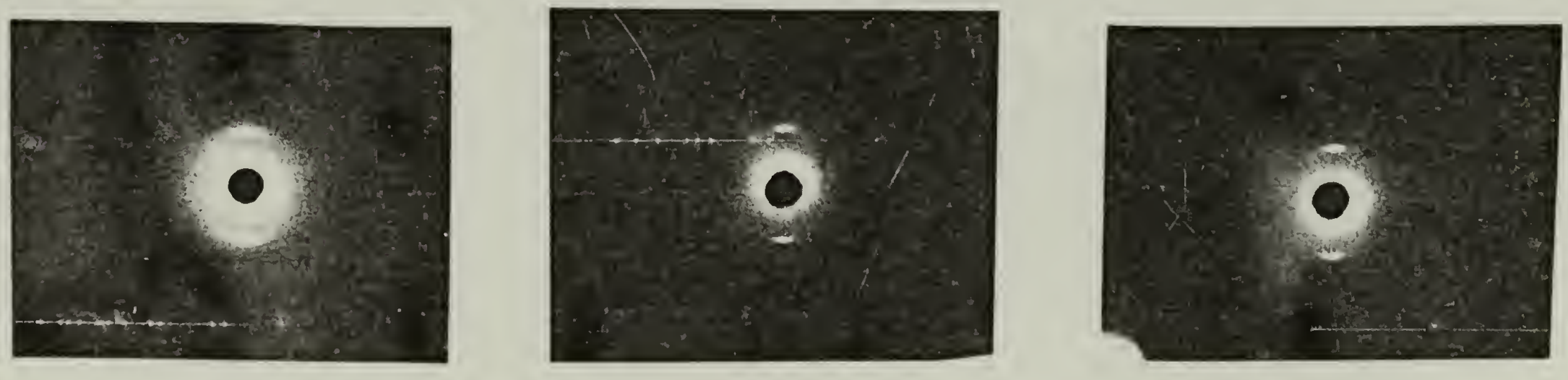

λ = 4.0

λ = 5.0

λ = 6.0

Figure 74b

T = 265°C

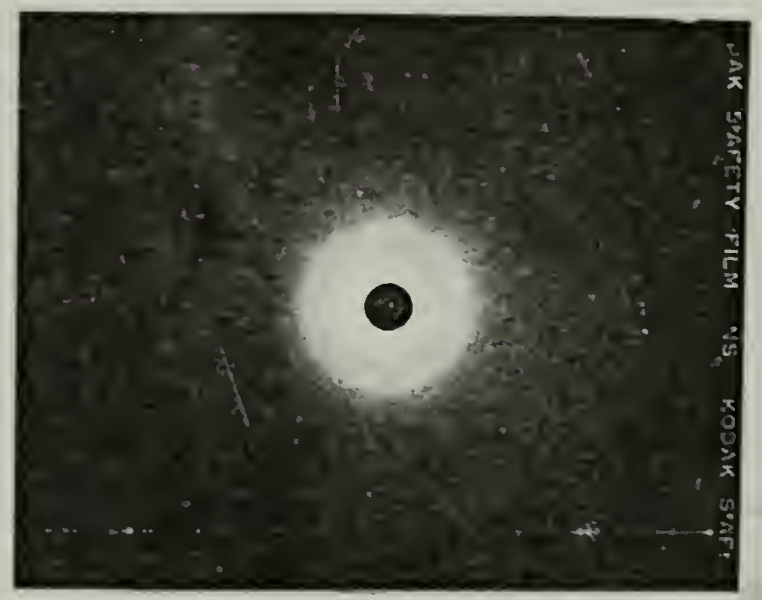

λ = 2.0

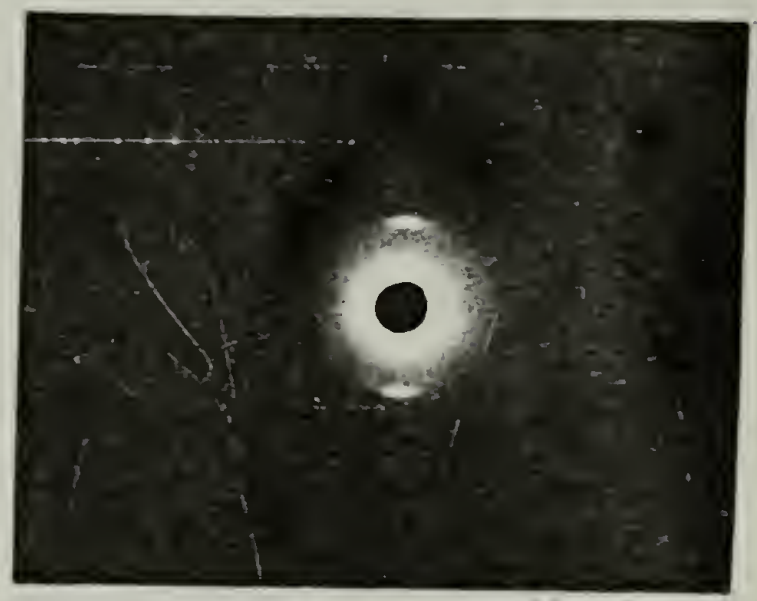

λ = 3.0

S.D.

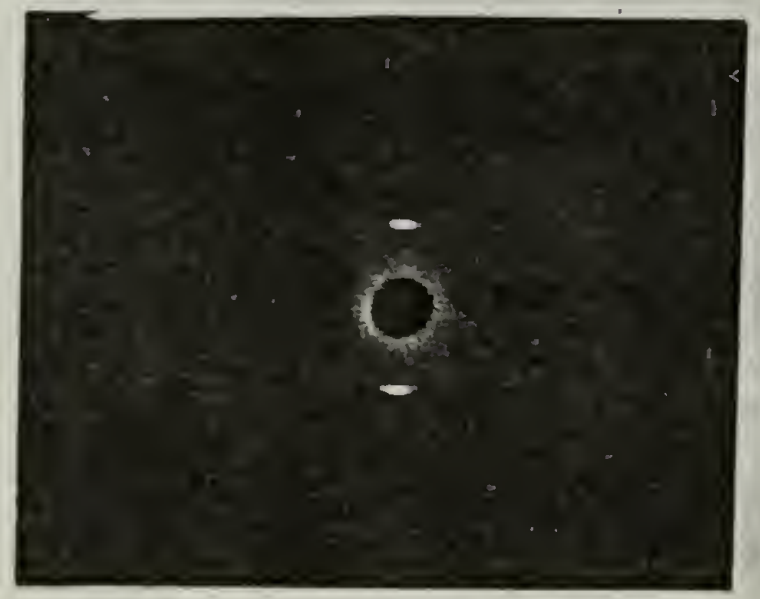

λ = 4.0

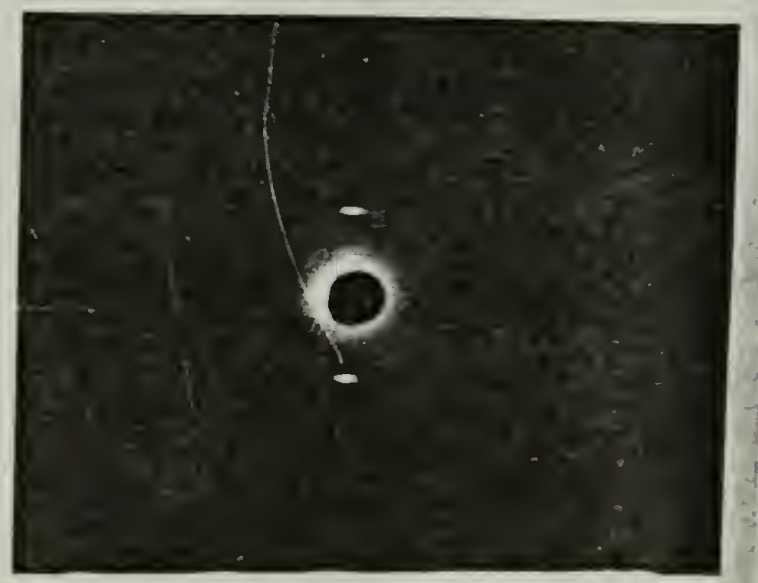

λ = 5.0

Figure 75

T = 285°C

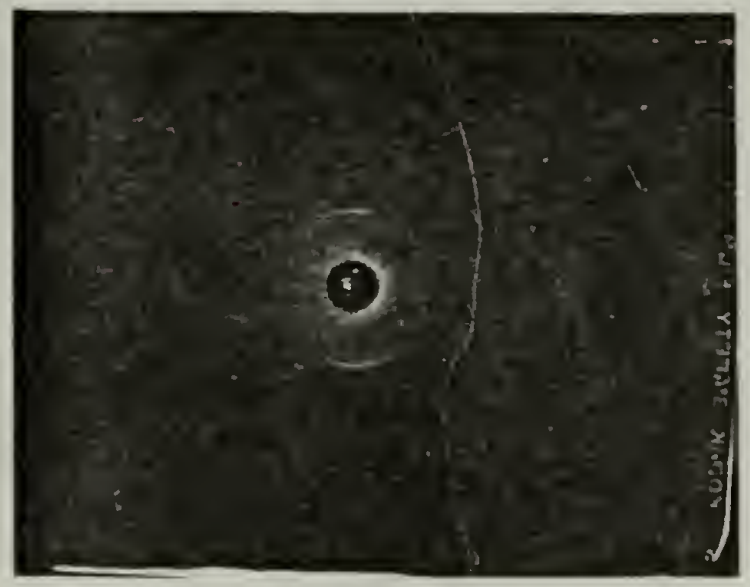

λ = 2.0

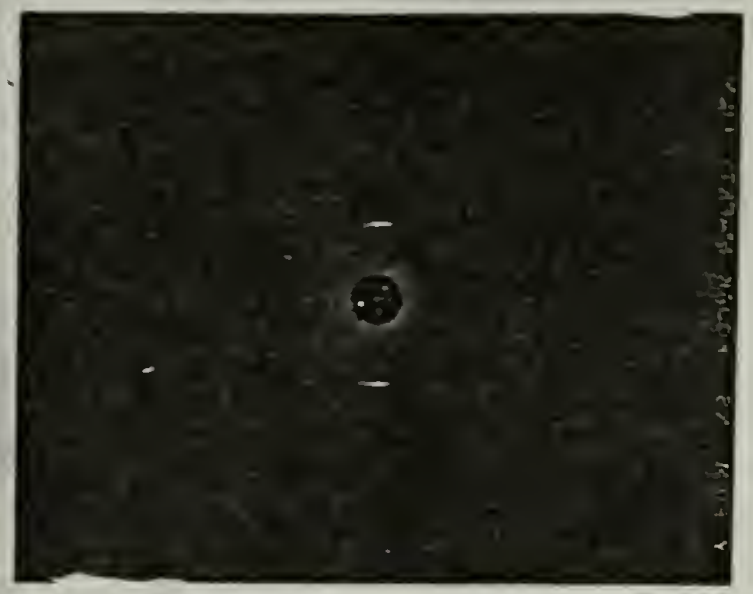

λ = 3.0

⟷ S.D.

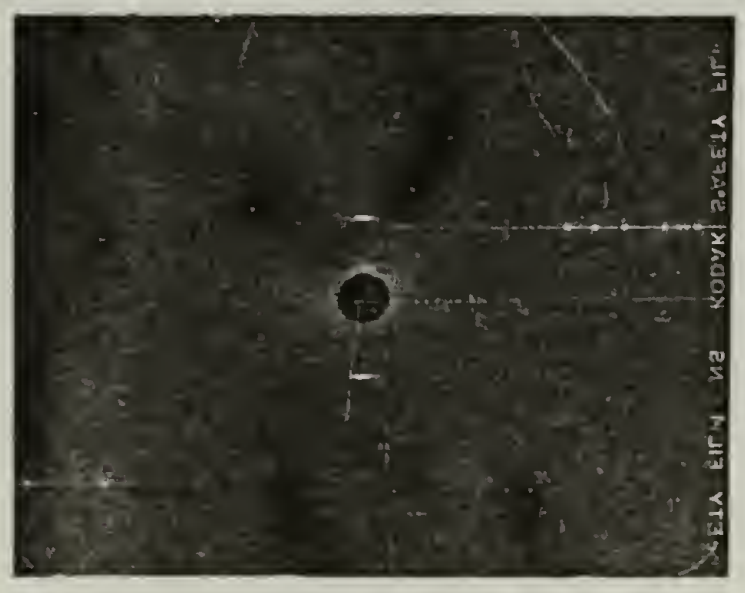

λ = 4.0

λ = 5.0

Figure 26

T = 300°C

λ = 1.0

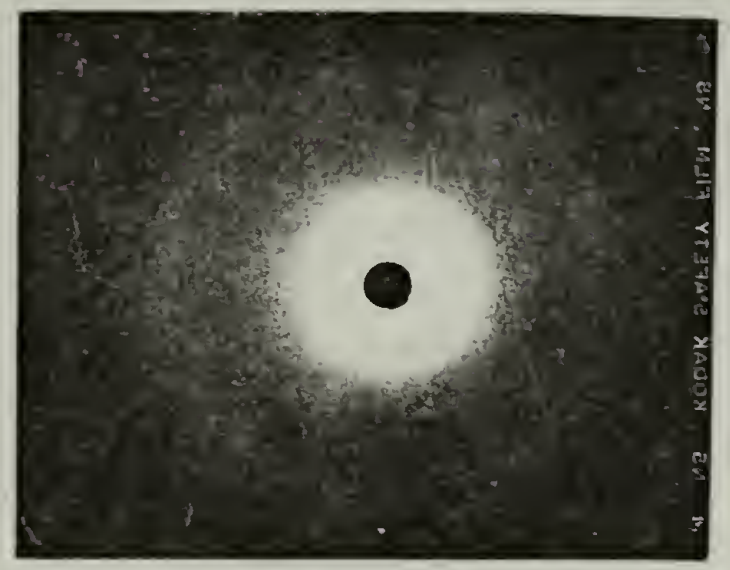

λ = 2.0

λ = 3.0

⟷ S.D.

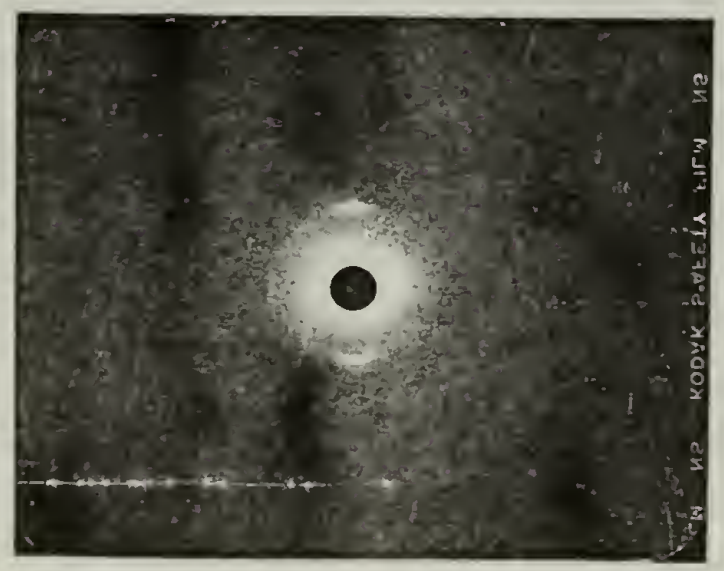

λ = 4.0

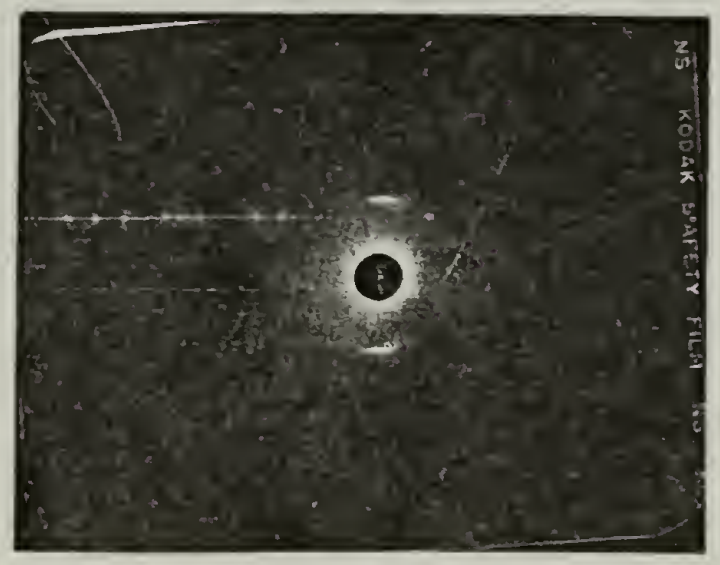

λ = 5.0 (30 min)

λ = 5.0 (120 min)

Figure 77

T = 260°C

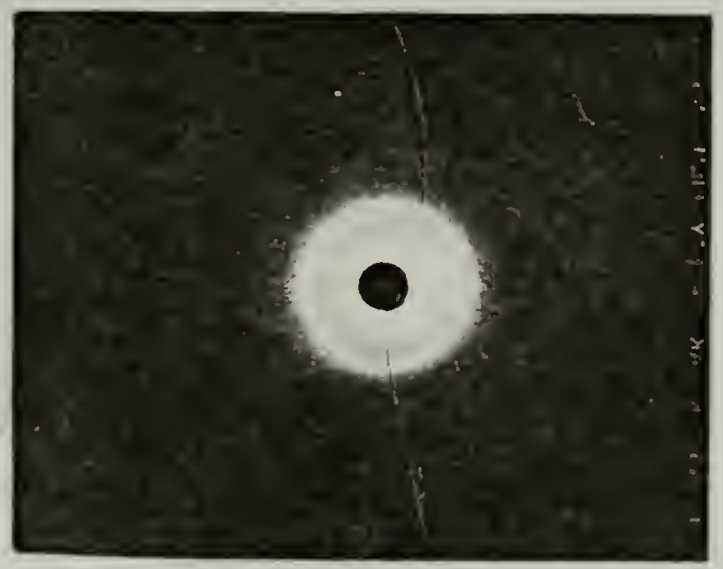

λ = 2.0

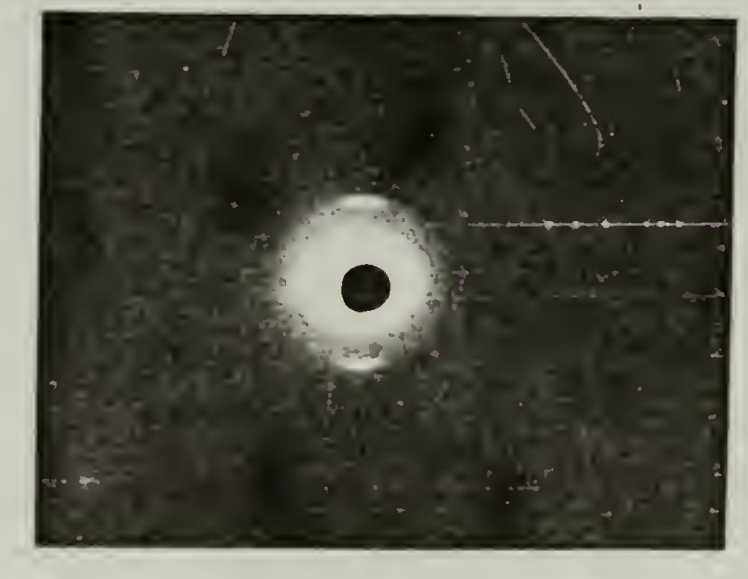

λ = 3.0

Figure 78a

T = 320°C

λ = 2.0

S.D.

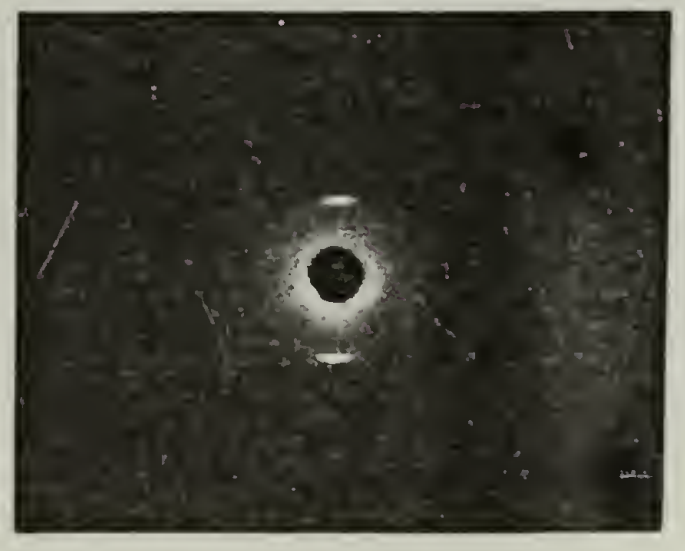

λ = 3.0

Figure 78b

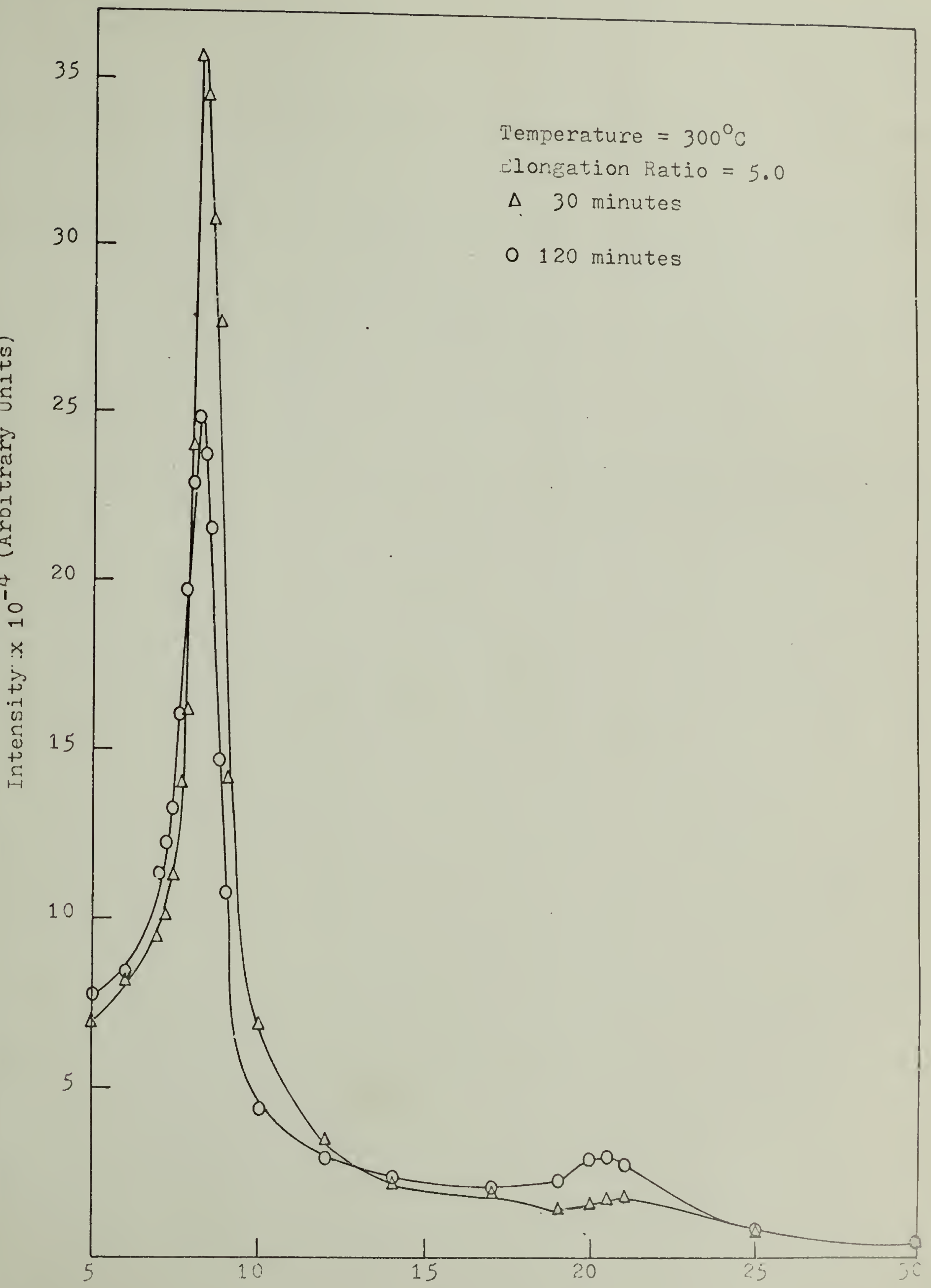
Temperature = 300°C
Elongation Ratio = 5.0
Δ 30 minutes
O 120 minutes
Intensity x 10⁻⁴ (Arbitrary Units)
35
30
25
20
15
10
5
5
10
15
20
25
2θ Degree

Figure 79

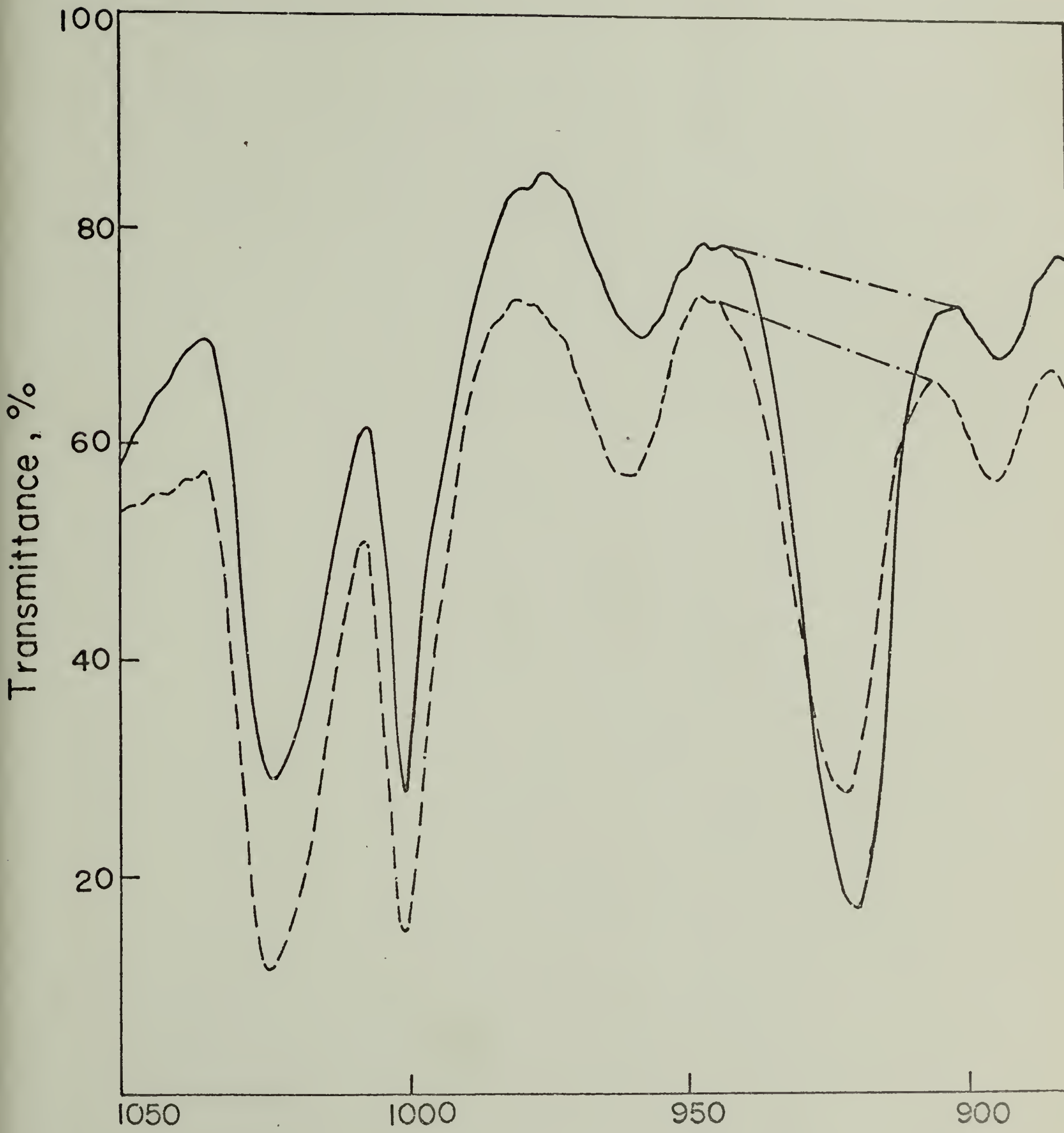
100
80
60
40
20
Transmittance, %
1050
1000
950
900
WAVE NUMBER CM-1

Figure 80

T = 240°C

λ = 2.0

λ = 3.0

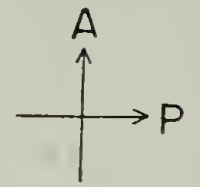

⟷ S.D.

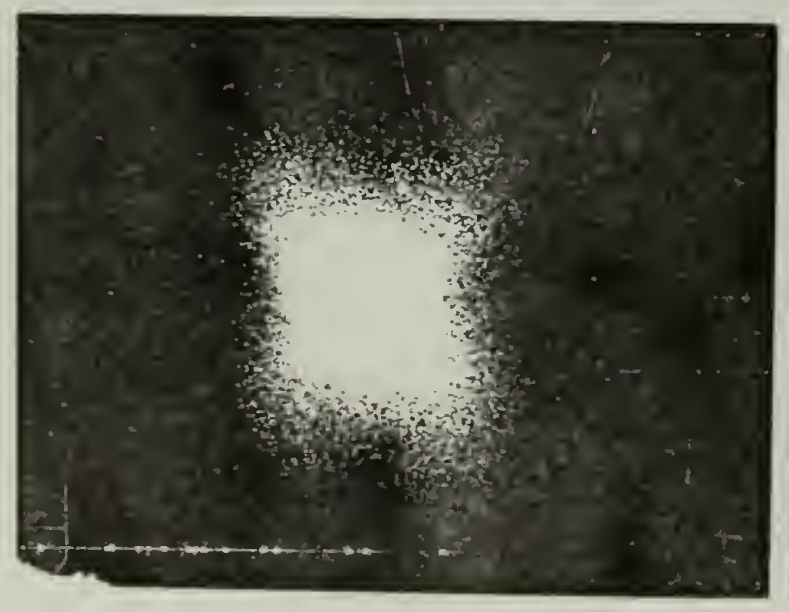

λ = 4.0

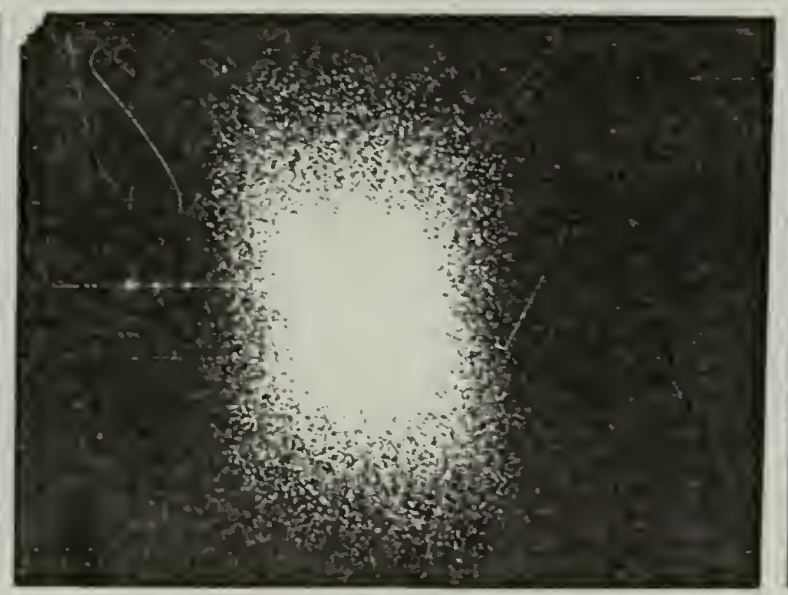

λ = 5.0

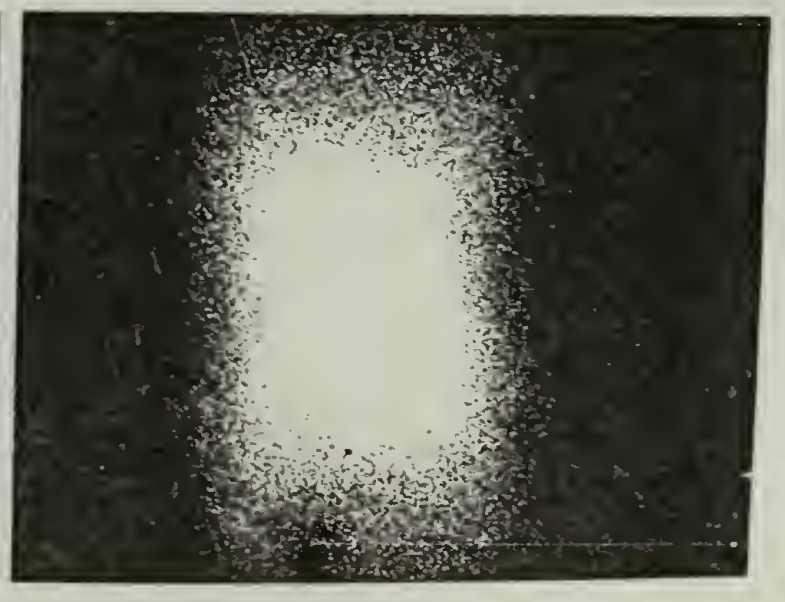

λ = 6.0

Figure 31

T = 250°C

λ = 1.0

λ = 2.0

A

P

S.D.

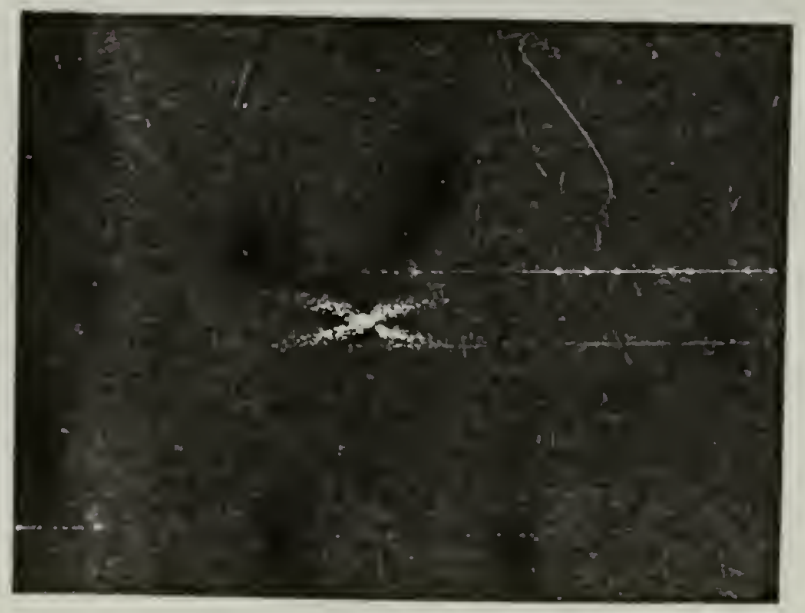

λ = 3.0

λ = 4.0

Figure 82

T = 260°C

λ = 2.0

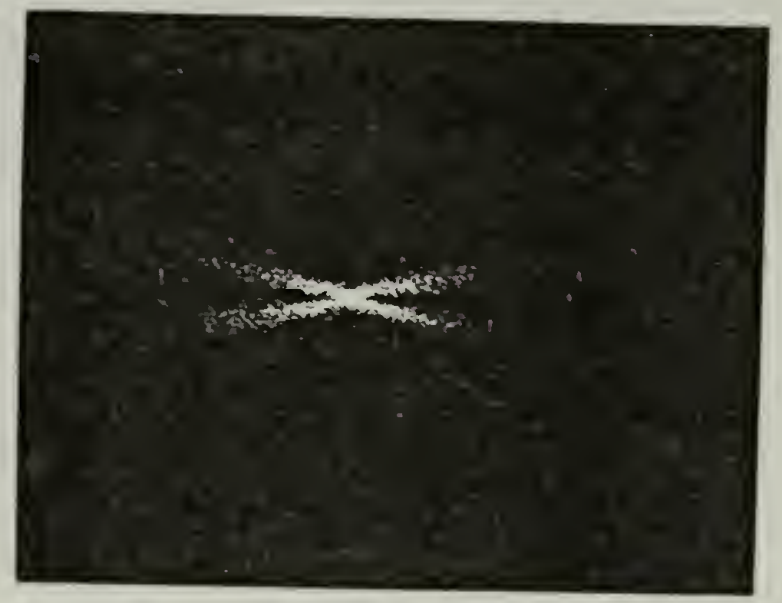

λ = 3.0

Figure 83a

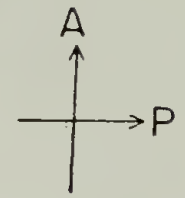

S.D.

T = 300°C

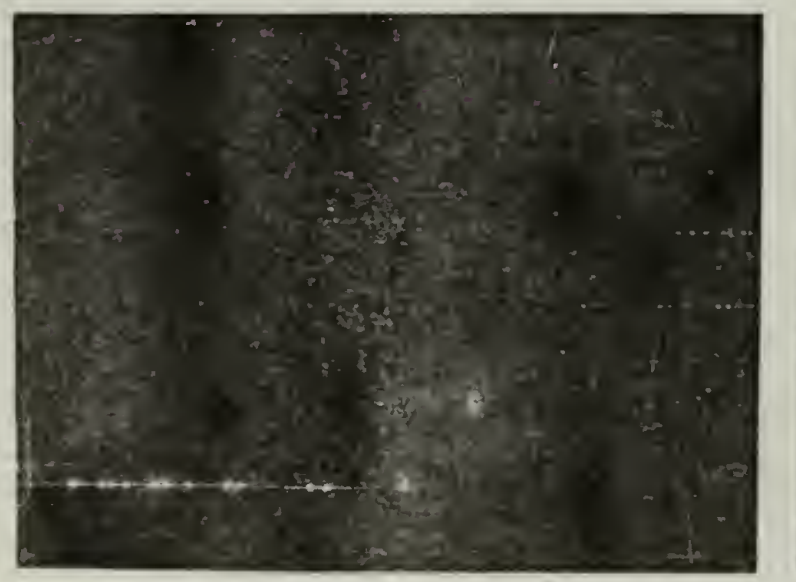

λ = 2.0

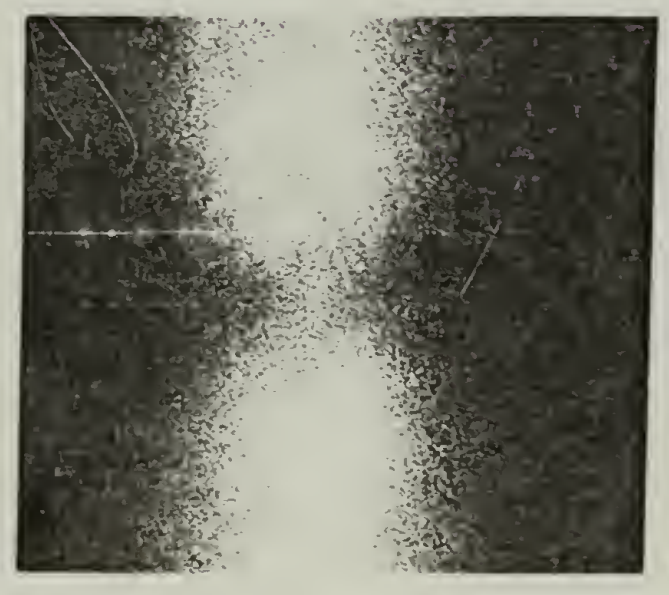

λ = 2.5

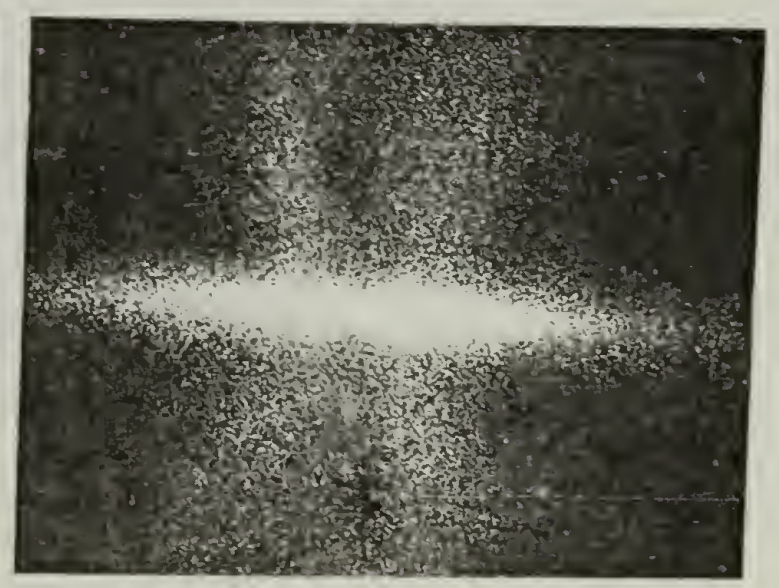

λ = 3.0

Figure 83c

T = 275°C

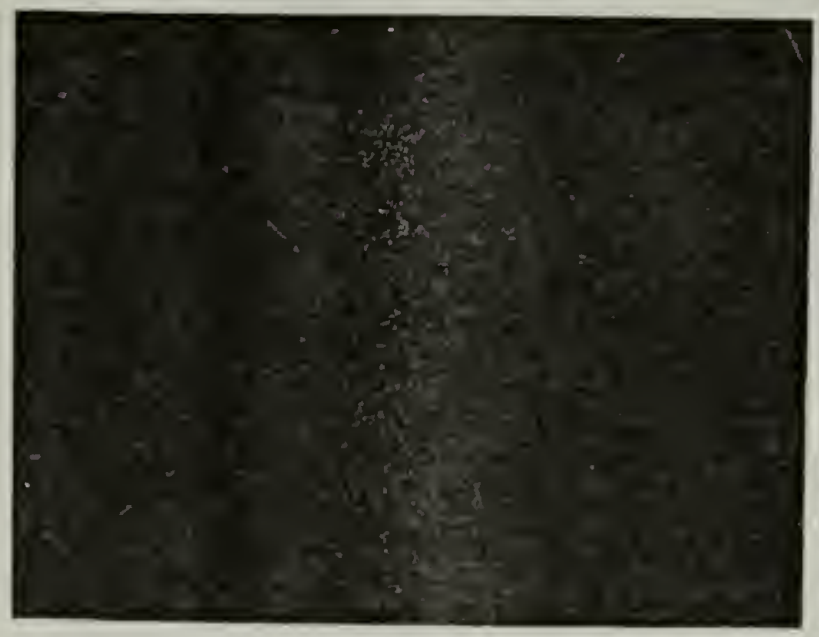

λ = 1.75

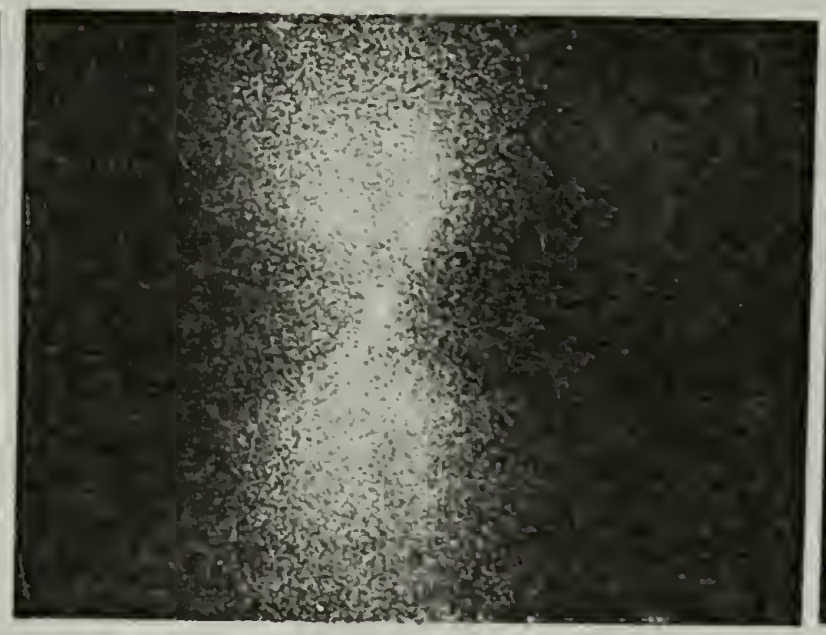

λ = 2.0

A
P
S.D.

λ = 2.25

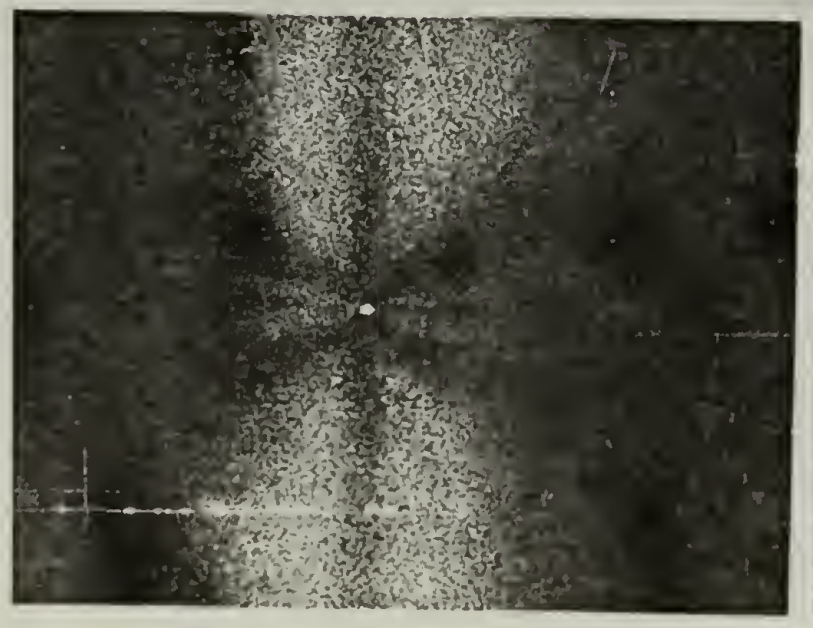

λ = 2.5

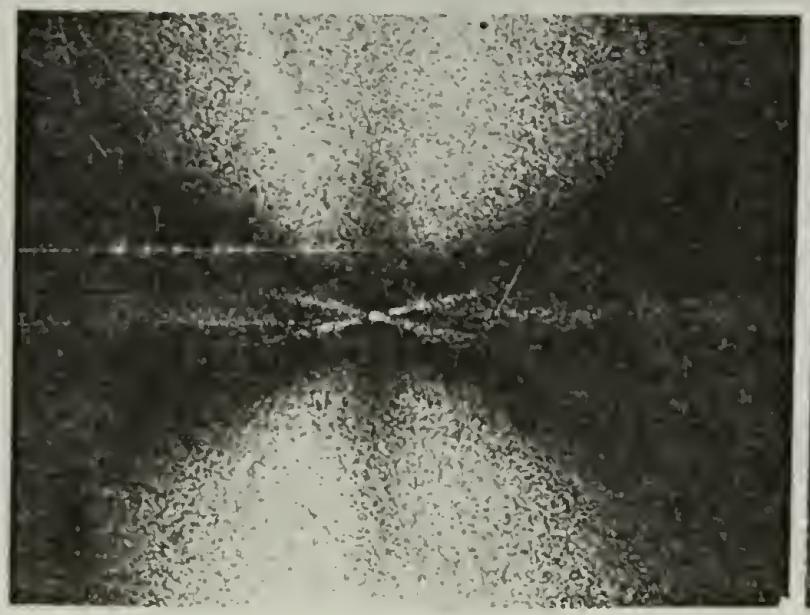

λ = 2.75

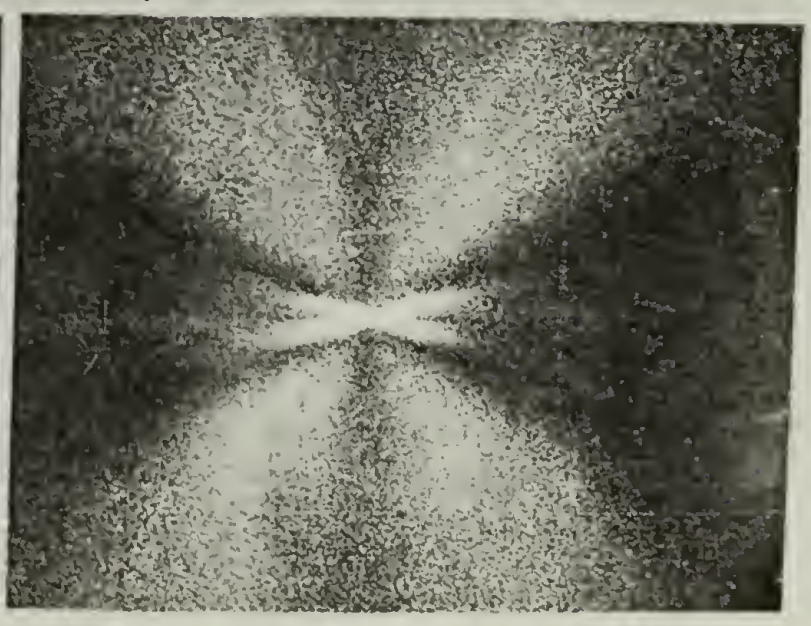

λ = 3.0

Figure 84

T = 275°C

λ = 3.1

λ = 3.25

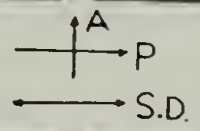

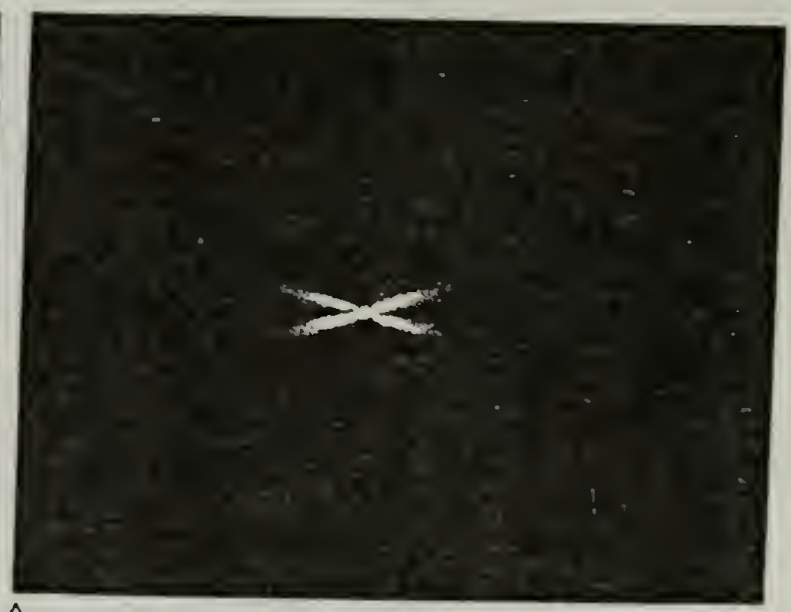

λ = 3.5

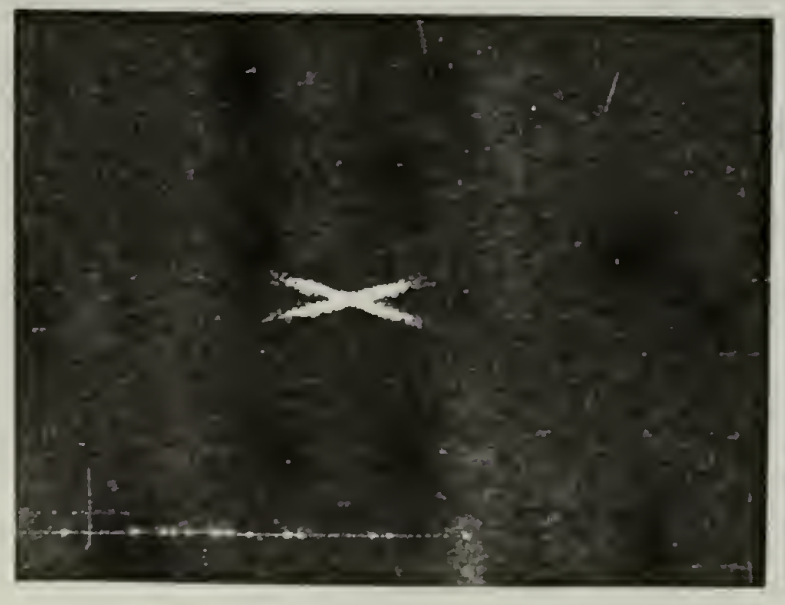

λ = 4.0

λ = 4.5

λ = 5.0

Figure 24b

T = 265°C

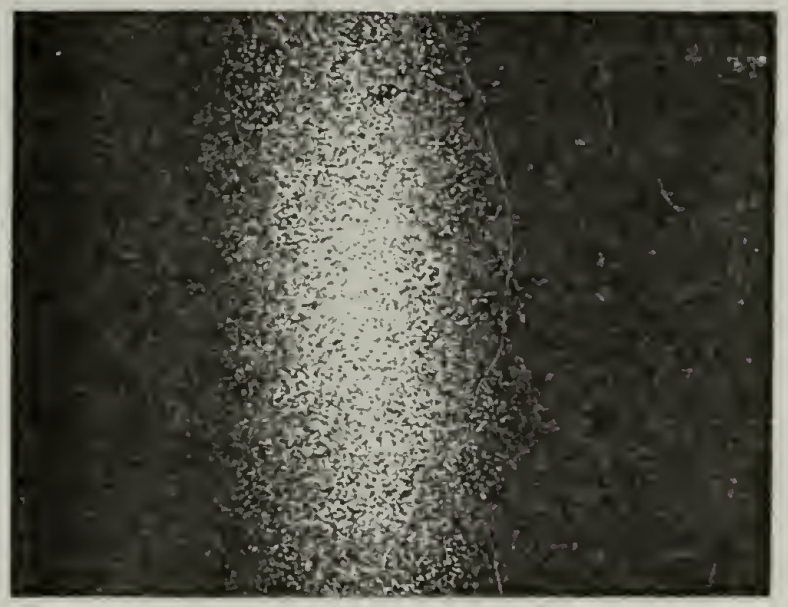

λ = 2.0

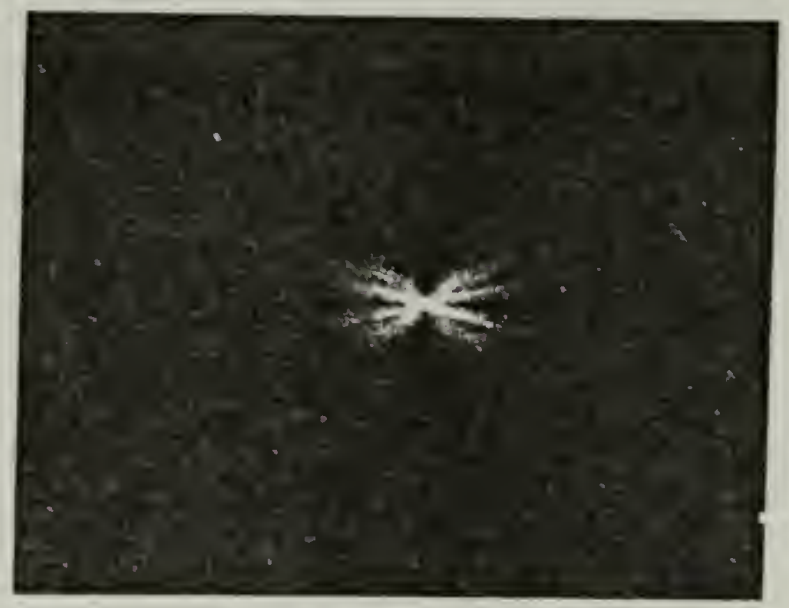

λ = 3.0

λ = 4.0

λ = 5.0

Figure 15

T = 285°C

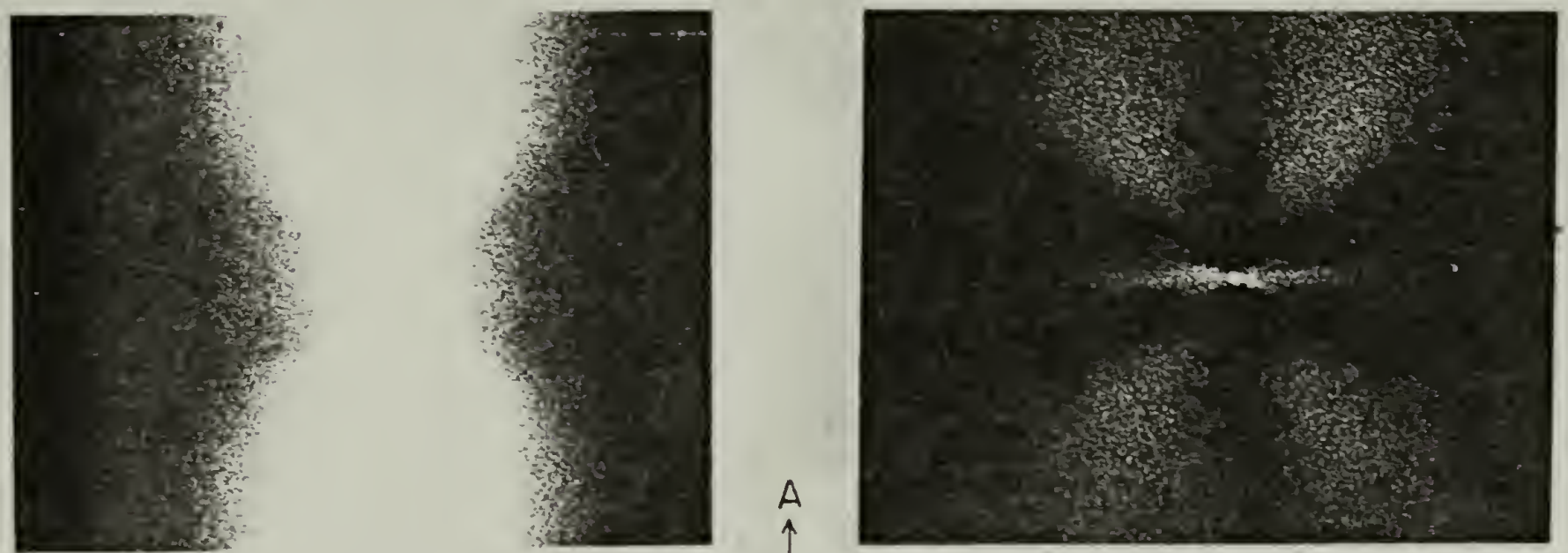

λ = 2.0

λ = 2.5

λ = 3.0

λ = 4.0

Figure 96

LIST OF TABLES

TABLE

TABLE I

The Effect of Temperature on the Half-Time, $t_{1/2}$, at Elongation Ratio 3.0

(°C) Temperature	(Min) Time
260	1.2
265	1.1
275	1.0
285	0.5
300	0.65
320	1.1

TABLE II

The Effect of Elongation on the Half-Time, $t_{1/2}$, at the Temperature of 275°C

$(\frac{L}{L_o})$ Elongation Ratio	(Min) Time
2.0	15.0
2.1	4.5
2.25	2.5
3.0	1.0

TABLE IIIA

Bond and Molecule	Denbigh		Bunn and Daubeny	
	(c.c.) $b_l \times 10^{25}$	(c.c.) $b_t \times 10^{25}$	(c.c.) $b_l \times 10^{25}$	(c.c.) $b_t \times 10^{25}$
C-C	18.8	0.2	10.0	2.5
N-H	5.8	8.4	5.8	8.4
C-H	7.9	5.8	8.2	6.0
C-C (aromatic)	22.5	4.8	22.5	4.8
C-N	15.9	8.9	13.8	2.2
	123.0	63.8	124.5	64.8

TABLE IIIB

Palarizabilities	$x10^{25}$(c.c.) Denbigh	$x10^{25}$(c.c.) Bunn and Daubeny
P_a	32.2	30.2
P_b	22.0	27.4
P_c	42.8	36.3
P_d	111.2	114.7
P_e	259.3	252.4
P_f	244.9	249.3

TABLE IV

°C Temperature	$\lambda = \frac{L}{L_o}$	$f' = \frac{D-1}{D+2}$	$-\Delta_T$	$f = \frac{\Delta_T}{\Delta^\circ}$
210	1.1	0.007	0.031	0.006
210	1.3	0.016	0.082	0.015
210	1.5	0.019	0.088	0.019
220	6.0 (M1)	0.117	0.058	0.127
230	1.1	0.004	0.015	0.004
230	1.3	0.009	0.040	0.008
230	1.5	0.013	0.055	0.012
240	4.0 (M2)	0.138	0.067	0.147
240	5.0 (M2)	0.142	0.070	0.153
240	6.0 (M2)	0.147	0.075	0.164
240	6.0 (M1)	0.110	0.042	0.092
260	3.0	0.157	0.092	0.201
260	6.0 (M1)	0.068	0.024	0.053
320	2.0	0.010	0.004	0.009
320	3.0	0.094	0.052	0.114

TABLE V

^{o}C Temperature	$\lambda = \frac{L}{L_o}$	$f' = \frac{D-1}{D+2}$	$-\Delta_T$	$f = \frac{\Delta_T}{\Delta^{\circ}}$
275	1.5	0.004	0.015	0.003
275	2.0(90)*	0.047	0.023	0.049
275	2.1(90)	0.083	0.043	0.094
275	2.25(90)	0.094	0.058	0.127
275	3.0(15)	0.155	0.123	0.270
275	3.0(30)	0.159	0.130	0.284
275	3.0(60)	0.163	0.135	0.295
275	3.0(90)	0.166	0.140	0.307
275	3.5(30)	0.168	0.155	0.340
275	4.0(30)	0.172	0.173	0.378
275	4.5(30)	0.185	0.199	0.436
275	5.0(30)	0.192	0.232	0.507

* The figures indicate the time (min) for isothermal crystallization

TABLE VI

°C Temperature	$\lambda = \frac{L}{L_o}$	$f' = \frac{D-1}{D+2}$	$-\Delta_T$	$f = \frac{\Delta_{T'}}{\Delta^\circ}$
265	2.0 (120)*	0.050	0.023	0.049
265	3.0 (90)	0.149	0.110	0.241
265	3.0 (60)	0.162	0.120	0.263
265	3.0 (120)	0.164	0.135	0.295
265	4.0 (30)	0.169	0.143	0.316
265	4.0 (120)	0.170	0.147	0.322
265	5.0 (120)	0.180	0.165	0.361
285	3.0 (30)	0.162	0.136	0.301
285	3.0 (90)	0.172	0.140	0.310
285	4.0 (120)	0.188	0.178	0.390
285	5.0 (120)	0.176	0.147	0.322
300	3.0 (120)	0.150	0.076	0.160
300	3.0 (90)	0.160	0.078	0.170
300	4.0 (30)	0.167	0.107	0.233
300	4.0 (90)	0.153	0.094	0.205
300	5.0 (15)	0.187	0.089	0.195
300	5.0 (30)	0.169	0.082	0.179
300	5.0 (120)	0.080	0.042	0.092

TABLE VII

CM^{-1} Wave Number	Symmetry	Orientation Function		
		T= 275°C = 5.0	T = 275°C = 2.1	T = 265°C = 4.0
418	A_1	0.165	0.037	———
451	B_1	0.715	0.446	0.638
500	B_2	-0.086	-0.022	-0.098
565	B_1 , B_2	0.0	0.0	———
616	B_2	-0.194	-0.102	-0.174
924	B_1	0.192	0.091	0.169
966	A_1	-0.190	-0.079	-0.183
1022	B_2	-0.134	-0.041	-0.171
1594	B_2	-0.114	-0.113	———
1912	A_1 , B_2	-0.213	-0.091	———

APPENDIX I

The Computer Program for the Calculation of Relaxation Study

PROGRAM RELAX

```
1 PROGRAM AMOR RELAX
5 DIMENSION A(20),B(100),C(100),D(100),E(20),EM(100),ES(100),
10C F(100),R8100),RO(100),ST8100),TT(100)
15C STG(100),RR(100),EE(20)
35 READ 40,R1,WL,DGF
40 FORMAT(S,1X,F5.2,2X,E10.3,2X,F6.1)
50 READ 60,TE,DO,SLO,WO,NL,MT
60 FORMAT(S,1X,F6.1,2X,F5.1,2X,F5.2,2X,F5.2,2X,I3,2X,I3)
70 READ 80,(E(J),J=1,NL)
80 FORMAT(S,1X,8(F4.1,1X))
105 DO 110 J=1,NL
106 ES(J)=E(J)-1.0
110 CONTINUE
125 PRINT 126,TE
126 FORMAT(* TEMP = *,F5.1)
127 READ 128,((RO(J),J=1,NL)
128 FORMAT(S,1X,9(F6.2,1X))
140 PRINT 142,E(J)
142 FORMAT(///* ELONGATION RATIO = *,F4.1)
145 PRINT 146
146 FORMAT(//*        TIME        STRESS        E        BIREF        SOC*)
150 A(J)=WO*DO*0.001*(2.54)**2.0/E(J)
155 EE(J)=SQRT(E(J))
160  D(J)=DO*0.001*2.54/EE(J)
162 READ,(R(I),I=1,MT)
164 READ,(F(I),I=1,MT)
166 READ,(TT(I),I=1,MT)
170 DO 210 I=1,MT
175 STG(I)=F(I)/A(J)
180 ST(I)=STG(I)*DGF
185 EM(I)=ST(I)/ES(J)
188 RR(I)=(R(I)-RO(J))/R1
190 B(I)=RR(I)*WL/D(J)
200 C(I)=B(I)/ST(I)
210 PRINT 220,TT(I),ST(I),EM(I),B(I),C(I)
220 FORMAT(5X,F5.1,2X,E9.3,2X,E9.3,1X,E9.3,4X,E9.3)
222 MT=MT+3
230 CONTINUE
240 END
READY.
```

APPENDIX II

The Computer Program for the Calculation of Stress Induced Crystallization Study

PROGRAM T1T

```
10 PROGRAM INSFX(INPUT,OUTPUT,DATA,TAPE5=DATA)
20 DIMENSION E(20),R(100),A(20),D(20),ST(100),B(100),C(100),
30+ TT(100),EM(100),ES(100),RO(100)
31 DIMENSION F(100),XC(100),RFA(100),X(50),XX(50),X1(50),XX1(50)
35 R1=5.36
36 WL=0.0000546
40 READ(5,42)FCI,FCO,SOC
41 42 FORMAT(4X,F5.2,F4.1,2X,E75)
50 READ(5,52)TE,DO,SLO,WO,NL,MT
51 52 FORMAT(3X,F6.1,1X,F4.1,1X,F5.2,1X,F5.2,1X,I2,1X,I3)
70 READ(5,72)(E(J),J=1,NL)
71 72 FORMAT(3X,F5.2)
73 READ(5,75)(R(I),I=1,10)
74 75 FORMAT(3X,10(F5.1,1X))
78 79 FORMAT(3X,5(F6.1,1X))
80 READ(5,75)(F(I),I=1,10)
83 READ(5,75)(TT(I),I=1,10)
86 READ(5,75)(RFA(I),I=1,10)
90 92 FORMAT(3X,2(F5.1,1X))
105 DO 110 J=1,NL
106 ES(J)=E(J)-1.
109 110 CONTINUE
140 DO 218 J=1,NL
150 A(J)=WO*DO*0.001*2.54*2.54/E(J)
155 D(J)=DO*0.001*2.54/SQRT(E(J))
169 PRINT 171,TE
170 171 FORMAT(* TEMP = *,F5.1)
172 PRINT 174,E(J)
173 174 FORMAT(///*ELONGATION RATIO = *,F5.2)
175 PRINT 177
176 177 FORMAT(//*  TIME  STRESS     E        BIREF        SOC        XC
178+ *       LOG      LOGI*)
179 DO 218 I=1,MT
180 ST(I)=(F(I)-FCO)*980.0/A(J)
185 EM(I)=ST(I)/ES(J)
186 RO(I)=R1*RFA(I)+17.4
190 B(I)=(R(I)-RO(I))*WL/R1/D(J)
200 C(I)=B(I)/ST(I)
205 XC(I)=(B(I)-ST(I)*SOC)/(BCI-ST(I)*SOC)
206 X(I)=1-XC(I)
207 XX(I)=-ALOG(X(I))
217 218 CONTINUE
220 XFG=XC(1)
222 DO 228 I=2,MT
223 IF(XC(I).GE.XFG)226,228
225 226 XFG=XC(I)
227 228 CONTINUE
```

```
230 DO 245 I=1,MT
231 X1(I)=1-XC(I)/XFG
232 IF(XC(I).GE.XFG)237,234
233 234 XX1(I)=-ALOG(X1(I))
235 GO TO 245
236 237 XX1(I)=0.0
243 245 CONTINUE
250 DO 270 I=1,MT
251 PRINT 260,TT(I),ST(I),EM(I),B(I),C(I),XC(I),XX(I),XX1(I)
255 260 FORMAT(F6.1,E9.3,E9.3,1X,E9.3,1X,E9.3,E10.4,F5.3,2X,F5.3)
268 270 CONTINUE
280 END
READY.
```

APPENDIX III

The Computer Program for the Calculation of Dynamic Birefringence

```
LIST DBS5
10 PROGRAM DBS
20 DIMENSION F(100),FR(100),FAF(100),ST(100),EMS(100),
30C SH(100),H(100),TH(100),RTD(100),BR(100),FAB(100),CB(100),
40C HA(100),B(100),SD(100),BRC(100),FRC(100),D(100),TD(100),
50C SOC(100),OME(100),SOK(100),SOKR(100),SOKI(100),T(100)
55 DIMENSION SBI(50),CF(10)
56 DIMENSION EMR(100),EMI(100)
60 READ,WL,DE,N,M,CFC
71 READ,(OME(J),J=1,M)
73 READ,(CF(J),J=1,M)
75 READ,(SBI(I),I=1,N)
77 READ,(T(I),I=1,N)
79 DO 495 J=1,M
80 READ,DO,SLO,SL,WO
85 PRINT 86,OME(J)
86 FORMAT(/////*    FREQUENCY = *,F6.3,*    CYCLES/SEC*)
99 READ,(FR(I),I=1,N)
100 READ,(FAF(I),I=1,N)
120 READ,(FRC(I),I=1,N)
150 READ,(BR(I),I=1,N)
160 READ,(FAB(I),I=1,N)
170 READ,(CB(I),I=1,N)
180 READ,(HA(I),I=1,N)
190 READ,(BRC(I),I=1,N)
210 E=SL/SLO
220 D=DO*0.001*2.54/SQRT(E)
230 A=WO*DO*0.001*2.54*2.54/E
240 DO 490 I=1,N
250 F(I)=FR(I)*FAF(I)*CFC*CF(J)
260 ST(I)=F(I)/A
270 EMS(I)=ST(I)/DE
280 SH(I)=FRC(I)/FR(I)
290 H(I)=ASIN(SH(I))
300 TH(I)=TAN(H(I))
310 EMR(I)=EMS(I)*COS(SH(I))
320 EMI(I)=EMS(I)*SIN(SH(I))
330 RTD(I)=BR(I)*FAB(I)*CB(I)/HA(I)
340 B(I)=RTD(I)*WL/D+0.5*SBI(I)
350 SD(I)=BRC(I)/BR(I)
360 D(I)=ASIN(SD(I))
370 TD(I)=TAN(D(I))
380 SOC(I)=B(I)/ST(I)
382 SOK(I)=B(I)/DE
384 SOKR(I)=SOK(I)*COS(D(I))
386 SOKI(I)=SOK(I)*SIN(D(I))
```

```
390 PRINT 400,T(I)
400 FORMAT(//*    TEMP = *,F6.1,*  DEGREE CENTIGRADE*)
410 PRINT 420
420 FORMAT(/*     E          ER         EI          BIRE        TANH   STRESS*)
430 PRINT 440,EMS(I),EMR(I),EMI(I),B(I),TH(I),ST(I)
440 FORMAT(2X,4(E9.3,1X),F6.3,1X,E9.3)
450 PRINT 460
460 FORMAT(/*     K          KR         KI          C           TAND*)
470 PRINT 480,SOK(I),SOKR(I),SOKI(I),SOC(I),TD(I)
480 FORMAT(2X,4(E9.3,1X),F6.3)
490 CONTINUE
495 CONTINUE
500 END
510 ENDPROG
```

APPENDIX IV

The Computer Program for the Correction of X-Ray Intensity

```
PROGRAM    X

10 PROGRAM X-RAY INTEN CORR
15 DIMENSION XI(50),BI(50),THETA2(50),THETA1(50),N(10),
16C AM(30),WW(30)
20 READ,NM,DEN
25 READ,(N(I),WW(I),AM(I),I=1,NM)
30 TOT=0.0
35 DO 50 I=1,NM
40 TOT=TOT+N(I)*WW(I)
50 CONTINUE
55 DO 65 I=1,NM
60 W(I)=N(I)*WW(I)/TOT
65 CONTINUE
70 SUM=0.0
75 DO 85 I=1,NM
80 SUM=SUM+W(I)*AM(I)
85 CONTINUE
90 U=SUM*DEN
95 READ,D,COHIN,MM
100 READ,((THEA2(I),BI(I)),I=1,MM)
105 READ,(XI(I),I=1,MM)
110 DO 200 I=1,MM
115 PAI=3.14159
118 RA2=(PAI/180.0)*THETA2(I)
120 RA1=RA2/2.0
125 THETA1(I)=THETA2(I)/2.0
135 SECA1=1.0/COS(RA1)
140 CRPOL=1.0+((COS(RA2))**2.0)
145 CRLOR=1.0/(SIN(RA2))
150 CRB=B(I)*EXP(-U*D*SECA1)
155 CRA=EXP(U*D*SECA1)/SECA1
160 COR3=XI(I)-CRB
165 COR2=COR3*CRPOL*CRA
175 CORR=COR1*CRLOR
180 CORF=CORR-COHIN
185 COR=CORF*(SIN(RA1)**2.0)*(COS(RA1))
190 PRINT 195,CORF,THETA1,COR,XI(I)
195 FORMAT(F10.0,F10.2,2F10.0)
200 CONTINUE
210 END
220 ENDPROG
READY.
```

BIBLIOGRAPHY

1. H. Davidge, J. Appl. Chem. 9, 553 (1959).
2. L. E. Nielsen, "Mechanical Properties of Polymers", Reinhold, New York (1962).
3. N. Kuwahara, S. Higashide, N. Nakara, and M. Kaneko. J. Polymer Sci., Part A-2, 7, 285 (1969).
4. D. J. William, Macromolecules, 3, 602 (1970).
5. L. R. G. Treloar, "The Physics of Rubber Elasticity", Oxford (1958).
6. Y. Abe, A. E. Tonell, and P. J. Flory, Macromolecules, 3, 294 (1970).
7. R. G. Crystal, Macromolecules, 4, 379 (1971).
8. J. H. Sharp, J. Phys. Chem., 71 1587 (1967).
9. Encyclopedia of Polymer Science and Technology, 11.
10. K. Tanikawa, S. Kusabayashi, H. Hirata, and H. Mikawa, Polymer Letters, 6, 275 (1968).
11. H. Hoegl, J. Phys. Chem., 69, 755 (1965).
12. M. Lardon, E. Lell-Doller, and J. A. Weigl, Molecular Crystal, 2, 241 (1967).
13. A. M. Herman and A. Rembaum, J. Polymer Sci., Part C, 17, 107 (1967).
14. C. E. Schildknecht, A. O. Zoss, and F. Grosser, Ind. Eng. Chem., 41, 2891 (1949).
15. O. F. Solomon, M. Dimonie, K. Ambrozh, and M. Tomesku, J. Polymer Sci., 52, 205 (1961).

16. J. Heller, D. O. Tieszen, and D. B. Parkinson, J. Polymer Sci., Part A, 1, 125 (1963).

17. J. Heller, D. J. Lyman, and .. A. Hewett, Makromol. Chem. 73, 48 (1964).

18. T. Matsuda, T. Higashimura, and S. Okamura, J. Macromol. Sci., Chem. 2, 43 (1968).

19. A. Kimura, S. Yoshimoto, Y. H. Jirata, S. Kusabayashi, H. Mikawa, and N. Kasai, J. Polymer Sci., Part A-2, 8, 643 (1970).

20. C. H. Griffiths, J. Polymer Sci., 13, 1167 (1975).

21. J. M. Schultz, "Polymer Material Science", Prentice-Hall, New Jersey (1974).

22. B. I. Sazhin, and N. G. Podosenova, Polymer Sci., (USSR), 6, 162 (1964).

23. V. A. Kargin, N. G. Podosenova, G. P. Andrianova, and B. I. Sazhin, Polymer Sci., (USSR), 9, 323 (1967).

24. L. E. Nielsen, "Mechanical Properties of Polymer and Composites" Vol. 2, Marrel Dekker, New York (1974).

25. L. E. Nielsen, and R. Buchdahl, J. Appl. Phys., 21, 488 (1950)

26. A. Keller, and J. G. Rider, J. Mater. Sci., 1, 389 (1966).

27. J. G. Rider, and E. Hargreaves, J. Polymer Sci., A2, 7, 829 (1969).

28. D. M. Gezovich and P. H. Geil, J. Mater, Sci., 6, 531 (1971).

29. I. M. Ward, J. Polymer Sci., C32, 175 (1971).

30. M. Parrish, and N. Brown in "Plastic Deformation of Polymers", Marrel Dekker, New York (1971).

31. G. A. Samara, and H. G. Drickammer, J. Chem. PHys., 37, 474 (1962).

32. E. F. Carr, Mol. Cryst. 7, 253 (1969).

33. R. S. Stein, in "Newer Methods of Polymer Characterization", Wiley, New York (1964).

34. R. J. Samuels, in "The Science and Technology of Polymer Film", Wiley, New York (1968).

35. G. L. Wilkes, Advan, Polym. Sci., 8, 91 (1971).

36. R. S. Stein, and R. W. Lenz, "Structure and Properties of Polymer Film", Plenum Press, New York (1973).

37. G. L. Wilkes, J. Macromol. Sci.-Revs. Macromol. Chem., C10 (2),149 (1974).

38. R. S. Stein, J. Polymer Sci., 31, 327 (1958).

39. R. S. Stein, S. Onogi, and D. A. Keedy, J. Polymer Sci., 57, 801 (1962).

40. J. C. Henncker, "Infrared Spectrometry of Industrial Polymer ", Academic Press, New York (1967).

41. R. S. Stein, J. Appl. Polymer Sci., 5, 96 (1961).

42. R. Zbinden, "Infrared Spectroscopy of High Polymers", Academic Press, New York (1964).

43. R. S. Stein, Polymer Eng. Sci., 9, 320 (1969).

44. B. E. Read, D. A. Hughes, D. C. Barnes, and F. M. M. Druvy, Polymer, 13, 485 (1972).

45. B. E. Read, et al, ibid, 13, 495 (1972).

46. R. S. Stein, and M. B. Rhodes, J. Appl. Phys., 31, 1873 (1960).

47. R. J. Samuels, J. Polymer Sci., A-2, 9, 2165 (1971).

48. S. B. Clough, J. J. van Aartsen, and R. S. Stein, J. Appl. Phys., 36, 3072 (1965).

49. T. Hasimoto, A. Todo, and H. Kawai, J. Polymer Sci., Phys. Ed., 11, 149 (1973).

50. M. B. Rhodes, and R. S. Stein, J. Appl. Phys., 42, 4570 (1971).

51. M. Moritani, N. Hayashi, A. Utsuo, and H. Kawai, Polymer J., 2, 74 (1971).

52. N. Hayashi, and H. Kawai, Polymer J., 3, 140 (1972).

53. R. J. Volungis, M. S. Thesis, University of Mass. (1955).

54. D. G. Legrand, Ph.D. Thesis, University of Mass. (1959).

55. R. S. Stein, F. H. Holmes, and A. V. Tobolsky, J. Polymer Sci., 14, 443 (1954).

56. L. E. Nielsen, and R. Buchdahl, J. Chem. Phys., 17, 839 (1949).

57. E. Catsiff and A. V. Tobolsky, J. Colloid Sci., 10, 375 (1955).

58. E. Catsiff and A. V. Tobolsky, J. Polymer Sci., 19, 111 (1956).

59. P. E. Rouse, J. Chem. Phys. 21, 1272 (1953).

60. B. F. Bueche, J. Chem. Phys. 22, 603 (1954).

61. B. H. Zimm, J. Chem. Phys. 23, 269 (1956).

62. M. L. William, R. F. Landel and J. D. Ferry, J. American Chem. Soc., 77, 3701 (1955).

63. J. D. Ferry, "Viscoelastic Properties of Polymers", Wiley, New York (1970).

64. J. J. Aklonis, W. J. Macknight, and M. Shen, "Introduction to Polymer Viscoelasticity", Wiley, New York (1972).

65. S. Onogi, D. A. Keedy, and R. S. Stein, J. Polymer Sci., 50, 153 (1961).

66. R. S. Stein, S. Onogi, and K. Sasaguri, and D. A. Keedy, J. Appl. Phys., 34, 80 (1963).

67. R. Yamada, and R. S. Stein, J. Appl. Phys., 36, 3005 (1965).

68. R. Yamada, N. Hayashi, S. Onogi and M. Horio, J. Polymer Sci., C5, 123 (1964).

69. B. E. Read, J. Polymer Sci., C5, 87 (1964).

70. B. E. Read, Polymer, 5, 1 (1964).

71. J. F. Rudd, Polymer Letter 3, 345 (1965).

72. D. G. Legrand, J. Polymer Sci., Part A-2, 931 (1964).

73. T. Ito, T. Oda, H. Kawai, T. Kawaguihi, D. A. Keedy, and R. S. Stein, Rev. Sci., Instr., 39, 1847 (1968).

74. H. Kawai, T. Ito, T. Oda, H. Hiratsuka, and S. Suehiro, Mem. Fac. Eng., Kyoto Univ., 35, 201 (1973).

75. T. Kyu, N. Yasuda, M. Tabushi, S. Nomura, and H. Kawai, Polymer J., 7, 108 (1975).

76. C. Chang, Ph.D., Thesis, University of Mass. (1973).

77. M. C. Child, and J. D. Ferry, J. Colloid Sci., 12, 327 (1957).

78. W. C. Child, and J. D. Ferry, ibid, 12, 389 (1957).

79. K. Dannhauser, W. C. Child, and J. D. Ferry, ibid, 13, 103 (1958).

80. P. R. Saunders, D. M. Stein, S. K. Kurath, C. Sakoonkim, and J. D. Ferry, ibid, 14, 222 (1959).

81. R. Simha and R. F. Boyer, J. Chem. Phys., 37, 1003 (1962).

82. J. G. Fox, and P. J. Flory, J. Appl. Phys., 21, 581 (1950).

83. R. Simha and C. E. Weil, J. Macromol. Sci.-Phys., B4, 215 (1970).

84. I. C. Sanchez, J. Appl. Phys., 45, 4204 (1974).

85. A. N. Gent, J. Polymer Sci., A, 3, 3787 (1965).

86. A. N. Gent,ibid, A-2, 4, 447 (1966).

87. W. Yau, and R. S. Stein, J. Polymer Sci., A-2, 6, 1 (1968).

88. H. Kim and L. Mandelkern, J. Polymer Sci., A-2, 6, 181 (1968).

89. S. B. Clough, J. Macromol. Sci.-Phys., B4, 199 (1970).

90. G. K. Kraus and J. T. Gruver, J. Polymer Sci., 10, 2009 (1972).

91. Y. Akana, M. S. Thesis, University of Mass. (1973).

92. A. V. Tobolsky and G. M. Brown, J. Polymer Sci., 17, 5471 (1955).

93. A. Keller, and M. J. Machin, J. Macromol. Sci.-Phys., B1, 41 (1967).

94. M. J. Hill and A. Keller, J. Macromol. Sci.-Phys., B3 (1), 153 (1969).

95. T. W. Hass, and B. Maxwell, Polymer Eng. and Sci., 9, 225 (1969).

96. A. Pereta, and C. G. Gogos, Polymer Engr. and Sci., 11, 19 (1971).

97. Z. Pelzbauer, and R. Manley, J. Macromol. Sci.-Phys., B4, 761 (1970).

98. A. J. Pennings, J. Polymer Sci., C16, 1799 (1967).

99. J. H. Southern, and R. S. Porter, J. Macromol. Sci.-Phys., B4, 541 (1970).

100. J. H. Southern, and R. S. Porter, J. Appl. Polymer Sci., 14, 2305 (1970).

101. E. S. Clark, Soc. Plastics Engrs. J., 23, 46 (1967).

102. K. Katayama, T. Amano and K. Nakamura, Kolloid-Z., 226, 125 (1968).

103. C. A. Garber, and E. S. Clark, J. Macromol. Sci.-Phys., B4, 499 (1970).

104. E. C. Bernhardt, "Processing of Thermoplastic Materials", Krieger, New York (1959).

105. W. R. Krigbaum, and R. J. Roe, J. Polymer Sci., A, 2, 4391 (1964).

106. P. J. Flory, J. Chem. Phys., 15, 397 (1947).

107. A. N. Gent, Trans. Faraday Soc., 50, 521 (1954).

108. P. J. Flory, Ind. Eng. Chem. 38, 417 (1946).

109. S. L. Dart and E. Guth, J. Chem. Phys., 13, 28 (1945).

110. S. L. Dart, R. L. Anthony, and E. Guth, Ind. Eng. Chem. 34, 1340 (1942).

111. I. M. Ward, "Mechanical Properties of Solid Polymers", John Wiley & Son, New York (1971).

112. L. E. Nielsen, "Mechanical Properties of Polymer and Composite", Vol. 1, Marrel Dekker Inc., New York (1974).

113. T. G. Fox, and P. J. Flory, J. Appl. Phys. 21, 581 (1950).

114. T. G. Fox and P. J. Flory, J. Polymer Sci., 14, 315 (1954).

115. R. C. Penwell, Private Communication.

116. P. Mears, "Polymers structure and Bulk Properties", New York (1965).

117. N. M. Prest, Private Communication.

118. R. S. Stein, J. Appl. Phys., 32, 1280 (1961).

119. K. G. Denbigh, Trans, Faraday Soc., 36, 936 (1940).

120. C. W. Bunn, and R. Daubeny, Trans. Faraday Soc., 50, 1173 (1954).

121. D. M. Saunders, Trans. Faraday Soc., 52, 860 (1956).

122. J. O. Hirschfelder, C. F. Curtiss, and R. B. Bird, "Molecular Theory of Gases and Liquids", John Wiley & Sons, New York (1954).

123. G. S. Whitley, J. Phys. Chem. 36, 198 (1932).

124. R. A. Sack, J. Polymer Sci., 54, 543 (1961).

125. C. R. Desper, and R. S. Stein, J. Appl. Phys., 37, 3990 (1966).

126. R. J. Samuels, in "The Science and Technology of Polymer Films", 1, 256 (1968).

127. C. W. Bunn, Proc. Roy. Soc. (London), A180, 40 (1940).

128. L. E. Alexander, and E. R. Michalik, Acta Cryst., 12, 105 (1959).

129. A. Bree, and R. Zwarich, J. Chem. Phys., 49, 3344 (1968).

130. M. F. Milagin, A. D. Gabarayeva, and I. I. Shishkin, Vysokomol. Soyed. A12, 513(1970).

131. W. Yau, and R. S. Stein, Polymer Letters, 2, 231 (1964).

132. P. H. Lindenmeyer, J. Polymer Sci., C-20, 145 (1967).

133. E. H. Andrew, Proc. Roy. Soc. (London), A77, 562 (1964).

134. M. H. Walter, J. Polymer Sci., A-1, 3091 (1963).

135. M. B. Rhodes, and R. S. Stein, J. Appl. Phys., 32, 1344 (1961).

136. M. Yasuniwa, C. Nakafuku, and T. Takemura, Polymer J. 4, 526 (1973).

137. M. Kyotani, and H. Kanestsuna, J. Polymer Sci., 12, 2331 (1974).

138. T. Hatakeyama, H. Kanestsuna, H. Kaneda, and T. Hashimoto, J. Macromol. Sci., Phys., B10, 359 (1974).

139. K. J. Smith, A. Greene, and A. Ciferri, Kolloid-Z. Z. Polym. 194, 49 (1964).

140. M. C. Morris, J. Appl. Polym. Sci., 8, 545 (1964).

141. J. T. Judge, and R. S. Stein, J. Appl. Phys. 32, 2357 (1961).

142. D. L. Magagnuni, A. Marchfiti, T. Matera, G. Pizzirani, and G. Turchi, European Polymer J., 10, 586 (1974).